

INTERACTION OF LUTEOLIN AND MITOXANTRONE WITH G-QUADRUPLEX DNA SEQUENCES

Ph.D. THESIS

by

SWETA TRIPATHI



**DEPARTMENT OF BIOTECHNOLOGY
INDIAN INSTITUTE OF TECHNOLOGY ROORKEE
ROORKEE-247 667 (INDIA)
DECEMBER, 2014**

INTERACTION OF LUTEOLIN AND MITOXANTRONE WITH G-QUADRUPLEX DNA SEQUENCES

A THESIS

*Submitted in partial fulfilment of the
requirements for the award of the degree
of*

DOCTOR OF PHILOSOPHY
in

BIOTECHNOLOGY

by

SWETA TRIPATHI



**DEPARTMENT OF BIOTECHNOLOGY
INDIAN INSTITUTE OF TECHNOLOGY ROORKEE
ROORKEE-247 667 (INDIA)
DECEMBER, 2014**

**©INDIAN INSTITUTE OF TECHNOLOGY ROORKEE, ROORKEE-2014
ALL RIGHTS RESERVED**



INDIAN INSTITUTE OF TECHNOLOGY ROORKEE ROORKEE

CANDIDATE'S DECLARATION

I hereby certify that the work which is being presented in the thesis entitled **“INTERACTION OF LUTEOLIN AND MITOXANTRONE WITH G-QUADRUPLEX DNA SEQUENCES”** is in partial fulfilment of the requirements for the award of the Degree of Doctor of Philosophy and submitted in the Department of Biotechnology of the Indian Institute of Technology Roorkee, Roorkee is an authentic record of my own work carried out during a period from August, 2009 to December, 2014 under the supervision of Dr. Ritu Barthwal, Professor, Department of Biotechnology, Indian Institute of Technology Roorkee, Roorkee.

The matter presented in this thesis has not been submitted by me for the award of any other degree of this or any other Institute.

(SWETA TRIPATHI)

This is to certify that the above statement made by the candidate is correct to the best of my knowledge.

Dated: December, 2014

(RITU BARTH WAL)
Supervisor

ACKNOWLEDGEMENTS

Life is full of twists and turns and we get lots of lessons throughout our journey. Research being one of the most important phases of this journey, which is full of excitement and challenges. Completing a Ph.D. seems to be a road in which you have to travel alone, but without the contribution from numerous people it would have been impossible for me to complete this journey. It's an immense pleasure for me to convey my sincere appreciation and gratitude to all of them.

First and foremost, I would like to thank Vaishnao maa for providing me the privilege to pursue my Ph.D. and the strength to complete it successfully in spite of the challenges I faced during this journey.

After Vaishnao maa, I would like to express my heartfelt gratitude to my parents, for their unconditional love, constant support and immense faith and encouragement. I dedicate this thesis to my parents.

I am heartily thankful to my advisor Dr. Ritu Barthwal whose encouragement, guidance and support from the initial to the final level enabled me to develop an understanding of the subject. This work would not have been possible without her undaunted enthusiasm, efforts, inspiration and remarkable patience. I am also grateful to her for giving a chance to avail all the facilities provided by the Central NMR facility, IIT Roorkee.

I would also like to thank my committee members Dr. G. S Randhawa, Dr. Partha Roy and Dr. Anil kumar for their supportive guidance throughout my degree. I owe particular thanks to Dr. Krishna Mohan Poluri for his valuable suggestions, time and support.

I offer my enduring gratitude to my fellow lab members Pradeep T.P., Padma, Zia Tariq, Shailja for providing healthy and friendly ambience in the lab. We had a great time both in and outside the lab. I also thank my seniors Dr. Asif Hassan, Dr. Lata Chauhan, Dr. Kushuma and Dr. Amit Kumar. I thank Padma for giving her valuable time in spite of her busy schedule. My special thanks to Pradeep without him my stay at Roorkee would not have been easier. We have spent five and half years together. He is a friend cum brother to me who helped me to learn a lot about how to use, maintain and troubleshoot different instruments in our lab. He has contributed a lot in successfully completing my Ph.D.

I am fortunate to have some good friends like Gargi, Megha, Priyanka, and Pooja. They kept me refreshed even during the stressful times. I can never forget the fun I had with Megha and I am thankful to her for emotional support she has provided during my thesis.

I thank Mr. Sher Singh and Pratibha for providing excellent food and special care in mess.

I cannot forget to thank my sister Julie, brother Kunal and jiju for their love and affection. They stood by me through thick and thin. I would like to mention my niece Tashi, who acts as a soothing balm for me. Last but not least my academic pursuits could have never been fully achieved without the unwavering support and love of my fiancée, Anand. I am extremely grateful for all of the sacrifices (including listening to me rant about crazy science things) he has made, that have allowed me to realize this part of my life.

Finally, I would like to acknowledge the Ministry of human Resources and Development, Govt. of India for financial assistance during my Ph.D.

My sincere apologies to those whom I could not mention personally one by one but I thank them equally.

(Sweta Tripathi)

Table of Contents

	Page No.
Acknowledgements	i-ii
Contents	iii-vi
List of Tables	vii-ix
List of Figures	xi-xviii
List of Abbreviations	xix-xx
Abstract	xxi-xxiv
Chapter 1	1-46
Introduction	1
1.1 General overview of DNA	1
1.1.1 Nitrogenous bases	1-2
1.1.2 Pentose sugar	3
1.1.3 Phosphate groups	4
1.2 DNA polymorphism	4-5
1.2.1 Canonical DNA structures	5
1.2.1.1 B-DNA	5-6
1.2.1.2 A-DNA	6
1.2.1.3 Z-DNA	6-7
1.2.2 Non-canonical DNA structures	7
1.2.2.1 Triplex-DNA	7-8
1.2.2.2 i-motif	8-9
1.2.2.3 G-quadruplex	9
1.3 G-quadruplex structure and stability	9-11
1.3.1 G-quadruplex structure and stability	11-14
1.3.2 Biological significance of G-quadruplexes	14
1.3.2.1 G-quadruplex location	14
1.3.2.2 Telomeric G-quadruplexes	14-15
1.3.2.3 Oncogenic promoter G-quadruplexes	15-16
1.3.2.4 RNA quadruplexes	17
1.3.2.5 G-quadruplex: as a target for anti-cancer drug design	17-18
1.3.2.5.1 Targeting Telomeres and telomerase	18-22
1.3.2.5.2 Targeting oncogenic promoter regions	22-23
1.3.3 G-quadruplex interactive ligands	23-27
1.3.4 Structural studies on G-quadruplex interactive ligands	27-33
1.4 Anthraquinones Derivatives	33-34
1.5 Mitoxantrone as a chemotherapeutic agent	34-35
1.6 Structure and Interaction of mitoxantrone with nucleic acids	35-36
1.7 Flavonoids	36-7
1.7.1 Structure and classification	37-38
1.7.2 Dietary intake and metabolism of flavonoids	38
1.7.3 Biological activities of flavonoids	38-40
1.7.4 Interaction of flavonoids with DNA	41-42
1.8 Luteolin as an anticancer and chemotherapeutic agent	42-43
1.9 Structural and pharmacological properties of Luteolin	43-44
1.10 Binding of luteolin to proteins and DNA	44-45
1.11 Scope of thesis	45-46

	Page No.
Chapter 2	
Materials and Methods	47-73
2.1 Chemicals and reagents	47
2.1.1 Buffer used in experiments	47
2.2 Absorbance measurements	47
2.2.1 Sample preparation	47-48
2.2.2 Methodology	48-49
2.3 Steady State and Life Time Fluorescence Measurements	48
2.3.1 Steady State measurements	48
2.3.1.1 Sample preparation	48
2.3.1.2 Methodology	48-50
2.3.1.3 Continuous Variation Analysis (Job plot)	51
2.3.2 Life Time Measurements	51
2.3.2.1 Sample preparation	51
2.3.2.2 Methodology	51-52
2.4 Circular Dichroism measurements	52
2.4.1 Sample preparation	52
2.4.2 Methodology	52-53
2.5 Nuclear Magnetic Resonance (NMR) spectral measurements	53
2.5.1 Sample preparation	53
2.5.1.1 Mitoxantrone-d-(TTAGGGT) ₄ complex	53
2.5.1.2 Luteolin-d-(TTAGGGT) ₄ and luteolin-d-(TTGGGGT) ₄ complex	54-55
2.5.2 Methodology	55
2.5.2.1 The Phenomenon of NMR	55-57
2.5.2.2 Chemical Shift	57-58
2.5.2.3 Spin-Spin Coupling (J coupling)	58
2.5.2.4 One-dimensional and Two-dimensional NMR Spectroscopy	58-67
2.5.2.5 Determination of three-dimensional structure	67-68
2.5.2.5.1 Resonance assignments of quadruplex	68-69
2.5.2.5.2 Sugar pucker conformations	69
2.5.2.5.3 Conformation about the glycosidic bond	69
2.5.2.5.4 Estimation of interproton distances	70
2.5.2.5.5 Restrained molecular dynamics methodology	70-71
2.6 Differential Scanning Calorimetry	71
2.6.1 Sample preparation	71
2.6.2 Methodology	71-72
2.7 Telomerase Repeat Amplification Protocol (TRAP) Assay	72
2.7.1 Telomerase enzyme isolation and methodology	72-73

	Page No.
Chapter 3	
Investigations on Binding, Stabilization and Inhibition properties of anticancer drug mitoxantrone with human G-quadruplex DNA.	75-92
3.1 Results and Discussion	75-91
3.1.1 Monitoring the MTX-quadruplex binding interactions using Absorption Spectroscopy	75-79
3.2.1 Measurement of Stoichiometry, Binding constant and Life time analysis of MTX-quadruplex using fluorescence spectroscopy	79-83
3.2.1.1 Continuous Variation Analysis (Job plot)	83-84
3.2.1.2 Life Time measurements	84-85
3.3.1 Analysis of Conformational changes and stability of quadruplex DNA upon MTX binding using Circular Dichroism Spectroscopy	86-89
3.3.2 Circular Dichroism Melting (T_m) studies	88-89
3.4.1 Differential Scanning Calorimetry (DSC) studies	89-90
3.5.1 Characterizing the telomerase inhibitory effects of MTX using Telomerase Repeat Amplification Protocol (TRAP) Assay	91
3.2 Conclusion	92
Chapter 4	
NMR Structure of Mitoxantrone bound to human G-quadruplex DNA	93-134
4.1: Results and Discussion	94-132
4.1.1 Resonance assignment of mitoxantrone	94-95
4.1.2 Resonance assignment of uncomplexed sequence d-(TTAGGGT) ₄	95-100
4.1.3 Resonance assignment of MTX-d-(TTAGGGT) ₄ complex	100-104
4.1.4 Effects of titrimetric addition of MTX	105-112
4.1.5 Temperature dependent studies revealing the stability of MTX-d-(TTAGGGT) ₄ complex	112-117
4.1.6 Phosphorous-31 NMR studies of MTX-d-(TTAGGGT) ₄ complex	117-120
4.1.6 Structural studies of MTX-d-(TTAGGGT) ₄ complex	120-129
4.1.7 Restrained Molecular dynamics studies of MTX-d-(TTAGGGT) ₄ complex	129-132
4.2 Conclusion	133-134

	Page No.
Chapter 5	
NMR analysis of luteolin interaction with human and <i>Tetrahymena</i>G-quadruplex DNA	135-210
5.1 Results and Discussion	136-208
5.1.1 Resonance assignment of luteolin	136-145
5.1.2 Resonance assignment of uncomplexed sequence d-(TTAGGGT) ₄	145
5.1.3 Resonance assignment of luteolin-d-(TTAGGGT) ₄ complex	146-150
5.1.4 Effects of titrimetric addition of luteolin	150-158
5.1.5 Temperature dependent studies revealing the stability of luteolin-d-(TTAGGGT) ₄ complex	158-161
5.1.6 Phosphorous-31 NMR studies of MTX-d-(TTAGGGT) ₄ complex	162-165
5.1.7 Structural studies of luteolin-d-(TTAGGGT) ₄ complex	165-171
5.1.8 Restrained Molecular dynamics studies of luteolin-d-(TTAGGGT) ₄ complex	171-174
5.1.9 Resonance assignment of uncomplexed sequence d-(TTGGGGT) ₄	175-180
5.1.10 Resonance assignment of luteolin-d-(TTGGGGT) ₄ complex	181-183
5.1.11 Effects of titrimetric addition of luteolin	184-190
5.1.12 Temperature dependent studies revealing the stability of luteolin-d-(TTGGGGT) ₄ complex	190-197
5.1.13 Phosphorous-31 NMR studies of MTX-d-(TTGGGGT) ₄ complex	197-200
5.1.14 Structural studies of luteolin-d-(TTGGGGT) ₄ complex	201-205
5.1.15 Restrained Molecular dynamics studies of luteolin-d-(TTGGGGT) ₄ complex	206-207
5.2 Characterization of the telomerase inhibitory effects of luteolin using TRAP Assay	207-208
5.3 Conclusion	208-210
Conclusions and Perspectives	211-214
List of Publications	215-216
References	217-248

List of Tables

	Page No.
Table 1.1: Data showing the length and sequence specificity of telomeric repeats from different organisms	15
Table 1.2 Sequence and topology of oncogenic promoter G-quadruplexes	16
Table 1.3 Novel telomerase inhibition-based strategies for targeting cancer	22
Table 1.4 Quadruplex-interactive ligands showing antitumor activity in various cancers	24-25
Table 1.5 Classification of flavonoids	39
Table 1.6 Dietary sources of flavonoids	40
Table 2.1 Concentration of mitoxantrone (D), d-(TTAGGGT) ₄ (N) in mitoxantrone-d-(TTAGGGT) ₄ complex at different D/N ratios	53
Table 2.2 Concentration of luteolin (D), d-(TTAGGGT) ₄ (N) in luteolin-d-(TTAGGGT) ₄ complex at different D/N ratios	54
Table 2.3 Concentration of luteolin (D), d-(TTGGGGT) ₄ (N) in luteolin-d-(TTGGGGT) ₄ complex at different D/N ratios	55
Table 2.4 Expected through bond correlation in Nucleic acids	61
Table 2.5 Short interproton distances in regular B-DNA in Å	63
Table 2.6 Short interproton distances in regular A-DNA in Å	64
Table 2.7 Proton and carbon chemical shift position in DNA	68
Table 3.1 Change in the absorption maxima (λ_{max}), O.D, and $\Delta\lambda$ at D (609 nm band) and M (659 nm band) on interaction of MTX with (TTAGGGT) ₄ at varying D/N ratios	77
Table 3.2 Change in the Fluorescence emission maxima (λ_{max}), fluorescence intensity, and $\Delta\lambda$ on interaction of MTX with (TTAGGGT) ₄ at varying D/N ratios	81
Table 3.3 The fluorescence lifetimes of MTX in the presence or absence of d-(TTAGGGT) ₄ in KBPES buffer(pH 7.0) at 298	85
Table 3.4 Change in the ellipticity (Θ) and λ_{max} for positive CD band (263 nm) and negative CD band (242 nm) on varying D/N ratios	87
Table 3.5 CD melting temperature (T_m) of d-(TTAGGGT) ₄ and its complex with MTX at D/N ratios 1.0, 1.5, 2, 2.5, 3.0 and its corresponding ΔT_m	89
Table 3.6 DSC-derived thermodynamic parameters associated with the interactions of MTX with d-(TTAGGGT) ₄	90
Table 4.1 Proton and carbon chemical assignments of MTX at 298 K	94
Table 4.2 Chemical shift (ppm) of d-(TTAGGGT) ₄ protons as a function D/N ratios at 298 K.	107-108
Table 4.3 Chemical shift (ppm) of d-(TTAGGGT) ₄ protons in uncomplexed state (δ_f) and that bound to MTX (δ_b) at D/N=2.0 at 298 K	109
Table 4.4 Chemical shift (ppm) of MTX protons as a function of D/N ratios at 298 K	110
Table 4.5 Chemical shift (ppm) of MTX protons from NOESY spectra of free MTX (δ_f) and MTX-d-(TTAGGGT) ₄ complex (δ_b) at D/N=1.0, 2.0 at 298 K.	111

	PageNo.
Table 4.6 Chemical shift (ppm) of d-(TTAGGGT) ₄ protons in MTX-d-(TTAGGGT) ₄ complex at D/N=2.0 as a function of temperature.	115
Table 4.7 Chemical shift (ppm) of MTX protons in MTX-d-(TTAGGGT) ₄ complex at D/N=2.0 as a function of temperature	116
Table 4.8 Chemical shift of ³¹ P resonances of the phosphate groups of d-(TTAGGGT) ₄ , in MTX-d-(TTAGGGT) ₄ complex at 298 K with increasing D/N ratios.	119
Table 4.9 Interproton NOE connectivities within MTX molecule in MTX-d-(TTAGGGT) ₄ complex at D/N=1.0 and 2.0 with different τ _m at 298 K, 308 K and 318 K.	121
Table 4.10 Intermolecular NOE connectivities between MTX molecule and d-(TTAGGGT) ₄ in MTX-d-(TTAGGGT) ₄ complex at 2.0 at 298 K.	122
Table 4.11 Intermolecular NOE connectivities and rMD distances between MTX molecule and d-(TTAGGGT) ₄ in MTX-d-(TTAGGGT) ₄ complex at 2.0 at 298 K.	122
Table 4.12 Experimental restraints and structure statistics of the final structure	131
Table 5.1 Proton chemical shift (ppm) of luteolin in DMSO-d ₆ of present work and its comparison with results reported in literature.	138
Table 5.2 Carbon chemical shift (ppm) of luteolin in DMSO-d ₆ of present work and its comparison with results reported in literature.	139
Table 5.3 The complete assignments of the ¹ H and ¹³ C chemical shift correlation of luteolin	142
Table 5.4 Connectivities and interproton distances (Å) from ROESY spectra of luteolin used in restrained molecular dynamics.	144
Table 5.5 Chemical shift (ppm) of d-(TTAGGGT) ₄ protons in uncomplexed state (δ _f) and that bound to luteolin (δ _b) at D/N=1.0 at 298 K	155
Table 5.6 Chemical shift (ppm) of d-(TTAGGGT) ₄ protons as a function D/N ratios at 298 K	156
Table 5.7 Chemical shift (ppm) of d-(TTAGGGT) ₄ protons in uncomplexed state (δ _f) and that bound to luteolin (δ _b) at D/N=2.0 at 298	157
Table 5.8 Chemical shift (ppm) of luteolin protons as a function of D/N ratios at 298 K	158
Table 5.9 Chemical shift (ppm) of luteolin protons from NOESY spectra of free luteolin (δ _f) and luteolin-d-(TTAGGGT) ₄ complex (δ _b) at D/N=1.0, 2.0 at 298 K.	158
Table 5.10 Chemical shift (ppm) of d-(TTAGGGT) ₄ protons in luteolin-d-(TTAGGGT) ₄ complex at D/N=1.0 as a function of temperature	160
Table 5.11 Chemical shift (ppm) of luteolin protons in luteolin-d-(TTAGGGT) ₄ complex at D/N=1.0 as a function of temperature	161
Table 5.12 Chemical shift of ³¹ P resonances of the phosphate groups of d-(TTAGGGT) ₄ , in luteolin-d-(TTAGGGT) ₄ complex at 298 K with increasing D/N ratios.	163
Table 5.13 Interproton NOE connectivities within luteolin molecule in luteolin-d-(TTAGGGT) ₄ complex at D/N=1.0 and 2.0 at 298 K.	166
Table 5.14 Intermolecular NOE connectivities between luteolin molecule and d-(TTAGGGT) ₄ in luteolin-d-(TTAGGGT) ₄ complex at D/N=1.0 and 2.0 at 298 K.	166

	Page No.
Table 5.15 Intermolecular NOE connectivities and rMD distances between luteolin molecule and d-(TTAGGGT) ₄ in luteolin-d-(TTAGGGT) ₄ complex at 2.0 at 298 K	167
Table 5.16 Experimental restraints and structure statistics of the final structure	173
Table 5.17 Chemical shift (ppm) of d-(TTGGGGT) ₄ protons as a function D/N ratios at 298 K	184
Table 5.18 Chemical shift (ppm) of d-(TTGGGGT) ₄ protons in uncomplexed state (δ_f) and that bound to luteolin (δ_b) at D/N=1.0 at 298 K	185
Table 5.19 Chemical shift (ppm) of luteolin protons as a function of D/N ratios at 298 K	186
Table 5.20 Chemical shift (ppm) of luteolin protons from NOESY spectra of free luteolin (δ_f) and luteolin-d-(TTGGGGT) ₄ complex (δ_b) at D/N=1.0 and 2.0 at 298 K	186
Table 5.21 Chemical shift (ppm) of d-(TTGGGGT) ₄ protons in luteolin-d-(TTGGGGT) ₄ complex at D/N=1.0 as a function of temperature	193
Table 5.22 Chemical shift (ppm) of d-(TTGGGGT) ₄ protons in luteolin-d-(TTGGGGT) ₄ complex at D/N=2.0 as a function of temperature	194
Table 5.23 Chemical shift (ppm) of luteolin protons in luteolin-d-(TTGGGGT) ₄ complex at D/N=1.0 as a function of temperature	195
Table 5.24 Chemical shift (ppm) of luteolin protons in luteolin-d-(TTGGGGT) ₄ complex at D/N=2.0 as a function of temperature	195
Table 5.25 Chemical shift of ³¹ P resonances of the phosphate groups of d-(TTGGGGT) ₄ in luteolin-d-(TTAGGGT) ₄ complex at 298 K with increasing D/N ratios	199
Table 5.26 Interproton NOE connectivities within luteolin molecule in luteolin-d-(TTAGGGT) ₄ complex at D/N=1.0 at 298 K	201
Table 5.27 Intermolecular NOE connectivities between luteolin molecule and d-(TTGGGGT) ₄ in luteolin-d-(TTGGGGT) ₄ complex at D/N=1.0 at 298 K.	201
Table 5.28 Intermolecular NOE connectivities and rMD distances between luteolin molecule and d-(TTAGGGT) ₄ in luteolin-d-(TTAGGGT) ₄ complex at 1.0 at 298 K	202
Table 5.29 Experimental restraints and structure statistics of the final structure.	206

List of Figures

		PageNo.
Fig. 1.1	Schematic showing the building blocks of a nucleotide	1
Fig. 1.2	Structure of nitrogenous bases purines and pyrimidines	2
Fig. 1.3	Different types of base pairing in nucleic acids	2
Fig. 1.4	Types of sugars present (A) and sugar conformations (B) in nucleic acids. (C) Glycosidic bond χ -angles for the anti- and syn-conformations of the nucleotide bases.	3
Fig. 1.5	Depiction of the backbone torsional angles of DNA (α , β , γ , δ , ϵ , ζ) along with the endocyclic torsion angles in the sugar ring (ν_0 - ν_4).	4
Fig. 1.6	Structure of B-DNA together with its helicodical parameters	5
Fig. 1.7	Structure of A-DNA together with its helicodical parameters	6
Fig. 1.8	Structure of Z-DNA together with its helicodical parameters	7
Fig. 1.9	(A) Schematic representation of triplex-DNA formation; (B) Structure of triplex-DNA; (C) Purine-motif.	8
Fig. 1.10	Structure of i-motif: Left the C•C ⁺ base pair; Right: 3D structure (Huppert, 2008)	9
Fig. 1.11	Structure of quadruplex: (A) a G-tetrad; (B) 3D structure; (C) syn and anti glycosidic confirmation of guanosine	10
Fig. 1.12	Poymorphisms present in G-quadruplexes (Yaku et al., 2012)	12
Fig. 1.13	Four possible orientations of quadruplex strands based on glycosidic torsion angles of guanosines: anti (black) and syn (cyan)-conformations.	13
Fig. 1.14	Schematic representation of different quadruplex folding; (A) anti-parallel structures left showing unimolecular quadruplex with lateral loops and varied grooves and right showing bimolecular quadruplex with diagonal loops and varied grooves; (B) left showing parallel quadruplex and right showing external loops. (Rujan <i>et al.</i> , 2005)	13
Fig. 1.15	(A) Telomeric DNA: Termini of eukaryotic chromosomes; (B) Different conformations of the unimolecular G-quadruplex formed by the four-repeat human telomeric sequence 5'-AGGG(TTAGGG) ₃ in Na ⁺ and K ⁺ solution	16
Fig. 1.16	Folding topology (a, c, e) and solution structure (b, d, f) of G-quadruplexes forming oncogenic promoter genes c-myc (PDB ID-2A5P), c-kit (PDB ID-2O3M), bcl-2 (PDB ID-2F8U) (Patel <i>et al.</i> , 2007)	18
Fig. 1.17	Structure of human telomere showing shelterin complex and loop (Cesare and Karlseder, 2012)	19
Fig. 1.18	Length of telomere and presence of telomerase (A); Fate of telomere in normal somatic cells and tumor cells (B); effect of telomere shortening in somatic cells and maintenance of telomere length in cancer cells, stem cells and germline cells (C)	21

	PageNo.
Fig. 1.19	Telomere mediated molecular therapeutics 21
Fig. 1.20	Stabilization of promoter G-quadruplex structure by small ligands (circle) regulates the transcription of oncogenes (Ma <i>et al.</i> , 2012) 23
Fig. 1.21	Modes of ligand binding to G-quadruplex structures (A) end stacking, (B) groove binding and (C) intercalation between the two successive G-tetrads 26
Fig. 1.22	Structure of mitoxantrone 35
Fig. 1.23	(A) Basic structure of flavonoid and (B) its glycosylation sites 37
Fig. 1.24	Biological activities of flavonoids 40
Fig. 1.25	(A) Structure of luteolin and (B) modulation of cell-signaling pathways by luteolin 43
Fig. 2.1	Schematic representation of UV-visible spectrophotometer 49
Fig. 2.2	Jablonski diagram showing the phenomena of fluorescence and phosphorescence 50
Fig. 2.3	Schematic representation of spectrofluorometer 51
Fig. 2.4	Energy levels for a nucleus with spin quantum number $\frac{1}{2}$ 56
Fig. 2.5	Precessional motion of the nucleus spinning on its axis in the presence of external magnetic field 56
Fig. 2.6	Flipping of the magnetic moment on absorption of the radiations 57
Fig. 2.7	The general scheme for two-dimensional spectroscopy 59
Fig. 2.8	Pulse scheme of COSY technique 60
Fig. 2.9	Pulse scheme of NOESY technique 62
Fig. 2.10	Pulse scheme of ROESY technique 64
Fig. 2.11	Pulse scheme of TOCSY technique 65
Fig. 2.12	Pulse scheme of HSQC technique 66
Fig. 2.13	Pulse scheme of HMBC technique 67
Fig. 3.1	The absorption spectra of 3 μ M MTX in the absence and presence of d-(TTAGGGT) ₄ at 298 K (a) at higher D/N (MTX/d-(TTAGGGT) ₄) ratios showing isobestic point; (b) at lower D/N ratios; (c) change in the absorption trend at these ratios. 76
Fig. 3.1	Change in the λ_{max} ($\Delta\lambda$) at varying D/N ratios at (d) 609 nm band and (e) 659 nm band 78

		PageNo.
Fig. 3.2	Plot of O.D versus D/N ratios at (a) 609 nm band and (b) 659 nm band	78
Fig. 3.3	Plot of 1/O.D versus D/N ratios at (a) 609 nm band and (b) 659 nm band	78
Fig. 3.4	Plot of [DNA]/ $\epsilon_a - \epsilon_f$ versus [DNA] (a) at 659 nm band for DNA concentrations 0.43-5.15 μM and (b) for DNA concentrations 6.84-32.5 μM . (c) at 609 nm band for DNA concentrations 0.43-5.15 μM and (b) for DNA concentrations 6.84-32.5 μM	79
Fig. 3.5	Fluorescence emission spectra of MTX in the absence and presence of d-(TTAGGGT) ₄ at 298 K at (a) higher D/N ratios (b) lower D/N ratios (c) change in the fluorescence emission trend at these ratios.(d) Change in the λ_{max} ($\Delta\lambda$) at varying D/N ratios. Excitation wavelength $\lambda_{\text{exc}} = 610 \text{ nm}$	80
Fig. 3.6	(a, b) change in the fluorescence intensity on varying D/N ratios	82
Fig. 3.7	The Stern-Volmer quenching plot of 3 μM MTX with DNA concentrations (a) full range of [DNA] i.e. 0.22-31.99 μM and (b) [DNA]= 0.88-2.66 μM	82
Fig. 3.8	Plot of $\log (F_0 - F)/F$ versus $\log [\text{DNA}]$ for DNA concentrations (a) 0.21-5.15 μM and (b) 6.84-32.15 μM	82
Fig. 3.9	Job plot for the binding of MTX to (TTAGGGT) ₄	83
Fig. 3.10	Fluorescence decay curves of free MTX and MTX-d-(TTAGGGT) ₄ complexes at varying D/N ratios in KBPES buffer (pH 7.0) at 298 K (a-c)	84-85
Fig. 3.11	Circular Dichroism (CD) spectra of 20 μM d-(TTAGGGT) ₄ in the absence and presence of MTX at 298 K at varying D/N ratios	86
Fig. 3.12	Plot of change in the ellipticity (Θ) versus varying D/N ratios for (a) positive CD band (263 nm) and (b) negative CD band (242 nm)	87
Fig. 3.13	Induced CD spectra of 20 μM MTX complexed with d-(TTAGGGT) ₄ at varying D/N ratios (a, b).	88
Fig. 3.14	(a) CD melting curves of 20 μM d-(TTAGGGT) ₄ in the absence and presence of MTX at D/N ratios 1.0, 2.0; (b) derivative plots at D/N ratios 1.0, 1.5, 2.0.(c) plot of change in melting temperature (T_m) versus D/N	88-89
Fig. 3.15	DSC thermograms of uncomplexed d-(TTAGGGT) ₄ and its complex with MTX at D/N ratios 0.5, 1.0, 1.5, 2.0	90
Fig. 3.16	Inhibitory effect of MTX on telomerase activity determined by TRAP assay	91
Fig. 4.1	Proton NMR spectra of 10 mM MTX in KBPES buffer at 298 K	95
Fig. 4.2	¹ H- ¹³ C HSQC spectra of mitoxantrone showing resonances of methylene and aromatic protons	95

		PageNo.
Fig. 4.4	Schematic representation of parallel-stranded G-quadruplex structure formed by oligonucleotide sequence d-(TTAGGGT) ₄	96
Fig. 4.5 (a)	1D proton spectrum of uncomplexed quadruplex sequence d-(TTAGGGT) ₄ showing exchangeable and non-exchangeable resonances	97
Fig. 4.5 (b)	1D proton spectrum of uncomplexed quadruplex sequence d-(TTAGGGT) ₄ showing sugar and methyl resonances	97
Fig. 4.6	G-tetrad showing NH-NH and NH-H8 connectivities that can be observable in NOESY experiments	98
Fig. 4.7	Expansion of the NOESY spectra of uncomplexed quadruplex sequence d-(TTAGGGT) ₄ at 298 K showing (a)NH-NH connectivity between adjacent imino protons. (b) Interstrand guanine NH connectivities to its own and 5' flanking base protons in A3-G4-G5-G6 segment	99
Fig. 4.8	Expansion of the NOESY spectra of uncomplexed quadruplex sequence d-(TTAGGGT) ₄ at 298 K showing (a)intrastrand base H8/H6-H1'sequential connectivity. (b) Intrastrand base H8/H6-H2'H2''sequential connectivity in T1-T2-A3-G4-G5-G6-T7 segment	100
Fig. 4.9	Expansion of the NOESY spectra of MTX-d-(TTAGGGT) ₄ complex at 298 K, D/N=2.0 showing (a)NH-NH connectivity between adjacent imino protons. (b) Interstrand guanine NH connectivities to its own and 5' flanking base protons in A3-G4-G5-G6 segment	102
Fig. 4.10	Expansion of the NOESY spectra of MTX-d-(TTAGGGT) ₄ complex at 298 K D/N=2.0 showing (a)intrastrand base H8/H6-H1'sequential connectivity. (b) Intrastrand base H8/H6-H2'H2''sequential connectivity in T1-T2-A3-G4-G5-G6-T7 segment	103
Fig. 4.11	Overlap of the uncomplex (red) and mitoxantrone complexed d-(TTAGGGT) ₄ (black) ¹ H- ¹³ C HSQC spectra at 318 K showing (a) aromatic protons of MTX. (b) Aliphatic protons of MTX	104
Fig. 4.12	1D ¹ H NMR spectra of MTX-d-(TTAGGGT) ₄ complex at 298 K showing change in the quadruplex and MTX proton resonances upon titration (a) imino proton region;(b, c)base and sugar regions	105-106
Fig. 4.13	Variation in the chemical shift of d-(TTAGGGT) ₄ protons on increasing D/N ratios at 298 K (a-c)	107
Fig. 4.14	Variation in the chemical shift of MTX protons versus increasing D/N ratios at 298 K (a, b).	110

		PageNo.
Fig. 4.15	1D ^1H NMR spectra of MTX-d-(TTAGGGT) $_4$ complex at 278 K showing change in the quadruplex and MTX proton resonances upon titration (a) imino proton region;(b) sugar region.	111-112
Fig. 4.16	1D ^1H NMR spectra of MTX-d-(TTAGGGT) $_4$ complex as a function of temperature at D/N=2.0 showing change in the quadruplex and MTX proton resonances (a) imino proton region;(b-c) base and sugar regions	113-114
Fig. 4.17	1D ^1H NMR spectra of imino protons region of d-(TTAGGGT) $_4$ and MTX-d-(TTAGGGT) $_4$ complex revealing the stability of complex with temperature	117
Fig. 4.18	Proton decoupled ^{31}P NMR spectra of d-(TTAGGGT) $_4$ in uncomplexed state and complexed with MTX with increasing D/N ratios at (a) 298 K; (b) as a function of temperature at D/N=2.0.	118-119
Fig. 4.19a-d	NOESY spectra of MTX-d-(TTAGGGT) $_4$ complex at D/N=1.0 and 2.0 at 298 K showing intermolecular NOE connectivities between 1/4OH,11NH, 6/7H protons of MTX molecule and d-(TTAGGGT) $_4$	123-125
Fig. 4.19e	NOESY spectra of MTX-d-(TTAGGGT) $_4$ complex at D/N=2.0 at 278 K showing NOE connectivities between 1/4OH proton of MTX with d-(TTAGGGT) $_4$	126
Fig. 4.19f-h	NOESY spectra of MTX-d-(TTAGGGT) $_4$ complex at D/N=2.0 showing intermolecular NOE connectivities between 1/4OH, 11NH, 6/7H protons of MTX molecule and d-(TTAGGGT) $_4$ as a function of temperature	127-129
Fig. 4.20	Front view of the final structure of MTX-d-(TTAGGGT) $_4$ complex obtained by restrained molecular dynamics simulations	131
Fig. 4.21	Close-up view of the MTX-d-(TTAGGGT) $_4$ interaction at T1pT2 and G6pT7 binding sites	132
Fig. 5.1	Proton NMR spectra of luteolin in DMSO-d $_6$ at 298 K	137
Fig. 5.2	Carbon NMR spectra of luteolin in DMSO-d $_6$ at 298 K	137
Fig. 5.3	^1H - ^{13}C HSQC spectrum of luteolin showing directly coupled aromatic protons resonances	140
Fig. 5.4	^1H - ^{13}C HMBC spectrum of luteolin showing long ranged coupling	141
Fig. 5.5	^1H NMR spectra of luteolin as a function of temperature showing the exchange of OH signals	141
Fig. 5.6	TOCY spectrum of luteolin	143

		PageNo.
Fig. 5.7	COSY spectrum of luteolin	143
Fig. 5.8	ROESY spectra of luteolin showing the intramolecular connectivities (a) of the aromatic protons and (b) of hydroxyl protons	144-145
Fig. 5.9	Minimized solution structure of luteolin by rMD	145
Fig. 5.10	Expansion of the NOESY spectra of luteolin-d-(TTAGGGT) ₄ complex at 298 K D/N=2.0 showing (a)NH-NH connectivity between adjacent imino protons. (b) Interstrand guanine NH connectivities to its own and 5' flanking base protons in A3-G4-G5-G6 segment	147
Fig. 5.11	Expansion of the NOESY spectra of luteolin-d-(TTAGGGT) ₄ complex at 298 K D/N=2.0 showing (a)intrastrand base H8/H6-H1'sequential connectivity. (b) Intrastrand base H8/H6-H2'H2"sequential connectivity in T1-T2-A3-G4-G5-G6-T7 segment	148
Fig. 5.12	Overlap of the uncomplex (red) and luteolin-d-(TTAGGGT) ₄ complex(black) ¹ H- ¹ H COSY spectra at 308 K showing meta coupled protons H5' and H6'of luteolin	149
Fig. 5.13	Overlap of the uncomplex (red) and luteolin complexed d-(TTAGGGT) ₄ (black) ¹ H- ¹³ C HSQC spectra at 308 K showing (a) aromatic protons of luteolin . (b) expansion of luteolin protons	149-150
Fig. 5.14	1D ¹ H NMR spectra of luteolin-d-(TTAGGGT) ₄ complex at 298 K showing change in the quadruplex and luteolin proton resonances upon titration (a) imino proton region;(b- d)base and sugar regions	151-154
Fig. 5.15	1D ¹ H NMR spectra of luteolin-d-(TTAGGGT) ₄ complex as a function of temperature at D/N=2.0 showing change in the quadruplex and luteolin proton resonances	159
Fig. 5.16	1D ¹ H NMR spectra of imino protons region of d-(TTAGGGT) ₄ and luteolin-d-(TTAGGGT) ₄ complex revealing the stability of complex with temperature	159
Fig. 5.17	Proton decoupled ³¹ P NMR spectra of d-(TTAGGGT) ₄ in uncomplexed state and complexed with luteolin with increasing D/N ratios at 298 K (a,b)	163-164
Fig. 5.18	Proton decoupled ³¹ P NMR spectra of luteolin-d-(TTAGGGT) ₄ as a function of temperature at D/N=1.0	165

	PageNo.
Fig. 5.19 (a-e) NOESY spectrum of luteolin-d-(TTAGGGT) ₄ complex at D/N=1.0 and 2.0 at 298 K showing intermolecular NOE connectivities between H6', H2', H8 and H6 protons of luteolin molecule and d-(TTAGGGT) ₄	168-171
Fig. 5.20 Front view of the final structure of luteolin-d-(TTAGGGT) ₄ complex obtained by restrained molecular dynamics simulations	171
Fig. 5.21 Close-up view of the luteolin-d-(TTAGGGT) ₄ interaction at T1pT2 and G6pT7 binding sites.	174
Fig. 5.22 Schematic representation of parallel-stranded G-quadruplex structure formed by oligonucleotide sequence d-(TTGGGGT) ₄	176
Fig. 5.23 1D proton spectrum of uncomplexed quadruplex sequence d-(TTGGGGT) ₄ showing exchangeable and non-exchangeable resonances (a-b).	176
Fig. 5.24 G-tetrad showing NH-NH and NH-H8 connectivities that can be observable in NOESY experiments	178
Fig. 5.25 Expansion of the NOESY spectra of uncomplexed quadruplex sequence d-(TTGGGGT) ₄ at 298 K showing (a)NH-NH connectivity between adjacent imino protons. (b) Interstrand guanine NH connectivities to its own and 5' flanking base protons in G3-G4-G5-G6 segment	178-179
Fig. 5.26 Expansion of the NOESY spectra of uncomplexed quadruplex sequence d-(TTGGGGT) ₄ at 298 K showing (a)intrastrand base H8/H6-H1'sequential connectivity. (b) Intrastrand base H8/H6-H2'H2"sequential connectivity in T1-T2-G3-G4-G5-G6-T7 segment	180
Fig. 5.27 Expansion of the NOESY spectra of luteolin-d-(TTGGGGT) ₄ complex at 298 K D/N=2.0 showing (a)NH-NH connectivity between adjacent imino protons. (b) Interstrand guanine NH connectivities to its own and 5' flanking base protons in G3-G4-G5-G6 segment	180
Fig. 5.28 Expansion of the NOESY spectra of luteolin-d-(TTGGGGT) ₄ complex at 298 K D/N=2.0 showing (a)intrastrand base H8/H6-H1'sequential connectivity. (b) Intrastrand base H8/H6-H2'H2"sequential connectivity in T1-T2-G3-G4-G5-G6-T7 segment	181
Fig. 5.29 Difference in the chemical shifts ($\Delta\delta$) of base protons on d-(TTGGGGT) ₄ (a, b) on binding of luteolin at D/N 2.0 at 298 K	186
Fig. 5.30a Proton NMR spectra of uncomplexed d-(TTGGGGT) ₄ and complex of luteolin with d-(TTGGGGT) ₄ at 298 K	187

Fig. 5.30	1D ^1H NMR spectra of luteolin-d-(TTGGGGT) ₄ complex at 298 K showing change in the quadruplex and luteolin proton resonances upon titration (b) imino proton region;(c- d)base and sugar regions	188-189
	Difference in the chemical shifts ($\Delta\delta$) of base protons on d-(TTAGGGT) ₄ (a, c) and d-(TTGGGGT) ₄ (b, d) on binding of luteolin	190
Fig. 5.32	1D ^1H NMR spectra of luteolin-d-(TTGGGGT) ₄ complex as a function of temperature at D/N=1.0 showing change in the quadruplex and luteolin proton resonances	191
Fig. 5.33	1D ^1H NMR spectra of luteolin-d-(TTGGGGT) ₄ complex as a function of temperature at D/N=2.0 showing change in the quadruplex and luteolin proton resonances	192
Fig. 5.34	1D ^1H NMR spectra of imino protons region of d-(TTGGGGT) ₄ and MTX-d-(TTGGGGT) ₄ complex revealing the stability of complex with temperature	196-197
Fig. 5.35	2D ^{31}P - ^1H HMBC spectrum of d-(TTGGGGT) ₄ at 298 K	198
Fig. 5.36	Proton decoupled ^{31}P NMR spectra of d-(TTGGGGT) ₄ in uncomplexed state and complexed with luteolin with increasing D/N ratios at 298 K	200
Fig. 5.37	Proton decoupled ^{31}P NMR spectra of d-(TTGGGGT) ₄ in uncomplexed state and complexed with luteolin as a function of temperature at D/N=1.0	200
Fig. 5.38	NOESY spectrum of luteolin-d-(TTGGGGT) ₄ complex at D/N=1.0 at 298 K showing intermolecular NOE connectivities between H2', H8 and H6 protons of luteolin molecule and d-(TTGGGGT) ₄	203-205
Fig. 5.39	Front and close view of the final structure of luteolin-d-(TTGGGGT) ₄ complex obtained by restrained molecular dynamics simulations	206-207
Fig. 5.40	Inhibitory effect of luteolin on telomerase activity determined by TRAP assay	208

ABBREVIATIONS

Å	Angstrom
α	Alpha
β	Beta
γ	Gamma
δ	Delta
ϵ	Epsilon
ζ	Zeta
Θ	Theta
π	Pi
λ	Lambda
ν	Nu
τ	Tau
°C	Degree Centigrade
μg	Microgram
μl	Microlitre
μM	Micromolar
bp	Base pair
1D	One Dimensional
2D	Two Dimensional
CD	Circular dichroism
COSY	Correlation Spectroscopy
D/N	Drug (MTX, Luteolin)/ Nucleic acid (quadruplex) molar ratio
D ₂ O	Deuterium oxide
DMSO	Dimethyl sulphoxide
DNA	Deoxyribonucleic acid
DSC	Differential Scanning Calorimetry
EDTA	Ethylenediaminetetracetic acid
eg.	For example
G	Guanine
H-bond	Hydrogen bond
h TERT	Human telomerase reverse transcriptase
h TR	Human telomerase RNA

HSQC	Heteronuclear Single Quantum Correlation
HMBC	Heteronuclear Multiple Bond Correlation
ICD	Induced CD
K	Kelvin
K_{SV}	Stern-Volmer quenching constant
K_b	Binding constant
mM	Milimolar
MTX	Mitoxantrone
NMR	Nuclear Magnetic Resonance
NOESY	Nuclear Overhauser Effect Spectroscopy
PDB	Protein data bank
ppm	Parts per million
rMD	Restrained molecular dynamics
RNA	Ribonucleic acid
ROESY	Rotating frame nuclear Overhauser Effect Spectroscopy
s	Seconds
T_m	Melting Temperature
TOCSY	Total Correlated Spectroscopy
TRAP	Telomerase Repeat Amplification Protocol
UV-vis	Ultra violet visible

Abstract

Telomeres are nucleoprotein complexes at the termini of linear chromosomes, which protect chromosomes from fusion and degradation. The extreme single stranded 3' end of the telomere comprises of simple tandem repeats of guanine-rich sequences (TTAGGG)_n in humans and other vertebrates, with the potential to adopt quadruplex fold. G-rich sequences are also found in other biologically significant regions of the genome such as immunoglobulin switch regions, gene promoter regions of important proto-oncogenes, 5' untranslated regions (UTRs) of many mRNAs and other sequences associated with human diseases. Telomeric DNA attrition on cell replication ultimately leads to cell senescence, although in the majority of cancers, telomeres are maintained by the enzyme telomerase, which is expressed in greatly enhanced levels in these cells. The action of telomerase is inhibited on folding of its single stranded DNA substrate into a quadruplex. One prominent strategy that emerged in last decade for telomerase inhibition is the stabilization of G-quadruplex structures of telomeric DNA. The G-quadruplex formation and stabilization is facilitated by small molecules via displacement of telomeric end capping protein hPOT 1, uncapping of telomere and subsequent initiation of DNA damage response-mediated cell death. The G-quadruplex interactive ligands like trisubstituted acridine compound BRACO-19, RHPS4, telomestatin, TMPyP4 and fluoro quinone derivative Quarfloxin, etc. exhibit anti cancerous activity in *in-vivo* tumor xenograft models. These ligands with their planar aromatic ring system stack effectively on planar G-tetrad via π - π interaction inducing replicative senescence in cancerous cells. However synthetic ligands exhibit toxic side effects such as cardiotoxicity, nausea, vomiting, etc. limiting their further application. This opens a window for compounds with similar efficacy but less toxicity. In this regard flavonoids, dietary plant derived polyphenols with extended aromatic ring system and biological properties viz. anti-oxidant, anti-cancer, anti-inflammatory and kinase inhibition are expected to be an ideal choice. They may possess activity comparable to their synthetic counterparts, with no apparent side effects and toxicity to normal cells, and hence offer an opportunity for more successful treatment of cancer.

In the present study, We have shown the interaction of flavonoid, luteolin and mitoxantrone (MTX), a well know chemotherapeutic synthetic anthraquinone derivative with human telomere single repeat sequence d-(TTAGGGT) and *Tetrahymena* Sequence d-(TTGGGGT), which form right handed parallel stranded G-quadruplexes in presence of K⁺ ion with anti glycosidic torsional angles.

The Ph. D. thesis work has been reported in the form of five chapters.

Chapter 1 reviews the literature on broad subject area of telomeres, telomerase enzyme, the strategies involved in telomerase inhibition and G-quadruplex interactive ligands. It also deals with biophysical and biochemical aspects of luteolin and mitoxantrone.

Chapter 2 deals with the materials and methods used in the present work. Binding mode and stoichiometry of ligand-G-quadruplex complexes are determined by absorption and fluorescence spectroscopy. The conformational changes due to binding are monitored by Circular Dichroism (CD) measurements. Structural elucidation of ligand-G-quadruplex complex is done using Nuclear Magnetic Resonance (NMR) techniques followed by restrained Molecular Dynamics (rMD) simulations. The results have been validated with a cell based Telomere Repeat Amplification Protocol (TRAP) assay.

Chapter 3 describes the exact binding mode, stoichiometry and conformational changes involved in mitoxantrone complexed with parallel G-quadruplex sequence d-(TTAGGGT)₄.

The UV-visible absorption spectrum of uncomplexed MTX shows four distinct bands at λ_{\max} 242, 276, 609 and 659 nm. We monitored the changes in the 662 nm peak as it is more sensitive to the change in mitoxantrone concentration and DNA. Upon addition of quadruplex to MTX, the absorbance maxima of both 659 and 609 nm peaks show hypochromicity accompanied by red shift of 15 and 11 nm, respectively. Presence of clear isobestic point at 677 nm indicates existence of single mode of interaction with a binding constant $2.23 \times 10^5 \text{ M}^{-1}$. Fluorescence intensity decreases on binding and is accompanied by 12 nm red shift, yielding binding stoichiometry (n) ~ 1.7 . This is in agreement with the data obtained by Job plot method of continuous variation analysis, which gives inflection point at 0.66. The binding leads to thermal stabilization of G-quadruplex with an increase in T_m of 13°C.

Chapter 4 describes structural studies of MTX complexed with d-(TTAGGGT)₄. Both one dimensional ¹H and ³¹P NMR and two dimensional experiments viz COSY, NOESY, ¹H-¹³C HSQC, ¹H-³¹P HMBC have been used for assignment of various resonances in uncomplexed and complexed states. MTX is titrated with d-(TTAGGGT)₄ at various Drug (D) to Nucleic acid (N) ratios up to 2.0 (D/N = 0.25 to 2.0) at different temperatures in the range of 278-318 K. Addition of MTX to d-(TTAGGGT)₄ did not induce significant chemical shift variation of phosphate and proton signals. A maximum upfield shift of 0.06 ppm is observed in all NH protons of quadruplex on binding while MTX protons 2/3 H, 1/4 OH and 11 CH₂ shift

upfield by 0.53 ppm, 0.48 ppm and 0.31 ppm, respectively. Presence of imino signals resonating between 10.0 and 11.5 ppm is indicative of formation of G-quadruplex structure. NH signals of uncomplexed d-(TTAGGGT)₄ disappear at 60 °C while that of complexed DNA disappeared at 85 °C, indicating stabilization of G-quadruplex on binding to MTX. NOESY spectra recorded with variable mixing times τ_m 100, 200, 250 ms are analysed at D/N = 1:1 and D/N = 2:1. The presence of all sequential connectivities between base-H1'/H2', H2'' and NH-NH protons, indicate that all G-quartets are intact. Intermolecular NOE connectivities between MTX protons 11 NH, 1/4 OH, 6/7 H and 12 CH₂ are observed with sugar (H1', H2'/H2'', H4', H5'/H5'') and CH₃ protons of T1, T2, and T7 bases of DNA. Absence of intermolecular NOEs between 11 NH-2/3 H, 11 CH₂-2/3 H, 6/7 H-2/3 H reveal that MTX does not exist as dimer in complex, instead two molecules of MTX (one at T1pT2 step and second at G6pT7 step) bind to one molecule of d-(TTAGGGT)₄ in the groove. Absence of significant downfield shift of ³¹P resonances (> 1.5 ppm) excludes the possibility of opening of base pair at any step to permit intercalative mode of binding. The observed NOE restraints have been used to build the structure of complex.

Chapter 5 deals with the structural studies of luteolin complexed with two G-quadruplex sequences d-(TTAGGGT)₄ and d-(TTGGGGT)₄, which occur in human and *Tetrahymena* telomeres, respectively and differ at third base position. On titrating luteolin with DNA up to D/N ratio 1.0 no significant change in chemical shift of d-(TTAGGGT)₄ protons is observed. However d-(TTGGGGT)₄ protons show shift in G6 NH, T7 H6, and T7 CH₃ protons on binding with luteolin accompanied by line broadening of imino signals. Aromatic protons H2', H6', H6, H8 and H3 of luteolin are shifted upfield on binding. All sequential connectivities, base- H1', H2'/H2'' and NH-NH are found to exist. Imino signals resonate between 10.0-11.5 ppm indicating that DNA remains in G-quadruplex form on complexation. G-quadruplex structure is stabilized on binding as the NH signals are found to persist at 80 °C, which disappear in uncomplexed DNA at 55 °C. Most of the intermolecular NOE contacts appeared between H2', H6', H6, H8 protons of luteolin and H1', H2'/H2'', CH₃ and NH of T1/T2/G6/T7 bases of d-(TTAGGGT)₄. In case of luteolin-d-(TTGGGGT)₄ complex, same luteolin protons are involved in making short contacts with G5H1', G6H1', G6H2'', G6 NH and T7H1' protons. The phosphate resonances of d-(TTAGGGT)₄ do not show any significant shift while that of d-(TTGGGGT)₄ show downfield shift of 0.12 ppm at G6pT7 step on binding. This is indicative of preferential binding of luteolin at G6pT7 step in case of d-(TTGGGGT)₄ whereas in d-(TTAGGGT)₄, additional binding site at T1pT7 exists.

Hence we conclude that both MTX as well as luteolin interact with G-quadruplex DNA. The results of TRAP assay confirm dose dependent telomerase inhibition by these ligands, which can be promising G4 ligands with implications towards G-quadruplex mediated telomerase inhibition for anticancer therapy.

Introduction

1.1 General overview of DNA

The central role played by DNA (Deoxyribonucleic acid) in biological systems is owing to its ability to store and transmit genetic information from generation to generation. Many cellular processes, for instance, replication, transcription and repair, which constitutes major steps in cell growth and division, is required for the development and functioning of an individual organism. To understand these mechanisms the basic structure of DNA has to be known. DNA basically is a polymer of nucleotide units and the unique sequence of these units (named gene) encodes the genetic information. Each nucleotide unit consists of three building blocks: (i) nitrogenous base, (ii) pentose sugar and (iii) phosphate groups (**Fig. 1.1**).

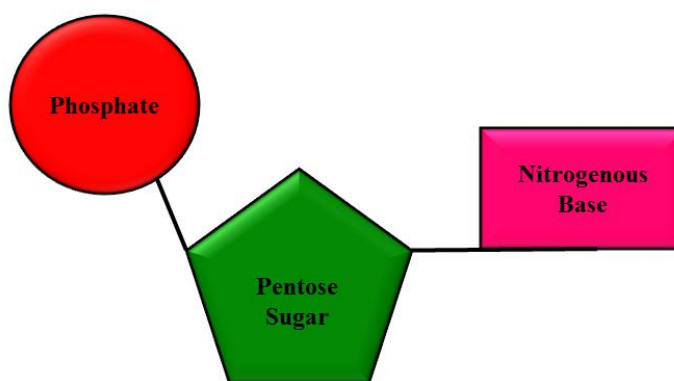


Fig. 1.1: Schematic showing the building blocks of a nucleotide.

1.1.1 Nitrogenous bases:

These are planar aromatic heterocyclic molecules, which are basically of two types: purines (R) and pyrimidines (Y). Purine consists of one five membered ring and one six membered ring that are fused together. Examples: Adenine (A) and Guanine (G). Pyrimidine consists of a six membered ring, namely: Thymine (T), Cytosine (C) and Uracil (U) the latter present in RNA in place of thymine (**Fig. 1.2**). These bases have complementary hydrogen bond donors and acceptors that are involved in formation of base pairs via hydrogen bonding, which aid in the stability of DNA. There are different types of base pairing (**Fig. 1.3**). The most common is Watson-Crick base pairing. This canonical base pairing is stabilized by hydrogen bonding interaction between complementary bases: adenine-thymine via two hydrogen bonds and guanine-cytosine via three hydrogen bonds (1). Thus G:C rich sequences provide more stability to DNA structure than that of A:T rich sequences.

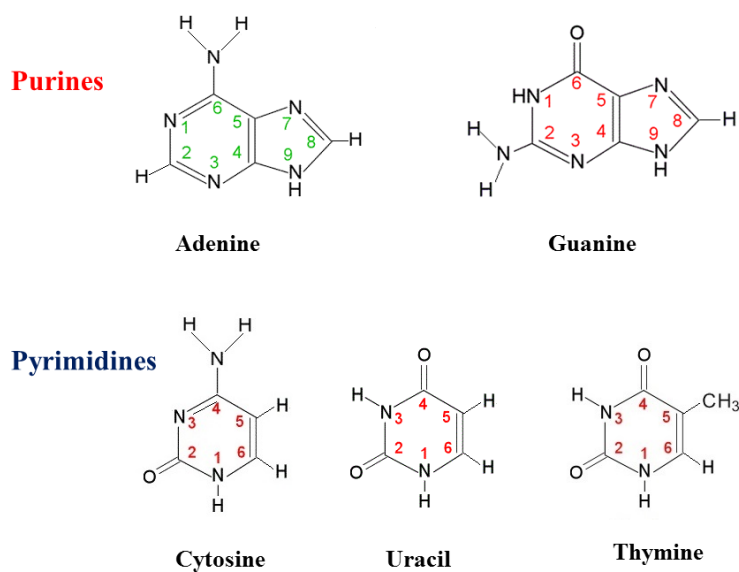


Fig. 1.2: Structure of nitrogenous bases purines and pyrimidines.

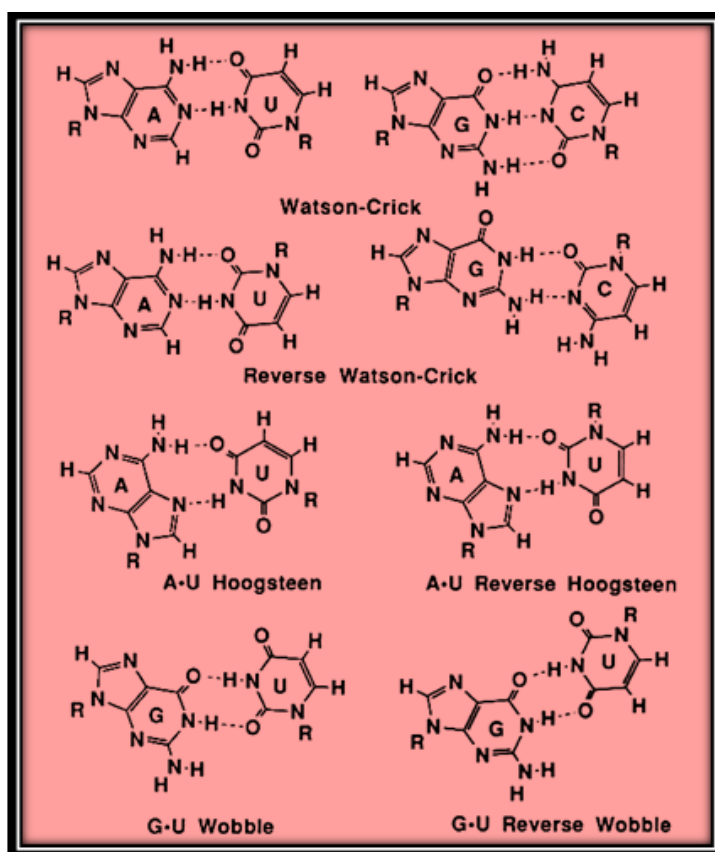


Fig. 1.3: Different types of base pairing in nucleic acids.

Among the other non-canonical base pairings like reversed Watson-Crick, Wobble, Hoogsteen and reversed Hoogsteen, Hoogsteen base pairing is involved in the formation of triplex and G-quadruplex DNA and also stabilizes these structures. This pairing involves the

hydrogen bonding between the major groove edge of purine N7 (acceptor) and C6 (donor) atoms with N3 (donor) and C4 (acceptor) atoms of pyrimidine base, respectively.

1.1.2 Pentose sugar:

Sugars play an important role in the conformation of nucleic acid structures. The sugar found in DNA is β -D-2-deoxyribose while that in RNA is β -D-Ribose (**Fig. 1.4A**). Deoxyribose sugar is non-planar and atoms puckered either above or below the reference plane and depending upon the position of sugar atoms with respect to this reference plane they adopt two conformations endo and exo form. They are further divided into two predominate conformations on the basis of endo form, i.e. N (C3'-endo) and S (C2'-endo) type conformations (**Fig. 1.4B**). B DNA has a predominance of S-type conformation while A DNA and RNA exist in N-type conformation. Sugar is covalently linked to a base via glycosidic bond, which constitute a nucleoside. Glycosidic bond is formed between C1'atom of sugar and N1 or N9 atom of pyrimidine and purine, respectively. The rotation along this bond χ_{CN} causes the base to place either above the sugar (*syn* conformation) or away from sugar (*anti* conformation) (**Fig. 1.4C**).

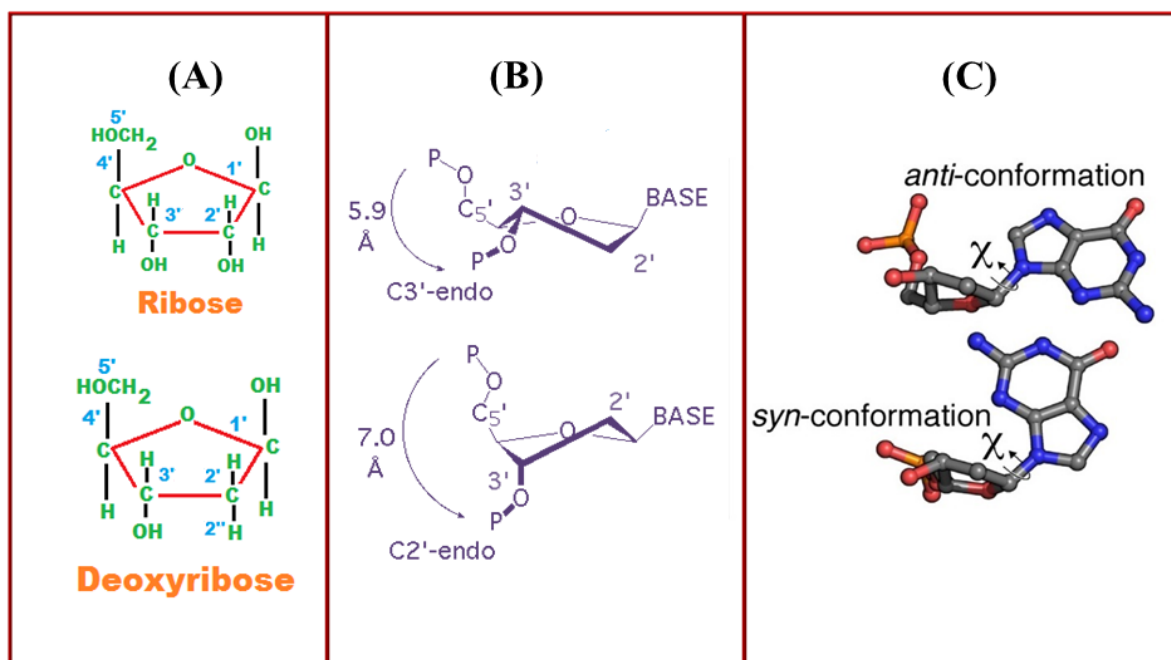


Fig. 1.4: Types of sugars (A), sugar conformations (B) and anti- and syn-conformations of the nucleotide bases (C) present in nucleic acids.

$$\chi \begin{cases} \text{O4'-C1'-N9-C4 (Purines)} \\ \text{O4'-C1'-N1-C2 (Pyrimidines)} \end{cases}$$

1.1.3 Phosphate groups

A nucleotide unit is formed by the attachment of phosphate group to the C5' atom of sugar in nucleoside. DNA is a polynucleotide in which each nucleotide is held together by phosphodiester bond, which constitute the backbone/strand of DNA. This bond is formed by the attachment of 5' phosphate of one nucleotide to the 3' hydroxyl of adjacent nucleotide. DNA strand is generally read from the 5'-3' direction and depending on strand polarity DNA adopt different conformations. Backbone of DNA is negatively charged which is stabilized by salt concentration and hydration. There are six torsion angles, namely α , β , γ , δ , ϵ and ζ (**Fig. 1.5**), which define the conformation of DNA backbone and help to minimize the repulsion within the DNA strands due to negatively charged phosphates.

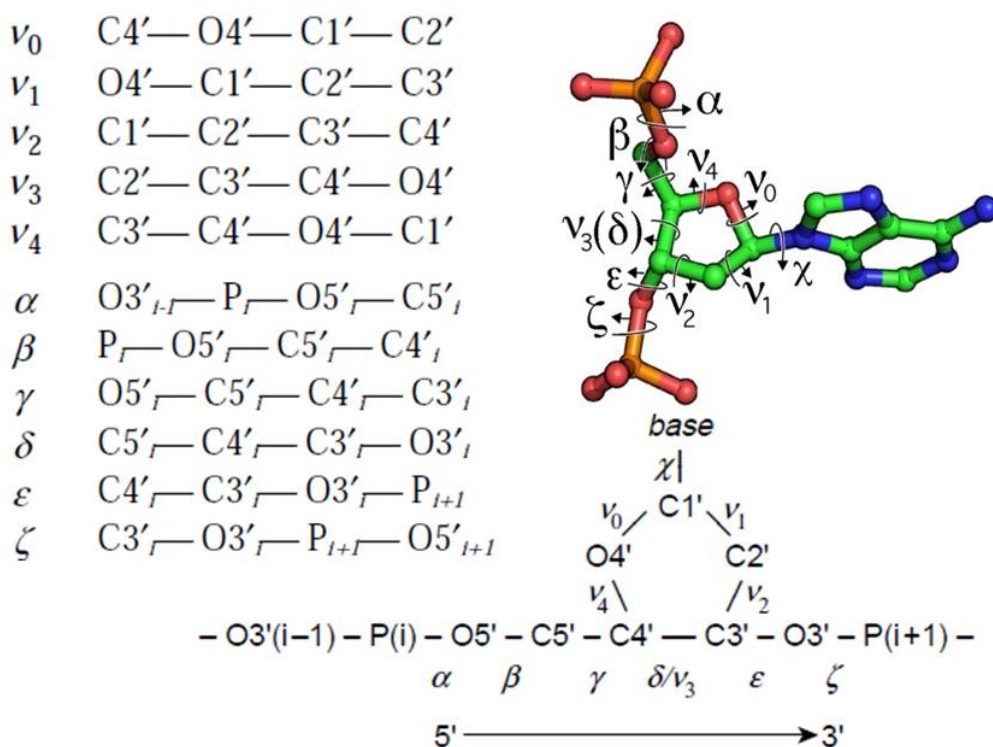


Fig. 1.5: Depiction of the backbone torsional angles of DNA (α , β , γ , δ , ϵ , ζ) along with the endocyclic torsion angles in the sugar ring (ν_0 - ν_4).

1.2 DNA polymorphism

The polymorphic nature of DNA is attributed to its environmental condition like salt concentration, hydration and also base sequences in which it resides. This polymorphism is basically on the ground of helicity. DNA basically exists in a double helical form, which is

known as the canonical form where two complementary strands are stabilized by different forces. These forces include; (i) base pairing - this is formed between complementary strands via hydrogen bond that stabilizes the duplex structure, (ii) base stacking – it minimizes the steric hindrance and stack adjacent bases via hydrophobic interaction due to the aromaticity of bases and, (iii) solvent interaction – it decreases the phosphate charge repulsion and also facilitates base stacking and base pairing.

1.2.1 Canonical DNA structures

Canonical DNA structures are the most prevalent double helical structures present inside the cells, which is basically three forms, i.e. A-DNA, B-DNA and Z-DNA. Variability among different types of DNA can easily be identified on the basis of helicoidal parameters such as; rise, pitch, tilt, roll, twist and number of bases per turn etc. Apart from these common duplex DNA, which orients in antiparallel fashion parallel-stranded duplex has also gain interest. Their formation is mediated either by low pH or through chemical modification and ligand interactions (Germann *et al.*, 1995).

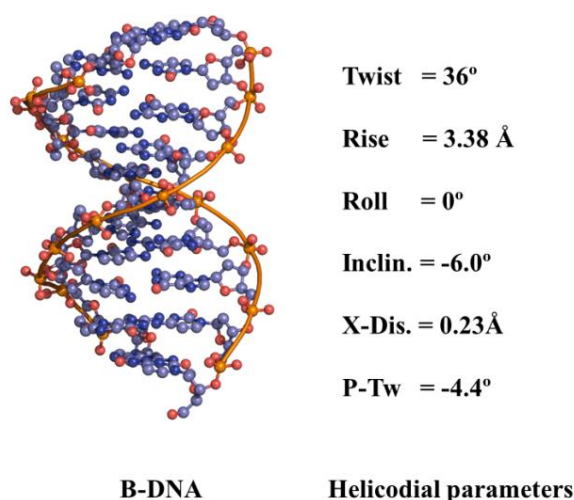


Fig. 1.6: Structure of B-DNA together with its helicoidal parameters.

1.2.1.1 B-DNA

Most commonly adopted canonical DNA confirmation within the genome is the B DNA, which was discovered by Watson and Crick in 1953. It is a right handed double helical structure where two complementary strands are aligned in an antiparallel fashion and are held together by Watson-Crick base pairing (**Fig. 1.6**). In this helical structure the base pairs are centrally

stacked and they are nearly perpendicular to the helical axis while the sugar phosphate forms the backbone of the helix. It also has two distinct grooves namely the major and the minor groove which arises due to the asymmetrical nature of glycosidic bond. Both grooves are similar in depth; major groove is wider compared to the minor groove hence providing accessibility to proteins. Minor groove is hydrated and it promotes stable hydrogen bonding, which add to the stability of DNA structure. All the bases are in *anti*-conformation while deoxyribose sugars are in C2' endo conformation. Sequence dependent structural variation generally occurs in B-DNA conformation depending upon environmental condition that facilitates protein recognition and binding.

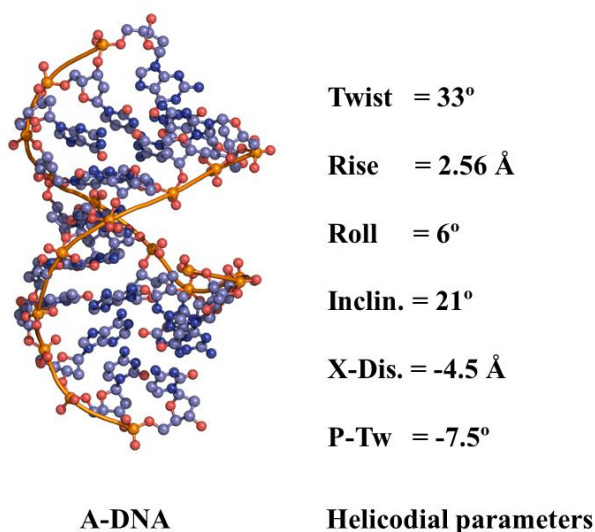


Fig. 1.7: Structure of A-DNA together with its helicoidal parameters.

1.2.1.2 A-DNA

A-DNA also adopt a right handed double helical antiparallel structure which differs from B-DNA with respect to sugar conformation which is C3' endo and base pair position that are tilted to the helix axis (**Fig. 1.7**). Due to the presence of C3' endo conformation the distance between the adjacent nucleotides is reduced. Tilting of base pairs result into a deeper and narrower major groove compared to the minor groove, which is broader and shallower. Transition from B to A form occurs in the presence of alcohol and dehydrating conditions. This transition is highly co-operative, reversible and kinetically fast. A-DNA generally occurs in DNA-RNA hybrid and in duplex RNA.

1.2.1.3 Z-DNA

This is an unusual duplex DNA, which is characterized by the presence of left-handed helix with zig-zag backbone (**Fig. 1.8**). The zig-zag pattern is due to the presence of alternate purine-

pyrimidine sequence such as GCGCGC which are in different conformations. Guanine adopts a C3' endo sugar conformation with *syn* glycosidic angle, whereas, cytosine is present in the C2' endo sugar conformation with *anti* glycosidic angle. Thus, the repeating unit is dinucleotide unlike a mononucleotide in B-DNA with a variable groove width. (Wang *et al.*, 1979). High salt concentration and negative supercoiling also promote Z-DNA formation. B to Z transition can occur with slow kinetics though the process is co-operative.

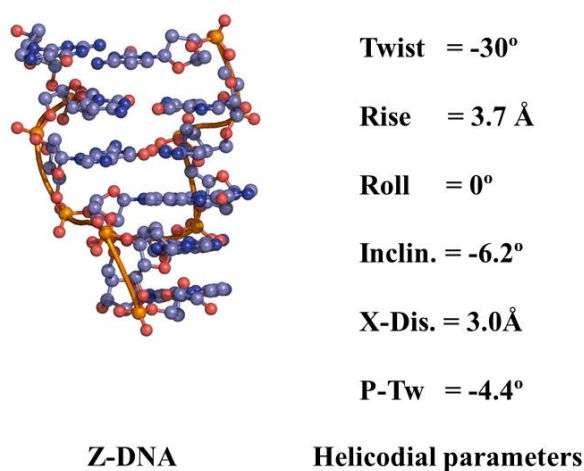


Fig. 1.8: Structure of Z-DNA together with its helicoidal parameters.

1.2.2 Non-canonical DNA structures

Apart from canonical DNA structures, DNA can adopt other structural forms during its participation in important cellular processes like replication, transcription and recombination. These structures result due to involvement of more than a double helix. Examples of such structures are triplex-DNA, G-quadruplex DNA, i- motif etc.

1.2.2.1 Triplex-DNA

As the name suggests triplex-DNA comprises of three stranded structure that occurs in homopurine-homopyrimidine mirror repeat sequences. This structure is known since 1957 (Felsenfeld *et al.*). In such a structure, a third oligonucleotide strand (also known as TFO - triplex forming oligonucleotide), can be either homopyrimidine or homopurine that bind to a homopurine-homopyrimidine duplex DNA in the major groove through Hoogsteen and reversed Hoogsteen hydrogen bonds respectively (**Fig. 1.9A**).

Formation of triplex helix can be achieved in two distinct fashions, which depends upon the nature of the TFO. It is named as pyrimidine (Pyr) motif and purine (Pur) motif.

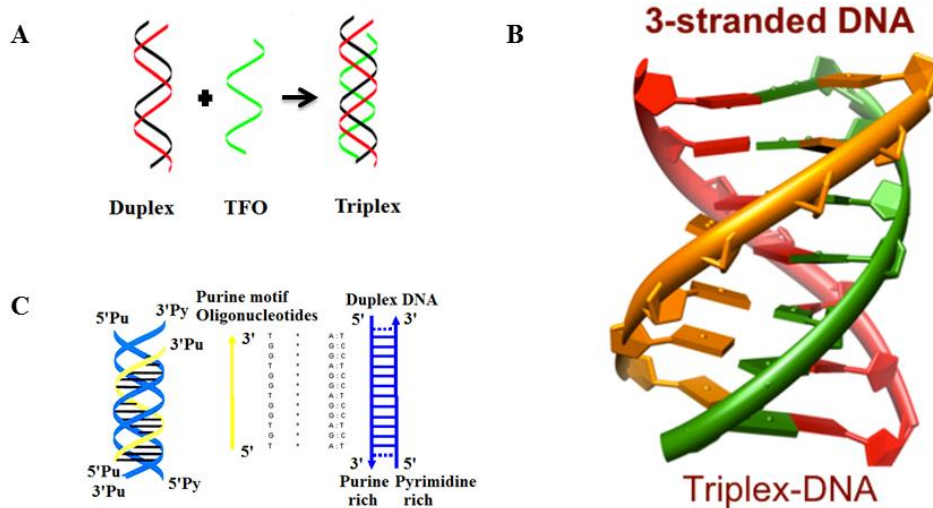


Fig. 1.9: (A) Schematic representation of triplex-DNA formation; (B) Structure of triplex-DNA; (C) Purine-motif.

In case of pyrimidine motif the homopyrimidine oligonucleotides bind in parallel orientation to the homopurine duplex via Hoogsteen base pairing between T and A:T and between C⁺ and G:C (Sun *et al.*, 1996). The latter triplex occurs at acidic pH which favors the protonation of cytosine at N3 atom. Similarly the purine motif involves the formation of a reversed Hoogsteen hydrogen bond between homopurine (A or G) and a homopurine strand of duplex (A * A:T and G * G:C) in an antiparallel fashion (Beal *et al.*, 1991) (**Fig. 1.9C**). Such triplex is formed at neutral pH. Triplex can be intramolecular or intermolecular depending upon invading strands. Intramolecular triplex is also known as H-DNA. Such DNA is present in eukaryotic promoter regions, recombination hotspots and also in prokaryotes (*E. coli*), where its biological role was not clear (van Dongen *et al.*, 1999). With the growing interest for gene targeting and mutagenesis triplex-DNA has been studied (Praseuth *et al.*, 1999).

1.2.2.2 i-motif

Telomeric region is rich in both G (guanine) and C (cytosine) repeat sequences which have the ability to form a four-stranded structure. When four-stranded structure is formed by C-rich sequences, it is referred as i-motif. It consists of two parallel stranded duplexes intercalated with hemi-protonated C.C⁺ pairs in a head to tail fashion (Mills *et al.*, 2002) (**Fig. 1.10**). In general, the i- motifs are stable at acidic pH.

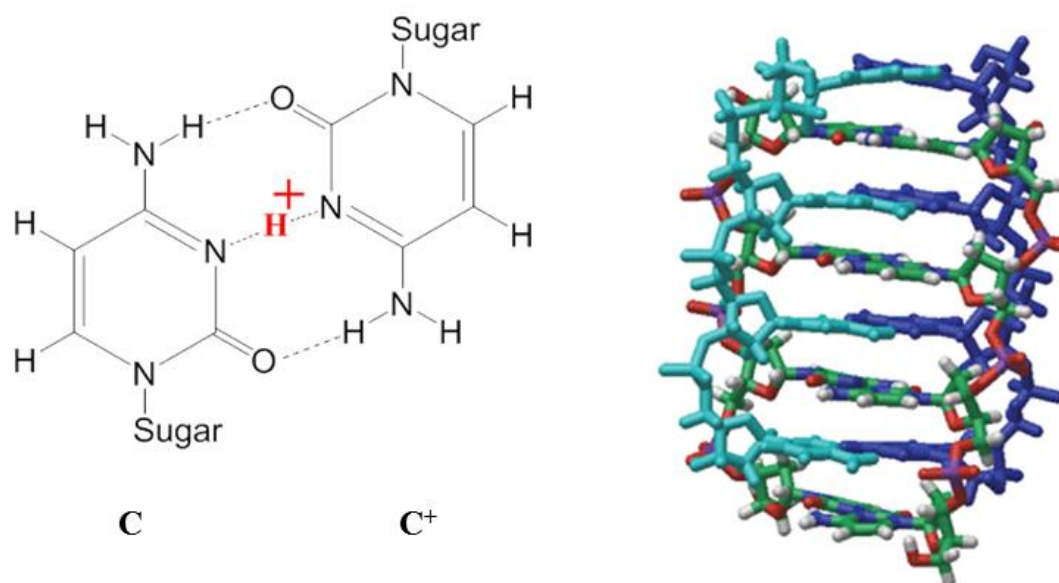


Fig. 1.10: Structure of *i*-motif: Left the C-C⁺ base pair; Right: 3D structure (Huppert, 2008).

1.2.2.3 G-quadruplex

Guanine (G) rich sequences present in the telomeric region, oncogenic promoter regions, immunoglobulin switch regions and 5'-untranslated regions of many mRNA (Patel *et al.*, 2007) have the ability to adopt a four-stranded structure known as G-quadruplex. Due to its functional role *in vivo*, it acts as a target for anti-cancer drug designing.

1.3 G-quadruplex structure and stability

Guanosine at higher concentration self-associates to form poly crystalline gels. In 1962 Gellert *et al* determined the tetrameric arrangement of guanine bases by crystallographic studies and described it as G-quartet arrangement. The four guanine bases form a square co-planar arrangement via Hoogsteen type hydrogen-bonding network (between N1H and C6=O and between N2H and N7) (**Fig 1.11A**). Each G-quartet is formed by eight hydrogen bonds, which acts as a major stabilizing force for quartet structure. These tetrad units are stacked onto one another in a helical fashion to form a secondary structure known as G-quadruplex (Neidle and Balasubramanian, 2006) The stability of this structure is further maintained by the presence of positively charged ion (Na⁺, K⁺) that circumvent the instability caused by centrally placed O6 carbonyl group (**Fig. 1.11B**). The overall stability of the final folded quadruplex structure depends upon the choice of cation, based on its size and shape which effectively coordinates with carbonyl oxygen atoms (Hud and Plavec., 2006). The stability of cations is in order: K⁺ >

$\text{Na}^+ > \text{Rb}^+ > \text{NH}_4^+ > \text{Cs}^+ > \text{Li}^+$. There is a cation based (especially Na^+ - K^+) conformational switching in quadruplex DNA, which has biological relevance (Sen and Gilbert, 1990). The human telomeric sequence $5'$ -AGGG(TTAGGG) $_3$ forms an anti-parallel “basket” type quadruplex structure in the presence of Na^+ ion (Wang and Patel, 1993) while the same sequence forms a “propeller” type structure in the presence of K^+ ion (Parkinson, 2002).

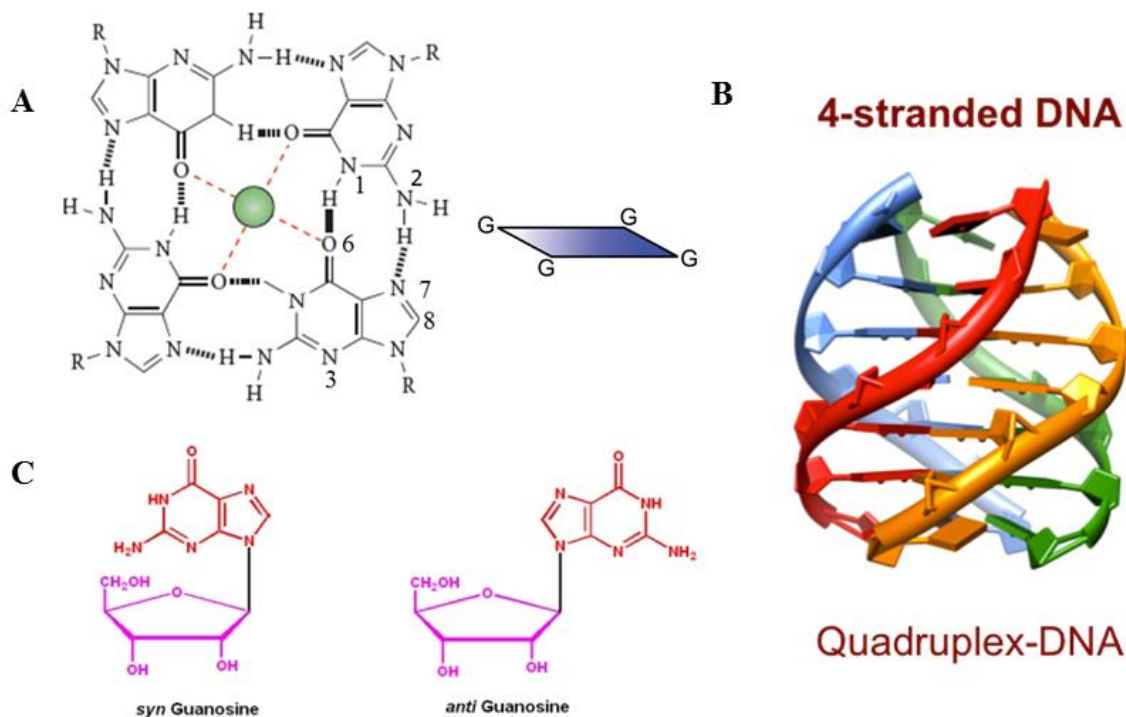


Fig. 1.11: Structure of quadruplex: (A) a G-tetrad; (B) 3D structure; (C) *syn* and *anti* glycosidic confirmation of guanosine.

Apart from the stability due to the presence of monovalent cations G-quadruplex structure in solution is also stabilized due to the hydrophobic interaction and Van der Waals force that occurs between the adjacent G-tetrads. The quadruplexes have four distinct grooves with varying width due to the variation in the glycosidic torsion angles (Kerwin, 2000) (**Fig. 1.11C**). In case of parallel quadruplex, where all the guanosines are in *anti*-glycosidic conformation the width (medium) of the four grooves are nearly same. In case of antiparallel structure, which has a different combination of *syn* and *anti*-glycosidic conformations show variation in all the four grooves that depends upon the types and topology of loops. For example, unimolecular quadruplex structure with lateral loops containing alternate *anti-syn-anti-syn* guanosines conformation between successive G-tetrads, results in a rectangular G-tetrad core with grooves of alternating wide-narrow-wide-narrow widths (Fig. 10A). Whereas bimolecular quadruplex with diagonal loops having *syn-syn-anti-anti* conformations of guanosines result into alternate wide, medium, narrow, medium grooves width between strands (Fig. 10A) (Rujan et al., 2005).

Hydration of these grooves with an ordered network of water molecules further add to the stability of quadruplex structures in the solution. This hydration is symmetrical in case of parallel stranded quadruplexes due to four-fold symmetry than that of *anti*-parallel quadruplexes.

1.3.1 Structural polymorphisms of G-quadruplex:

The polymorphic natures of G-quadruplexes are due to the variation of their molecularity, strand polarity, glycosidic conformation and topology of connective loops (**Fig. 1.12**) (Keniry, 2001).

1. **Strand Stoichiometry:** Quadruplexes can adopt various topologies depending upon the number of strands which participate in its formation. When one oligonucleotide strand participates in the quadruplex formation, it is known as unimolecular quadruplexes with intramolecular G-tetrad interactions. The G-quadruplex sequences which have the potential to form a unimolecular structure can be expressed as : $GmXnGmXoGmXpGm$, where m denotes the number of guanines involved in the formation of G-tetrad of a particular length, whereas Xn , Xo and Xp denotes the number of nucleotide residues that are involved in the formation of loops. Length of G-tract varies; it is equal in case of telomeric (vertebrate) sequences while in case of non-telomeric sequences it may or may not be the same.

Some guanine residues of the unequal G-tracts are present in loop regions. Similarly bimolecular quadruplex is formed by the association of two separate strands with identical sequences $XnGmXoGmXp$, while tetramolecular quadruplex result due to association of four separate strands ($XnGmXo$ or $GmXnGm$) (**Fig. 1.12**). Bimolecular and tetramolecular quadruplexes are also referred as intermolecular quadruplexes that basically consists of short G-tracts.

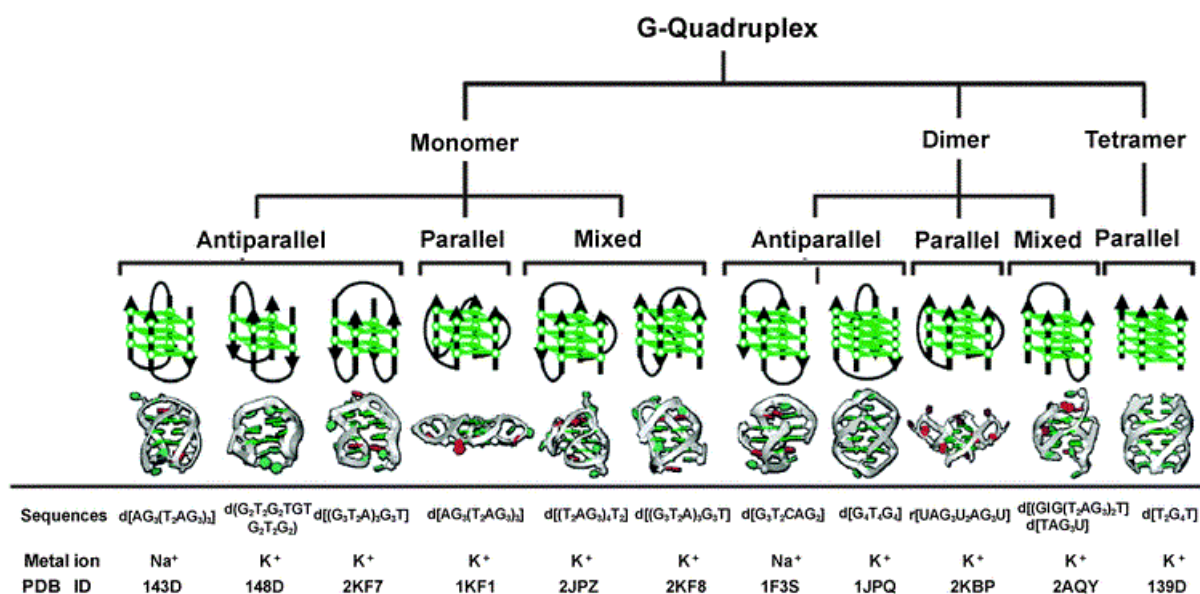


Fig. 1.12: Polymorphisms present in G-quadruplexes (Yaku *et al.*, 2012).

2. Strand Polarity: There are possibly four ways through which strands can be self-associated to form different quadruplex structures and their orientation are also related to the glycosidic conformation of the guanines (**Fig. 1.13**). The first possibility is that all the four strands are parallel, which can be seen in parallel stranded quadruplexes where all the strands run in the same direction (Phillips *et al.*, 1997; Wang and Patel, 1993 and Aboul-ela *et al.*, 1992). In second form out of the four strands three are in parallel form and fourth one is in the antiparallel form (Wang and Patel, 1995). In the third form two neighboring strands are in parallel form (orientation in one direction) and the remaining two are in the antiparallel form (oriented in opposite directions). In this form each strand has adjacent parallel and antiparallel form (Smith and Feigon, 1992). In the last form the strands are arranged in an alternate antiparallel fashion (Kang *et al.*, 1992 and Schultze *et al.*, 1994)

3. Glycosidic Torsion Angle Variation: Unlike B-DNA where the bases are in *anti*-conformation quadruplexes has both *syn* and *anti*-arrangement of guanines (**Fig. 1.11C**). Parallel quadruplexes consist of bases arranged in *anti*-conformation (Wang and Patel, 1992) while that of antiparallel quadruplexes has both *anti* and *syn*-conformations. The requirement of such conformation is to reduce the steric clashes between the adjacent bases (guanines) within G-tetrads. Glycosidic torsion angles not only determine the strand polarity but also the width of the four grooves in different quadruplexes.

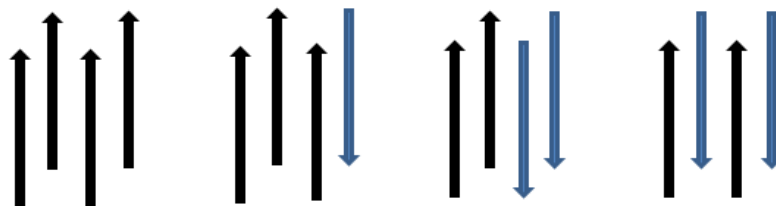


Fig. 1.13: Four possible orientations of quadruplex strands based on glycosidic torsion angles of guanosines: anti (black) and syn (cyan)-conformations.

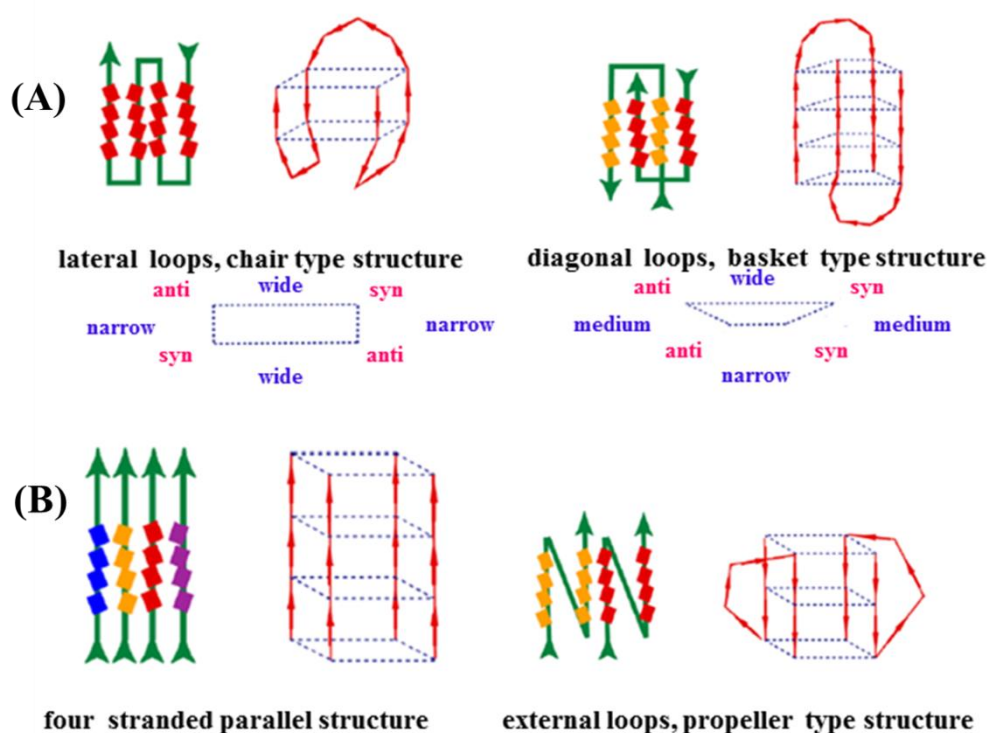


Fig. 1.14: Schematic representation of different quadruplex folding; (A) anti-parallel structures left showing unimolecular quadruplex with lateral loops and varied grooves and right showing bimolecular quadruplex with diagonal loops and varied grooves; (B) left showing parallel quadruplex and right showing external loops. (Rujan et al., 2005).

4. Connecting Loops: Loops are basically linkers that connect G-tracts and provide support to the stacked G-tetrads. They are present in unimolecular and bimolecular quadruplexes. The size and sequences of these linkers not only define the different forms of loop, but also add to the stability of quadruplex structures.

There are four major types of loops: (i) Lateral or edge-wise loops, which consists of two or more residues that connect two anti-parallel adjacent strands (**Fig. 1.14A**) (Wang and Patel, 1993; Macaya, 1993). (ii) Diagonal loops which consists of three or more residues that connect two opposite antiparallel strands (**Fig. 1.14A**) (Haider *et al.*, 2002). (iii) External loops also known as propeller loops or double chain reversal loops, which consist of both short length (one residue) and longer lengths of six or more residues connect adjacent parallel strands (**Fig. 1.14B**) (Kettani *et al.*, 2000; Parkinson *et al.*, 2002). Single residue supports a stack of three G-tetrads while for accommodating four G-tetrads at least two residues are required. (iv) V-shaped loops are present in the structure lacking support column and hence connect two corners of a G-tetrad core (Zhang *et al.*, 2001). Shorter linker sequences show preference for lateral and external loops while that of the longer shows preference for all the loops. Length of the linker also determines the structure of quadruplexes, where shorter length has a high propensity for parallel quadruplexes, increasing the length tends towards mixed (both parallel and anti-parallel) and anti-parallel forms of quadruplexes. Thymine is the most preferred base in the loop followed by adenines.

1.3.2 Biological significance of G-quadruplexes

1.3.2.1 G-quadruplex location

G-rich sequences are located in many biologically significant regions of the genome. The important sites are telomeric region (Blackburn, 1991), oncogenic promoter regions (Siddiqui-Jain *et al.*, 2002; Fernando *et al.* 2006), immunoglobulin heavy chain switch regions (Sen and Gilbert, 1998), recombination hot spot, 5'UTR regions (Kumari *et al.*, 2007) etc. Apart from these hot spots, systematic algorithmic search has been done to know the putative G-quadruplex forming oligonucleotides (QFOs) in the entire genome with a minimum of GGG repeats separated by linkers of short length that generally form stable quadruplex structures (Huppert *et al.*, 2007). It shows that such sequences are prevalent in the promoter regions of proto-oncogenes with nearly 375000 G-quadruplex motifs (Huppert and Balasubramanian, 2005).

1.3.2.2 Telomeric G-quadruplexes

Telomeres are nucleoprotein complexes found in the termini of the eukaryotic chromosomes, which helps in the stability and protection of the chromosomes. The extreme single stranded 3' end of the telomere comprises of simple tandem repeats of guanine-rich sequences that is present in humans and other vertebrates (**Table 1.1 and Fig. 1.15A**), with the potential to adopt

quadruplex fold (Huppert and Balasubramanian, 2005; Riethman, 2008; Neidle and Parkinson, 2003). Telomeric DNA is basically present in duplex form with single stranded 3' overhangs under physiological conditions and in the absence of proteins or small ligands, which induces quadruplex formation. There is an equilibrium between duplex/single-stranded and G-quadruplex form, which is dominant at lower pH and high temperature (Phan *et al.*, 2002). Many studies have been done on different telomeric sequences (human, Tetrahymena, Oxytricha and yeast), human telomere (hTelo) being one of the most important ones among them. The human telomeric sequence 5'-AGGG(TTAGGG)₃ form different structures in the presence of Na⁺ and K⁺ solution (Fig. 13B). The human telomeric sequence 5'-AGGG(TTAGGG)₃ form an anti-parallel “basket” type quadruplex structure in the presence of Na⁺ ion (Wang and Patel, 1993) while the same sequence form a “propeller” type structure in the presence of K⁺ ion (Parkinson, 2002). Later it was shown that these two forms coexist in solution in equilibrium (Phan *et al.*, 2006). Formation of G-quadruplex structures were also reported *in vivo* in the macronuclei of *Stylonychia lemnae* and in human cells, where they exhibit functional role (Schaffitzel *et al.*, 2001; Johnson *et al.*, 2008; Paeschke *et al.*, 2005).

Organism	Repeat	Length
<i>Oxytrichia</i>	TTTTGGGG	20 bp
<i>Euplotes</i>	TTTTGGGG	28 bp
<i>S. cerevisiae</i>	TG ₂₋₃ (TG) ₁₋₆	300 bp
<i>Tetrahymena</i>	TTGGGG	300-400 bp
<i>Arabidopsis</i>	TTTGGGG	2-15 kbp
<i>Mus spretus</i>	TTAGGG	5-15 kbp
<i>Homo sapiens</i>	TTAGGG	5-25 kbp
<i>Mus musculus</i>	TTAGGG	20-50 kbp

Table 1.1: Data showing the length and sequence specificity of telomeric repeats from different organisms.

1.3.2.3 Oncogenic promoter G-quadruplexes

QFOs are also prevalent in the promoter region (generally 1 kb upstream of the transcription start site (TSS)) of certain proto-oncogenes where they regulate the expression of certain genes (Dexheimer *et al.*, 2006) that are involved in the proliferation, development and transcriptional activity, which requires a high level of regulatory control. Examples of such genes are *c-myc* (Phan *et al.*, 2004; Simonsson *et al.*, 1998), *bcl-2* (Dai *et al.*, 2006), *HIF-1 α* (De Armond *et al.*, 2005), *c-kit* (Rankin *et al.* 2005; Fernando *et al.*, 2006), *VEGF* (Sun, *et al.*, 2005), *ki-ras* (Cogoi

et al., 2004), *Rb* (Xu and Sugiyama, 2006) and *RET* (Sun *et al.*, 2003). QFOs of promoter region exist in the form of duplex whose unwinding during the course of replication and transcription is necessary for the formation of quadruplex structure. Hence a duplex-quadruplex equilibrium exist that can be switched by quadruplex interactive ligands, which bind and stabilizes the either forms (Rangan *et al.* 2001).

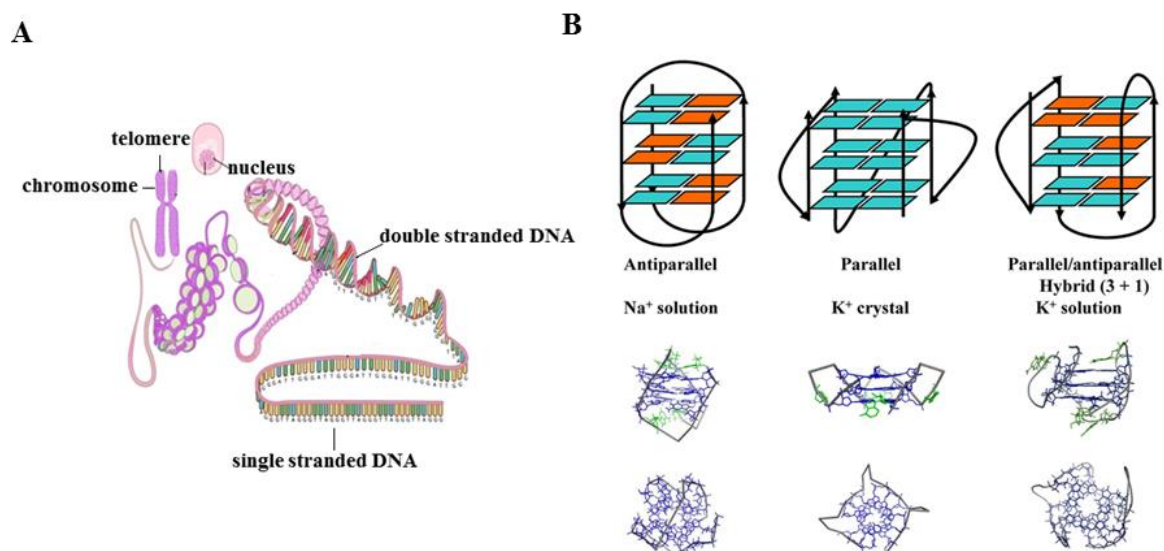


Fig. 1.15: (A) *Telomeric DNA: Termini of eukaryotic chromosomes;* (B) *Different conformations of the unimolecular G-quadruplex formed by the four-repeat human telomeric sequence 5'-AGGG(TTAGGG)₃ in Na⁺ and K⁺ solution.*

Gene	Sequence	Topology	Loops	PDB ID	Refs
c-myc	d(TGAG3TG2TGAG3TG4A2G2)	Parallel	3'P	2A5P	Phan <i>et al.</i> , 2005
c-myc	d(TGAG3TG3TAG3TG3TA2)	Parallel	3'P	1XAV	Ambrus <i>et al.</i> , 2005
bcl-2	d(G3CGCG3AG2A2T2G3CG3)	Mixed; Parallel and antiparallel	2'L 1'P	2F8U	Dai <i>et al.</i> , 2006
c-kit 1	d(AG3AG3CGCTG3AG2AG3)	Parallel	2'P	2O3M	Phan <i>et al.</i> , 2007
c-kit 2	d(CG3CG3CGCGAG3AG3T)	Parallel	3'P	2KQG and 2KQH	Hsu <i>et al.</i> , 2009
c-kit 2	d(CG3CG3CGCGAG3AG3T) d(CG3CG3CGCGAG3AG3T)	Parallel	3xP	2KYO and 2KYP	Kuryavyi <i>et al.</i> , 2010

Table 1.2: *Sequence and topology of oncogenic promoter G-quadruplexes.*

QFOs in the promoter region contain four or more G-tracts with varied number of guanine residues as well as intervening bases. Therefore, apart from generally adopted intramolecular

structure they can also exist in multiple conformations with varied loop isomers (**Table 1.2 and Fig. 1.16**) (Qin and Hurley, 2008).

1.3.2.4 RNA quadruplexes

Quadruplex is also found in RNA sequences, particularly in the 5' UTR regions. Since RNA exist in the single stranded form there is no constraint for duplex melting unlike DNA and more or less RNA quadruplexes are more stable than DNA quadruplexes. NMR study on r(UGGGGU) gave the first evidence of RNA quadruplex formation (Cheong and Moore, 1992), which was followed by some other crystal studies (Deng *et al.*, 2001; Pan *et al.*, 2003) that gave the evidence of a parallel stranded quadruplex. G-quadruplex motif was also found in the 5' UTR of N-ras oncogene. Formation of G-quadruplex in this region is marked by the deregulation of NRAS protein, which otherwise shows increase in its expression level in the absence of quadruplex formation or its mutation (Kumari *et al.*, 2007).

Apart from these locations, there are several proteins which either stabilize or disrupt G-quadruplex formation (Maizels, 2006; Fry, 2007). β -subunit of telomere binding protein of *Oxytricha* (Fang and Cech, 1993) and RAP1 of *Saccharomyces cerevisiae* (Giraldo and Rhodes, 1994) are the proteins which promote G-quadruplex formation. MutS α protein and AID have a significant role in the recombination of immunoglobulin switch regions (Larson *et al.*, 2005; Duquette *et al.*, 2005). Human POT1 which cap the telomere ends, disrupt the quadruplex formation (Zaug *et al.*, 2005). Some family of helicases and nucleases also disrupt of G-quadruplex structures by unwinding and cleaving the quadruplexes. A very good example is the RecQ helicases, whose absence result in chromosome instability causing Bloom and Werner syndrome (Huber *et al.*, 2006; Sun *et al.*, 1998).

1.3.2.5 G-quadruplex: as a target for anti-cancer drug design

G-rich sequences are located in many biologically significant regions of the genome such as telomere, promoter regions of important proto-oncogenes, immunoglobulin switch regions, 5' UTRs of many mRNAs and other sequences associated with human diseases. Formation and stabilization of quadruplex structures within these regions regulates several physiological and pathological processes.

For example formation of quadruplex structure within the telomeric region interferes with telomerase activity and their formation within the oncogenes regulates the gene expression in majority of cancer cells that is responsible for cell immortality. Inducing the formation and enhancing the stability of G-quadruplex in the telomeric region of human chromosome with

small ligands is considered to be a prominent strategy for telomerase inhibition. (Wheelhouse *et al.*, 1998). The G-quadruplex formation and stabilization is facilitated by small molecules via displacement of the telomeric end capping protein hPOT 1, uncapping of telomere and subsequent initiation of DNA damage response-mediated cell death. Similarly formation and stabilization of the quadruplex structure within oncogenic promoter region down-regulate the oncogenes. Hence G-quadruplexes can act as a potential target for broad-spectrum anticancer therapies (Han and Hurley, 2000). Targeting G4-structures within the telomeric region and oncogenic promoter regions as well as mRNA are one the most probable mechanism in the way to anti-cancer drug designing.

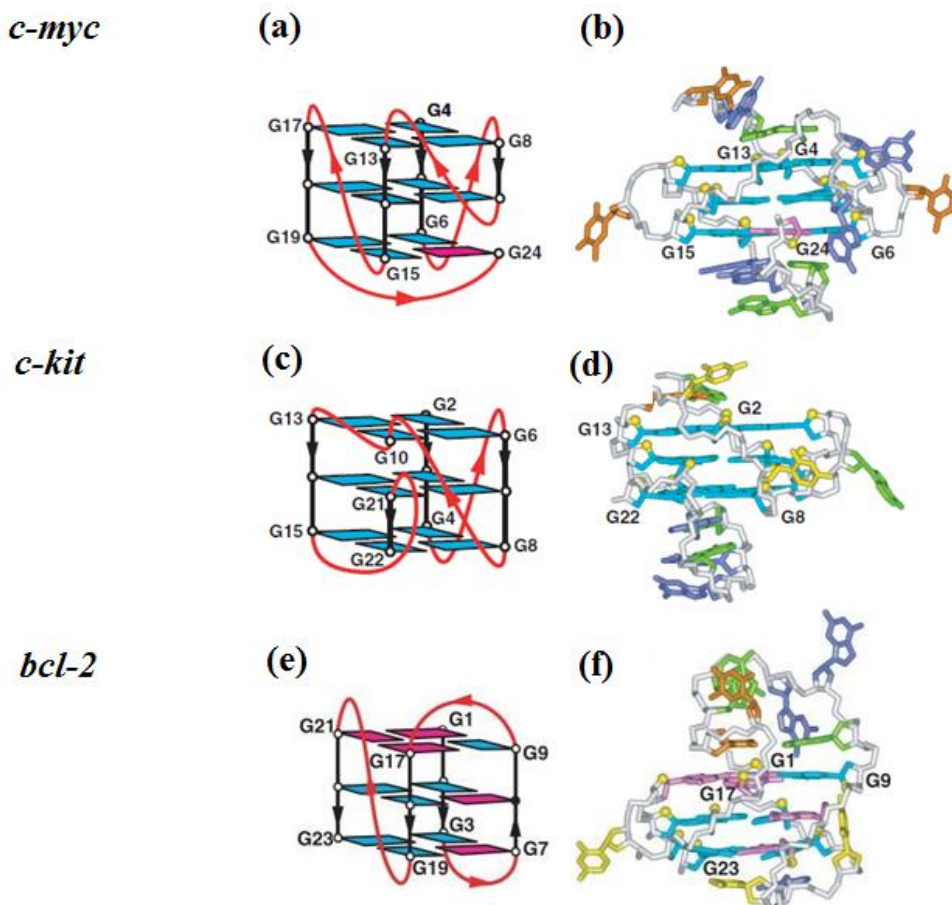


Fig. 1.16: Folding topology (a, c, e) and solution structure (b, d, f) of G-quadruplexes forming oncogenic promoter genes *c-myc* (PDB ID-2A5P), *c-kit* (PDB ID-2O3M), *bcl-2* (PDB ID-2F8U) (Patel *et al.*, 2007).

1.3.2.5.1 Targeting telomeres and telomerase

Telomeres are the specialized regions (Fig. 1.17) found in the termini of the eukaryotic chromosomes, which protect chromosomes from fusion and degradation (Blackburn, 1991; Griffith *et al.*, 1999). It consist of a double-stranded region (3-15 kb) followed by an extreme

single stranded 3' end (150-200 nucleotides) that comprises of simple tandem repeats of guanine-rich sequences that is present in humans and other vertebrates, with the potential to adopt quadruplex fold (McElligott and Wellinger, 1997; Wright *et al.*, 1997). Telomere is present in loops and capped form to protect chromosomal end from being recognized as damaged DNA and subsequent apoptosis mediated cell death (Conomos *et al.*, 2013). Such looping and capping is facilitated by a group of protein complex known as shelterin, which binds to both double-stranded and single-stranded telomeric DNA (De Lange, 2005).

Shelterin is a six protein complex, which consist of telomeric repeat binding factor 1 and 2 (TRF1, TRF2), TRF1-interacting nuclear factor 2 (TIN2), Repressor/activator protein 1(Rap1), Telomerase associated protein 1(TPP1) and Protection Of Telomere 1(POT1) (Blackburn, 2000; Zhong *et al.*, 1992; Broccoli *et al.*, 1997; Bilaud *et al.*, 1997). TRF1, TRF2 and POT1 recognize the hexanucleotide repeats (TTAGGG) and binds directly to telomeric DNA (Broccoli *et al.*, 1997; Baumann and Cech, 2001; Colgin *et al.*, 2003) while TIN2 and TPP1 mediate the six protein complex assembly (O'Connor *et al.*, 2006).

TRF2 also help in making 3'-G-rich single-stranded telomeric DNA into a large duplex loop (telomere loop, t-loop) by folding back this strand and invading the duplex region to form a displacement loop (D-loop) (Griffith *et al.*, 1999).

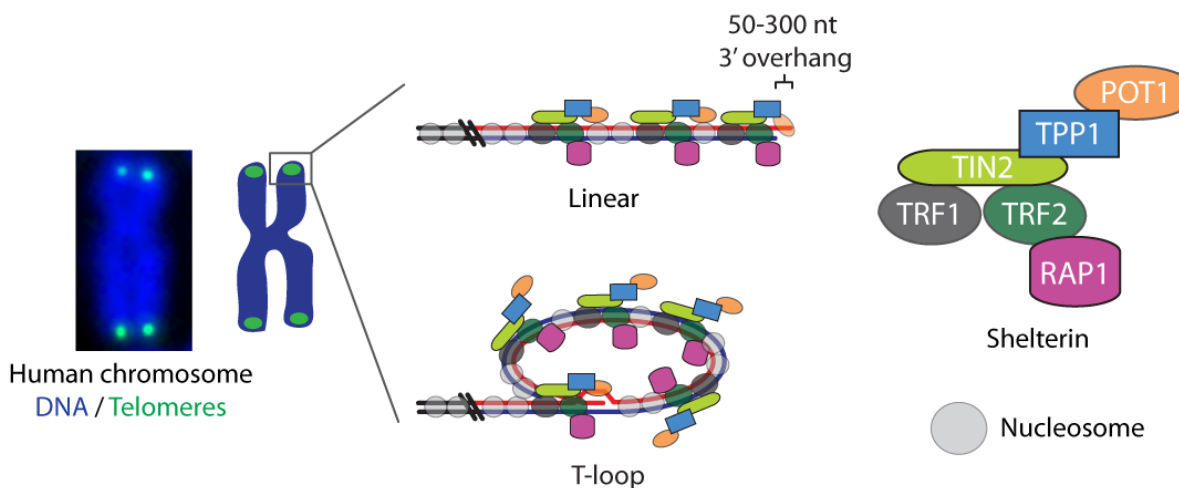


Fig. 1.17: Structure of human telomere showing shelterin complex and loop (Cesare and Karlseder, 2012).

Length of telomere is cell-type dependent, for example, in case of somatic cells it's ~6-8 kb while in case of germline cells it is 10–20 kb (**Fig. 1.18A**). The length of telomere in case of somatic cells decreases (50–200 bases) progressively with every successive round of cell division due to the inability of DNA polymerase to replicate the extreme 3' end of lagging strand of chromosome (i.e., the end replication problem) (Mocellin *et al.*, 2013; Bryan and Cech, 1999) (**Fig. 1.18B**). As a result the telomere is eroded and when it reaches a critical

length (the Hayflick limit) the cells stop dividing and enter into a state of replicative senescence, which eventually leads to apoptotic cell death (Harley *et al.*, 1990; Allsopp and Harley, 1995) (**Fig. 1.18C**). In case of cancer cells (85%), germ cells, stem cells the length of the telomere is maintained constantly in the presence of a reverse transcriptase enzyme named telomerase, which add the hexameric (5'-TTAGGG-3') repeats to the extreme 3' end of the human telomere (Greider and Blackburn, 1985) (**Fig. 1.18B, C**).

Telomerase is a ribonucleoprotein complex, which contain three important components apart from other regulatory proteins (eg., pontin and reptin), which not only constitute this holoenzyme but also help with their assembly. The first component is the hTR (human Telomerase RNA), which is an RNA subunit that has 11 nucleotides template complementary to the 3' end of the telomeric DNA (Feng *et al.*, 1995). The second component is hTERT (human Telomerase Reverse Transcriptase), a 120 kDa protein, which is active as a dimer that constitute the catalytic subunit of the enzyme that catalyzes the addition of hexameric repeats to the 3' end of the chromosomes (Nakamura *et al.*, 1997; Beattie *et al.*, 2001). The third component is a protein named dyskerin (DKC1) that binds to the hTR. These three components play a vital role in telomerase activity as well as lengthening of telomere (Ishikawa, 1997; Weinrich *et al.*, 1997; Beattie *et al.*, 1998).

Telomere elongation occurs in three basic steps: Firstly the RNA template hybridize to 3' end of the telomeric DNA, secondly, this hybridization is followed by the addition of hexanucleotide repeats at this end, thirdly the translocation of the template RNA occur at the 5' direction for the next round of hexanucleotide addition (Nugent and Lundblad, 1998). This cycle is repeated for the elongation of telomere, which will compensate the telomere attrition owing to end replication effect and nuclear action. Though the cancer cells have short telomeres (4-6 kb) presence of high telomerase activity in these cells are responsible for their prolonged proliferation, which leads to their immortality (Weinrich *et al.*, 1997; Kim, 1997; Shay and Gazdar, 1997; Kim *et al.*, 1994). On the other hand somatic cells have inactive telomerase, therefore telomerase inhibition act as a potential broad-spectrum anticancer therapy with less cytotoxicity inside the normal cells (Neidle and Kelland, 1999; Neidle and Parkinson, 2002; Gellert *et al.*, 2005). There are several strategies to inhibit the activity of the telomerase enzyme, which is shown in **Table 1.3** (Sharma *et al.*, 1997). Most of the strategies target the telomerase components and its associated proteins. Induction and stabilization of G-quadruplex architecture by small molecules is now emerging as a potential anticancer approach. (Alberti *et al.*, 2003; Mergny *et al.*, 2001; Zahler *et al.*, 1991) (**Fig. 1.19**). The G-quadruplex formation and stabilization is facilitated by small molecules via displacement of the telomeric end

capping protein hPOT 1, uncapping of telomere and subsequent initiation of DNA damage response-mediated cell death (Gowan *et al.*, 2002).

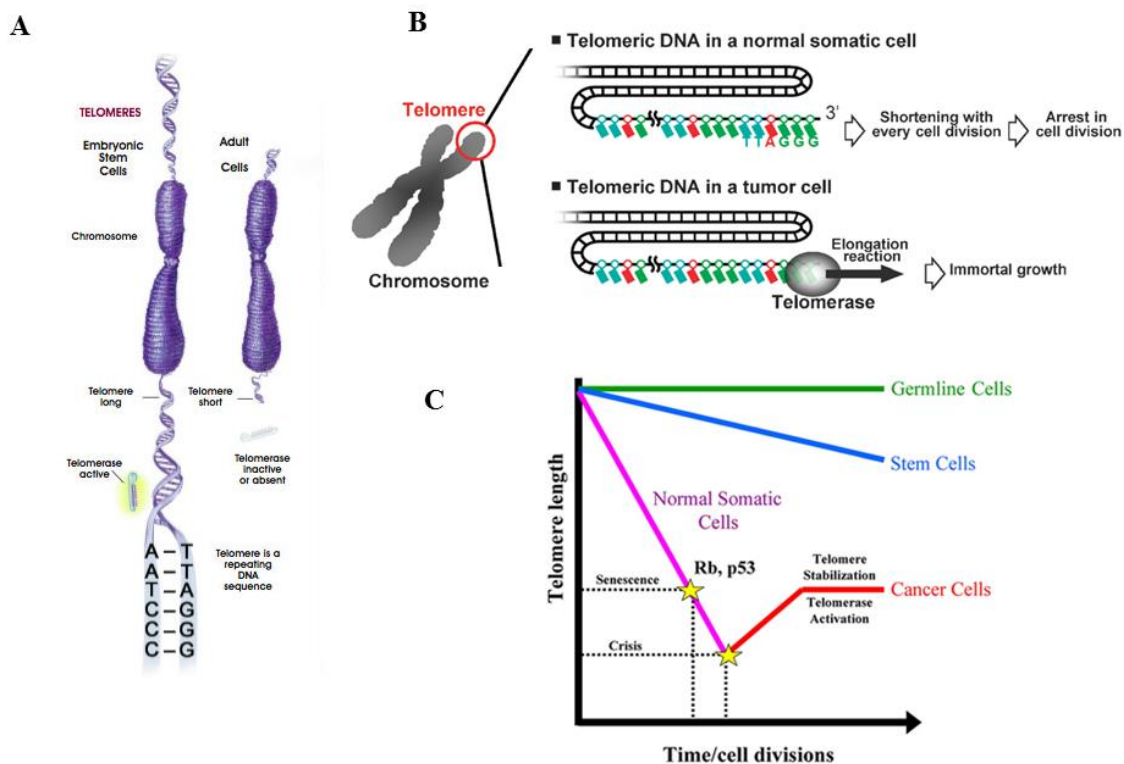


Fig. 1.18: Length of telomere and presence of telomerase (A); Fate of telomere in normal somatic cells and tumor cells (B); effect of telomere shortening in somatic cells and maintenance of telomere length in cancer cells, stem cells and germline cells (C).

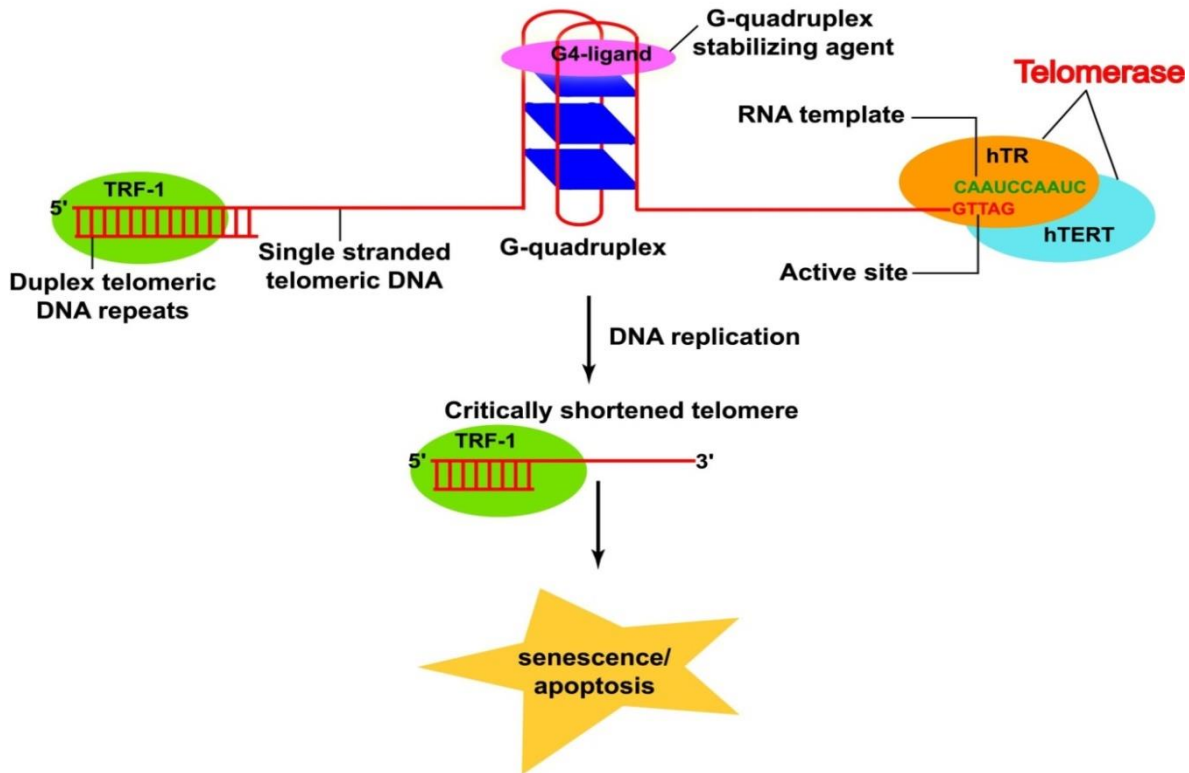


Fig. 1.19: *Telomere mediated molecular therapeutics.*

Target	Approach	Mechanism and consequence	Examples	References
hTERT	RNAi-based TERT knockdown Oligonucleotide antagonist (biochemical active site inhibitor) Telomerase immunotherapy	TERT mRNA degradation and gene silencing TERT enzymatic inhibition Activate immune system to kill telomerase-positive tumor cells that express TERT	Small-interfering RNAs (siRNA) AZT (3'-azido-2',3'-dideoxythymidine), BIBR1532 CD8 ⁺ -induced TERT antigen-expressed cancer cell lysis	Lai <i>et al.</i> , 2007; Cunningham <i>et al.</i> , 2007 Fletcher <i>et al.</i> , 2001; Daly and Martens, 2007 Li <i>et al.</i> , 2007
hRT	Antisense oligonucleotides Hammerhead ribozymes RNAi technique	hTR degradation and telomerase transcriptase template dysfunction	2',5'-oligoadenylate (2-5A) antisense system	Kondo and Kondo, 2007; Li <i>et al.</i> , 2007
Telomerase associated proteins	Interfere telomerase-associated proteins and relative signal pathways	Influence telomerase activity and/or TERT expression	Tankyrase I MAP signal pathway	Ohishi <i>et al.</i> , 2007; Xu, 2007
Telomere-disrupting agents	Designing of G-quadruplex-stabilizing molecules	Rapid induction of cell death via telomere uncapping and telomerase inhibition	Porphyryns Amidoanthraceans Pentacyclic acridine	Rezler <i>et al.</i> , 2002; Gowan <i>et al.</i> , 2001

Table 1.3: Novel telomerase inhibition-based strategies for targeting cancer**1.3.2.5.2 Targeting oncogenic promoter regions**

Formation of G-quadruplex structures within the promoter regions of certain oncogene results in the down-regulation of oncogene transcription, which in turn suppresses the production of oncogenic proteins that are involved in proliferation, development and transcriptional activity (**Fig. 1.20**). Once G-quadruplex is formed within this region, it prevents the binding of transcription machinery to the promoter region (Huppert, 2008) or halts its proceeding along the DNA. Hence it regulates the expression of genes. In few cases there is an increase in the transcription upon G-quadruplex formation (Catasti *et al.*, 1996). There are number of oncogenic promoters where G-quadruplex motifs are present. The well-studied oncogene among them is the *c-myc*, which encodes a protein named MYC, a transcription factor. Their expression is tightly regulated in normal cells for controlling cell growth, proliferation, differentiation and apoptosis (Marcu *et al.* 1992). Overexpression of this oncoprotein owing to the mutation of *c-myc* gene, result into uncontrolled proliferation responsible for causing a wide variety of human cancers for examples colon, cervical, myeloid leukemias, glioblastomas, osteosarcomas etc. (Lutz *et al.*, 2002; Chung and Levens, 2005; Wierstra and Alves, 2008; Brooks and Hurley, 2009). 90% of the total *c-myc* transcription is regulated by nucleosome hypersensitivity element (NHE) III1, which is present in its P1 promoter (Bossone *et al.*, 1992; Cooney *et al.*, 1988). Purine-rich strands of this element form intramolecular G-quadruplex, which act as a transcriptional repressor. MYC protein also induces the activity of telomerase by increasing the expression of hTERT (Wang, 1998).

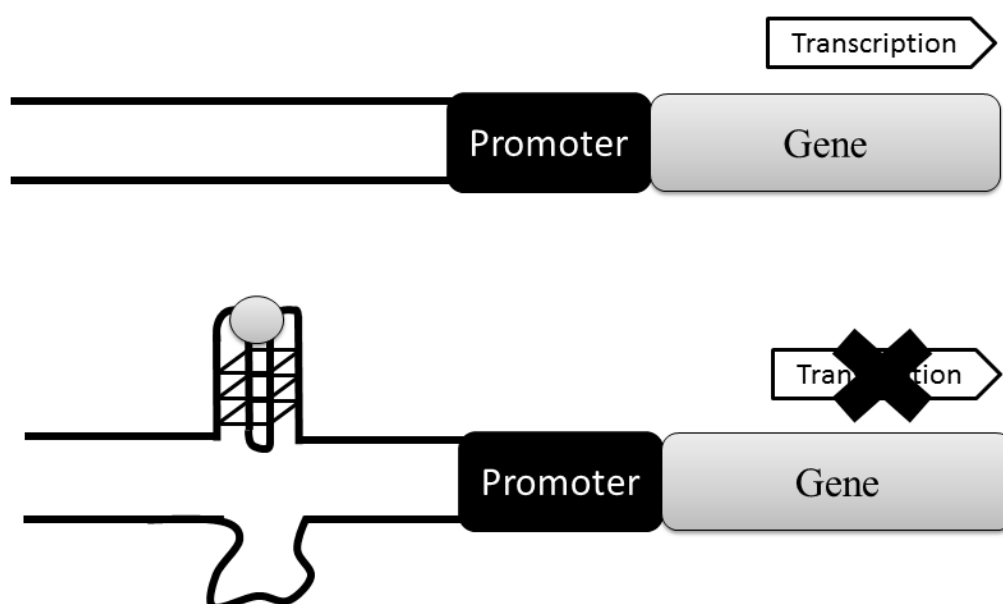
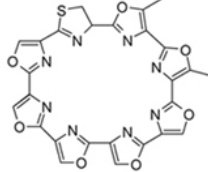
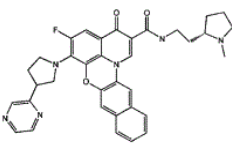


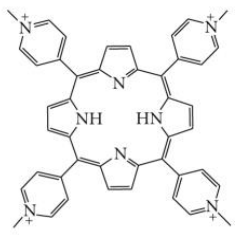
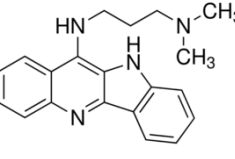
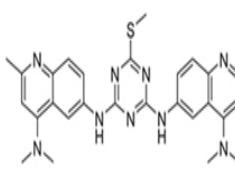
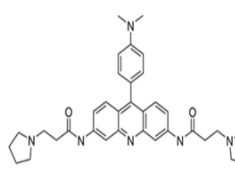
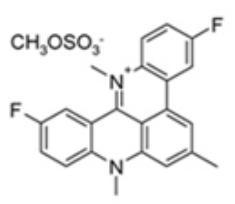
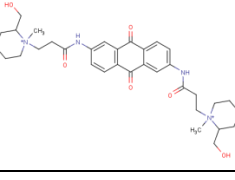
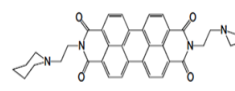
Fig. 1.20: Stabilization of promoter G-quadruplex structure by small ligands (circle) regulates the transcription of oncogenes (Ma *et al.*, 2012).

Stabilizing the oncogenic promoter G-quadruplexes by G-quadruplex interacting ligands can act as a good strategy against cancer (Balasubramanian *et al.*, 2011). Binding of a G-quadruplex-interactive ligand TMPyP4 to quadruplex structures of *c-myc* and *ki-ras* genes causes the down-regulation of these genes (Seenisamy *et al.*, 2004; Siddiqui-Jain *et al.*, 2002).

1.3.3 G-quadruplex interactive ligands

Stabilization of G-quadruplex structures with small ligands is one of the prominent strategies against a wide range of cancers. There are wide numbers of ligands both natural and synthetic that interact with G-quadruplexes, which are in their pre-clinical and clinical trials (Nicoludis *et al.*, 2012; Yang and Okamoto, 2010; Liu *et al.*, 2007). The prerequisite of ligands to be a good quadruplex binder are the presence of planar aromatic ring systems, side chains of minimum of $-(CH_2)_2-$ length with cationic substituent groups like amine, pyrrolidine, piperidine etc. (Monchaud and Teulade-Fichou, 2008, Sun *et al.*, 1997) and selectively towards quadruplexes over duplexes.

Ligand	Structure	Tumor model tested	Antitumor activity	Reference
Telomestatin		Neuroblastoma, myeloma, acute leukemia and glioma stem cells	Telomerase inhibition, telomere length reduction Inhibition of proto-oncogene c-Myb expression Antiproliferative activity, apoptosis induction and increased chemosensitivity Impairs cancer stem cell survival and growth	Shin-ya <i>et al.</i> , 2001; Tauchi <i>et al.</i> , 2003; Sumi <i>et al.</i> , 2004; Shamma <i>et al.</i> , 2004;
Quarfloxin		breast cancer, pancreatic cancer	Selective for telomeric G-quadruplex than duplex and single stranded DNA highly selective for the MYC G-quadruplex disrupt the binding of rDNA quadruplexes and nucleolin, inhibit ribosome biogenesis induce apoptosis	Kim <i>et al.</i> , 2003; Drygin <i>et al.</i> , 2009;

TMPyP4 (Cationic porphyrin)		Myeloma, cervical, pancreatic, breast, colon, prostate cancer and osteosarcoma , neuroblastoma and retinoblastoma	MYC and hTERT inhibition Blockage of telomerase elongation Antiproliferative activity	Rha <i>et al.</i> , 2000; Fujimori <i>et al.</i> , 2011;
SYUIQ-5 and other quindoline derivatives		Leukemia, Burkitt's lymphoma, human epithelial carcinoma, nasopharyngeal carcinoma	MYC and hTERT inhibition Antiproliferative activity cellular senescence; apoptosis induction	Zhou <i>et al.</i> , 2006; Liu <i>et al.</i> , 2007; Zhou <i>et al.</i> , 2009
Triazine derivatives		Melanoma, mouth, lung, colon cancer as well as, lung adenocarcinoma	Impairs the splicing machinery of hTERT by stabilizing quadruplexes located in the hTERT intron 6 Telomere shortening Antitelomerase activity, senescence and cancer cell growth arrest	Riou <i>et al.</i> , 2002; Gomez <i>et al.</i> , 2003; Gomez <i>et al.</i> , 2004
BRACO-19 3,6,9- trisubstituted acridine		Breast and prostate cancer, uterus and vulval carcinoma	Decreases hTERT expression Induction of cellular senescence; cessation of cell growth	Read <i>et al.</i> , 2001; Gowan <i>et al.</i> , 2002
Pentacyclic acridines (RHPS4)		Melanoma, breast and vulval cancer	Telomerase inhibition Telomere capping disruption Apoptosis via PARP-1 activation Cell cycle perturbations and decrease in cancer cell growth Increased sensitivity to chemotherapy	Leonetti <i>et al.</i> , 2004; Cookson <i>et al.</i> , 2005; Phatak <i>et al.</i> , 2007;
Amidoanthra quinone derivatives		60 different human cancer cell lines	Telomerase inhibition High anti-proliferative activity	Huang <i>et al.</i> , 2008
Perylene derivatives (PIPER)		Melanoma, colon and breast carcinomas and osteosarcoma	Selective for telomeric G-quadruplex with respect to duplex genomic DNA. Telomerase inhibition	Micheli <i>et al.</i> , 2009; Franceschini <i>et al.</i> , 2012

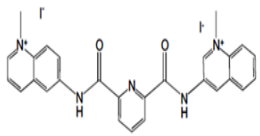
		and colorectal carcinoma cell		
307A 2,6-pyridindicarboxamide derivative		Glioma and osteosarcoma	Equipotent against MYC and telomeric G-quadruplexforming sequences Inhibiting proliferation and induce apoptosis	Pennarun <i>et al.</i> , 2005

Table 1.4: *Quadruplex-interactive ligands showing antitumor activity in various cancers*

Presence of aromatic ring systems facilitates stacking of these ligands effectively on planar G-tetrad via π - π interaction while cationic side chains interact with the grooves of the G-quadruplexes.

Based on the structure of quadruplexes and ligands there is basically three modes of binding: (i) end-stacking on the terminal G-tetrads (ii) Intercalation between the two successive G-tetrads (iii) groove binding (**Fig. 1.21**). Some ligands due to the presence of certain moieties also interact with the loops. Binding forces are basically non-covalent comprising of hydrophobic interactions, hydrogen bonding and electrostatic interactions.

Apart from small ligands G-quadruplexes in the form of aptamers are also of growing interest against certain proteins like thrombin, HIV-1 integrase (Bock *et al.*, 1992; Aviñó *et al.*, 2012, 2013; Wyatt *et al.*, 1994; de Soultrait *et al.*, 2002). Many biophysical techniques along with molecular modeling studies have been employed for knowing the structure and mechanism of quadruplex-ligand interactions. In order to evaluate the anti-cancerous nature of ligands cell based *in vitro* assays are conducted, the most important one is TRAP (Telomere Repeat Amplification Protocol) assay, which is used to measure the inhibition of relative telomerase activity by G-quadruplex interactive ligands (De Cian *et al.*, 2008).

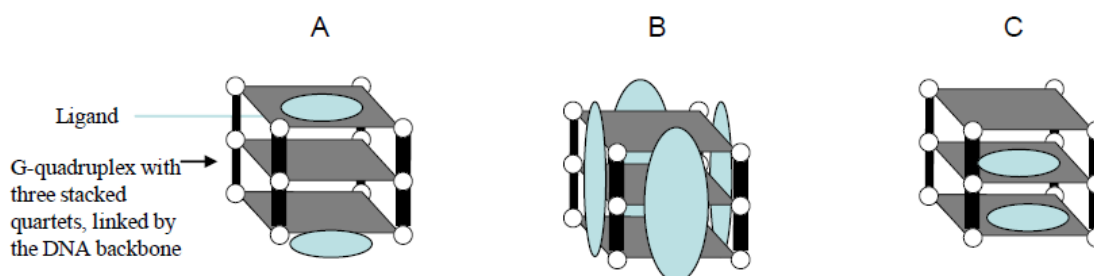


Fig. 1.21: *Modes of ligand binding to G-quadruplex structures (A) end stacking, (B) groove binding and (C) intercalation between the two successive G-tetrads.*

There are basically two ways through which stabilization of G-quadruplex structures leads to anticancer therapy. There are several ligands which induce and stabilize G-quadruplex structures in telomeric region that leads to the uncapping of telomere as well as the inhibition of telomerase activity. Uncapping result in the displacement of the telomeric end capping protein hPOT1 while stabilization of G-quadruplex structures further halt the elongation of telomere by telomerase, which leads to telomere shortening (Balasubramanian and Neidle, 2009). Both uncapping of telomere and telomerase inhibition induces DNA damage response-mediated cell death. Uncapping of the telomere is a fast pathway with short-term effects, whereas telomerase inhibition has long-term effects though it's a slow pathway. Stabilization of G-quadruplex structures in oncogenic promoter regions lead to the down-regulation of oncogene transcription by preventing the binding of transcription machinery, or their proceeding along DNA, which in turn suppresses the production of oncogenic proteins that are involved in proliferation, development that leads to cancer. Some of the ligands like trisubstituted acridine compound BRACO-19 (Burger *et al.*, 2005), polycyclic compound fluorinated pentacyclicquinol[4,3,2-kl]acridium cation (RHPS4) (Phatak *et al.*, 2007), telomestatin (Tauchi *et al.*, 2003), cationic porphyrin, 5,10, 15, 20-tetrakis-(N-methyl-4-pyridyl)porphyrin (TMPyP4) and fluoro quinone derivative Quarfloxin exhibit anti cancerous activity *in vivo* tumor xenograft models (Neidle, 2010) (**Table 1.4**). Right after the synthesis of the first G-quadruplex interactive ligand 2,6-diamidoanthraquinone, which inhibit telomerase activity *in vitro* (Sun *et al.*, 1997) many synthetic G-quadruplex interactive compounds were designed which belong to diverse chemical classes.

The most important classes are:- anthraquinone derivatives, acridine derivatives (Read *et al.*, 2001; Gowan *et al.*, 2001), ethidium derivatives (Koeppel *et al.*, 2001), fluoroquinolones, porphyrins (Wheelhouse *et al.*, 1998), perylenes (Rossetti *et al.*, 2005), piperazines, carbazole derivatives, fluoroquinophenoxazines (Duan *et al.*, 2001), alkaloids (Franceschin *et al.*, 2006). A database known as G4LDB (<http://www.g4ldb.org>) is built, which has a collection of all the known G-quadruplex-interactive ligands that provide a platform for the study of these ligand and their discovery (Li *et al.*, 2013).

1.3.4 Structural studies on G-quadruplex interactive ligands

Several biophysical studies have been carried out to probe the quadruplex-ligand interactions. Though these studies provide invaluable structural information (binding constant, stoichiometry, stability and other thermodynamic parameters) related to conformational changes under various conditions. However, only NMR spectroscopy and X-ray

crystallography give detailed structural analysis on atomic resolution, which helps in a structure-based drug designing approach. Most of the high resolution structures of quadruplex-ligand used human and protozoan ciliates as structural models for studying quadruplex specific ligands.

These models are simple and predominately exist in single conformation that provides easier interpretation of ligand-quadruplex interactions. Sequence with longer G tracts exists in different forms, which coexist in solution in equilibrium, making the interpretation of ligand-quadruplex interactions difficult.

Anthraquinone and Acridine derivatives

Several molecular modelling studies were carried out for a variety of anthraquinone derivatives along with TRAP assay to evaluate their anticancer property through telomerase inhibition (Sun *et al.*, 1997). The model used for modelling studies was a well characterized NMR structure of human 22 mer telomeric sequence. The result proposed the concept of end-stacking, which was later confirmed by crystallographic, NMR and biophysical data. Till date, there is not a single X-ray crystal/NMR structure available on G-quadruplex structures with anthraquinone derivatives. But a crystal structure of the anti-cancer anthracycline daunomycin with the tetramolecular quadruplex formed from four strands of d-(TGGGGT) has been determined (Clark *et al.*, 2003). The crystal data showed that daunomycin binds to the G-quadruplex structure in an end stacking mode. Six daunomycins arrange in two layers of three molecules each and stacks into the terminal 5'-GT segment of the two end to end stacking quadruplexes. Hence the binding stoichiometry is three daunomycin molecules end stack to a quadruplex structure, which is stabilized by π - π interaction between daunomycin-daunomycin and daunomycin-quadruplex. The sugar moiety of daunomycin molecule interacts with the groove of quadruplex through hydrogen bonding or Van der Waals interaction. Therefore three of the four quadruplex grooves were occupied by sugar moiety of three daunomycin molecules.

In a similar study Clark *et al.*, 2012 shows the effect of terminal thymine nucleotide on daunomycin interaction to tetramolecular quadruplex structure. The crystal studies of d-(GGGG)₄- daunomycin in the presence of Na⁺ ions shows that daunomycin binds in an end stacking mode, but with a higher order aggregation structure. The four daunomycin molecules arrange in a plane with nose to nose arrangement, four such daunomycin layers stack between the two GGGG quadruplex layers. The binding arrangement shows d(3'-GGGG-5')₄-Dau-Dau-Dau-Dau-d(5'-GGGG-3')₄. 'Dau' denotes a layer of four daunomycin molecules. The stability of this complex structure stems from the extensive pi-pi stacking between daunomycin-

daunomycin aromatic chromophore layer and between daunomycin-terminal guanosine bases. The complex shows the perfect 4-fold symmetry. The 5'-terminal guanine shows glycosyl orientation of *syn* due to the square planar orientation of Na^+ ion.

The tricyclic acridine chromophore with a central ring nitrogen atom was originally developed (Harrison *et al.*, 1999) as an alternative to the anthraquinones, in order to circumvent the poor aqueous solubility of many amidoanthraquinone derivatives. BSU 6039, BRACO-19, RHPS4 are some examples of acridine, which are known G-quadruplex binders. In 2003 Haider and co-workers solved the crystal structure of 3,6-bis-[3-pyrrolidino-propionamide] acridine (BSU6039), a disubstituted acridine with *Oxytricha nova* telomeric DNA sequence d(GGGGTTTTGGGG) at 1.75 Å resolution in the presence of K^+ condition. This sequence forms a hairpin dimer with thymine loops present diagonally across the top and bottom G-tetrad with alternating *syn-anti* guanines. BSU6039 forms a 1:1 complex with this quadruplex structure, with acridine ring stacking on the terminal G-tetrad. π - π interaction between terminal two guanine bases and acridine chromophore acts a stabilizing force for the binding interaction. BSU6039 contains two aminoalkylamido side-chains, both of which position themselves near the quadruplex grooves. The O2 atom of the loop thymine T2 forms a hydrogen bond with the acridine ring nitrogen, which is protonated in $\text{pH} > 7.0$.

In search of better acridine derivative with enhanced selectivity towards G-quadruplex structures than duplex structures, a 3,6,9-trisubstituted acridine ligand BRACO-19 with an anilino group at the 9-position was developed. It showed enhanced quadruplex binding along with extensive *in vitro* anti-cancer activity. The substitution of side chain facilitates its binding to each grooves of quadruplex. This selectivity was proved by molecular modeling studies. The interaction of BRACO-19 with bimolecular human telomere repeat sequence d(TAGGGTTAGGGT) was studied at 2.5 Å using X-ray diffraction studies by Campbell *et al.*, 2008. Binding model shows a single molecule of BRACO-19 sandwiching between two molecules of bimolecular quadruplexes at the 3' end, hence end stacking mode of binding. Drug stacks asymmetrically on the end of quadruplex stabilized by π - π stacking interaction with two terminal guanine bases. The substituents at 3- and 6- position of BRACO-19 extend into grooves of G-tetrad hence further stabilizing the complex. The cationic ring nitrogen present on the axis of K^+ ion channel acts as a stabilizing factor to hold two quadruplexes.

Polycyclic acridines have been synthesized in order to increase the π - π stacking interaction with terminal G-quartet. RHPS4 is an example of polycyclic acridine whose interaction with parallel stranded quadruplex sequence d-(TTAGGGT)₄ was reported by Gavathiotis *et al.* ¹H and ¹⁹F studies of the complex d-(TTAGGGT)₄-RHPS4 shows that drug

is in fast exchange with quadruplex DNA. The titration data shows that line width broadens at drug/DNA ratio 0.5 and again sharpens as drug/quadruplex ratio increases to 2. This behavior shows that RHPS4 is in fast exchange with d-(TTAGGGT)₄. All the central G-tetrad core i.e G3-G4-G5 are intact, which clearly indicates that RHPS4 is not intercalating between any of G-tetrads. Proton chemical shift perturbations and 24 intermolecular NOE contacts with 5'-ApG step and 5'-GpT step indicates RHPS4 stacks on either side of G-tetrad. Restrained molecular dynamics based on the distance restraints obtained from NOESY and intermolecular peaks confirms the stacking of RHPS4 on G-tetrad on either side.

Porphyrin

Cationic porphyrins are one of the important G-quadruplex interactive ligand, which stabilizes the quadruplex structures with the extended aromatic surface. TMPyP4 is one of them, which binds to quadruplex with high affinity. Although it does not possess high selectivity for quadruplex DNA compared to duplex DNA (Ren and Chaires, 1999). Both NMR and X-ray structures are available for TMPyP4-quadruplex complex. The crystal structure of TMPyP4 complexed with a human telomeric bimolecular quadruplex having a parallel topology at 2.0 Å resolution was reported by Parkinson *et al.*, in 2007. Two molecules of TMPyP4 interact with quadruplex. One molecule stacked perpendicularly at TTA propeller loop while the other molecule stacked between two quadruplexes. However, the later TMPyP4 molecule is not stacked between G-quartets, but rather between A·T base pairs formed from the reorganization of the loops. Direct end-stacking was not possible because of the presence of 4 N-methyl pyridyl groups in TMPyP4 that were non-planar with respect to the porphyrin core. On the contrary to this the NMR structure of TMPyP4 with the *c-myc* promoter quadruplex (Phan *et al.*, 2005) showed the stacking of TMPyP4 on G-quartet. The complex showed a large upfield shifts in the imino resonances along with the presence of slow exchange between bound and free forms.

In an attempt to elucidate the mode of interactions between TmPyP4 and human G-quadruplex repeat sequence (TTAGGG)₄ Mita *et al.*, used NMR and spectroscopic techniques. The results showed that TmPyP4 interacts and stabilizes the human tetramolecular G-quadruplex repeat sequence (TTAGGG)₄. Upon interaction with TmPyP4, the aromatic protons of quadruplex step A3pG4 show significant line broadening effect and upfield shifts. Specific intermolecular contacts exist between ortho and meta protons of TmPyP4 with A3H2, A3H8, T2H4', A3H1', A3H4', G4H1' and G4H4' protons of quadruplex. This indicates the binding of TmPyP4 to A3pG4 step of quadruplex molecule. The upfield shift of imino protons of G4 and

G5 is due to the ring current effect upon porphyrin binding to DNA. In a plausible model explained on the basis of NMR studies, it was shown that planar TmPyP4 stacks on the A3pG4 step covering two or all four bases of adenine residue. The N-methyl pyridinium side chain of TmPyP4 is present near the DNA backbone and this cationic side chain helps in the binding thermodynamics by forming electrostatic interaction with negatively charged phosphate backbone of quadruplex DNA.

Perylene

The first NMR based quadruplex ligand complex structure was proposed by Laurence Hurley group in 1998 (Fedoroff *et al.*, 1998). Both one dimensional and two dimensional NOESY NMR techniques were used to study the binding interaction of PIPER (3, 4, 9, 10-perylenetetra-carboxylic diimide) with human tetramolecular repeat sequences. They used four different sequences like d-(TTAGGGTT)₄, d-(TTAGGGTTA)₄, d-(TTAGGG)₄ and d-(TAGGGTTA)₄, to distinguish between end-stacking and intercalation mode of binding. Addition of PIPER to d-(TTAGGGTTA)₄ resulted in gradual disappearance of GNH resonances and gradual appearance of new resonances in the corresponding up-field region. Due to the broadening of resonances after addition of PIPER, only two complexes namely d-(TTAGGG)₄ and d-(TAGGGTTA)₄ were further studied to get the structure through NOESY correlations. Based on the chemical shift perturbation and NOEs it was shown that PIPER binds on the terminal G-quartet plane of d-(TTAGGG)₄ by end-stacking mode. A single molecule of PIPER stacks between the two molecules of quadruplex, with two quadruplex structures arranged in head-to-tail fashion. But a different type of binding was observed when PIPER interacts with quadruplex sequence with 3' overhang sequences, like in d-(TAGGGTTA)₄. The presence of NOEs with G5pT6 step protons shows that PIPER binding site, as the (GGG)₄ core remains intact, it was predicted that the drug binds to d-(TAGGGTTA)₄ quadruplex sequence by threading intercalation mode.

Non-planar ligands

Structural studies are also available for groove binding ligands. Distamycin, a well known groove binder and its analogues are most talked quadruplex binders. Many studies have been carried out by different research groups. In one such study Antonio Randozzo *et al.*, 2007 reported the detailed NMR structure of distamycin A binding to a parallel G-quadruplex structure d-(TGGGGT)₄. Chemical shift perturbation and intermolecular NOE peaks show that distamycin A exists as dimer in head to tail fashion and binds to two opposite grooves of d-

(TGGGGT)₄. The BMI (Binding mode index) values obtained by saturation transfer difference (STD)-NMR study also supports the binding of distamycin A to d-(TGGGGT)₄. To prove the distamycin A is interacting in groove region they also used modified DNA sequence 8-bromo guanosine in the second G of G2-G3-G4-G5 stretch, d-(TGG-BrGGT)₄. This modified oligonucleotide forms a parallel quadruplex sequence, but bulky Br protrudes out in the groove region, which prevents the binding of distamycin A to this quadruplex DNA.

In another study Cosconati and co-workers (Cosconati *et al.*, 2010) replaced amidinium group by an uncharged N-methyl amide group in distamycin molecule. GNH and GH8 proton signals of all four G-tetrad steps show upfield shift upon interaction with the ligand, on the contrary both terminal T H6 and CH₃ signals show downfield shift. 12 drug head-to-tail dimer NOEs were observed similar to distamycin molecule (Martino *et al.*, 2007). And 14 NOEs were observed between Dist-A analogue with d-(TGGGGT)₄ quadruplex. Hence it was evident that Dist-A analogue binds to groove and 3' end of quadruplex d-(TGGGGT)₄ quadruplex structure as head-to-tail dimer.

In an attempt to know the interaction of non-planar G-quadruplex ligands Li *et al.*, studied the interaction of two non-planar alkaloids peimine and peiminine, with human tetramolecular quadruplex forming sequence d-(TTAGGGT)₄. The results showed that drug binds as a monomer in two separate grooves. Addition of peimine/peiminine to d-(TTAGGGT)₄ results in downfield shift G4, G5 proton resonances and upfield shift of G6 proton resonances, apart from these, T2H6, T2CH₃, A3H8, A3H2, G5H8, T7CH₃ proton resonances also show downfield shift. The 2:1 NOESY spectra acquired at 100 ms and 300 ms show very few intermolecular peaks due to signal overlapping, the important among them are peiminine 23- positioned methyl protons with T2H2', T2H2'', A3H2' protons, and 19-positioned methyl group with T2H2' proton. As these two studied alkaloids lack extended planar aromatic ring structure for π - π stacking on G-quartets, and based on the obtained intermolecular peaks between peiminine and d-(TTAGGGT)₄, the authors clearly conclude the two alkaloid molecule binds as a monomer in the two grooves of G-quadruplex structure. The thermal stabilization experiments based on CD spectroscopy revealed the both peimine and peiminine stabilizes quadruplex DNA by 13-14°C. Studies have been conducted on the interaction of isoquinoline alkaloids like berberine, coralyne with human telomeric quadruplex DNA (Bhadra and Kumar, 2011). Among all the alkaloids tested coralyne showed highest binding affinity. The binding affinity of coralyne is also higher for duplex DNA and RNA owing to its intercalative mode of binding (Pal *et al.*, 1998; Sinha and Kumar, 2009). But till date there are no structural studies on its binding to DNA owing to its strong aggregation properties, which

would lead to an extensive line broadening of NMR signals. On the other hand, both NMR and molecular modelling studies are available for berberine and its derivatives with different quadruplex structures. Berberine and its derivatives stabilize the quadruplex structure basically through end-stacking mode (Bessi *et al.*, 2012; Franceschin *et al.*, 2006, Zhang *et al.*, 2007).

Apart from typical end-stacking or groove binding interactions some ligands show dual mode of interactions simultaneously. One such ligand is cyanine dye 2,2'-diethyl-9-methyl-selenocarbocyanine bromide (DMSB). Gai *et al.*, in 2013 showed that cyanine dye 2,2'-diethyl-9-methyl-selenocarbocyanine bromide (DMSB) binds to d-(TGGGGT)₄ in a dual mode, where in one site drug binds as dimer and as a monomer in the second site. The initial addition of DMSB to d-(TGGGGT)₄ i.e D/N ratio 0.5 to 2, results in the broadening of aromatic and methyl protons belongs G5pT6 step. DMSB binds to quadruplex DNA in monomer mode (M-mode) in this D/N ratio. G6-NH show up-field shift and T6-H6 and T6-CH₃ show downfield shift (> 0.1 ppm), hence DMSB stacks as monomer between G5 and T6 nucleotides as end stacking mode. Further increase in D/N ratio from 3:1 to 8:1 results in the sharpening of G5-NH, G5-H8, T6-CH₃, T6-H6 resonances and show little change in chemical shift position in this D/N range. This clearly indicates the filling up of this site, but proton resonances of T1 and G2 step shows dramatic shift, and broaden remarkably. G2-NH proton shifts maximum downfield (~0.3ppm). This clearly shows the different binding behavior, as drug binds other than stacking, as it involves T1, G2 and G3 steps. Based on these observations authors proposed the structure of DMSB bound d-(TGGGGT)₄ tetramolecular quadruplex. One drug binds to G5pT6 step as a monomer by external stacking and a head to tail dimer DMSB molecule binds to T1pG2pG3 step in groove region. Trimethine cyanine analogs have been synthesized by Nanjunda *et al.*, which shows higher affinity for parallel stranded G-quadruplex structure and the primary mode of interaction is end-stacking, which is revealed by NMR spectroscopy.

Modification of existing ligands with different substituent groups are, in practice, in search of better ligand with specificity towards a particular G-quadruplex structure and their delivery within cells. In the current thesis, I have investigated the G-quadruplex interactions with ligands from two different families; (a) mitoxantrone (MTX) - a synthetic anthraquinone derivative and (b) luteolin – a naturally occurring flavonoid.

1.4 Anthraquinones Derivatives

Anthraquinones (AQs), also known as 9, 10-anthracenedione are a class of structurally related anthracene with a molecular formula of C₁₄H₈O₂. Several derivatives of anthraquinone are

synthesized, which have diverse role both in industry and medicine. They are mostly known in the form of chemotherapeutic agents that interfere with cellular processes (replication, transcription etc.) and enzymes that are involved in these processes by intercalating into DNA. The most common anthraquinone based compounds are anthracycline, which form an important class of antibiotic to combat several cancers. Modification of existing compounds has been done in a way to design new ligands with increased efficacy to interact with DNA and hence can be used to inhibit several diseases.

Apart from its interaction with the duplex DNA and RNA they have gained importance in interacting with non-canonical structures like G-quadruplexes, which in turn exhibit its property to inhibit telomerase activity.

Amidoanthraquinone derivatives were the first class of G-quadruplex interactive ligands that showed telomerase inhibition (Zahler *et al.*, 1991; Sun *et al.*, 1997) due to the stabilization of G-quadruplex structures. It has already been mentioned in G-quadruplex-interactive ligands section that the prerequisite of ligands to be a good quadruplex binder are the presence of planar aromatic ring systems, side chains of minimum of $-(CH_2)_2-$ length with cationic substituent groups like amine, pyrrolidine, piperidine etc. (Monchaud and Teulade-Fichou, 2008, Sun *et al.*, 1997). Anthraquinone based ligands fall under this category, which fulfill the requirement of planar rings for stacking interactions to the G-quartets and the presence of side chains with cationic group facilitate its interaction to the grooves of quadruplexes. Several anthraquinone derivatives were synthesized in order to investigate the relation between structure and activity for telomerase inhibition. Molecular modeling studies along with TRAP assay was done on different anthranthraquinone derivatives, which shows that these derivatives bind to G-quadruplex structures via threading intercalation mode and stabilizes them, thus inhibiting the telomerase enzyme (Read *et al.*, 1999). Substitution of the terminal side chains of anthraquinone with a range of amino acids (Phe, lys, Arg etc.) i.e. peptidyl-anthraquinones to yield 1,4-, 1,5-, 1,8-, 2,6- and 2,7- isomers not only enhances their interactions with quadruplex groove regions thereby improving selectivity towards-quadruplex structures but also inhibit telomerase activity by inducing cell senescence with lower toxicity (Shan *et al.*, 2013; Zagotto *et al.*, 2011; Zagotto *et al.*, 2008). It has also been suggested that the addition of fourth planar aromatic system to the tricyclic chromophore might improve the interaction between the compounds and quadruplex groove regions (Huang *et al.*, 2009). More recently several aryl ethynyl anthraquinones showed that primer extension by DNA polymerase can be blocked at 5-10 μ M concentrations of ligands. The stabilization of Tel24 and HTS G-quadruplexes was found to be $\Delta T_m = 25-30$ °C for various ligands and the results correlated well with the docking

studies (Percivalle *et al.*, 2014). There are no structural studies of anthraquinone-G-quadruplex complexes reported so far in the literature, either by x-ray crystallography or NMR techniques but crystal structure is available for anthracycline drug daunomycin.

The first crystal structure of complex involving a parallel DNA quadruplex, d-(TGGGGT)₄-daunomycin complex, showed that daunomycin binds to the G-quadruplex structure in an end stacking mode (Clark *et al.*, 2003). A recent high resolution crystal structure of parallel inter molecular DNA quadruplex, d-(GGGG)₄-daunomycin complex, shows two quadruplexes in which four daunomycin molecules are sandwiched with syn, anti, anti, anti-conformations (Clark *et al.*, 2003) and showed no guanosamine groove insertions as seen in earlier daunomycin-d-(TGGGGT)₄ structure (Clark *et al.*, 2003) having all anti conformations. Since there are no structural studies of anthraquinone-G-quadruplex complexes reported so far in the literature, we have done the structural studies of a very well-known anthraquinone derivative mitoxantrone (MTX) with human telomere single repeat sequence d-(TTAGGGT).

1.5 Mitoxantrone as a chemotherapeutic agent

Mitoxantrone, a synthetic anthraquinone derivative, is a well-known chemotherapeutic agent, which was synthesized in replacement of cardiotoxic anthracycline drugs like doxorubicin and daunomycin (Murdock *et al.*, 1979). It shows enhanced antitumor activity and it reduces the dose related cardiotoxicity thus making it a promising drug than anthracyclines (Bonadonna *et al.*, 1969; Neidle and Waring, 1983). It is used singly or in combination with other anticancer drugs against several cancers such as metastatic breast cancer, acute leukemia and non-Hodgkin's lymphoma (Smith, 1983; Faulds *et al.*, 1991; Tsavaris *et al.*, 2004; Hagemester *et al.*, 2005). Cytotoxicity of MTX lies partly in its intercalative binding to cellular DNA, RNA and histone proteins which lead to unwinding of DNA helix followed by condensation of nucleic acid and partly as topoisomerase II inhibitor (Kapuscinski *et al.*, 1981; Lown *et al.*, 1985; Krishnamoorthy *et al.*, 1986; Hajihassan and Chadegani, 2009, 2011; Kapuscinski and Darzynkiewicz, 1986; Smith *et al.*, 1990; Capranico *et al.*, 1994). Its cytotoxicity is also due to the formation of interstrand crosslinks in DNA mediated by the oxidation of mitoxantrone, which is catalyzed by myeloperoxidase, an enzyme present in neutrophils and monocytes (Panousis *et al.*, 1994; 1995). *In vitro* mitoxantrone-DNA adduct was formed by the activation of formaldehyde that in turn stabilizes the DNA and also halt the progression of polymerase and exonuclease activity (Parker *et al.*, 1999).

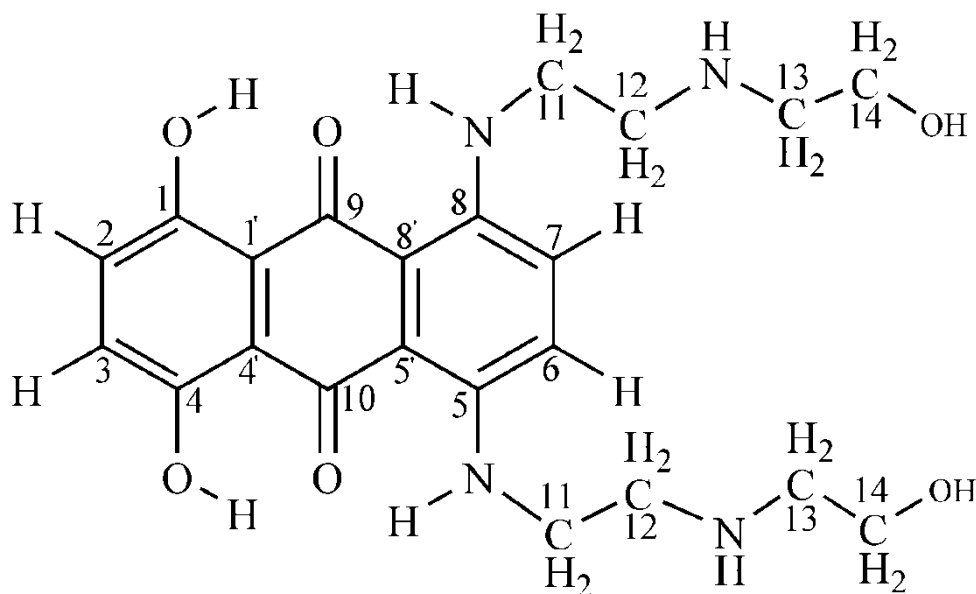


Fig. 1.22: Structure of mitoxantrone.

1.6 Structure and Interaction of mitoxantrone with nucleic acids

MTX is basically a 1,4-dihydroxy-5,8-bis[2-[(2-hydroxyethyl)amino] ethyl]amino]-9,10-anthracenedione (**Fig. 1.22**) that have three planar aromatic rings which aids in its intercalative binding to DNA while with two cationic side chains that facilitate its interaction towards groove. Presence of ethyldiamine substituents in side chains and 1,4-OH group on the aromatic nucleus are responsible for its activity and efficacy (Murdock *et al.*, 1979; Bailly *et al.*, 1996). It has two characteristic absorption bands of MTX at λ_{\max} 610 and 662 nm owing to the hydrogen bonding and charge transfer of these two substituents to the anthraquinone ring (Kapusinski *et al.*, 1981; Lee and Dutta, 1989).

The 662 nm band of MTX is sensitive to the MTX concentration and pH. MTX aggregates at higher concentration of drug and pH beyond 7 due to the deprotonation of $-\text{NH}$ groups on the side chains (Enache and Volanschi, 2010). MTX is a symmetrical compound and formation of dimer or higher order aggregates is marked by the stacking of aromatic chromophore and formation of intermolecular hydrogen bonds between 11NH and 1,4OH groups (Davies *et al.*, 1999). Self-aggregation of mitoxantrone can easily be identified by NMR experiments (NOESY experiments). Presence of intermolecular NOEs between 11 NH-2/3 H, 11 CH₂-2/3 H, 6/7 H-2/3 H reveals the existences of head to tail dimer of MTX.

Several biophysical studies along with *in vitro* assays were carried out on the interaction of MTX with natural and synthetic DNA in order to gain insight into its mechanism of action. MTX has shown some specificity towards CG sites and its aromatic chromophore intercalates in a perpendicular mode along the DNA axis while the side chains interact with the major

grooves (Lown *et al.*, 1985a; Islam *et al.*, 1985). This fact is also supported by a kinetic study conducted by Krishnamoorthy *et al.*, where mitoxantrone shows the slower dissociation rate from poly d(G–C)₂ than poly d(A–T)₂ driven by SDS. MTX interact with CG rich tetra and hexanucleotides sequences in 1:1 and 2:1 stoichiometry, respectively, revealed by NMR spectroscopy (Lown *et al.*, 1985b; Kotovych *et al.*, 1986).

Binding of mitoxantrone to DNA results in red shift of 662 nm and 610 nm absorption bands accompanied by hypochromicity, which is an indicative of intercalative interaction. This red shift is owing to the inaccessibility of MTX chromophore to form an H-bond with solvent water. MTX also shows a dual mode of interaction with duplex DNA that occur via both partial intercalation and groove binding (Lown *et al.*, 1985a; Bowden *et al.*, 1985) with high affinity.

The interaction of MTX with hairpin structures and RNA is different to that of DNA. There are only two NMR reports on the binding of MTX to hairpin (d-(GCGAAGC) (Kostjukov *et al.*, 2007) and tau pre m-RNA (Zheng *et al.*, 2009). Binding of MTX results in the stabilization of stem loop of tau pre m-RNA while it shows the external stacking in case of hairpin structure. Such binding plays an important role in modulating the RNA activity and hence its role in certain diseases. It will be quite interesting to know the interaction of MTX with non-canonical structures like G-quadruplexes whose modulation results in the inhibition of telomerase activity.

1.7 Flavonoids

Flavonoids are dietary plant derived polyphenols, which are ubiquitously present in various parts of plant like fruits, leaf, flower, seeds, nuts, grains and vegetables. Apart from these locations they are also present in spices, various medicinal plants and beverages like tea, wine (Kuhnau, 1976; Middleton, 1998; Beecher, 2003). They also impart colors to flowers, fruits and leaves (Brouillard and Cheminat, 1988). Research on flavonoids began in 1930 with the identification of the flavonoid rutin, which was isolated from oranges. Previously this substance was referred as vitamin P and till date more than 8000 flavonoids have been discovered (Ranaud and de Lorgeril, 1992; De Groot and Raven, 1998). Much attention on flavonoids were sought with the discovery of French paradox, i.e., where there is an inverse relation between the incidence of coronary heart disease and consumption of red wine and saturated fats (Ranaud and de Lorgeril, 1992).

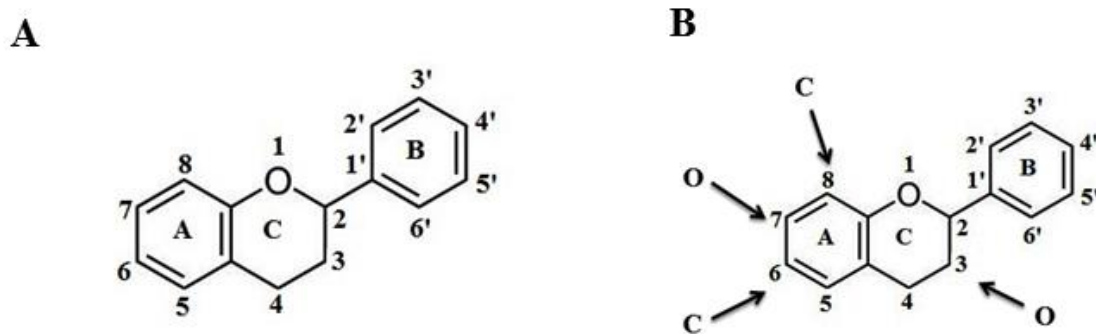


Fig. 1.23: (A) Basic structure of flavonoid and (B) its glycosylation sites.

Flavonoids are generally present in the form of glycosides apart from aglycone, methylated, acylated and sulphate forms (Stobiecki *et al.*, 1999; Iwashina, 2000; Cuyckens *et al.*, 2003). The glycosylation is responsible for the solubility of flavonoids in water, protection against cytoplasmic damage and hence it is easily stored in cell vacuoles (Justesen *et al.*, 1998)

1.7.1 Structure and classification

Flavonoids have a common phenylbenzopyran (C₆-C₃-C₆) carbon framework consisting of two benzene rings (A and B) and a heterocyclic pyran ring (C) (**Fig. 1.23A**), which are synthesized via the phenylpropanoid pathway (Ferreyra *et al.*, 2012). They are classified on the basis of the oxidation and unsaturation of C ring along with the attachment of the B ring to C ring carbon (Hughes *et al.*, 2001) (**Table 1.5**). Mostly B ring is attached at the second carbon of the C ring, e.g. flavones, flavanols while in case of isoflavones it is attached at the third carbon of C ring. When the B ring is linked at fourth carbon it is referred as neoflavonoids. On the above basis flavonoids are classified into various subgroups such as flavones, flavonols, flavanols, Flavanones, Flavanonol, Isoflavones, anthocyanidins, neoflavonoids, chalcones and aurones (Winkel-Shirley, 2001).

Further, within an individual subgroup division occur on the basis of the number and nature of substituents on the rings, which is basically hydroxylation and glycosylation (**Fig. 1.23B**) (Robards and Antolovich, 1997). Hydroxylation usually occurs at 3, 5, 7, 3', 4' and 5' positions. Glycosylated form is more prevalent in plants, which is basically of two types O-glycosides and C-glycosides. In case of O-glycosides sugar is bound to the -OH of aglycone while in case of C-glycosides, it is directly bound to the carbon of aglycone. The most favoured glycosylation sites for O-glycosides are 3 or 7 -OH group and that of C-glycosides are 6 or 8 carbon (Fig. 21B) (Rijke *et al.*, 2006; Cavaliere *et al.*, 2005). The commonly involved sugars are glucose,

galactose, rhamnose, arabinose along with some other higher saccharides like rutinose and neohesperidose (Middleton, 1984; Robards et al., 1997). In some case of flavonoids the acylated derivatives of glycosides are also present.

1.7.2 Dietary intake and metabolism of flavonoids

Flavonoids are usually present in our daily diet owing to its presence in various food sources such as fruits, vegetables, tea, red wine, various medicinal plants, etc. (**Table 1.6**) (Larson, 1988; Cook and Samman, 1996). Its daily intake depends upon the type of food consumed worldwide and is generally greater than that of vitamin C, vitamin E and carotenoids. Its average intake is 50 and 800 mg/day. Flavonols followed by flavones and soya isoflavones are the major flavonoids present in food. Out of the total flavanols and flavones intake of 23 mg/day quercetin, a flavonol constitute 16 mg/day (Heim et al., 2002). Level of flavonoids also varies depending upon preparation and processing of food. In some cases its level decreases upon processing (Gil-Izquierdo et al., 2001). The metabolism and absorption of flavonoids depend upon its structure, size, solubility and other properties. It is prominently present in the form of flavonoid glycosides in various plants and food (Williamson, 2004) except catechins.

Aglycones and flavonoid glucosides are readily absorbed in the small intestine and further metabolized to methylated, glucuronidated, or sulphated form (Manach *et al.*, 2004) while flavonoid glycosides goes to the colon, where they are converted to aglycan form by colon bacteria (Hollman *et al.*, 1999), which aid in their metabolism and absorption. Bioavailability of various flavonoids varies and it's generally low owing to its limited absorption and rapid elimination. Quercetin is also an example of flavonoid, which possess this problem. In rder to probe this problem Govil *et al.*, have studied the interaction of quercetin with a model membrane DPPC. Formation of H-bonds between polar head group of membrane and hydroxyl groups of quercetin is the reason for its lack of membrane permeability. The most available flavonoid is isoflavones.

1.7.3 Biological activities of flavonoids

Flavonoids show many beneficial effects both in plant and animal kingdoms and their biological activities (**Fig. 1.24**) are directly related to their structural properties. Most of their activities lie owing to its antioxidant nature as well as modulator of certain enzymes involved in the cell-signaling pathways. Presence of planar aromatic rings as well as hydrogen bonding capacities due to –OH groups facilitates their binding to proteins and DNA. Apart from duplex DNA studies flavonoids were also known to bind to the G-quadruplex structures and in some

case it induces the formation and stabilization of G-quadruplex structure, which indicates flavonoids as potent G-quadruplex ligands (Jin *et al.*, 2009; Jin *et al.*, 2010). Furthermore, flavonoids exhibit wide range of biological activities such as anti-oxidant, anti-microbial, anti-inflammatory, anti-cancer, hepatoprotective etc (Rice-Evans *et al.*, 1996; Cushnie and Lamb, 2005; Mishra *et al.*, 2013; Middleton and Kandaswami, 1992; Davis and Matthew, 2000).

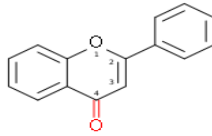
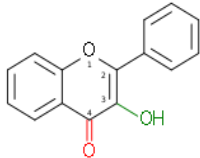
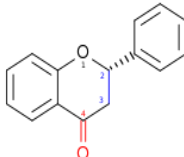
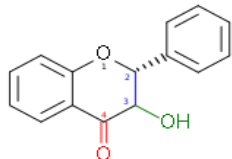
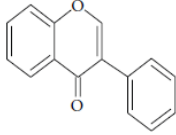
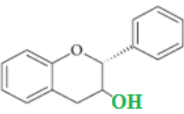
Group	Description	Skeleton		Structural formula	Examples
		Functional groups			
		3-hydroxyl	2,3-dihydro		
Flavone	2-phenylchromen-4-one	no	no		Luteolin, Apigenin Chrysin
Flavonol or 3-hydroxyflavone	3-hydroxy-2-phenylchromen-4-one	yes	no		Quercetin, Kaempferol, Myricetin
Flavanone	2,3-dihydro-2-phenylchromen-4-one	no	yes		Hesperetin, Naringenin,
Flavanonol or 3-Hydroxyflavone	3-hydroxy-2,3-dihydro-2-phenylchromen-4-one	yes	yes		Taxifolin
Isoflavone	3-phenylchromen-4-one	no	no		Genistein, Daidzein, Glycitein
Flavan-3-ol	2-phenyl-3,4-dihydro-2H-chromen-3-ol	yes	yes		Catechin Epicatechin

Table 1.5: Classification of flavonoids.

Class	Flavonoid	Dietary source	References
Flavanol	(+)-Catechin (-)-Epicatechin Epigallocatechin	Tea	Lopez <i>et al.</i> , 2000
Flavone	Chrysin, apigenin Rutin, luteolin, and luteolin glucosides	Fruit skins, red wine, buckwheat, red pepper, and tomato skin	Hara <i>et al.</i> , 1995; Kreft <i>et al.</i> , 1999; Stewart <i>et al.</i> , 2000.
Flavanol	Kaempferol, quercetin, myricetin, and tamarixetin	Onion, red wine, olive oil, berries, and grapefruit.	Stewart <i>et al.</i> , 2000.
Flavanone	Naringin, naringenin, taxifolin, and hesperidin	Citrus fruits, grapefruits, lemons, and oranges	Rousseff <i>et al.</i> , 1987; Miyake <i>et al.</i> , 2000.
Isoflavone	Genistin, daidzin	Soyabean	Reinli and Block, 1999.
Anthocyanidin	Apigenidin, cyanidin	Cherry, easberry, and strawberry	Hertog <i>et al.</i> , 1992; Stewart <i>et al.</i> , 2000.

Table 1.6: Dietary sources of flavonoids.

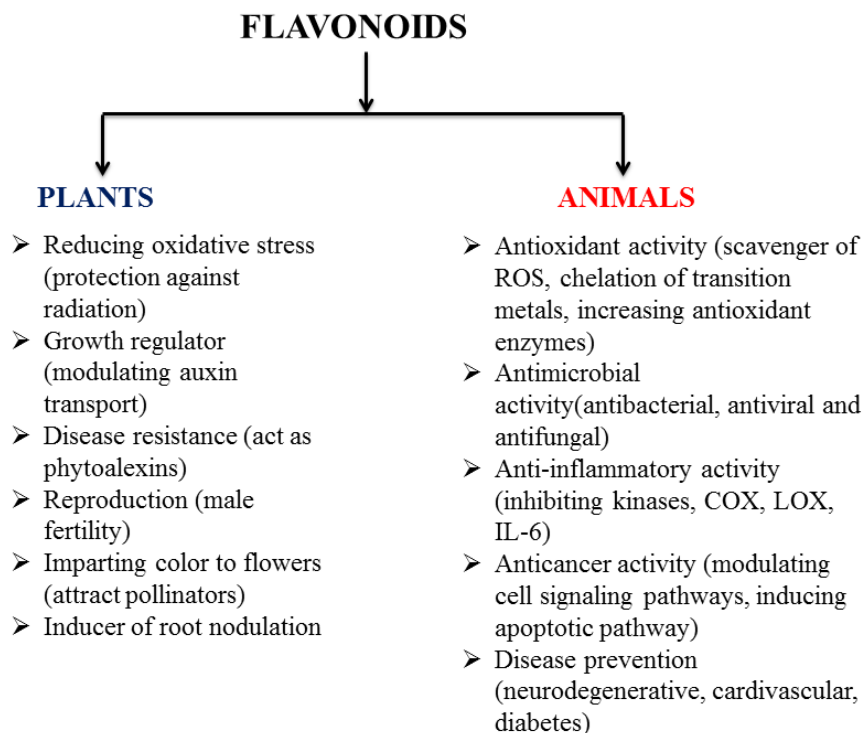


Fig. 1.24: Biological activities of flavonoids.

1.7.4 Interaction of flavonoids with DNA

Numerous studies exist that explain the mode of interaction of flavonoids with duplex, triplex and quadruplex DNA molecules. The first report of flavonoid binding to DNA structure was of quercetin binding to calf thymus DNA (Alvi *et al.*, 1986). Melting studies showed that quercetin stabilizes the DNA by about 4°C. Quercetin and luteolin are the two the most widely studied flavonoids, which binds duplex DNA by intercalation or external binding (Solimani *et al.*, 1995; Chowdhury *et al.*, 2002). In order to investigate the mode of binding of flavonoid with duplex DNA Nerdal *et al.*, used NMR spectroscopy. They have shown the interaction of flavonoid glycoside kampeferol 7-O-neohesperdioside (K7-neo) with *E. coli* lac promoter containing dodecamer sequence d-(GCGTATGTTGCG). The presence of sequential connectivities between base H8/H6 with sugar H1'/H2'/H2'' excludes the intercalative mode of binding. Later on the basis of NOE connectivities between K7-neo aglycone protons H3' and H5' with the A5 H1' of DNA showed minor groove binding. The binding was stabilized by the formation of H-bond between the hydroxyl groups of K7-neo with DNA bases and phosphate group. Wan *et al.*, used ESI-MS technique to investigate the binding of flavonoids (both aglycone and glycosides) with triplex-DNA. The results revealed that the binding of flavonoids to triplex-DNA is governed by the position of hydroxyl groups, saccharide on aglycone skeleton. Flavonoid glycosides exhibit higher binding affinities towards the DNA triplexes than their aglycone counterparts. Reports are also available on the interaction of flavonoids with quadruplex-DNA.

The first report on the interaction of flavonoid with quadruplex DNA was reported by Sun *et al.*, in 2006. They studied the interaction of quercetin with monomeric and dimeric G-quadruplexes using absorption, fluorescence, CD and one dimensional NMR spectroscopy. The UV-visible study showed a red shift in the 371 nm absorbance band of quercetin upon interaction with both the quadruplexes. The fluorescence intensity increased upon binding to quadruplex but the increase in the intensity was different for both the quadruplexes. Based on the ¹H NMR and CD studies, it was predicted that the quercetin bind to monomeric form of G-quadruplex structure through end-stacking mode while that of dimeric G-quadruplex structure through groove binding.

Similar studies were conducted by Sun *et al.*, for rutin, but they have chosen blunt ended (d-(TTAGGG)₄, d-(TTAGGGG)₄) and interlocked (d-(GGGT)₄) quadruplexes. Upon

interaction with G-quadruplex structure, a red shift (bathochromic shift) in the 356 nm absorption band of rutin was observed and there was an increase in the fluorescence intensity. The bathochromic shift and increase in emission intensity was more for blunt end stacked d-(TTAGGG)₄ and d-(TTAGGGG)₄ structures when compared to interlocked d-(GGGT)₄ G-quadruplex structure. The proton NMR studies showed that the addition of rutin results in the decomposition of blunt end stacked G-quadruplex structures to its monomer form. The imino proton resonance of terminal G-quartet residue in d-(TTAGGG)₄ and d-(TTAGGGG)₄ structures show upfield shift, but the terminal imino proton resonances of interlocked d-(GGGT)₄ sequence show no shift in position. These results clearly explain that rutin binds to terminal G-quartet via stacking interaction.

Apart from the above mentioned flavonoids, daidzin, an important isoflavone present in soy compounds also shows the stabilization of G-quadruplex structure (Li *et al.*, 2006). ESI-MS studies showed that daidzin interacts with human telomeric antiparallel G-quadruplex structure dAG₃(T₂AG₃)₃ under molecular crowding condition in the stoichiometric ratio of 1:2. The electrophoretic mobility shift assay also confirmed the formation of daidzin-d[AG₃(T₂AG₃)₃] complex. Based on the docking and CD thermal melting studies, it was revealed that the daidzin-quadruplex complex was stabilized through π - π stacking interaction and H-bonding interactions that result between daidzin and quadruplex bases.

The knowledge that isoflavones acts as G-quadruplex ligands were also supported by the work of Zhang *et al.*, 2009. The interaction of isoflavones daidzein and genistein and their glycoside form daidzin and genistin, with human G-quadruplex sequence d[AG₃(T₂AG₃)₃] and its related duplex DNA were studied through spectroscopic techniques like UV-vis, fluorescence, CD, ESI-MS and molecular modeling. The study revealed that isoflavones stabilizes the quadruplex structure while they destabilized their related duplex-DNA.

Sengupta *et al.*, showed the interaction of medicinally important plant flavonoid fisetin with unimolecular DNA sequence d(T₂AG₄)₄ using spectroscopic and chromatographic studies. The result showed the binding of fisetin in the hydrophobic region of quadruplex loop, which results in an increase in its average fluorescence life time. These preliminary results indicate fisetin to be a prospective candidate as a quadruplex ligand.

1.8 Luteolin as an anticancer and chemotherapeutic agent.

Luteolin is best known flavonoid, which has shown anticancer activity both *in vitro* and *in vivo* (Seelinger *et al.*, 2008; Lin *et al.*, 2008). It targets a wide range of cancers mediated by radiation, ROS, hormones, carcinogens etc. Its anticancer property is related to its antioxidant

and anti-inflammatory properties. Daily intake of luteolin containing food reduces the incidence of cancer and also the formation of carcinogens (such as amines, nitroso compounds, etc.) in food. It also shows radioprotective activity by reducing the damage due to ionizing radiation (Shimoi *et al.*, 1994).

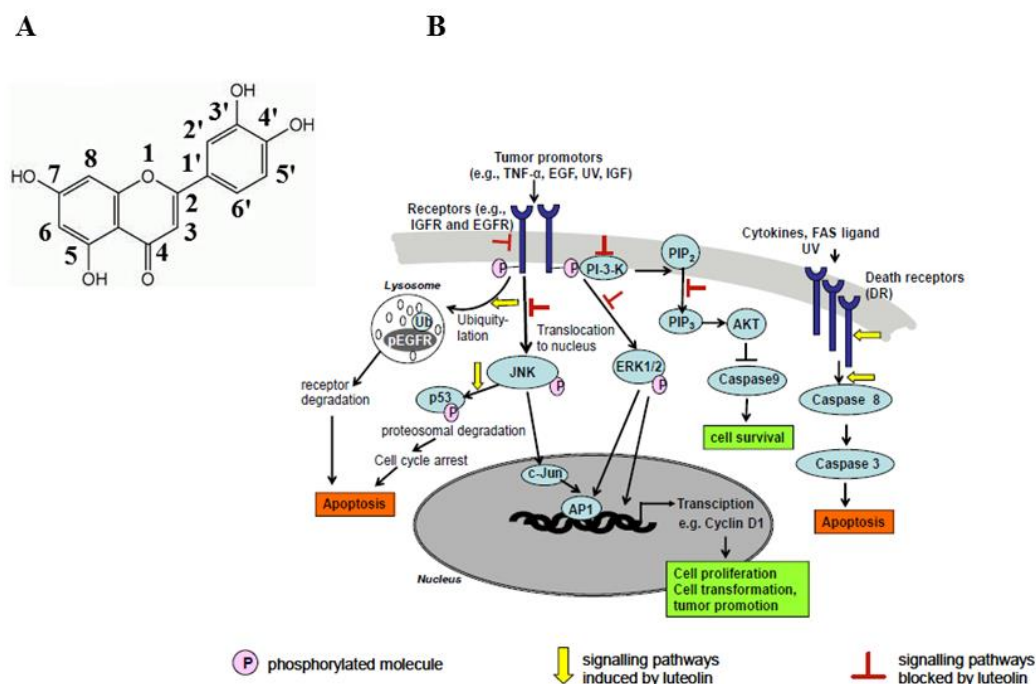


Fig. 1.25: (A) Structure of luteolin and (B) modulation of cell-signaling pathways by luteolin.

There are many mechanisms which show its cancer chemo-preventive activity the best being the modulation and inhibition of cell-signalling pathways that is responsible for the proliferation, angiogenesis, apoptosis etc., which is shown in **Fig.1.25**. It not only shows the inhibition of topoisomerase I and II, but also sensitizes cancer cells towards apoptosis mediated by TNF (Chowdhury *et al.*, 2002; Shi *et al.*, 2004). These properties show the therapeutic potential of luteolin, which can work in accordance with other well-known anticancer agents.

1.9 Structural and pharmacological properties of Luteolin

Luteolin, 3', 4', 5, 7-tetrahydroxyflavone and its glycosides are widely distributed in many botanical families and the most common source of it is artichoke, thyme, pepper, celery, etc. Luteolin is characterized by the presence of catechol moiety at "B" ring, two -OH groups at 5 and 7 positions on "A" ring and a double bond (2-3 position) in conjugation with a 4-keto group in the "C" ring. The "A" and "C" rings are planar while the "B" ring is flexible. Luteolin is present in both aglycone and glycosides form, most commonly being O-glycosides (e.g.

cynaroside) together C-glycosides (e.g. oreintin). O-glycosylation preferably occur at 7th position on A ring while that of C-glycosylation at 6 and 8 positions. The structure of the luteolin has been characterized using various experimental and theoretical techniques (Cox *et al.*, 2003; Owen *et al.*, 2003; Leopoldini *et al.*, 2004), which shows that it forms both intramolecular and intermolecular hydrogen bondings. Intramolecular hydrogen bonding occurs between C5-OH group of the “A” ring and 4-oxo group in the “C” ring while the OH groups at “B” ring and C7 are involved in intermolecular hydrogen bondings. Spectral characteristic of luteolin is due to the “A” and “B” ring and various substitutions over it. Luteolin has two major absorption bands: band I at 349 nm signify absorption due to ring B and that at 258 nm band II mark the absorption owing to ring the ring “B” (Kumar and Pandey, 2013). Since the band II overlap with that of DNA absorption band changes in luteolin upon binding can easily be made by monitoring band I.

Most of the activities of luteolin including its antioxidant property are due to the presence of an *ortho*-catechol moiety at the “B” ring and double bond (2-3 position) in conjugation with a 4-oxo group in the “C” ring. “A” and “C” rings are planar while the “B” ring is flexible. Luteolin has many health benefits and has been used in traditional medicines for a long time owing to its pharmacological properties like antioxidant, anti-inflammation, anti-allergy and anticancer (Lopez-Lazaro, 2009; Brown *et al.*, 1998; Ueda *et al.*, 2002; Seelinger *et al.*, 2008; Lin *et al.*, 2008).

1.10 Binding of luteolin to proteins and DNA

Luteolin interaction with macromolecules occurs due to the presence of aromatic rings and hydrogen bonding capabilities. Binding of luteolin depends upon the pH of the solution and with increasing the pH towards an alkaline condition results in an increase in binding. Binding studies of luteolin with both proteins (e.g. BSA and HSA) and DNA were reported. Binding of luteolin to BSA was studied by Yang *et al.*, using spectrophotometric techniques like CD, fluorescence spectroscopy. The result showed that upon binding the fluorescence emission of BSA was quenched by luteolin and the quenching mechanism was static. The binding occurs in 1:1 stoichiometry with a binding constant of 10^5 . The forces involved in the binding were mainly hydrophobic interactions and hydrogen bonding. Luteolin has also been reported to inhibit the activity of *mdr* transporter protein. The inhibition was due to the binding of polar group of luteolin (C-5, C-4, and C-3') to the ATP binding domains of protein (Nissler *et al.*, 2004). Similarly the binding of luteolin with calf thymus DNA was also determined by Zhang *et al.*, using absorption spectroscopy, fluorescence spectroscopy and viscosity measurements.

The result showed that luteolin binds to CT DNA with high affinity with a binding constant of $4.52 \times 10^4 \text{ L/mol}^{-1}$. The binding mode is basically intercalative, which is proved by several facts like the binding constant, increase in viscosity upon binding, displacement of acridine orange. The forces involved in the binding are hydrophobic interactions and hydrogen bonding. On contrary to the study of Zhang *et al.*, Bi *et al.*, proved groove binding of luteolin to fish sperm DNA. In an attempt to determine the binding of flavonoid aglycones and glycosides to duplex DNA Wang *et al.*, used ESI-MS technique, which showed that the presence of 4'-OH is necessary for binding to DNA while the presence of sugars at A and B rings increases the binding to duplex DNA over their aglycone counterpart. An intercalative mode of binding was suggested for flavonoid aglycones. Presence of tertiary amines and substitution of sulfur atom with an oxygen atom enhance the potency of flavonoid derivatives towards DNA binding (Ragazzon *et al.*, 2009). However, no such interaction studies for luteolin have been reported with G-quadruplex.

1.11 Scope of thesis

Guanine rich sequences are located in many biologically significant regions of the genome such as telomere, gene promoter regions of important proto-oncogenes, immunoglobulin switch regions, 5' untranslated regions (UTRs) of many mRNAs and other sequences associated with human diseases have the ability to adopt a four-stranded structure known as G-quadruplex. Formation and stabilization of quadruplex structures within these regions regulates several physiological and pathological processes. For example formation of quadruplex structure within the telomeric region interferes with telomerase activity, and their formation within the oncogenes regulates their gene expression in majority of cancer cells that is responsible for cell immortality. Inducing the formation and enhancing the stability of G-quadruplex in the telomeric region of human chromosome with small ligands is considered to be a prominent strategy for telomerase inhibition. This has led to structure-based drug designing of molecules specific to G-quadruplex that can act as a potential target for broad-spectrum anticancer therapies (Han and Hurley, 2000). Several families of ligands have been evaluated for telomerase inhibition but lack of structural data of G-quadruplex-Ligand complexes has restricted their therapeutic applications. The present thesis presents deep insights into the structural interactions of human G-quadruplex forming telomere single repeat sequence d-(TTAGGGT) with a luteolin (flavonoid) and MTX-mitoxantrone, (a synthetic anthraquinone derivative), and *Tetrahymena* G-quadruplex forming telomere single repeat sequence d-(TTGGGGT) with a luteolin. The structural characterization of *Tetrahymena* G-quadruplex

with MTX has been characterized in our lab previously (Pradeep *et al*, Manuscript under preparation). Both the sequences form right handed parallel stranded G-quadruplexes in presence of K⁺ ion with anti glycosidic torsion angles. Both luteolin and mitoxantrone have planar aromatic ring systems, which can easily interact with the planar surface of G-quartet and the presence of cationic side chains and hydroxyl group aid in its interaction to the grooves of quadruplexes. Till date not a single X-ray crystal/NMR structure is available on G-quadruplex structures with anthraquinone derivatives and flavonoid complexes. The binding interactions of telomeric G-quadruplex sequences with these ligands were studied by various biophysical techniques such as; absorption, fluorescence, circular dichroism (CD) and nuclear magnetic resonance. They provide insights into the affinity, stability and stoichiometry of the G-quadruplex-ligand complex. Further, structural elucidation of ligand-G-quadruplex complex was obtained using nuclear magnetic resonance (NMR) techniques in combination with restrained molecular dynamics (rMD) simulations.

Finally, TRAP assay reactions were carried out with these ligands to assess their ability towards telomerase enzyme inhibition, which in turn can throw light about their anticancer property. In a nutshell, these studies provided thought provoking insights into the structure-function paradigm of quadruplex-ligand interactions and highlighted their biological significance. Henceforth, these results can facilitate a rational structure-based drug design approaches in order to synthesize novel therapeutic molecules that can specifically interact with G-quadruplexes, and regulate telomerase inhibition to avoid cancer cell progression.

Materials and methods

This chapter deals with the materials and experimental techniques involved in studying the interaction of G-quadruplex forming oligonucleotides with ligands, which are potentially of pharmaceutical interest. Spectroscopic techniques such as absorption, fluorescence, circular dichroism (CD) and nuclear magnetic resonance were used to give insight about the affinity, stoichiometry and structure of G-quadruplex-ligand complex. Telomere Repeat Amplification Protocol (TRAP) assay was done to check the ability of these ligands to inhibit telomerase enzyme, which in turn can give an idea about their anticancer property.

2.1 Chemicals and reagents

The desalted oligonucleotide d-(TTAGGGT), d-(TTGGGGT), mitoxantrone hydrochloride (MTX), luteolin, deuterium oxide (D₂O), dimethyl sulphoxide (DMSO) with isotopic purity 99.96 %, 3-(Trimethylsilyl) propionic-2,2,3,3-d₄ sodium acid salt (TSP) used as internal reference for NMR were purchased from Sigma Chemical Co., USA. Chemicals like di potassium hydrogen phosphate (K₂HPO₄), potassium chloride (KCl) and ethylene diamine tetra acetic acid (EDTA) etc. used for phosphate buffer preparation were purchased from Merck. TRAPeZe XL Telomerase Detection Kit (S7707) used for TRAP assay was supplied by Merck Millipore. Mitoxantrone, luteolin and DNA sequences were used without further purification.

2.1.1 Buffer used in experiments

All the spectroscopic experiments were performed in 20 mM KBPES buffer (pH 7.0) containing 100 mM KCl, 10 mM K₂HPO₄ and 1 mM EDTA. 100 mM KCl was required for the formation of parallel stranded quadruplex and the presence of EDTA suppress paramagnetic impurities responsible for line broadening in NMR experiments. All the experiments except melting studies were conducted at 25°C.

2.2 Absorbance measurements

2.2.1 Sample preparation

The oligonucleotide sequence d-(TTAGGGT) was dissolved in 20 mM KBPES buffer (pH 7.0), and heated at 90 °C for 5 minutes and was allowed to cooled overnight at room temperature. The sample was stored at 4°C and shaken gently at regular intervals to ensure its homogeneity. The concentration of oligonucleotide sequence and MTX were determined spectrophotometrically at λ_{max} 256 nm (per strand $\epsilon = 69800 \text{ M}^{-1} \text{ cm}^{-1}$) and λ_{max} 659 nm ($\epsilon = 20900$

$M^{-1}cm^{-1}$) (Babayan *et al.*, 1998), respectively using the Beer Lambert's law.

$$A = \epsilon.c.l$$

Where,

A= Absorbance

c = Concentration of solution (in moles/ liter)

ϵ = Molar extinction coefficient (in $M^{-1}cm^{-1}$)

l = Path length of quartz cuvette (in cm)

The stock solution of MTX was prepared by dissolving 1 mg of MTX into 1 mL of KBPES buffer (pH 7.0).

2.2.2 Methodology

Absorbance measurements were recorded on CARY-100 Bio-spectrophotometer (Varian, USA) equipped with a Peltier thermostatic cell holder using quartz cuvette with optical path length of 1 cm. This is the most common and simplest technique (**Fig. 2.1**) used for the qualitative and quantitative measurements of quadruplex-ligand interaction. Any compound absorbs a particular wavelength of light depending upon the presence of chemical group/chromophore on it. DNA due to presence of conjugated rings shows absorption in the range of 200-260 nm while most of ligands show absorption in the visible range. In order to get an idea about the interaction between G-quadruplex and ligand the maximum peak position (λ_{max}) of ligand was monitored in the absence and presence of G-quadruplex sequence. The extent of binding was determined by the magnitude of this shift. Titration experiments were conducted to get information regarding binding constant and stoichiometry. For titration studies the concentration of MTX was kept constant (3 μM) and the quadruplex sequence was added progressively from stock solution into it in order to achieve Drug to quadruplex Nucleotide (D/N) ratio ranging from 0.08 to 6.7. The samples were incubated for one hour at 25 °C and the spectra were recorded in the wavelength range of 200 nm to 800 nm. The absorbance obtained at $\lambda_{max} = 659$ nm was used to calculate the intrinsic binding constant since it's more sensitive to the change in mitoxantrone concentration and DNA doesn't have any absorbance in this region, using the following equation (Benesi and Hildebrand, 1949):

$$\frac{[DNA]}{\epsilon_a - \epsilon_f} = \frac{[DNA]}{\epsilon_b - \epsilon_f} + \frac{1}{K(\epsilon_b - \epsilon_f)} \quad \dots\dots\dots (1)$$

where [DNA] = N, the concentration of d-(TTAGGGT)₄, K is the equilibrium constant for binding, ϵ_a is the apparent extinction coefficient obtained by calculating ratio of observed absorbance of drug-DNA complex to the drug concentration ($A_{obs}/[D]$), ϵ_f corresponds to the

extinction coefficient of the drug in its unbound form and ϵ_b refers to the extinction coefficient of drug in bound form. The binding constant K was obtained from the intercept-to-slope ratios of the plot of $[\text{DNA}]/\epsilon_d - \epsilon_f$ vs. $[\text{DNA}]$.

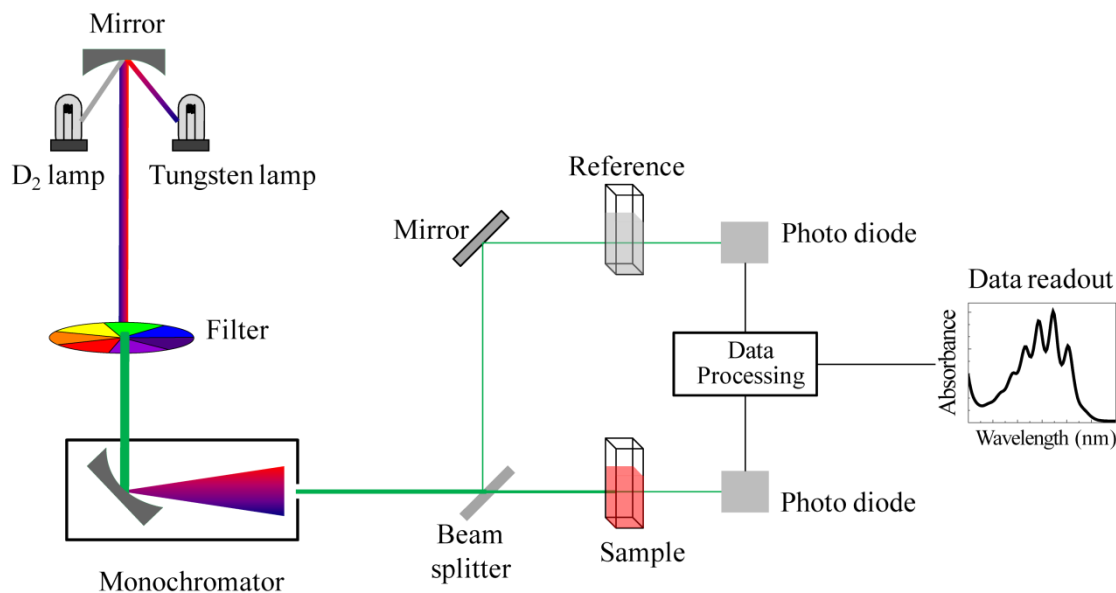


Fig. 2.1: Schematic representation of UV-visible spectrophotometer.

2.3 Steady State and Life Time Fluorescence Measurements

2.3.1 Steady State measurements

2.3.1.1 Sample preparation

To reduce the error due to changes in sample condition the fluorescence emission spectra were recorded for the samples used in absorbance measurements. The result thus obtained depends upon the sensitivity of the technique used.

2.3.1.2 Methodology

Fluorescence experiments were performed on “Fluorolog-3 Spectrofluorimeter LS55” (make HORIBA JobinYvonSpex®) using 1 cm path length quartz cuvette polished on all the four sides of a right angle beam path. The samples were excited using the excitation wavelength (λ_{exc}) of 609 nm with emission in the wavelength range of 630 to 750 nm. Fluorescence spectroscopy is very sensitive to the change in the environment of drug chromophore. Most of the ligands exhibit fluorescence due to presence of aromatic rings and function groups present on it. Such compounds when excited at a particular wavelength emit light in the form of fluorescence (**Fig. 2.2; Fig. 2.3**). Since the intrinsic fluorescence of G-quadruplex sequence is too low to be detected the fluorescence property of mitoxantrone was used to monitor the

changes upon interaction with quadruplex sequence d-(TTAGGGT)₄. Free mitoxantrone exhibits fluorescence emission (λ_{em}) at 677 nm when excited at 609 nm. Wide range of interaction affect emission spectrum as this process occur at a slower time scale (10^{-8}) and both shift and shape of the band give information about the binding mode and orientation of ligand, which can be measured by fluorescence quenching (**Fig. 2.2**). The fluorescence quenching constant, K_{sv} , was evaluated using Stern-Volmer equation [Lakowicz, 2006]:

$$F_0/F = 1 + K_{sv} [\text{DNA}] \quad \dots\dots\dots (2)$$

Where F_0 and F are the intensity of fluorescence in the absence and presence of DNA, respectively, and K_{sv} is the Stern-Volmer quenching constant, which is a measure of quenching efficiency of DNA. K_{sv} was obtained from the slope of the plot of F_0/F vs. [DNA] using titration data. Depending upon the quenching mechanism binding constant and stoichiometry can be calculated.

When quenching phenomenon is static and the ligand binds to independent equivalent sites the binding constant K_b and binding stoichiometry (n) of the complex can be determined using the following equation (Liu *et al.*, 2012):

$$\log [(F_0 - F)/F] = \log K_b + n \log [Q] \quad \dots\dots\dots (3)$$

Where quencher concentration $[Q] = [\text{DNA}] = N$, K_b is the binding constant and n is number of ligands binding to DNA. Plot of $\log [(F_0 - F)/F]$ vs. $\log [\text{DNA}]$ yielded K_b and n .

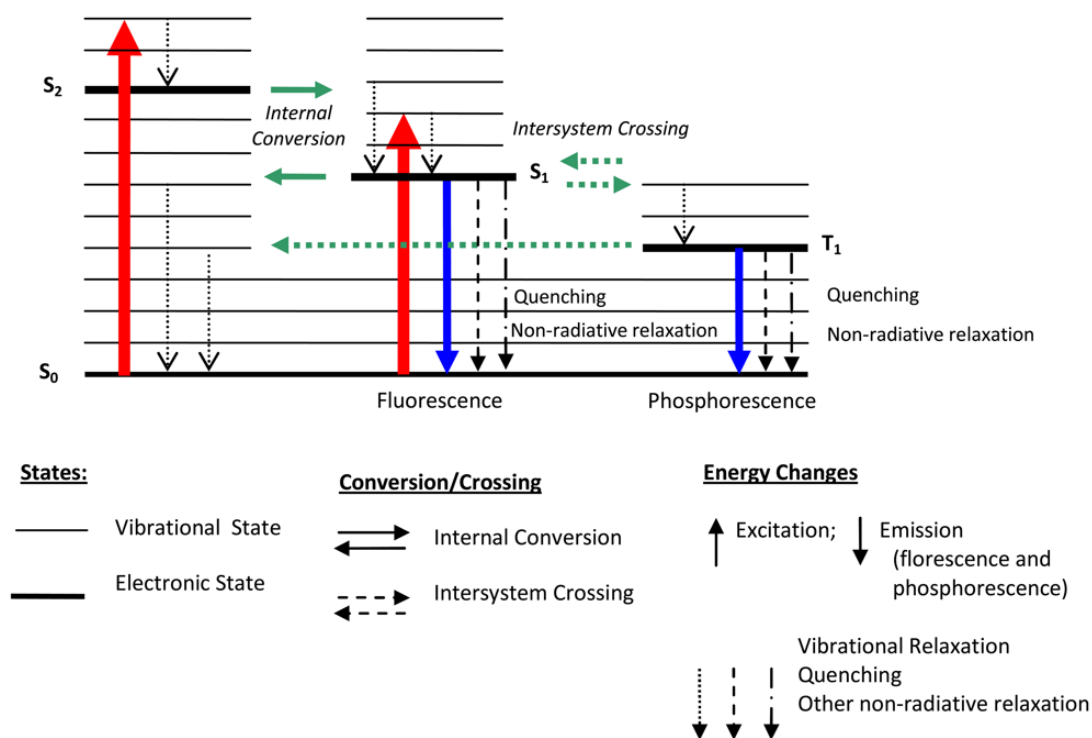


Fig. 2.2: Jablonski diagram showing the phenomena of fluorescence and phosphorescence.

2.3.1.3 Continuous Variation Analysis (Job plot)

Binding stoichiometry through fluorescence can also be determined by the method of continuous variation (Job plot) [Job, 1928; Huang, 1982]. In this method the total concentration of DNA and MTX were held constant (3 μM) but their relative mole fractions were varied. The fluorescent intensity was measured at a wavelength of $\lambda_{em} = 677$ nm using $\lambda_{exc} = 609$ nm. The difference in fluorescence intensity ($\Delta F = F - F_0$) of free MTX and its complex with d-(TTAGGGT)₄ was plotted versus the mole fraction of MTX. The inflection point gives the mole fraction of the MTX bound to d-(TTAGGGT)₄. The binding stoichiometry of MTX was obtained from $n = [(1 - \chi_{\text{ligand}}) / \chi_{\text{ligand}}]$, where n is the number of binding sites and χ_{ligand} is the mole fraction of ligand (MTX) at the intersection points of the two slopes obtained.

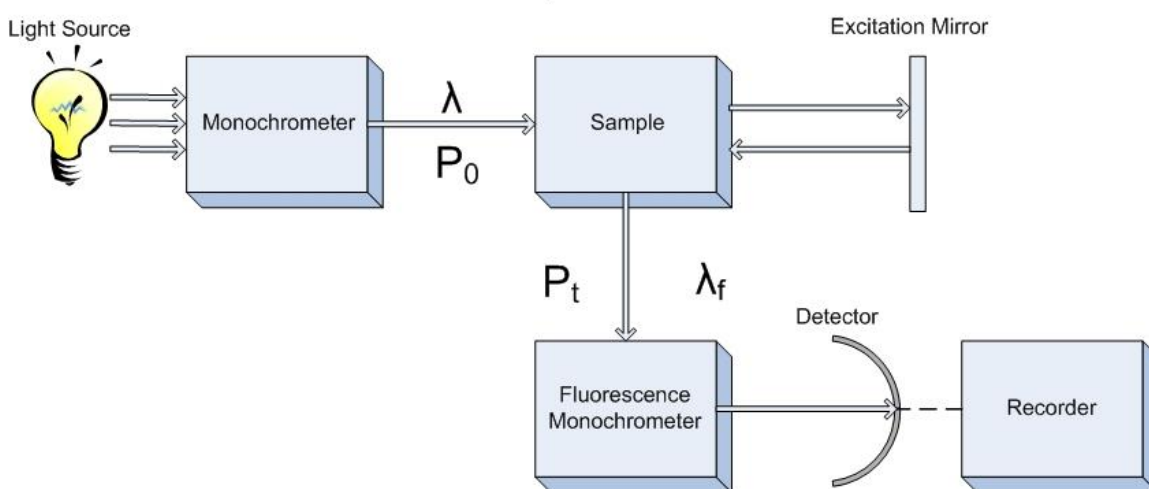


Fig. 2.3: Schematic representation of spectrofluorometer.

2.3.2 Life Time Measurements

2.3.2.1 Sample preparation

For this study mitoxantrone concentration was kept constant (3 μM) and quadruplex sequence was added to make a final volume of 1 ml sample of different D/N ratios 0.5, 1.0, 1.5 and 2.0.

2.3.2.2 Methodology

Time resolved fluorescence measurements were performed using FluoroLog®-TCSPC, (make HORIBA Jobin Yvon Spex®) using a 10 mm path length quartz cuvette operating in time correlated single photon counting (TCSPC) mode and ready to perform time domain lifetime spectroscopy building up a histogram of the sample's fluorescent decay. Fluorescence life time of free and bound chromophore differs which can be resolved on experimental time scale. Time-Resolved fluorescence studies can give an idea of the binding modes of ligand-DNA

complex depending upon their fluorescence decay profile. The samples were excited by a fixed-wavelength Nano LED of 635 nm with a pulse duration of <200 ps. All decay traces were measured using 2048 channel analyzer. Typical parameters for these experiments were: time resolution = 0.2 ns, accuracy = ± 0.5 ns, speed = 150 nm/s, TAC range = 100 ns. The data were fitted using a reconvolution method of the instrument response function producing best chi square fitting values and errors were given as standard deviation obtained from the fits. All the measurements were carried out three times to check the reproducibility and to obtain the average values of the life time for MTX and its complex with 7-mer DNA quadruplex.

2.4 Circular Dichroism measurements

2.4.1 Sample preparation

Titration was performed by keeping the concentration of DNA quadruplex constant (20 μM) and varying the mitoxantrone concentration in the D/N range 0.2–2.6. In order to examine induce CD band another set of CD data was recorded. In this set of experiment, the concentration of mitoxantrone was kept constant (20 μM) and DNA quadruplex concentration was varied in the range D/N = 0.06-4.00. For melting studies MTX was added progressively from a stock solution to a fixed concentration (20 μM) of quadruplex to get D/N ratio of 1, 1.5, 2.0, 2.5 and 3. T_m was measured for each complex, so obtained.

2.4.2 Methodology

CD measurements were carried out on “Applied Photophysics” (Model Chirascan, UK) spectropolarimeter equipped with a programmable temperature controlled cell holder using a rectangular quartz cell of 0.1 cm path length. All spectra were acquired in the wavelength range 200–700 nm with a 1nm slit width at 1 nm interval and were averaged over 3 scans. Interaction of a chiral molecule with circularly polarized light result into CD. The extent of absorption of left circularly polarized light (L-CPL) and right circularly polarized light (R-CPL) by a chiral molecule differ, result into positive and negative CD signal. It is generally expressed in the form of molar ellipticity ($[\Theta]$) or millidegrees. It can be used to study the conformational polymorphism of quadruplex DNA and the change in its structure due to environmental conditions or after binding to ligands. Thus, it's a powerful technique to monitor drug-DNA interaction. The position and magnitude of CD bands reveal the conformation adopted by G-quadruplex sequences. A positive CD band around 260-265 nm and a negative band around 240-245 nm are the signature of parallel stranded G- quadruplex whereas a positive band at 295 nm and a negative band at 260 are indicative of an antiparallel conformation (Spada *et al.*, 2010; Kypr *et al.*, 2012). DNA is a chiral molecule, which give a CD signal in UV region while

most ligands are achiral and do not exhibit CD signal. Hence quadruplex concentration was fixed and MTX was titrated to monitor change in the quadruplex conformation due to binding. A titration curve, which is a plot of molar ellipticity at λ_{\max} in our case at 264 nm or λ_{\min} at 243 nm vs D/N ratio gives idea about binding stoichiometry. Sometimes a chiral ligand when binds tightly to DNA give induce signal in the absorbance wavelength range of bound ligand. The shape and sign of the induced CD (ICD) band reflect the mode of binding. A strong and positive ICD is characteristic of groove binding and that of weak and negative (or slight positive band) ICD band is an intercalative/end-stacking mode (end-stacking is prominent in quadruplex) (Ellestad, 2012). Thermal melting experiments were acquired by using a Peltier temperature controller system (Quantum Northwest Peltier) accessory to an accuracy of 0.1 °C. The uncomplexed d-(TTAGGGT)₄ and its complex with MTX at D/N ratio of 1.0, 1.5, 2.0, 2.5, 3.0 were heated from 20 °C to 90 °C with an increment of 5 °C and 5 min stabilization time between two measurements. T_m was calculated by plotting the ellipticity at 264 nm versus temperature. Increase in T_m gives the extent of thermal stability G-quadruplex structure upon ligand binding.

2.5 Nuclear Magnetic Resonance (NMR) spectral measurements

2.5.1 Sample preparation

2.5.1.1 Mitoxantrone-d-(TTAGGGT)₄ complex

The d-(TTAGGGT) with a single strand concentration 8.8 mM was dissolved in 500 μ l of 90 % H₂O: 10 % D₂O (v/v) 20 mM KBPES buffer (pH 7.0). A stock solution of mitoxantrone (18.33 mM) was prepared in 20 mM KBPES buffer. The mitoxantrone–quadruplex complex at different D/N ratios up to 2.0 (D/N = 0.25 0.5, 0.75, 1.0, 1.25 1.5, 1.75 and 2.0) was prepared by titrating 15 μ l of mitoxantrone at each step from a 18.33 mM solution into the d-(TTAGGGT)₄.

Concentration of d-(TTAGGGT) ₄ (mM)	Concentration of mitoxantrone (mM)	D/N
2.20	0.00	-
2.13	0.53	0.25
2.06	1.03	0.50
2.00	1.50	0.75
1.94	1.94	1.00
1.88	2.36	1.25
1.83	2.74	1.50
1.78	3.12	1.75
1.73	3.47	2.00

Table 2.1: Concentration of mitoxantrone (D), d-(TTAGGGT)₄ (N) in mitoxantrone-d-(TTAGGGT)₄ complex at different D/N ratios.

2.5.1.2 Luteolin-d-(TTAGGGT)₄ and luteolin-d-(TTGGGGT)₄ complex

The d-(TTAGGGT) and d-(TTGGGGT) with single strand concentration 8.24 mM and 12.28 mM were dissolved in 500 µl of 90 % H₂O: 10 % D₂O (v/v) 20 mM KBPES buffer (pH 7.0). A stock solution of luteolin was prepared in DMSO-d₆. The concentration of oligonucleotide sequences and luteolin were determined spectrophotometrically at λ_{\max} 256 nm (per strand $\epsilon = 69800 \text{ M}^{-1} \text{ cm}^{-1}$ for d-(TTAGGGT) and $65900 \text{ M}^{-1} \text{ cm}^{-1}$ for d-(TTGGGGT)) and λ_{\max} 348 nm ($\epsilon = 20417 \text{ M}^{-1} \text{ cm}^{-1}$), respectively. 6µl of 42.75 mM of luteolin was titrated in 500µl of 2.06mM d-(TTAGGGT)₄ to make 1:1 complex similarly 6µl of luteolin 62.5mM was added in 500 µl of 3.07 d-(TTGGGGT)₄ to make 1:1 complex at different D/N ratios up to 1.0 (D/N = 0.25 0.5, 0.75 and 1.0).

The concentration of d-(TTAGGGT)₄(N₁) in total volume of 506 ul is determined as follow:

$$N_1 \times V_1 = N_2 \times V_2$$

$$N_1 \times 506 = 2.06 \times 500$$

$$N_1 = 2.03 \text{ mM}$$

The concentration of luteolin in this solution is determined as follows:

$$N_3 \times V_3 = N_4 \times V_4$$

$$N_3 \times 506 = 42.75 \times 6$$

$$N_3 = 0.507 \text{ mM}$$

Similarly the N₁ of d-(TTGGGGT)₄ = 2.96 mM and N₃ of luteolin = 0.741mM

Table 2.2 and 2.3 shows the concentration of luteolin (D), d-(TTAGGGT)₄ (N) and d-(TTGGGGT)₄ in luteolin-d-(TTAGGGT) and luteolin-d-(TTGGGGT) complex at different D/N ratios.

Concentration of d-(TTAGGGT) ₄ (mM)	Concentration of luteolin (mM)	D/N
2.06	0.00	-
2.03	0.50	0.25
2.00	1.00	0.50
1.98	1.48	0.75
1.95	1.95	1.00
1.92	2.40	1.25
1.89	2.84	1.50
1.86	3.27	1.75
1.84	3.69	2.00

Table 2.2: Concentration of luteolin (D), d-(TTAGGGT)₄ (N) in luteolin-d-(TTAGGGT)₄ complex at different D/N ratios.

Concentration of d-(TTGGGGT) ₄ (mM)	Concentration of luteolin (mM)	D/N
3.00	0.00	-
2.96	0.74	0.25
2.92	1.46	0.50
2.88	2.16	0.75
2.84	2.84	1.00
5.38	2.69	2.00

Table 2.3: Concentration of luteolin (D), d-(TTGGGGT)₄ (N) in luteolin-d-(TTGGGGT)₄ complex at different D/N ratios.

2.5.2 Methodology

NMR is a powerful technique which gives insight to the three dimensional structure, stability, dynamics and intermolecular interactions of macromolecules and its complex with ligand. Apart from its application in structural biology it also has important application in medical diagnosis and drug designing (Sharma *et al.*, 2009; Kumar *et al.*, 2012, 2014). The solution structure determined by NMR mimic the natural one present in the cell, which is the main advantage of this technique over X-Ray crystallography. Now-a-days low temperature NMR under supercooled conditions is used, which give better insight into biomolecular systems, especially small molecules. This is because at lower temperature the exchange rate as well as the dynamics is slow, which allows to probe the conformational equilibria of biomolecules (Spring and Germann, 2012).

2.5.2.1 The Phenomenon of NMR

NMR is observed in the sample containing NMR active nuclei (¹H, ¹³C, ¹⁵N and ³¹P), which have two or more allowed spin states (spin $I \geq 1/2$). Number of allowed spin states for any nuclei can be calculated by $2I + 1$, where I = nuclear spin number. Therefore, for nucleus with spin $1/2$ there are 2 allowed states (Fig. 1). Such nucleus behaves like a tiny magnet having the same energy for the 2 states in the absence of external magnetic field. When placed in an external magnetic field the spin of NMR active nuclei distributes themselves into discrete energy level with the separation by:

$$\Delta E = h \gamma B_0$$

Where ΔE = energy difference between 2 states, γ = gyromagnetic ratio, unique constant of a particular nucleus, B_0 = external magnetic field. Thus, they are aligned either partially parallel (α spin with lower energy) or antiparallel (β state with higher energy) to the direction of external magnetic field.

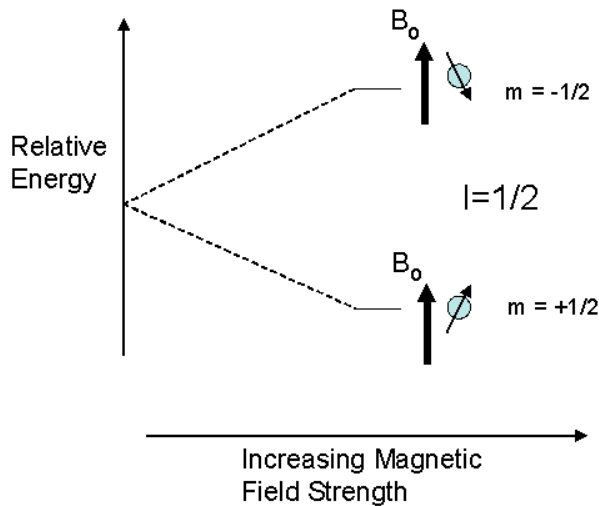


Fig. 2.4: Energy levels for a nucleus with spin quantum number $1/2$.

A spin cannot align perfectly to B_0 it will experience a permanent torque from B_0 . The nuclei due to the presence of the nuclear magnetic moment (owing to spin) precess (**Fig. 2.4**) with a frequency known as Larmor frequency (ω_0) about the axis of external magnetic field (B_0), which is given by:

$$\omega_0 = \gamma B_0$$

Where, γ is proportionality constant, ω_0 is the Larmor frequency in radians/second and B_0 is the magnitude of the applied magnetic field.

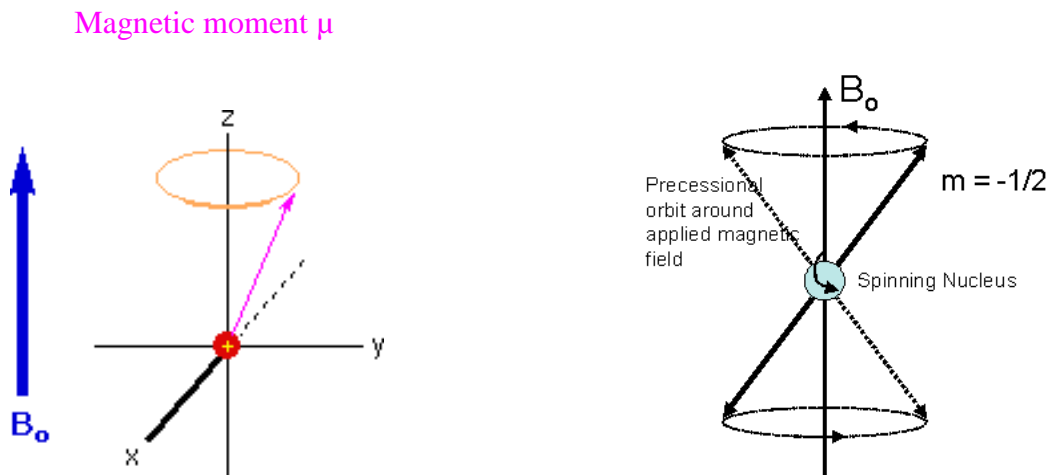


Fig. 2.5: Precessional motion of the nucleus spinning on its axis in the presence of external magnetic field

When the frequency of the applied RF (radio frequency) is same as that of Larmor frequency the nuclei flips from the lower energy state to the higher energy state (**Fig. 2.5; Fig. 2.6**) and the net magnetization M_z oriented along the Z-axis can flip to any desired angle relative to M_z . To achieve the best signal to noise ratio the net magnetization precess along x-y plane, which

increase the amplitude of a signal. The magnetization then returns to its equilibrium through different relaxation pathway. This can be achieved either through spin-lattice (T_1) relaxation or spin-spin relaxation (T_2). Spin-lattice relaxation occurs through the interaction of excited nuclei with the lattice, which depends upon the motion of molecules. Spin-spin relaxation involves the interaction of one spin with another spin which causes either or both spins to return to the equilibrium. T_2 depends upon the magnetic field homogeneity and size of the molecule. Fast spin-spin relaxation or decay leads to the broad signal while that of slow leads to sharp signal, which is due to the dependence of T_2 to the line width of the signal ($(\Delta\omega)_{1/2} = 1 / \pi T_2$).

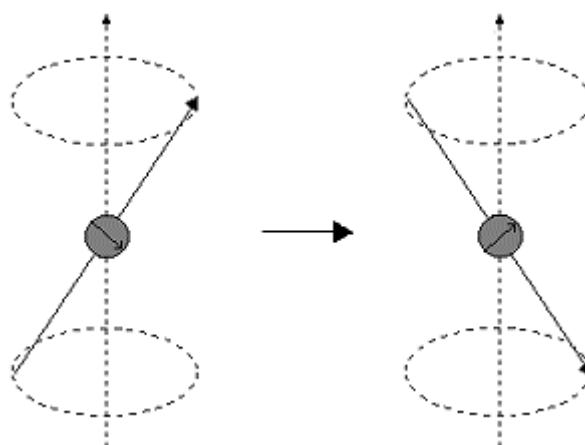


Fig. 2.6: *Flipping of the magnetic moment on absorption of the radiations.*

2.5.2.2 Chemical Shift

Electrons with spin ($1/2$) present in the vicinity of nucleus resist the applied magnetic field B_0 and it shields the nucleus from experiencing the full magnetic field. Thus the effective magnetic field around the nucleus is less than the applied field by σ which is represented as:

$$B_{\text{eff}} = B_0 (1 - \sigma)$$

Where, σ is the shielding constant which depends on the nature of electrons around the nucleus.

The greater the electron density around a nucleus greater will be the nuclear shielding. Chemical shift δ is presented in parts per million (ppm) which is measured relative to reference compound. Tetramethylsilane, $\text{Si}(\text{CH}_3)_4$ (TMS) is often used as reference for ^1H and ^{13}C NMR. Chemical shift is expressed as:

$$\delta = 10^6 \times \left(\frac{\delta_{\text{ref}} - \delta_{\text{obs}}}{\delta_{\text{ref}}} \right)$$

Where, δ_{ref} is the position observed for a reference compound and δ_{obs} is the position of the signal of interest. The position of chemical shift infers the chemical environment around the nucleus. It's an important parameter used to measure change upon the binding of ligand to the DNA.

2.5.2.3 Spin-Spin Coupling (J coupling)

Apart from the effective magnetic field the nuclei also experience a magnetic field due to the presence of other nuclei close by. When 2 nuclei experienced same chemical environment they are referred as equivalent while those having different environment are non-equivalent. Spin-spin coupling occurs when 2 non-equivalents nuclei which are connected through the bond (≤ 3 bond length) affect each other's effective magnetic field. This coupling results in the splitting of absorption lines owing to the magnetic interaction between 2 nuclei. The distance between 2 such splitting is named as J coupling constant and it is measured in Hertz (Hz). These coupling constants play an important role in the prediction of sugar puckering and backbone conformations. The presence of both chemical shifts and coupling constant in proton NMR spectrum gives quantitative information regarding the intermolecular resonance, which helps in estimating the purity of compounds. Thus it's an important analytical tool that can be used in metabolomics, pharmaceuticals (Joshi *et al.*, 2003; Bharti and Roy, 2012; Bhatia *et al.*, 2013).

2.5.2.4 One-dimensional and Two-dimensional NMR Spectroscopy

The NMR data were collected on Bruker Avance 500 MHz FT-NMR spectrometer equipped with broadband probe (BBO) and triple inverse probe (TXI) and processed on Topspin version 2.1 software. One-dimensional (1D) NMR spectra were generated by using zg30/zgpr and zgpg30 pulse programs for ^1H and ^{31}P , respectively, and the signals were Fourier transformed from time domain to frequency domain. Parameters used were: 65536 data points with 64-128 numbers of scans, spectral width of 20 ppm and a delay time of 1.5 s. Receiver gain was optimized in each instance to obtain the best signal to noise ratio. The removal of water signal was accomplished using Watergate suppression (zgpr pulse program). It's an important procedure when dealing with aqueous environment. Many computational methods have been employed to reduce the intensity of residual water signal. In this respect a new processing algorithm WAVEWAT is used to suppress the onresonance water signal in NMR spectra (Günther *et al.*, 2002). In temperature variable experiments, constant temperature is maintained

in the range 275–363 K using temperature control accessory (Bruker Variable Temperature Unit, BVTU).

Two-dimensional (2D) NMR was introduced to overcome the shortcomings of 1D NMR. Small molecules can easily be interpreted by analysis the 1D spectra, but for large, complex molecules assignment of all the resonances is not an easy task due to overlapping of signals. Sometimes isotopic labeled oligonucleotides especially ^{15}N labeled are used to resolve this complexity. It helps in probing the interaction between DNA and ligands (Kieper *et al.*, 1998). 2D NMR thus provides a second dimension to the existing spectrum, which not only made the interpretation easier, but also provides lots of valuable information regarding the structure of large, complex molecules. In two-dimensional (2D) NMR the signal is recorded as a function of two time variables, t_1 and t_2 , and the resulting data Fourier transformed twice to yield a spectrum, which is a function of two frequency variables (**Fig. 2.7**). Magnetization transfer is an important parameter or integral part of 2D NMR experiments. Transfer of magnetization through bond (scalar) and space (dipolar) acts as an important mode of magnetization relaxation process in molecules. Chemical bond between two atoms acts a bridge through which nuclear magnetic dipole of one atom can interact with neighboring atoms through their shared electrons. This relaxation process is called as T_2 relaxation and numerous NMR experiments have been developed to utilize this process and provide information about the structure of a molecule of interest.

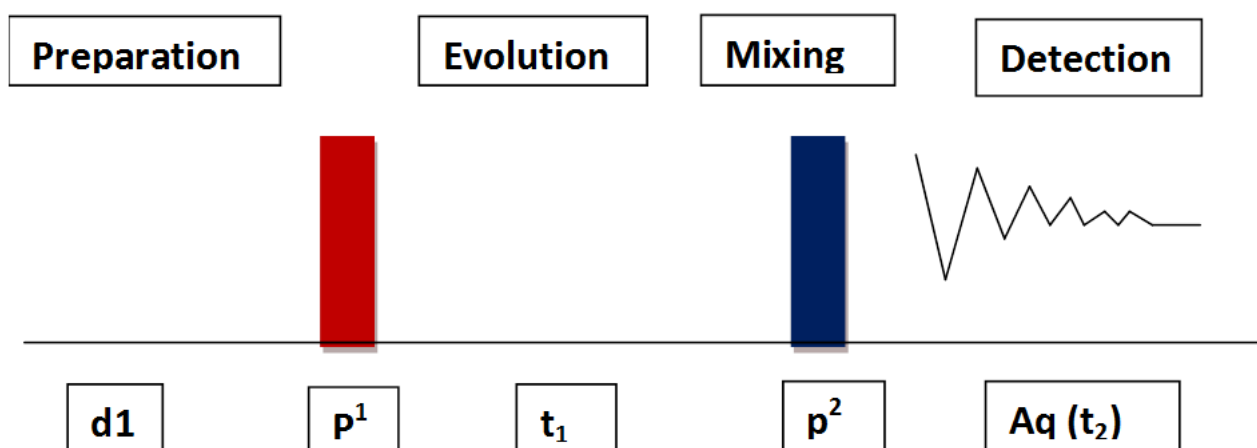


Fig. 2.7: The general scheme for two-dimensional spectroscopy.

The standard two dimensional (2D) phase sensitive experiments viz. Nuclear Overhauser Effect Spectroscopy (NOESY), Rotating frame nuclear Overhauser Effect Spectroscopy (ROESY)

Total Correlated Spectroscopy (TOCSY), Correlation Spectroscopy (COSY), Double Quantum Filtered Correlation Spectroscopy (DQF-COSY) Heteronuclear Single Quantum Correlation (HSQC) and Heteronuclear Multiple Bond Correlation (HMBC) (Wuthrich et al. 1980; Ernst and Braunschweiler 1983) were used for assignment of various resonances in uncomplexed and complexed states using standard procedures. COSY, DQF-COSY, TOCSY are homonuclear 2D experiments that utilize J coupling for the assignment of sugar protons. NOESY is also a homonuclear 2D experiment used for the assignment of sugar and base protons which are connected through space (distance smaller than 5\AA). It is helpful for the deduction of three dimensional structures. NOESY experiments were carried out at different temperatures from 278-318K with variable mixing times τ_m 100, 200, 250ms. HSQC and HMBC are heteronuclear 2D experiments which give correlation of protons with directly attached heteronuclei and 2 or 3 bond away, respectively.

COSY

The COSY experiment (homonuclear *C*ORrelated Spectroscop*Y*) is one of the most powerful and important two-dimensional NMR experiments, originally developed by Jeener. The spin $\frac{1}{2}$ nuclei which are connected by a scalar coupling with a coupling constant of J Hz show two doublets in a one dimensional experiments, but in two dimensional COSY spectrum will show a pair of symmetrical cross peaks between the diagonal peaks of two spins. Hence COSY experiment correlates chemical shifts of the same nucleus in both dimensions. In bio molecules many spin systems have a variety of coupling constants ranging from large geminal couplings of 15 Hz or more, through typical vicinal couplings of a few Hz, down to long-range couplings of a fraction of a Hz. The initial $\pi/2$ (90°) pulse excites the spin system which evolves during the regularly-incremented delay t_1 . The second pulse is called the mixing pulse and may have any flip angle, α . For many applications, $\alpha = \pi/2$ or $\alpha = \pi/4$.

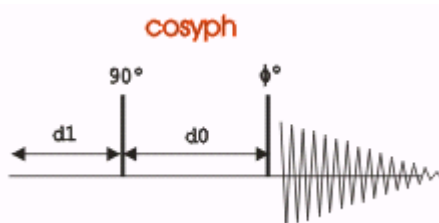


Fig. 2.8: Pulse scheme of COSY technique.

The simple COSY experiment consists of a four important steps; they are excitation pulse (90°), an evolution time (t_1), a mixing pulse, and then detection (**Fig. 2.8**). Before the start of the experiment the spin system should reach equilibrium. The first 90° pulse rotates the equilibrium

magnetization to the transverse plane and generates single-quantum coherence. During the evolution time t_1 , the single-quantum coherence evolves, resulting in F_1 frequency labeling of the detected coherence. The last pulse transfers the magnetizations between spins via the scalar coupling between them. Finally, the correlated coherence is detected as the FID in the detection period. The coherence selection is achieved by the gradient pulses following each RF pulse. The cross peaks appear as symmetrically placed pairs above and below the main diagonal.

Experimental parameters:

The Pulse program used was Cosygpqf, which uses gradient pulses for coherence transfer. Quadrature detection (QF) method was used in F_1 direction, with a spectral width of 20 ppm. The size of the FID consists of 2048 data points in F_2 direction at 256 steps in F_1 direction, acquired for 56 scans. Pre scan delay (d1) 1.5 second was used between each experiment. The time domain data were converted into the frequency domain and following processing parameters were used. Sine bell window function was used, with a line broadening factor of 0.3 Hz in F_1 direction and 1 Hz in F_2 direction.

Various important through bond ^1H - ^1H coupling constants are present in nucleic acids, especially between the sugar ring protons, which helps in identifying numerous resonances and puckering pattern of sugar ring. **Table 2.4** lists the through bond correlation expected in Nucleic acids (A DNA/B-DNA).

Bond correlations	Aromatic bases
3J	H5-H6 (Cytosine)
4J	CH ₃ -H6 (Thymine)
	Sugar
3J	H1'-H2', H1'-H2''
2J, 3J	H2'-H2'', H2'-H3'
3J	H2''-H3'
3J	H3'-H4'
3J	4'H-5'H, 4'H-5''H
2J	5'H-5''H

Table 2.4: Expected ^1H - ^1H through bond correlation in Nucleic acids.

NOESY:

NOESY (Nuclear Overhauser effect spectroscopy) is one of the most commonly used two dimensional technique applied to the assignment of protons and structural determination of biological macromolecules like nucleic acids, proteins and carbohydrates. Its basic principle is based on Nuclear Overhauser Effect or NOE, which is a relaxation phenomenon used to derive information on short internuclear distances. These distances can be used to derive three dimensional structural details. The origin of NOE can be explained by the knowledge of Solomon equations and molecular relaxation mechanisms, apart from dipole-dipole interactions. **Fig. 2.9** shows the NOESY pulse sequence used in the present work which consists of three $\pi/2$ (90°) pulses separated by certain delay times (d). The first delay time d_1 is the recycling delay between two experiments/scans in which the precessing magnetization relaxes to the equilibrium ground state. The first $\pi/2$ pulse (p1) converts longitudinal z magnetization into transverse spin magnetization. This is followed by second delay period (d_0), during which the transverse magnetization precesses around the z axis, so that at the end of t_1 each nucleus has precessed through an angle ωt_1 , where ω is the angular frequency of the nucleus compared with the reference frequency, or in other words its chemical shift difference from the carrier, which in a quadrature detection experiment is in the center of the spectrum. The second $\pi/2$ pulse (p1) rotates this transverse magnetization to the longitudinal one in the pulse direction i.e in the xz plane. The phases of the pulses are cycled in subsequent pulse sequences so that any residual transverse magnetization following the second pulse is canceled out. Thus, the only magnetization that is added constructively as a result of the complete phase cycle is that resulting from the magnetization that is along the z axis after the second pulse. The first two pulses have therefore achieved a frequency labeling of magnetization, in which each magnetization vector now has an intensity modulated both by t_1 and by its frequency. The period between the second and third pulses is the mixing period (d_8 in Bruker instrument) τ_m during which the NOE build up occurs. By the end of this mixing period, magnetization in the z direction has modified by NOE cross relaxation. The final $\pi/2$ pulse (p1) reads the magnetization present in z direction and converts it into a transverse magnetization, which is then detected. This experiment is repeated for a series of regularly incremented t_1 values and stored as a matrix of points.

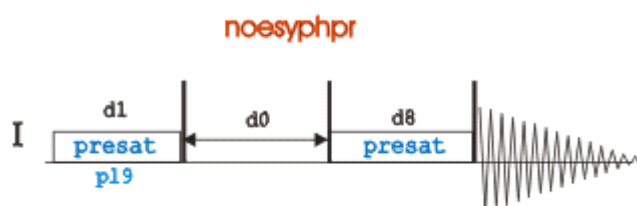


Fig. 2.9: Pulse scheme of NOESY technique.

In common with most other two-dimensional experiments, NOESY spectra are normally presented as square plots containing a line of diagonal peaks and symmetrically placed cross peaks. The two dimensions in NOESY experiment were labeled as $F_1, F_2 (\omega_1, \omega_2)$ where 1 and 2 refer respectively to the indirectly and directly detected dimensions.

In NOESY experiments, cross connectivities originate from cross relaxation between two nuclei that are close to each other in space, hence called as dipolar-dipolar coupling. Therefore, appearance of a NOE cross peak is interpreted as a short distance between the two nuclei at the chemical shifts of the cross peak. The appearance of NOE cross connectivity for a pair of proton within a molecule under study depends upon the close proximity of the two protons, generally less than the 5\AA , mixing time (τ_m) and sensitivity of the instrument. In some cases spin diffusion results in the appearance of connectivities between protons which are at a distance longer than 5\AA . To minimize this lower mixing time value in the range of 50-200 ms was used.

Experimental parameters: The Pulse program used was *noesyphpr*, which uses phase sensitive detection with pre-saturation pulse for water suppression. States TPPI method of detection was used in F_1 direction, with a spectral width of 20 ppm. The size of the FID consists of 2048 data points in F_2 direction at 256 steps in F_1 direction, acquired for 56 scans. Pre scan delay (d1) 1.5 seconds was used between each experiment. One of the important parameters taken care of before NOESY experiment is mixing time (τ_m), that is D8 of 100, 200 and 250 ms was used in the present study. Exact transmitter offset position (O1P) for suppression of the solvent water peak was determined by gs mode.

The data were processed using the Bruker Topspin 2.1 processing software. The time domain data were converted into the frequency domain and following processing parameters were used. Quadrature Sine bell window function was used, with a line broadening factor of 0.3 Hz in F_1 direction and 1 Hz in F_2 direction.

With increase in multidimensional NMR experiments need for the advance processing of NMR data is required, which is achieved by NMRLAB. It's a MATLAB base NMR data processing toolbox (Günther *et al.*, 2000).

Residue n	Residue n		Residue n+1			
	H2''	H6/H8	H6/H8	H5	CH ₃	NH
H1'	2.6	3.8	3.1		3.8	
H2'	1.75	2.1	3.9	3.2	2.8	

H2''	-	3.5	2.3	2.8	2.4	
H6/H8		-			3.2	
NH						3.8

Table 2.5: Short interproton distances in regular B-DNA in Å.

Residue n	Residue n		Residue n+1		
	H2''	H6/H8	H6/H8	H5	CH ₃
H1'	2.3	3.8	4.0		
H2'	1.75	3.8	1.6	3.0	2.8
H2''	-	3.5	3.2		
H6/H8		-		3.7	3.1

Table 2.6: Short interproton distances in regular A-DNA in Å.

ROESY:

ROESY (Rotating frame nuclear Overhauser effect spectroscopy) is an alternative to the NOESY experiment used for the determination of dipolar coupling in molecules with intermediate molecular weight. The pulse program used for ROESY experiment was *roesyphpr* (Fig. 2.10) Acquisition and processing parameters were similar to NOESY experiment except for mixing time, which can be set by changing p15. ROESY experiment was used to determine the conformation of ligands i.e. mitoxantrone, luteolin used in the present studies.

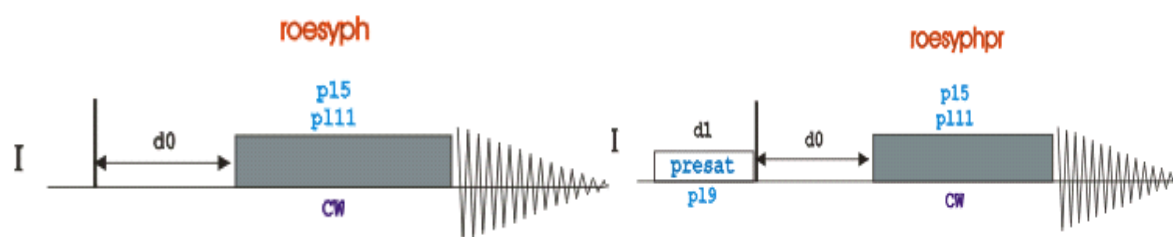


Fig. 2.10: Pulse scheme of ROESY technique.

TOCSY

TOCSY (Total correlation spectroscopy) is also called as two dimensional HOHAHA (homonuclear Hartmann-Hahn) experiment. This experiment reveals both scalar and relayed scalar coupling connectivities (Davis and Bax, 1985). The proton of interest show correlations with all other protons in that spin system, which results in a 2D correlation map. This experiment plays an important role in identifying sugar ring protons in DNA. Due to the presence of glycosidic bond, TOCSY correlation breaks between two sugars or between sugar and nitrogenous base in DNA.

The basic pulse sequence of the TOCSY experiment (**Fig. 2.11**) follows the same principles of the other homonuclear 2D experiments like COSY and NOESY. After an excitation with 90° ^1H pulse, transverse magnetization evolves during a free variable evolution t_1 period, then isotropic mixing sequence (typically 50-100 msec) was used to transfer magnetization between spins via the strong scalar coupling Hamiltonian, with the result that magnetization can be transferred through several couplings during the mixing time.

The isotropic mixing is usually performed applying a WALTZ, MLEV or DIPSI pulse train, and it can be inserted into two z-filters and, in such case, isotropic mixing is performed on the longitudinal magnetization. The TOCSY pulse sequence can also be combined with some solvent suppression scheme.

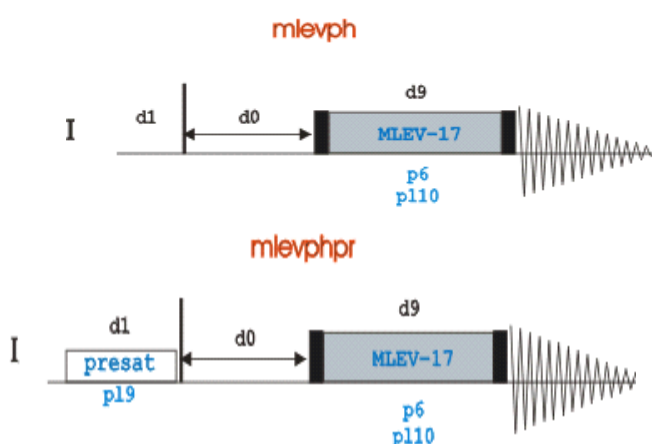


Fig. 2.11: Pulse scheme of TOCSY technique.

Experimental Parameters:

The *mlevphpr* pulse program was used to get the TOCSY correlation map. STATES-TPPI method of detection was used in F_1 direction, with a spectral width of 20 ppm. The size of the FID consists of 2048 data points in F_2 direction at 256 steps in F_1 direction, acquired for 56 scans. Pre scan delays (d_1) 1.5 seconds were used between each experiment. The time domain data were converted into the frequency domain and following processing parameters were used. Sine bell window function was used, with a line broadening factor of 0.3 Hz in F_1 direction and 1 Hz in F_2 direction.

HSQC

The HSQC (Hetero Sequential Quantum Coherence) is a heteronuclear two dimensional experiments developed used to determine the proton coupled directly to the heteroatom (X nucleus like spin $\frac{1}{2}$, ^{13}C , ^{15}N or ^{31}P). In a ^1H - ^{13}C HSQC experiment all the protons attached directly to carbon (^{13}C) nucleus through one bond (C-H) produces a correlation map consists of

^{13}C (heteronucleus, X in F_1 dimension) and ^1H (proton in F_2 dimension) via the direct heteronuclear coupling $1J(\text{X-H})$.

This gives chemical shift of each bonding pair atoms and hence information about the coupling constant between them.

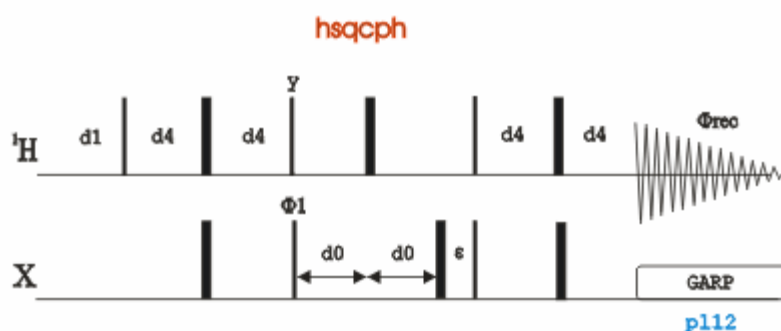


Fig. 2.12: Pulse scheme of HSQC technique.

Experimental Parameters:

The natural abundance ^1H - ^{13}C HSQC experiment was done by using pulse program *hsqcetgpsi* (**Fig. 2.12**) with an acquisition mode of echo-antiecho in F_1 direction, the size of the FID is 1024 data points in F_2 direction with 400 scans in F_1 direction. The spectral width of 200 ppm in F_1 direction and 16 ppm in F_2 direction was used. Delay (d1) of 1.5 seconds was used between each acquisition. 56 scans with 16 dummy scans were used. Q Sine window function was used for window function in both dimensions, with line broadening factor of 1Hz in F_2 and 0.3Hz in F_1 direction. Shifted square sine bell (SSB) function of 2 was used.

HMBC

The HMBC (Hetero Multiple Bond Correlation spectroscopy) is a heteronuclear two dimensional experiment, which provides correlation between ^1H and any X nuclei (X nucleus like spin $\frac{1}{2}$, ^{13}C , ^{15}N or ^{31}P) which are separated by two, three or four bond away (3J, 4J). The direct one bond correlation that is HSQC type correlation is suppressed. The coupling between the nucleus directly relates to the intensity of the observed correlation. Along with the HSQC experiment, HMBC is one of the widely used techniques for the structural determination of natural compounds. $^{31}\text{P}/^1\text{H}$ coupling provides an unambiguous assignment of nucleotides by providing structural information regarding sugar phosphate backbone of DNA oligomers (Otter *et al.*, 1986).

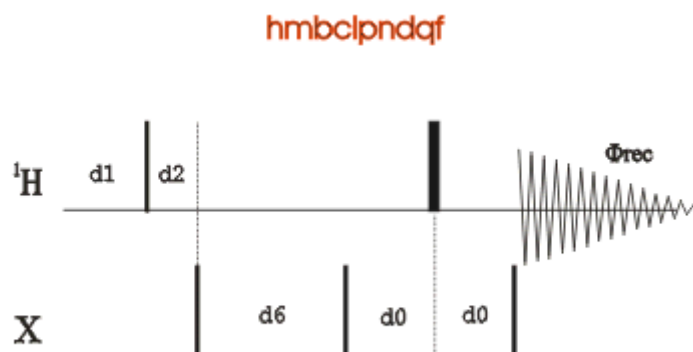


Fig. 2.13: Pulse scheme of HMBC technique.

Experimental Parameters:

The natural abundance ^1H - ^{13}C and ^1H - ^{31}P HMBC experiment was done by using pulse program hmbc1pndqf, which uses gradient pulses for coherence selection, with an acquisition mode of quadrature (QF) in F_1 direction, the size of the FID is 2048 data points in F_2 direction with 256 scans in F_1 direction. The spectral width of 200 ppm in F_1 direction and 16 ppm in F_2 direction was used for ^1H - ^{13}C HMBC experiments and for ^1H - ^{31}P HMBC experiments spectral width of 40 ppm in F_1 and 20 ppm in F_2 direction and. Delay (d1) of 1.5 seconds was used between each acquisition. 56 scans with 16 dummy scans were used. Q Sine window function was used for window function in both dimensions, with line broadening factor of 1Hz in F_2 and 0.3Hz in F_1 direction. Shifted square sine bell (SSB) function of 2 was used.

2.5.2.5 Determination of three-dimensional structure

The first step in determining the three-dimensional structure is to assign all the resonances present in a particular structure. The most common and important assignment is the proton resonances. **Table 2.7** shows the positions of proton and carbon resonances. The proton resonances are basically divided into two categories. The first one is the imino and amino exchangeable protons of bases. The second one is the non-exchangeable protons, which consist of bases H8/H6 protons, methyl protons and sugar protons. In order to assign exchangeable protons the experiments were carried out in H_2O and that of non-exchangeable in D_2O . The strategies involved for resonance assignment is of two types. First the J correlated experiments were carried out to assign the spin coupled system, which basically exist within sugar. Once this was done the assigned coupled systems were correlated with their corresponding nucleotides, which can be achieved by NOESY experiments. Sequential connectivities exist, which probe all the nucleotides. With the help of these connectivities the sequence assignments

were completed. Further the non-overlapping NOE connectivities were used for distance calculation. These distances were used as constraints for building the final structure.

Deoxyribose	¹ H (δ ppm)	¹³ C (δ ppm)
H1'	5.2–6.7	84–91
H2' and H2''	0.9–3.9	37–44
H3'	4.1–5.6	72–82
H4'	3.8–5.0	84–89
H5' and H5''	3.3–4.6	62–72
Nucleoside		¹³ C
AH2	7.3–8.4	153–155
CH5	4.5–6.5	92–99
CH6 and TH6	6.5–8.1	139–143
TCH ₃	0.8–1.6	13.5–15
AH8 and GH8	7.4–8.5	137–142
		¹⁵ N (δ ppm)
A, C and G NH ₂ (b and nb)	6.2–9.0	79–81(A), 74–76 (G), 96–98 (C)
NH imino proton of GNH and TNH	10–15	_147 (G), 158–160 (T)

Table 2.7: Proton and carbon chemical shift position in DNA.

2.5.2.5.1 Resonance assignments of quadruplex

Oligonucleotide sequence d-(TTAGGGT), form a right handed parallel stranded G-quadruplex in presence of K⁺ ion with *anti* glycosidic torsion angles. All the 4 strands have the same orientation in 5' to 3' direction. Due to the presence of right handed helical geometry the standard assignment which is used for B-DNA can be employed for parallel stranded G-quadruplex also. This assignment included both exchangeable and non-exchangeable protons of quadruplex. Formation of quadruplex can be easily monitored by the observation of exchangeable imino and amino proton resonances. The number of the imino resonances present is directly related to the number of guanosine residue participated in G-tetrad formation. Presence of imino signals resonating between 10.5 and 12.00 ppm is indicative of the formation of G-quadruplex structure while that at 12-13 ppm is suggestive of duplex DNA (Webba da Silva, 2007). NOESY spectra also give evidence for G-tetrad formation due to the presence of interstrand NOEs between guanine imino proton to its own and its 5' flanking base protons in A3-G4-G5-G6 segment of d-(TTAGGGT)₄ sequence (Wang and Patel, 1992). Such long range NOE cannot be possible within same strand. Classical sequential assignment used for nucleic acid was employed for the assignment of the nonexchangeable protons of quadruplex (Wuthrich, 1986), which were done by observing NOE connectivities between base H8/H6

protons to its own and its 5' flanking H1'/H2'/H2'' sugar protons. 5'-anti-3'- anti conformation can also be determined by these connectivities.

2.5.2.5.2 Sugar pucker conformations

Torsional/dihedral angle restraints can easily be provided by vicinal coupling constants (3J) through Karplus relations (Karplus, 1959).

$$^3J(\theta) = A \cos^2 \theta + B \cos \theta + C$$

Where θ = dihedral angle; A, B and C are constants.

In general the nucleotides exhibit two types of conformations; (i) S-type and, (ii) N-type. The S-type conformation is dominant in B DNA and quadruplex DNA, whereas A DNA and RNA exist in N-type conformation. Identification of S- and N-type conformation can be easily identified using spin-spin coupling/J-coupling.

S-type and N-type sugar puckering can easily be identified by measuring the coupling constant $J_{1'2'}$.

$J_{1'2'} = 8$ Hz for C2' endo (S-type)

$J_{1'2'} = 0-2$ Hz for C3' endo (N-type)

Apart from this an intense $J_{3'4'} \sim 10$ Hz and a weak $J_{2'3'}$ coupling show the predominance of N and S-type sugar conformations, respectively.

Moreover, the Five vicinal coupling (3J) constants, that exists in deoxyribose sugar H1'-H2', H1'-H2'', H2'-H3', H2''-H3' and H3'-H4' can be determined by a combination of DQF-COSY spectrum and Karplus equation.

2.5.2.5.3 Conformation about the glycosidic bond

Different conformation of quadruplex occurs on the basis of *anti* and *syn* conformation of guanosine residue involved in G-tetrad formation. The relative magnitudes of the intranucleotide and internucleotide (H8/H6)-H1' and (H8/H6)-(H2', H2'') cross peaks in NOESY spectra at different mixing times gives an idea about *syn* and *anti*-conformation (Hosur *et al.*, 1985).

Syn conformation – It is characterized by the presence of a strong NOE between base H8/H6 and H1' protons (2.5 Å). Weak NOEs between NH1' (n - 1)-*syn*GH8 and base to H2'/2''.

Anti-conformation - It is characterized by the presence of a medium NOE between base H8/H6-H1' (3.7 Å). Presence of a strong NOE between base H8/H6 to H2' than that with H2''.

2.5.2.5.4 Estimation of interproton distances

NOESY experiments were recorded at different mixing times in order to get NOE build up curve, which will help to distinguish between cross peaks generated from direct dipolar interaction (the NOE) or as a result of spin diffusion (Hosur *et al.*, 1988). At the lower mixing time spin diffusion rate is slow and the observed cross peaks are the one whose distances are shorter that is two protons are close through space. Initially the intensity of cross peaks increase with mixing time, but later at a higher mixing time due to multi spin relaxation, diffusion rate is fast and distance based NOE cross peaks does not exist and the intensity of all the cross peaks are same. Interprotons distances were achieved by measuring the intensities of cross peaks in the “linear regime” through two-spin approximation, where only the rates of dipolar magnetization transfer between proximal spins *i* and *j* was monitored as follows:

$$r_{ij} = r_{ref} (I_{ij} / I_{ref})^{1/6} \dots\dots\dots (4)$$

Where r_{ij} = distance between two protons *i* and *j*, r_{ref} = reference distance, I_{ij} = intensity of *i* and *j* and I_{ref} = reference intensity.

Cross peaks in the NOESY spectra were integrated and intensities were translated into interproton distances using thymine H6-CH₃ as the reference distance (3.00 Å) using the SPARKY software (T.D Goddard DGK, University of California, San Francisco, USA 2004). A range of ±0.5 Å was provided to avoid any errors in integration. The NOEs were categorized as very strong(ss), strong (s), medium (ws), weakly and very weakly intense with corresponding distances set range set in the range of ss 1.8–2.5 Å, s 2.5–3.0 Å, ws 3.0–3.5 Å, w 3.5–4.0 Å, ww 4.0–5.0 Å for the respective protons.

2.5.2.5.5 Restrained molecular dynamics methodology

The initial structure of d-(TTAGGGT)₄ was built using the biopolymer module in INSIGHT II, version 2005 (Accelrys Inc., San Diego, California) on Silicon Graphics Fuel workstation. The force constant was fixed as 40 kcal mol⁻¹ Å⁻² for hydrogen bonds during the simulation. The energy of the molecule was minimized using 1000 steps each of Steepest Descent and Conjugate Gradient to remove any internal strain due to short contacts in starting structure using a CFF91 force field in discover software version 2005 (Accelrys Inc., San Diego, California). Dielectric constant was fixed at 1.0 for calculation of electrostatic interactions. Conformational search was performed using the following simulated annealing restrained molecular dynamic protocol. The molecule was heated to a temperature of 800 K in steps of 100 K so that the chances of the molecule being trapped in local minima become lost and it can reach global minima. Molecular dynamics were carried out for 100 ps (1000 iterations with time step of 1 fs) at 800 K during which 100 structures were saved at regular intervals of 1 ps.

Each of them was then slowly cooled at 300 K in steps of 100 K. The force constants for NOEs for strong, medium and weak peaks were held constant as 25, 15 and 10 kcal mol⁻¹ Å⁻², respectively. At the end of simulated annealing all the structures were minimized by 1000 steps of Steepest Descent until a predefined convergence limit of root mean square derivative of <0.001 kcal mol⁻¹ Å⁻¹ was reached.

2.6 Differential Scanning Calorimetry

2.6.1 Sample preparation

The concentration of DNA quadruplex was held constant (20 μM) and was titrated with MTX to achieve D/N 1.0 and 2.0.

2.6.2 Methodology

DSC experiments were carried out using a Microcal VP-DSC. A scan rate of 60°C/h was used within a temperature range of 20-90 °C throughout the experiments. Before acquiring the sample scan the baseline was recorded by filling the KBPES buffer in both the sample and the reference cell. The experiment was repeated twice on separate fillings. The DSC thermograms, a plot of heat capacity versus temperature were obtained by subtracting with the baseline (buffer-buffer), at every D/N only the ligand of specific concentration dissolved in buffer was used for obtaining baseline by carrying out ligand-ligand run. The data were examined using Origin 7.1 software and were fitted in a two transition non-two-state model. Each transition gave a melting temperature (T_m), calorimetric (ΔH_{cal}) and van't Hoff enthalpies (ΔH_v).

DSC is one of the direct and sensitive technique to characterize the energetic behind the conformation transition of G-quadruplexes and other macromolecules. It gives an idea regarding *them*, ΔH_{cal} , ΔH_v associated with the transition process. The enthalpy change provides information regarding the state to which a particular system belongs in a given range of temperature. The basic principle of DSC is to measure the enthalpy change of the solution of macromolecule as a function of temperature change. This is achieved by keeping the temperature of both the sample and reference cell constant. This constant temperature is maintained by measuring the power to achieve the above state. The temperature of both the cells increased in a linear fashion. The solution of biological molecules was kept in the sample cell while the reference cell contains the buffer solution (in case of free DNA & buffer ligand in D/N). With increase in temperature the macromolecules undergo a transition in a cooperative manner. This transition is either being a protein denaturation or DNA dissociation is due to the destruction of the binding forces which stabilizes the native structure. This disruption change the enthalpy of the system and the calorimeter either remove or provide energy to the sample to match with that of the reference cell. The raw output is in the form of power versus

temperature, which is converted into apparent excess heat capacity. Thus a DSC data is a curve of excess heat capacity versus temperature.

2.7 Telomerase Repeat Amplification Protocol (TRAP) Assay

Inhibition of telomerase enzyme by mitoxantrone/luteolin was evaluated by using the TRAP assay. The assay was performed using TRAPeze XL Telomerase Detection Kit (S7707) supplied by Merck Millipore. It's a PCR based amplifluor primer containing kit used for the detection of telomerase activity in cell extracts. The assay conditions and protocols followed were those as provided by manufacturer kit.

2.7.1 Telomerase enzyme isolation and methodology

MCF-7 breast line cancer cells (passage 15) were harvested and approximately 100,000 cells were pelleted by centrifugation. The pellet was washed thrice with PBS and freshly used for enzyme isolation or stored at -80°C for further use. To isolate telomerase enzyme, the cell pellet was resuspended in 200 μL of CHAPS Lysis buffer (0.5 % CHAPS, 10 mM Tris-HCl, 1mM MgCl_2 , 1 mM ethylene glycol tetraacetic acid (EGTA), 5 mM β -mercaptoethanol, 0.1mM benzamidine, 10 % glycerol), and incubated in ice for 30 minutes. The lysate was centrifuged at 10,000 RPM for 20 minutes at 4°C , supernatant was transferred to a fresh tube and the protein concentration was determined using the Bradford's method of protein estimation. The supernatant was divided into aliquots and stored at -80°C or used directly for TRAP assay. 50 μL of TRAP reaction mixture consisted of 100 mM Tris-HCl (pH 8.3), 7.5 mM MgCl_2 , 315 mM KCl, 0.25 % Tween 20, 5 mM EGTA, 0.5 mg/mL BSA, 60 μM of dATP, dGTP, dTTP, dCTP, and the oligonucleotides TS primer (5'-AATCCGTCGAGCAGAGTT-3'), RP Amplifluor primer [5'-(CCCTTA)3CCTAA-3'], K2 Amplifluor primer (5'-ATCGCTTCTCGGCCTTTT-3') and TSK2 template (5'-AATCCGTCGAGCAGAGTTAA AAGGCCGAGAAGCGAT-3'), 2 units of Taq Polymerase (500 ng/ μL), to 2 μL of cell extract. The reaction mix with enzyme was incubated at 30°C for 30 minutes. Then required concentration of ligand was added to the reaction mix and a 4 step PCR reaction was carried out as follows, $94^{\circ}\text{C}/30$ seconds, $59^{\circ}\text{C}/30$ seconds, $72^{\circ}\text{C}/1$ minute this step is repeated for 36 cycles, this followed by a $72^{\circ}\text{C}/3$ minute extension step.

Since it's an amplifluor primer containing kit, PCR products were directly quantified using spectrofluorimeter (Horiba Jobin Yvon). 20 μL of assay mixture was diluted to 600 μL with 10 mM Tris-HCl pH 7.4, 0.15 M NaCl and 2 mM MgCl_2 containing buffer. The fluorescence of the sample was measured in 1 cm path length cuvette by collecting emission scan after exciting fluorescein at 495 nm and sulphorhodamine at 600 nm, respectively. The

relative fluorescence intensity was measured using,

$$\Delta F/\Delta R = (FL_0 - FL_{neg}) / (R_0 - R_{no\ taq}),$$

Where, $\Delta F/\Delta R$ is net fluorescence increase or decrease, which is the measure of telomerase activity, FL_0 and R_0 are the fluorescence intensity of fluorescein and sulforhodamine of each sample, FL_{neg} is fluorescence intensity of the telomerase negative control, $R_{no\ taq}$ is fluorescence intensity of the Taq negative control.

Investigations on Binding, Stabilization and Inhibition properties of anticancer drug mitoxantrone with human G-quadruplex DNA.

Guanine rich sequences are located in many biologically significant regions in the human genome (e.g. telomere, promoter, oncogene), and have the ability to assemble as G-quadruplex structures by folding. Ligands which induce and stabilize G-quadruplex structures cause telomerase inhibition and interfere with gene regulation. Several classes of G-quadruplex interactive ligands (both synthetic and natural) have been studied, which are in their pre-clinical and clinical trials (Nicoludis *et al.*, 2012; Yang and Okamoto, 2010; Liu *et al.*, 2007). Amidoanthraquinone derivatives were the first class of G-quadruplex interactive ligands that showed telomerase inhibition (Zahler *et al.*, 1991, Sun *et al.*, 1997). Mitoxantrone, a synthetic anthraquinone derivative, is a well-known chemotherapeutic agent against various cancers such as metastatic breast cancer, acute leukemia and non-Hodgkin's lymphoma. It shows enhanced antitumor activity, which has been attributed to its intercalative binding to cellular DNA, RNA and histone proteins that leads to unwinding of DNA helix followed by condensation of nucleic acid and partly as a topoisomerase II inhibitor. Several studies have been carried out on the interaction of mitoxantrone with duplex DNA and RNA, but there is no report on its interaction with G-quadruplex DNA. In order to gain insights into its mechanism of action with G-quadruplex structures, I have characterized the interaction of mitoxantrone (MTX) with human G-quadruplex sequence using multiple optical spectroscopic and thermodynamic techniques.

3.1 Results and Discussion

3.1.1 Monitoring the MTX-quadruplex binding interactions using Absorption Spectroscopy

Mitoxantrone shows four distinct absorption bands at $\lambda_{\text{max}} = 242, 276, 609$ and 659 nm. Both the bands in the visible region, 609 and 659 nm, are affected on binding to nucleic acids (Kapusinski *et al.*, 1980; Varani *et al.*, 2009; Shilpa *et al.*, 2013a, b) while the 659 nm band is particularly sensitive to the concentration and the formation of dimers in solution at concentrations $> 7 \mu\text{M}$ (Kapusinski *et al.*, 1980). We have monitored changes in 609 and 659 nm peaks on titrating DNA quadruplex with MTX since DNA itself does not absorb in the visible range of spectra. Upon progressive addition of DNA quadruplex to a fixed concentration of MTX ($3 \mu\text{M}$), the absorbance decreased continuously accompanied by a red shift in both the bands. The observed decrease in absorbance was 43% and 54% at 609 and 659 nm, respectively at $D/N = 0.56$ accompanied by corresponding $\Delta\lambda_{\text{max}} = 11$ and 15 nm (**Fig. 3.1a**). The higher wavelength band apparently shows an isobestic point at $\lambda = 677$ nm which is not

sharp, but the lower wavelength absorption band has no such isobestic point. Further addition of DNA quadruplex ($D/N = 0.56-0.08$) reversed the trend of absorption intensity which started increasing (**Fig. 3.1b**) but the λ_{\max} remained unaltered.

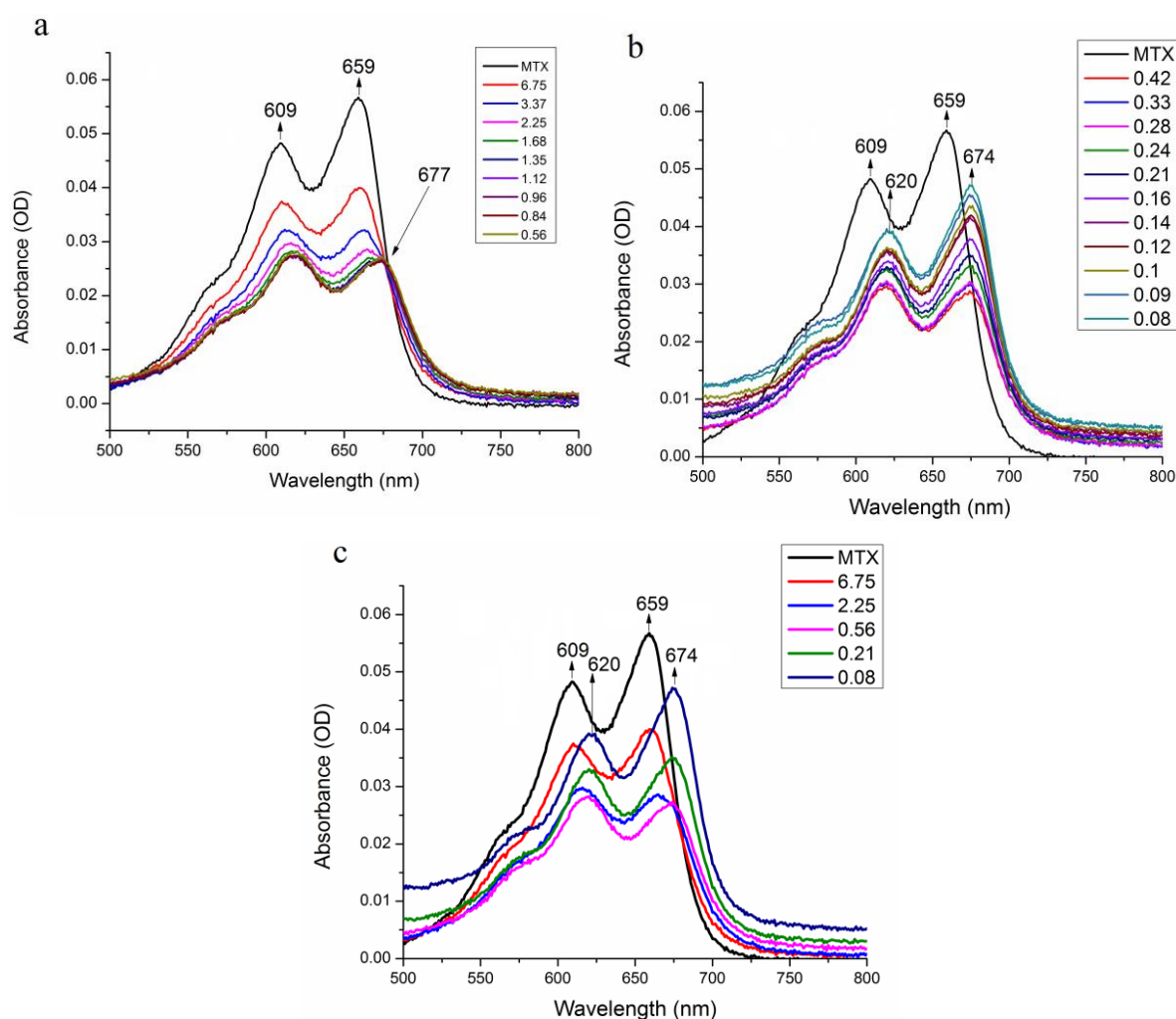


Fig. 3.1: The absorption spectra of 3 μM MTX in the absence and presence of $d\text{-(TTAGGGT)}_4$ at 298 K (a) at higher D/N ($\text{MTX}/d\text{-(TTAGGGT)}_4$) ratios showing isobestic point; (b) at lower D/N ratios; (c) change in the absorption trend at these ratios.

The absorbance of 674 nm peak increased much more (45%) than corresponding 620 nm peak (28%) (**Fig. 3.1b**, **Table 3.1**). There is no isobestic point in either of the two bands at lower D/N ratios ($D/N = 0.56-0.08$) indicating existence of multiple conformations or multiple stoichiometries of bound complexes. The change in absorbance (**Fig. 3.1c**) and λ_{\max} (**Figs. 3.1d**, **e**) of both the bands is minimal in the range of $D/N \sim 1-2$ (**Figs. 3.2a**, **b**). The plot of reciprocal of absorbance $1/A$ versus D/N (**Figs. 3.3a**, **b**) shows a point of inflection at $D/N \sim 1-2$ indicating a likely stoichiometry of 1:1 and 2:1 in the MTX-quadruplex complex.

D/N	$\lambda_{\max} D$	OD D	$\Delta\lambda D$	$\lambda_{\max} M$	OD M	$\Delta\lambda M$
∞	609	0.048	0	659	0.056	0
6.75	610	0.037	1	659	0.039	0
3.37	612	0.032	3	662	0.032	3
2.25	614	0.029	5	665	0.028	6
1.68	616	0.028	7	669	0.026	10
1.35	616	0.027	7	669	0.026	10
1.12	616	0.027	7	670	0.026	11
0.96	616	0.027	7	671	0.026	12
0.84	618	0.027	9	673	0.026	14
0.56	618	0.028	9	674	0.026	15
0.42	620	0.029	11	674	0.028	15
0.33	620	0.030	11	674	0.029	15
0.28	620	0.030	11	674	0.030	15
0.24	620	0.032	11	674	0.033	15
0.21	620	0.032	11	674	0.035	15
0.16	620	0.033	11	674	0.037	15
0.14	620	0.035	11	674	0.041	15
0.12	620	0.035	11	674	0.041	15
0.10	620	0.036	11	674	0.043	15
0.09	620	0.039	11	674	0.045	15
0.08	620	0.039	11	674	0.047	15

Table 3.1: Change in the absorption maxima (λ_{\max}), O.D, and $\Delta\lambda$ at D (609 nm band) and M (659 nm band) on interaction of MTX with (TTAGGGT)₄ at varying D/N ratios.

The hypochromism at D/N = 6.7–0.56 and hyperchromism at D/N = 0.56–0.08 shows the existence of at least two apparent modes of binding mechanisms one at higher MTX concentration and other at lower concentration. In case of duplex DNA where end stacking is not significant a red shift ≥ 15 nm and hypochromicity $\geq 35\%$ is indicative of intercalative binding (Pasternack *et al.*, 1983; Krugh *et al.*, 1975). The predominant mode of binding in quadruplex DNA is end-stacking and groove binding. Hence this red shift (due to decrease in π - π^* transition energy) is characteristic of end stacking interactions of the aromatic chromophore of MTX with base pairs of DNA, which prevents it from forming an H-bond with solvent water (Lee and Dutta, 1989; Yang *et al.*, 2005). This dual mode of interaction can be quite justifiable on the ground that the interaction of MTX with duplex DNA occurs via both partial intercalation and groove binding (Lown *et al.*, 1985; Bowden *et al.*, 1985; Neidle, 1978). The intrinsic binding constant has been evaluated by plotting $[DNA]/\epsilon_a - \epsilon_f$ with respect to $[DNA]$ using equation 1 (chapter 2 section 2.2.2). The data at 659 nm fit into two straight lines yielding affinity constant $K = 3.04 \times 10^6$ and $2.35 \times 10^5 \text{ M}^{-1}$ in the range D/N = 6.7–0.56 and 0.42–0.08, respectively (**Figs. 3.4a, b**). This gives a corresponding value of 8653 and $14793 \text{ M}^{-1}\text{cm}^{-1}$ for

the extinction coefficient of the drug in bound form (ϵ_b) as compared to the value of 20900 M⁻¹cm⁻¹ for unbound MTX (ϵ_f).

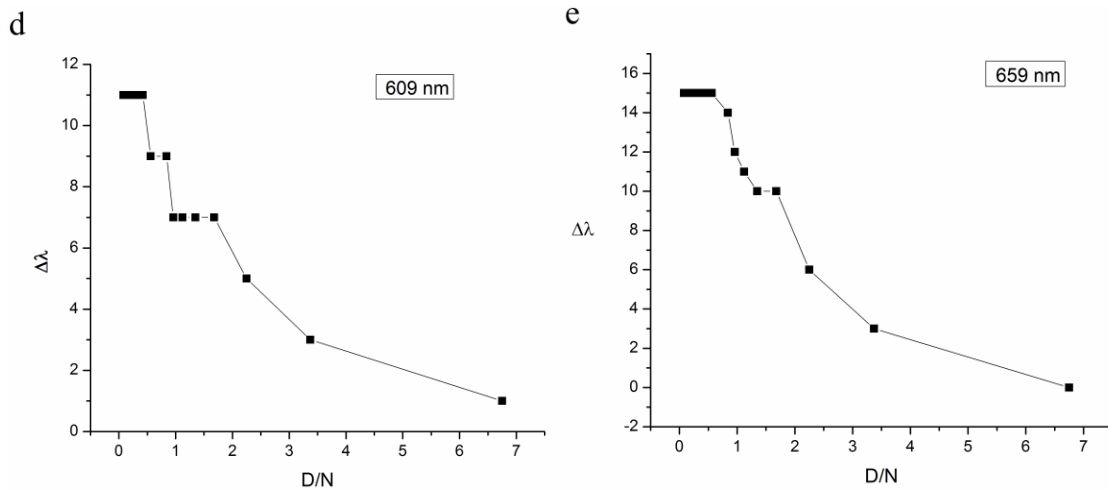


Fig. 3.1: Change in the λ_{max} ($\Delta\lambda$) at varying D/N ratios at (d) 609 nm band and (e) 659 nm band.

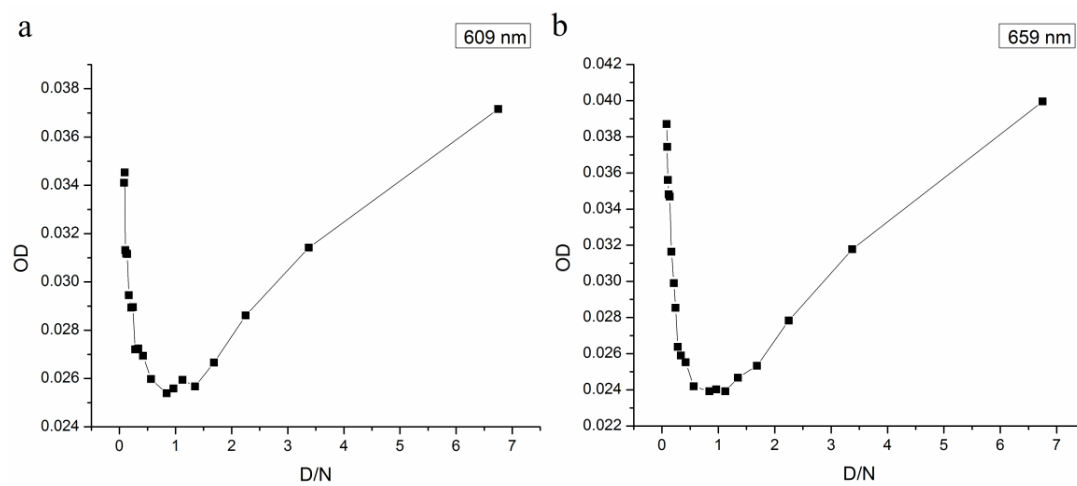


Fig. 3.2: Plot of O.D versus D/N ratios at (a) 609 nm band and (b) 659 nm band.

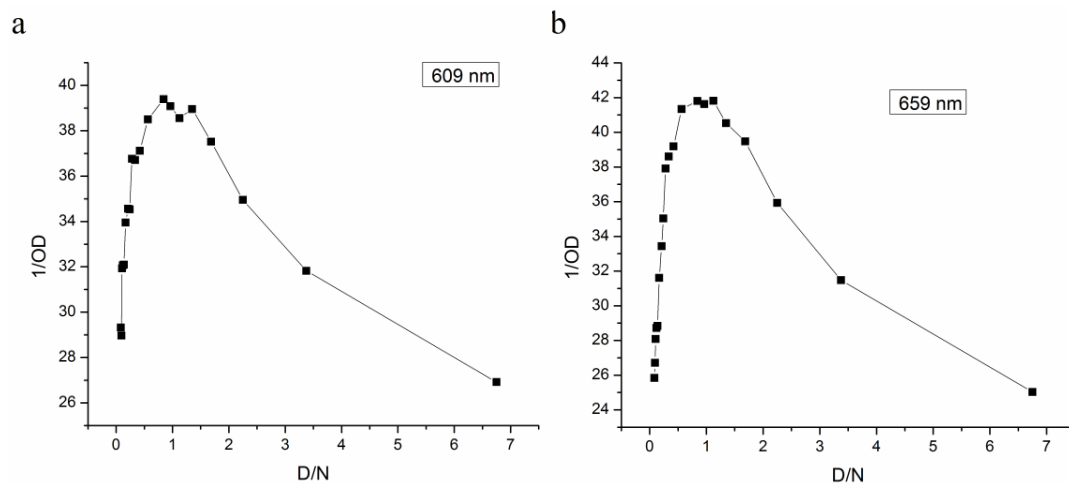


Fig. 3.3: Plot of 1/O.D versus D/N ratios at (a) 609 nm band and (b) 659 nm band.

Similar analysis has been carried out for the absorption peak at 609 nm (**Figs. 3.4c, d**) which yields a value of $K = 2.88 \times 10^6$ and $2.81 \times 10^5 \text{ M}^{-1}$ in the range $D/N = 6.7 - 0.56$ and $0.42 - 0.08$, respectively. This value is in agreement with that reported in literature [Yang *et al.*, 2005; Ibrahim, 2001], which hereby indicates high affinity of MTX with DNA. Existences of multiple binding sites or multiple stoichiometries in the ligand-DNA quadruplex have earlier been reported in literature on binding of TMPyP4 and TPrPyP4 to parallel G-quadruplex (Wei *et al.*, 2010; Kovaleva *et al.*, 2013; Freyer *et al.*, 2007) and duplex DNA (Shilpa *et al.*, 2013a, b).

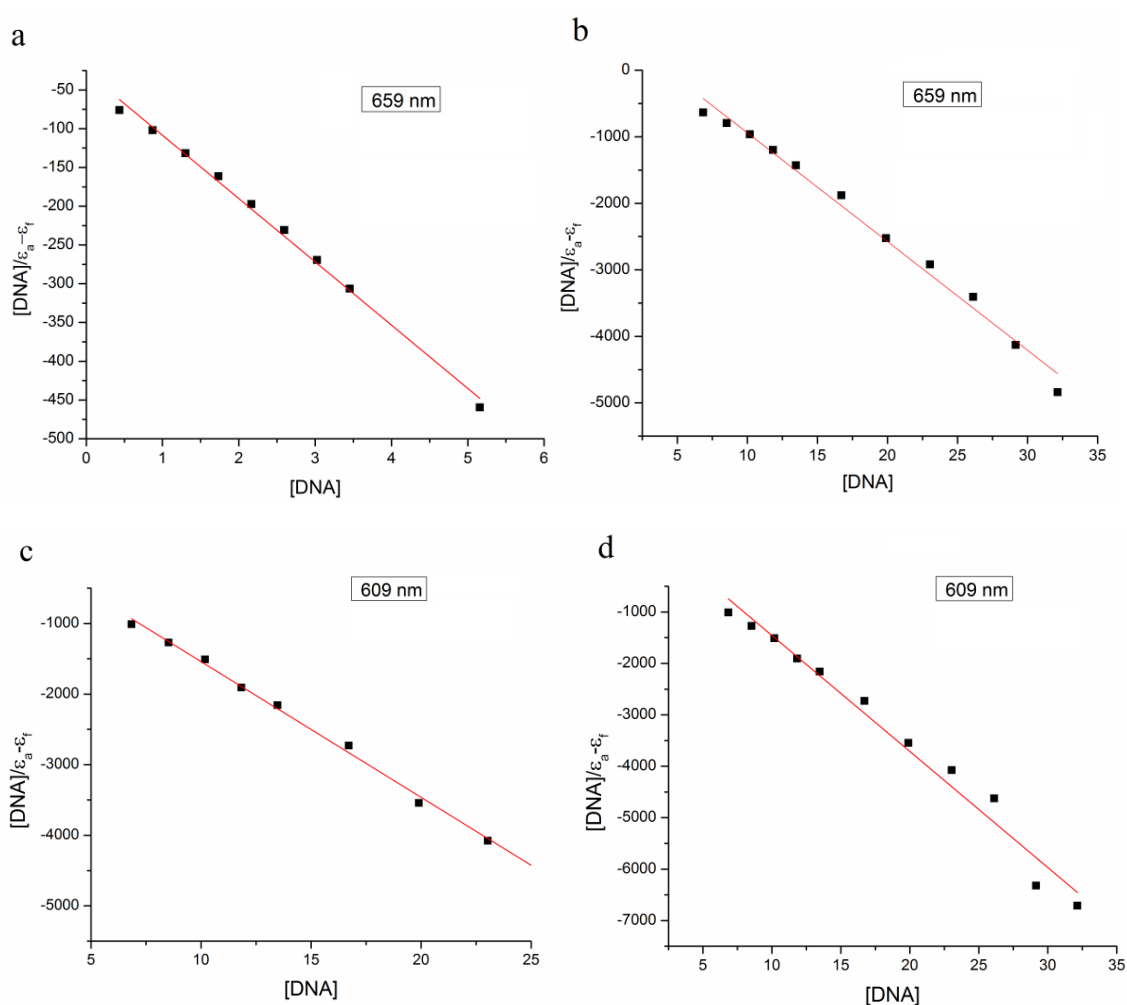


Fig. 3.4: Plot of $[DNA]/\epsilon_a - \epsilon_f$ versus $[DNA]$ (a) at 659 nm band for DNA concentrations 0.43-5.15 μM and (b) for DNA concentrations 6.84-32.5 μM . (c) at 609 nm band for DNA concentrations 0.43-5.15 μM and (d) for DNA concentrations 6.84-32.5 μM .

3.2.1 Measurement of Stoichiometry, Binding constant and Life time analysis of MTX-quadruplex using fluorescence spectroscopy

Fluorescence spectroscopy is very sensitive to the change in the environment of drug chromophore. Most of the ligands exhibit fluorescence due to presence of aromatic rings and function groups present on it. Since the intrinsic fluorescence of DNA is too low to be detected

the fluorescence property of mitoxantrone was used to monitor the changes upon interaction with quadruplex sequence $d\text{-(TTAGGGT)}_4$. When excited at $\lambda_{\text{ex}} = 609 \text{ nm}$, MTX shows a well resolved emission band with a maxima (λ_{em}) at 677 nm. Upon successive additions of DNA quadruplex to a fixed concentration of MTX ($3 \mu\text{M}$), a strong quenching of fluorescence was observed, which was accompanied by a progressive shift in λ_{em} (**Fig. 3.5a**) in the range $D/N = 13.5\text{--}0.67$. The fluorescent intensity decreased by 88% (**Table 3.2**), indicating a strong interaction of MTX with DNA quadruplex. Further addition of MTX with DNA quadruplex reversed the trend of change in fluorescent intensity (**Fig. 3.5b**) as also observed in absorbance measurements. The fluorescence increased rapidly, by a factor of eight (**Fig. 3.5b**) on variation of D/N from 0.67 to 0.08. The emission wavelength increases rapidly on adding DNA quadruplex at $D/N = 13.5\text{--}2.0$, shows minor shift at $D/N = 2.0\text{--}0.56$ and levels off to a value of 689 nm at $D/N = 0.56$ (**Fig. 3.5d**).

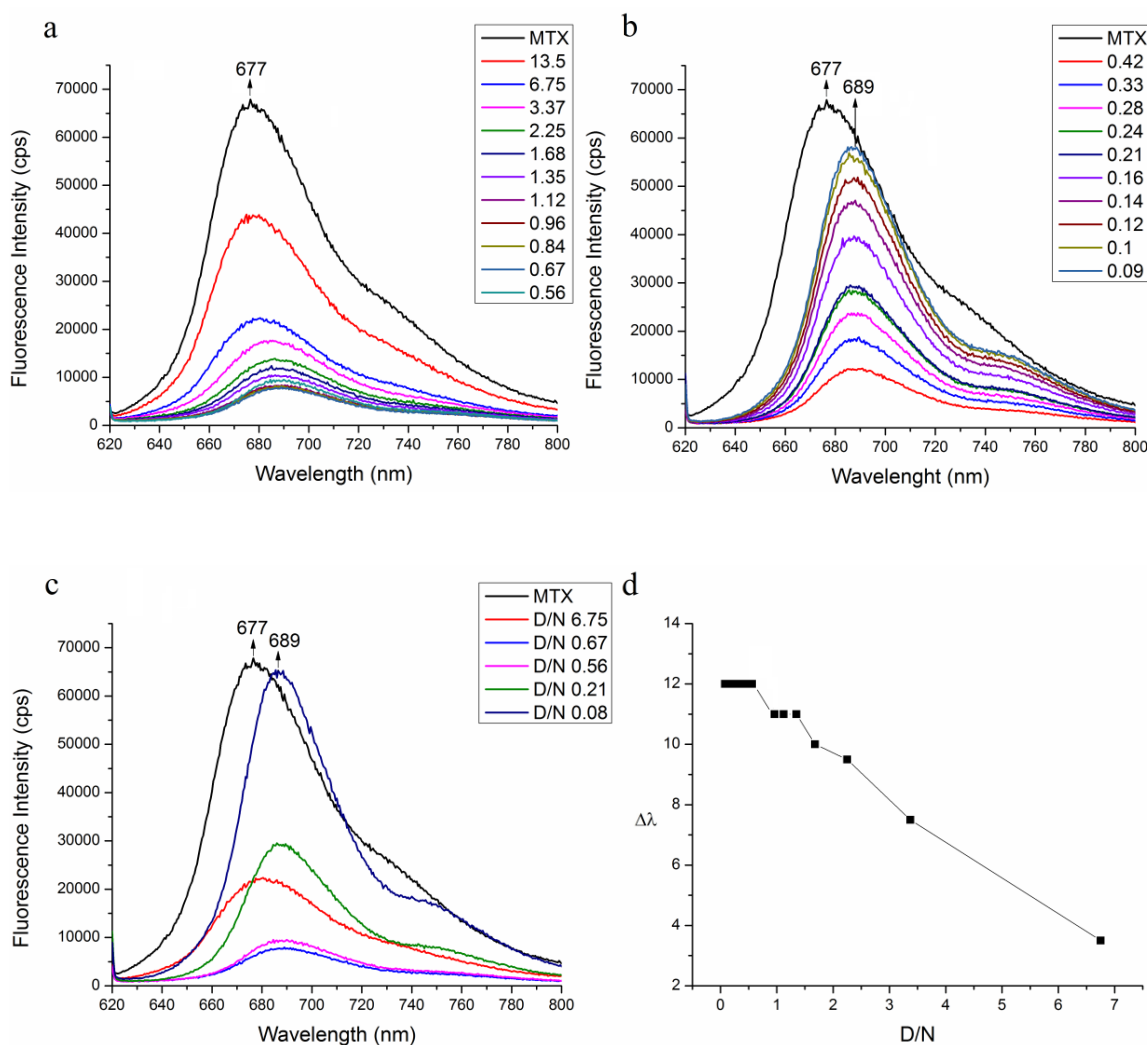


Fig. 3.5: Fluorescence emission spectra of MTX in the absence and presence of $d\text{-(TTAGGGT)}_4$ at 298 K at (a) higher D/N ratios (b) lower D/N ratios (c) change in the fluorescence emission trend at these ratios. (d) Change in the λ_{max} ($\Delta\lambda$) at varying D/N ratios. Excitation wavelength $\lambda_{\text{exc}} = 610 \text{ nm}$.

The fluorescence intensity on the other hand, shows a clear point of inflection, that is, a change in trend at $D/N = 0.56$ (**Fig. 3.6a, b**). The Stern-Volmer quenching constant K_{sv} was determined using equation 2: $-F_0/F = 1 + K_{sv} [DNA]$ (Chapter 2 section 2.3.1.2) which was linear and obtained as $2.87 \times 10^6 M^{-1}$ for $D/N = 3.37-1.12$ (**Fig. 3.7a, b**). This shows that only one type of quenching process occurs, either static or dynamic quenching (Lakowicz, 2006). The binding constant K and the stoichiometry (n) of MTX-d(TTAGGGT)₄ complex has been determined by plotting $\log [(F_0 - F)/F]$ versus $\log [DNA]$ by using the equation 3 (Chapter 2 section 2.3.1.2).

D/N	λ_{max}	Fluorescence Intensity	$\Delta\lambda$
∞	677	67078	0
13.5	677	43228	0
6.75	680.5	22374	3.5
3.37	684.5	17710	7.5
2.25	686.5	13888	9.5
1.68	687	11952	10
1.35	688	10366	11
1.12	688	8252	11
0.96	688	8122	11
0.84	689.5	8150	12.5
0.67	690	7762	13
0.56	689	9190	12
0.42	689	12130	12
0.33	689	18584	12
0.28	689	23778	12
0.24	689	27772	12
0.21	689	28854	12
0.16	689	39414	12
0.14	689	45988	12
0.12	689	51846	12
0.10	689	55772	12
0.09	689	57648	12

Table 3.2: Change in the Fluorescence emission maxima (λ_{max}), fluorescence intensity, and $\Delta\lambda$ on interaction of MTX with (TTAGGGT)₄ at varying D/N ratios.

We obtained $K=3.22 \times 10^6 M^{-1}$, $n=0.9$ and $K=1.69 \times 10^8 M^{-1}$, $n=1.7$ for $D/N = 6.75- 0.56$ and $D/N = 0.42-0.08$, respectively. Thus the fluorescence data points toward a stoichiometry of 1 and 2 (**Figs. 3.8a, b**). At lower D/N ratio the concentration of DNA is higher so drug will get more preferred binding site and all the sites will be occupied by drug hence we got higher binding constant. At this ratio approximately two drugs bind to DNA quadruplex while at higher drug concentration owing to external binding the binding constant as well stoichiometry is less compared to that of lower drug concentration.

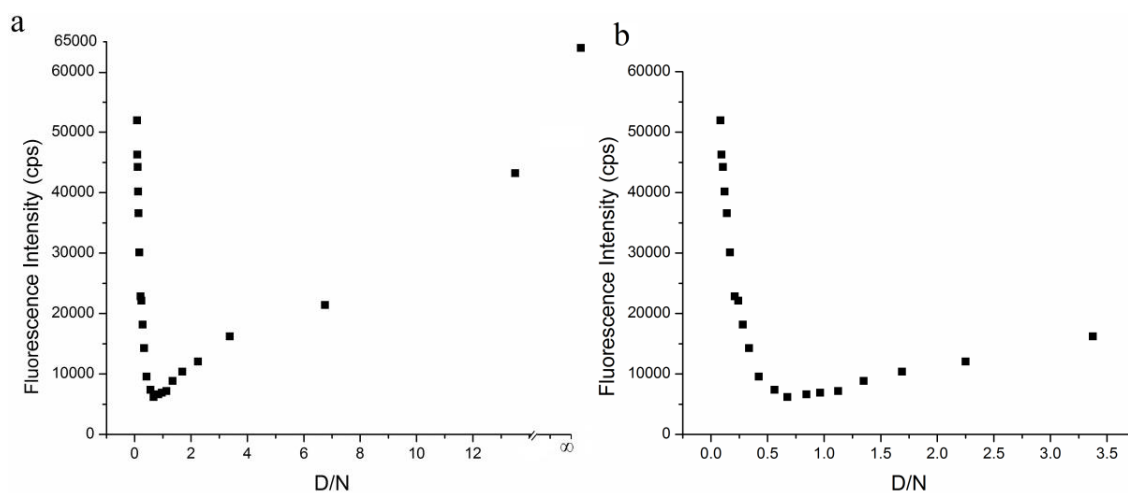


Fig. 3.6: (a, b) change in the fluorescence intensity on varying D/N ratios.

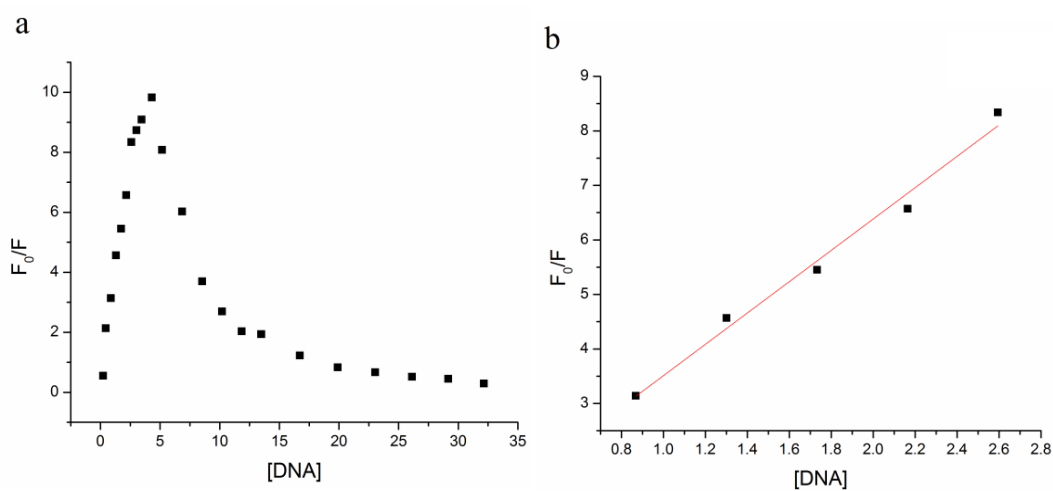


Fig. 3.7: The Stern-Volmer quenching plot of $3 \mu\text{M}$ MTX with DNA concentrations (a) full range of [DNA] i.e. $0.22\text{--}31.99 \mu\text{M}$ and (b) $[\text{DNA}] = 0.88\text{--}2.66 \mu\text{M}$.

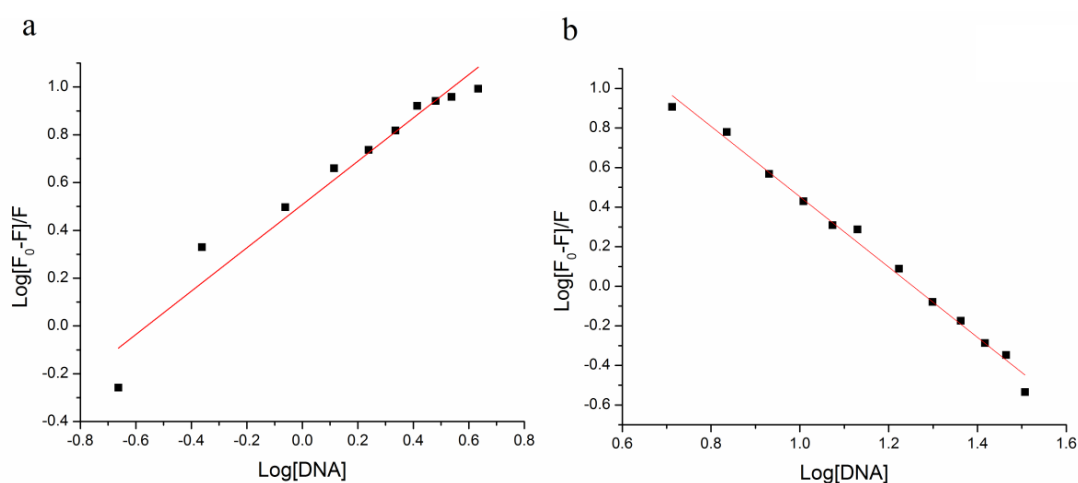


Fig. 3.8: Plot of $\log (F_0 - F)/F$ versus $\log [\text{DNA}]$ for DNA concentrations (a) $0.21\text{--}5.15 \mu\text{M}$ and (b) $6.84\text{--}32.15 \mu\text{M}$.

Similar behavior was also observed in case of binding of porphyrin to parallel G-quadruplex sequence d-(GGGGTTTTGGGG)₄ (Wei *et al.*, 2010). Our fluorescence data corroborate the findings from that of absorption and shows good affinity to the quadruplex with a binding stoichiometry of 2:1.

3.2.1.1 Continuous Variation Analysis (Job plot)

Since binding of MTX to DNA quadruplex showed formation of multiple complexes having different stoichiometry, we chose to establish the stoichiometry independently by the method of continuous variation Job plot (Job, 1928; Huang, 1982) using fluorescence. The total concentration of DNA and MTX was held constant (3 μ M) but their relative mole fractions were varied. The fluorescent intensity was measured at a wavelength of $\lambda_{em}=677$ nm using $\lambda_{ex}=609$ nm at 298 K. The difference in fluorescence intensity $\Delta F=F-F_o$ of free MTX (F_o) and its complex (F) with d-(TTAGGGT)₄ was plotted as a function of mole fraction of MTX (Fig. 8). The inflection point indicated by a change in slope gives the mole fraction of the MTX bound to d-(TTAGGGT)₄. The binding stoichiometry of MTX was obtained from $n= [(1-\chi_{ligand})/\chi_{ligand}]$, where n denotes the number of binding sites and χ_{ligand} denotes the mole fraction of ligand (MTX) at the intersection points of the two slopes obtained.

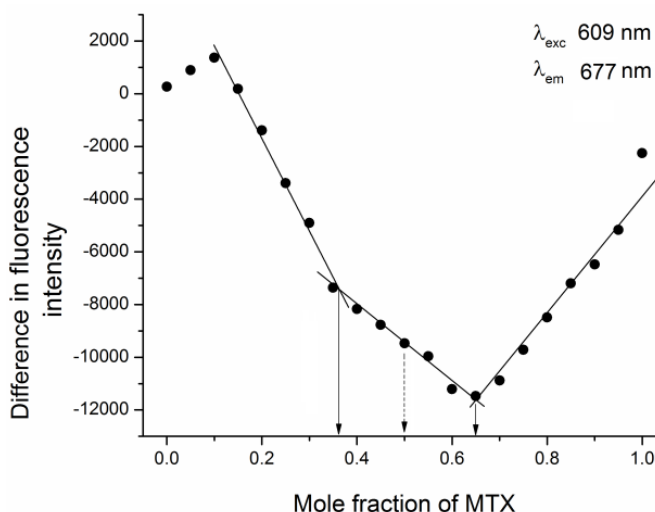


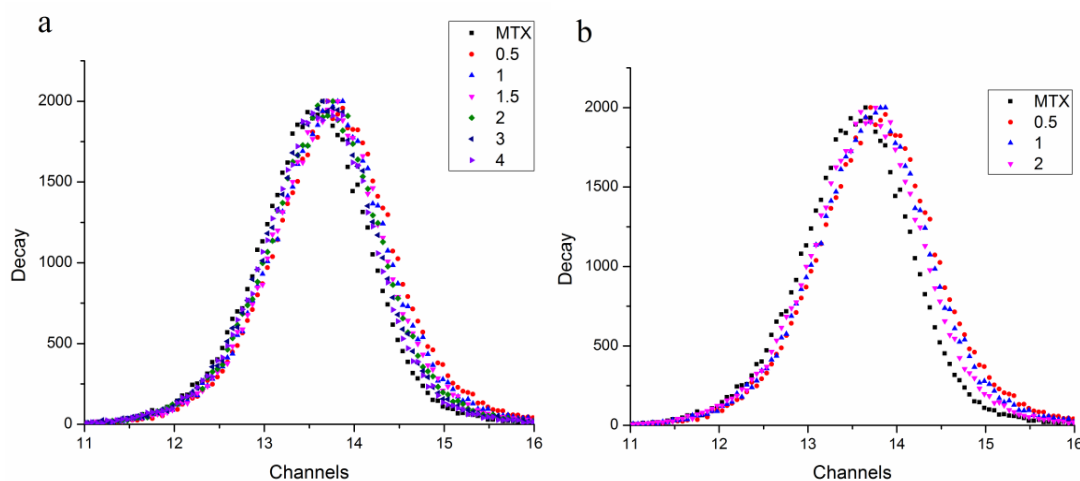
Fig. 3.9: Job plot for the binding of MTX to (TTAGGGT)₄.

Examination of Job plot (**Fig. 3.9**) shows change in slope corresponding to the mole fraction of MTX as 0.35 and 0.65 which corresponds to stoichiometry of 0.5:1 and 2:1 in MTX:d-(TTAGGGT)₄ complex. A careful inspection of the data shows the possibility of stoichiometry of 1:1 at mole fraction of MTX = 0.5 (**Fig. 3.9**), which is perhaps less evident due to the presence of multiple stoichiometries in this range. A similar result was also obtained in the

literature (Li *et al.*, 2006) with parallel G-quadruplex sequence d-(TTAGGGT)₄. This stoichiometry was consistent results obtained in fluorescence studies.

3.2.1.2 Life Time measurements

Fluorescence life time of free and bound chromophore differs which can be resolved on experimental time scale. Time-Resolved fluorescence studies can give an idea of the binding modes of ligand-DNA complex depending upon their fluorescence decay profile. The fluorescent decay of 3 μ M uncomplexed MTX is essentially monoexponential giving a life time value of 0.140 and 0.135 ns in separate experiments, which compares well with that reported in the literature (Lin and Struve, 1991; Koningstein *et al.*, 1992). The fluorescence decay profiles of MTX-d-(TTAGGGT)₄ complexes at varying D/N ratios (**Figs. 3.10a–c**) showed that the lifetime of MTX increases on binding to quadruplex. This increase in the life time is due to shielding of the MTX chromophore from solvent, which resembles to its life time of aprotic solvent (Lin and Struve, 1991). The decay profiles are biexponential and yield two sets of average values of a life time, that is, $\tau = 0.45$ ns and $\tau = 0.23$ ns at D/N = 0.5-2.0 (**Table 3.3**), which can be attributed to the presence of two species. The amplitude of longer life time decreases with D/N. Since the higher stoichiometries complex is expected to be the dominant species at D/N \sim 2, it may be inferred that the complex having $\tau = 0.23$ ns is 2:1 MTX-DNA complex with a relative abundance of 82%. The amplitude of this signal reaches a saturation of 88%-89% at D/N = 3.0-4.0 and excess MTX may be present as uncomplexed form yielding lower values of life time ($\tau = 0.15$ -0.19 ns). This life time is attributed to the externally bound MTX to quadruplex because on intercalation the life time increases about three to four times to that of free ligand. Ethidium bromide a classical intercalator shows an increase in life time $\tau = 22.2$ ns to that of free $\tau = 1.6$ ns upon binding to duplex DNA (Malathi *et al.*, 2003).



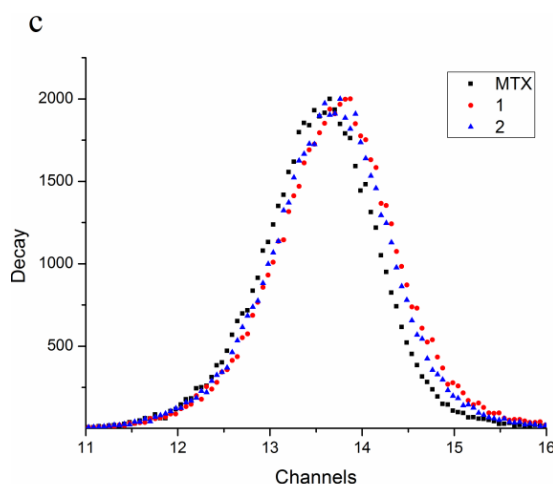


Fig. 3.10: Fluorescence decay curves of free MTX and MTX-d-(TTAGGGT)₄ complexes at varying D/N ratios at 298 K (a-c).

	τ_1 (ns)	τ_2 (ns)	α_1	α_2	χ^2
MTX	0.14	-	100	-	1.14
0.5	0.45	0.26	44.65	55.35	1.16
1	0.47	0.23	29.95	70.05	1.30
1.5	0.44	0.21	23.08	76.92	1.20
2	0.44	0.21	18.26	81.74	1.20
3	0.47	0.15	11.79	88.21	1.19
4	0.59	0.19	10.85	89.15	1.11

Table 3.3: The fluorescence lifetimes of MTX in the presence or absence of d-(TTAGGGT)₄ at 298 K (where τ denotes fluorescence lifetimes and α denotes amplitude).

3.3.1 Analysis of Conformational changes and stability of quadruplex DNA upon MTX binding using Circular Dichroism Spectroscopy

CD spectroscopy is a very sensitive technique to monitor ligand-DNA interaction. In order to study the conformational polymorphism of DNA and the change in its structure after binding to ligands, we have recorded CD spectra on titrating MTX with DNA quadruplex. Since MTX is optically inactive, change in conformation of quadruplex can be monitored in the UV region. **Fig. 3.11** shows the CD spectra of d-(TTAGGGT)₄ in the absence and presence of MTX at varying D/N ratios. We observed a positive CD band at 263 nm and a negative band at 242 nm, which are the signature peaks of parallel stranded G-quadruplex (Spada *et al.*, 2010; Kypr *et al.*, 2012; Ellestad, 2012). Apart from these two bands, positive band at 210 nm was also observed. Positive band at 263 nm has been attributed to the anti glycosidic arrangement of guanosine residue in G-quadruplex. Sequence d-(TTAGGGT)₄ thus forms a right handed parallel stranded quadruplex in presence of K⁺ ion with anti glycosidic torsional angle.

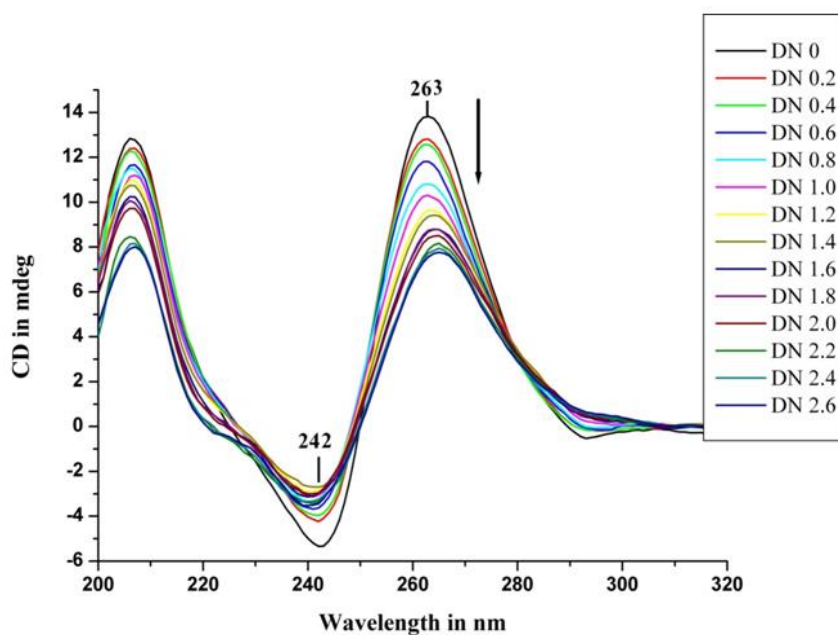


Fig. 3.11: Circular Dichroism (CD) spectra of $20 \mu\text{M}$ $d\text{-(TTAGGGT)}_4$ in the absence and presence of MTX at 298 K at varying D/N ratios.

With the addition of MTX the ellipticity of both 263 and 242 nm bands decreases, which may be attributed to the change in glycosidic bond rotation and consequently due to stacking arrangement of bases. The change in the ellipticity of 263 and 242 nm bands is accompanied by red and blue shift, respectively by a total of 3 nm (**Table 3.4**). The negative CD band at 242 nm does not shift until $D/N > 0.4$ and levels off at $D/N > 2.2$. The positive CD band on the other hand, does not shift until $D/N > 1.2$ is reached and levels off at $D/N > 2.4$. **Fig. 3.12a** shows the change in ellipticity of the positive band as a function of added MTX to quadruplex ratio (D/N), which gave an inflection point at ~ 1.22 and ~ 2.1 indicating a 1:1 and 2:1 stoichiometry. The change in ellipticity of 242 nm band shows slope change at ~ 0.48 and 1.5 (**Fig. 3.12b**). The maximum change in ellipticity, $\Delta\epsilon$, over the observed range of D/N for positive band at 263 nm is ~ 6.3 mdeg and that of negative band at 242 nm ~ 1.8 mdeg. When an achiral ligand binds to chiral DNA an induced CD (ICD) bands are observed within the absorption region of bound ligand. The shape and sign of ICD band determine the mode of binding. Groove binding results in a strong and positive ICD band while intercalators usually show weak and negative ICD band (Ellestad, 2012). Therefore in order to look for induced band of achiral MTX due to binding to chiral DNA, a different set of experiment was done in which the MTX concentration was kept constant at $20 \mu\text{M}$ and DNA quadruplex was progressively added to it.

D/N	Milideg. 242	λ_{\max} 242	Milideg. 263	λ_{\max} 263
(TTAGGGT) ₄	-5.341	242	13.824	263
0.2	-4.234	242	12.820	263
0.4	-3.957	242	12.572	263
0.6	-3.680	241	11.818	263
0.8	-3.345	240	10.816	263
1	-3.130	241	10.299	263
1.2	-2.902	241	9.638	263
1.4	-2.700	241	9.424	264
1.6	-3.133	240	8.786	264
1.8	-2.999	241	8.794	264
2	-3.047	240	8.516	265
2.2	-3.413	241	8.163	265
2.4	-3.344	239	7.946	265
2.6	-3.523	239	7.717	266

Table 3.4: Change in the ellipticity (Θ) and λ_{\max} for positive CD band (263 nm) and negative CD band (242 nm) on varying D/N ratios.

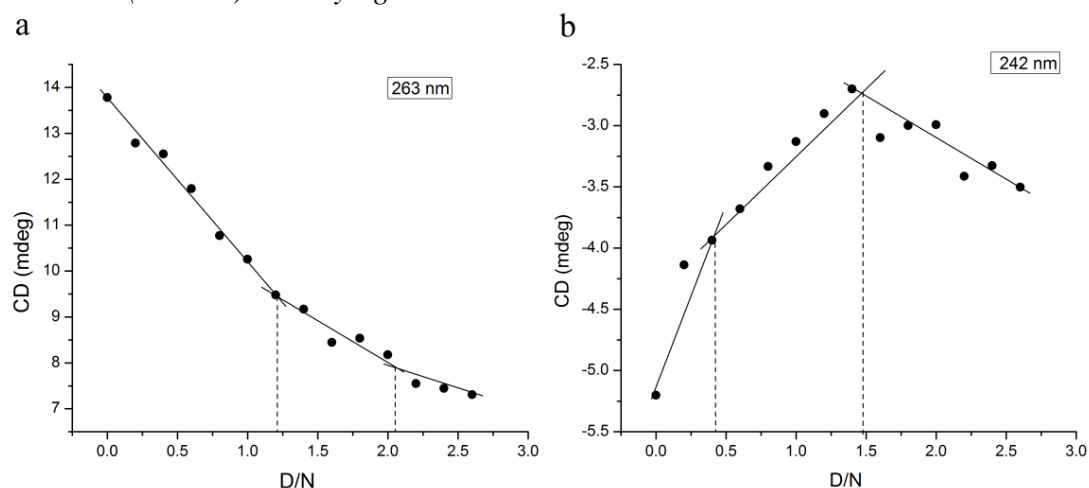


Fig. 3.12: Plot of change in the ellipticity (Θ) versus varying D/N ratios for (a) positive CD band (263 nm) and (b) negative CD band (242 nm).

The induced negative CD (ICD) band having ellipticity = 0.8–0.9 mdeg, appeared at 639 nm and lies within the range of absorption of MTX molecule, which is a clear proof of formation of bound complex of MTX-d-(TTAGGGT)₄ (Figs. 3.13a, b). This clearly shows that MTX binds to quadruplex in an end-stacking mode out of two apparently binding modes observed in absorption and fluorescence studies. The intensity of ICD signal did not vary significantly with D/N within the limits of experimental error and apparently remain same at D/N > 0.5.

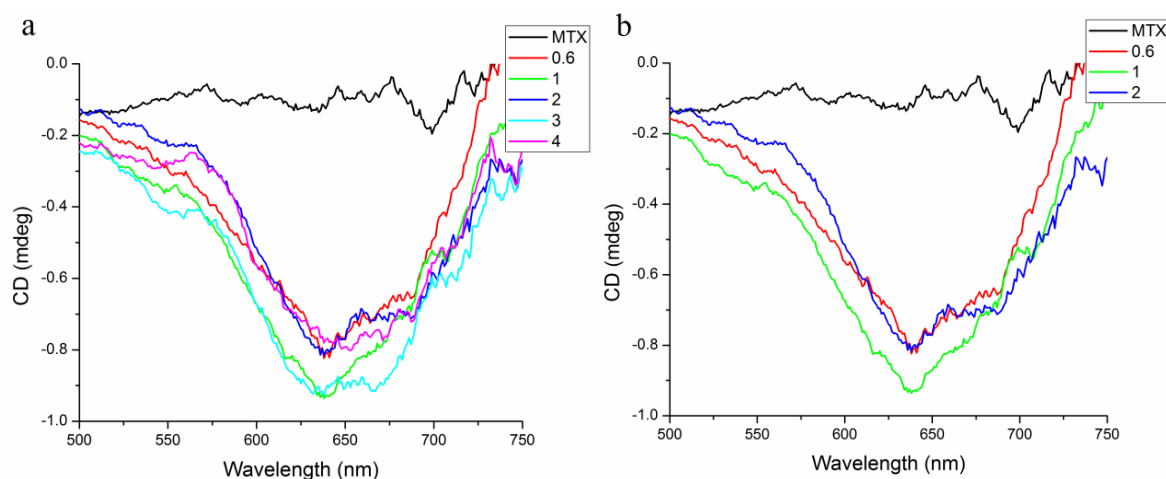
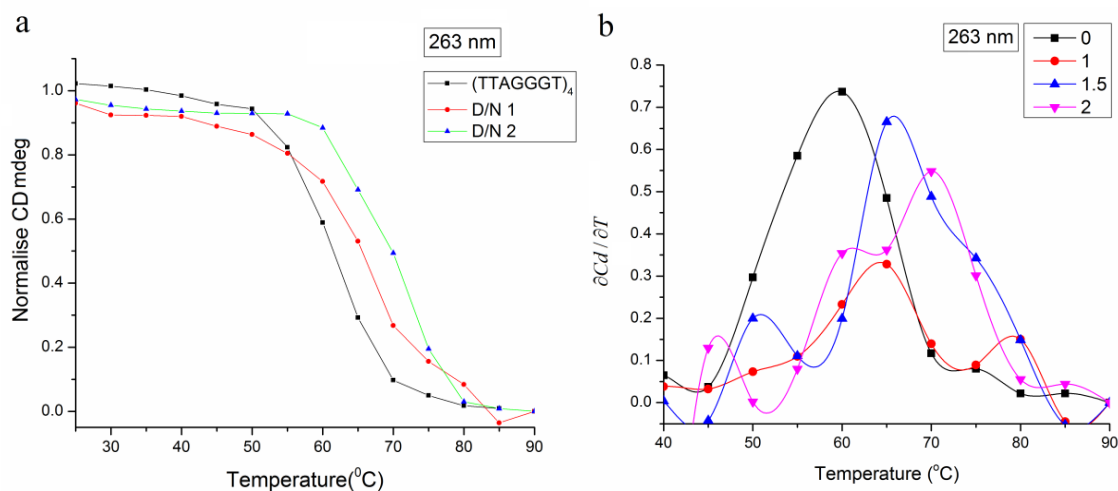


Fig. 3.13: Induced CD spectra of 20 μM MTX complexed with $d\text{-(TTAGGGT)}_4$ at varying D/N ratios (a, b).

3.3.2 Circular Dichroism Melting (T_m) studies

Thermal stability of quadruplex upon binding to MTX has been monitored using CD spectroscopy. MTX was added progressively to a fixed concentration (20 μM) of quadruplex and the ellipticity at 263 nm was recorded as a function of temperature. The melting profile of uncomplexed quadruplex and its complex with MTX at D/N = 1–3 are shown in **Fig. 3.14a**, which clearly shows increase in T_m due to binding of MTX leading to stabilization of G-quadruplex. The change in T_m was better manifested in the plot of derivative of CD signal with respect to temperature (**Fig. 3.14b**) and has been plotted as a function of D/N ratio (**Fig. 3.14c**, **Table 3.5**). The uncomplexed quadruplex sequence $d\text{-(TTAGGGT)}_4$ gives $T_m = 58^\circ\text{C}$. T_m increases linearly and gets saturated at D/N = 2.0 to a value of 71°C (**Table 3.5**), with a total increase at saturation, $\Delta T_m = 13^\circ\text{C}$. The results establish that a maximum of two MTX molecules bind to DNA quadruplex and the highest stoichiometric ratio in MTX-DNA quadruplex complex is 2:1.



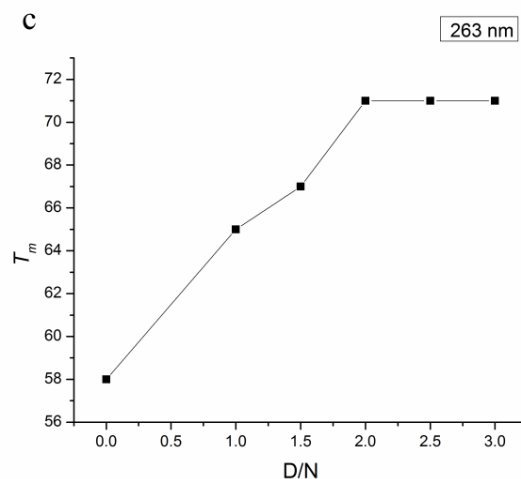


Fig. 3.14: (a) CD melting curves of 20 μ M d -(TTAGGGT)₄ in the absence and presence of MTX at D/N ratios 1.0, 2.0; (b) derivative plots at D/N ratios 1.0, 1.5, 2.0.(c) plot of change in melting temperature (T_m) versus D/N.

D/N	T_m (°C)	ΔT_m
d -(TTAGGGT) ₄	58	
1	65	7
1.5	67	9
2	71	13
2.5	71	13
3	71	13

Table 3.5: CD melting temperature (T_m) of d -(TTAGGGT)₄ and its complex with MTX at D/N ratios 1.0, 1.5, 2, 2.5, 3.0 and its corresponding ΔT_m

Stability of quadruplex by ligand binding in groove and end stacking results in increase of T_m by 13-14°C on the binding of peimine and its analogue peiminine to human telomeric DNA (Li et al., 2009) and 11°C on the stacking of Actinomycin D on the terminal G-tetrad (Hudson et al., 2009) while intercalating drug RHPS4 shows an increase of T_m by 20°C. Hence we can say that the observed stability lies in the range of groove binding and end stacking.

3.4.1 Differential Scanning Calorimetry (DSC) studies

The thermal stability of quadruplex upon binding to MTX was also measured using DSC. The melting curve of uncomplexed quadruplex fits in a single state thermal transition giving $T_m \sim 64$ °C while that of complexed showed a two-state thermal transition. The first melting transition showed an increase in the thermal stability of quadruplex to 71-72 °C on increasing the MTX to quadruplex ratios. The second transition has a melting temperature of 55-56 °C. (Fig. 3.15, Table 3.6). Presence of two melting transitions have already been reported in literature (Hudson et al., 2009) for longer repeat human quadruplex sequence that is,

d[AGGG(TTAGGG)₃]. The reason for such transition in case of the latter is either due to the existence of two conformers or due to the formation of a stable intermediate. This is quite possible as intramolecular human quadruplex (d[AGGG(TTAGGG)₃]) is found to coexist in two forms, which is in equilibrium in solution. The sequence d-(TTAGGGT)₄ predominantly form a single parallel stranded G-quadruplex structure, which will be discussed later in chapter 4. So a two melting transition in this case may be due to the presence of two independent binding site. Presence of 2:1 stoichiometry in MTX-d-(TTAGGGT)₄ complex is already being discussed in this chapter, which was strengthened by the finding of NMR studies (will be discussed in chapter 4). The affinity of both the binding varies, so the increase in thermal transition is due the binding of first MTX molecule with higher affinity. Thus, in a nutshell we can say that MTX forms a stable complex with quadruplex sequence d-(TTAGGGT)₄, which is responsible for the enhanced stability of complex compared to that of uncomplexed quadruplex.

Table 3.6:
DSC-deriv

D/N	T _{m1} (°C)	ΔH ₁ (cal/mol)	ΔH _{v1} (cal/mol)	T _{m2} (°C)	ΔH ₂ (cal/mol)	ΔH _{v2} (cal/mol)
0	63.95 ± 0.06	50.23 × 10 ³	54.21 × 10 ³	-	-	-
1	71.35 ± 0.07	52.51 × 10 ³	73.78 × 10 ³	55.28 ± 0.39	46.78 × 10 ³	35.11 × 10 ³
2	72.04 ± 0.07	53.06 × 10 ³	75.49 × 10 ³	56.46 ± 0.56	35.03 × 10 ³	35.88 × 10 ³

ed thermodynamic parameters associated with the interactions of MTX with d-(TTAGGGT)₄.

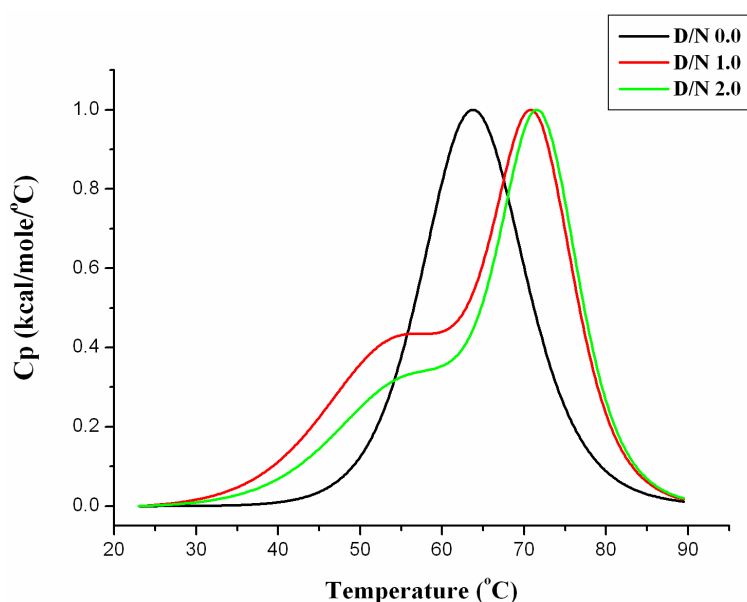


Fig. 3.15: DSC thermograms of uncomplexed d-(TTAGGGT)₄ and its complex with MTX at D/N ratios 0.5, 1.0, 1.5, 2.0.

3.5.1 Characterization the telomerase inhibitory effects of MTX using Telomerase Repeat Amplification Protocol (TRAP) Assay

Formation of G-quadruplex in the telomeric region of human chromosome followed by its stabilization with small ligands, leads to the uncapping of telomere as well as the inhibition of telomerase activity. It's a prominent strategy for anticancer therapy. Cancerous cells like MCF-7 have high level of telomerase activity, hence the telomerase extracted from this cell line was used as positive control. For negative control the reaction mixture was heated to inactivate telomerase activity. The telomerase inhibitory effect of mitoxantrone was tested at increasing concentrations in the range of 0.1–10 μM . Since it's a fluorescence based assay so PCR products were directly quantified using a spectrofluorimeter. The relative fluorescence intensity $\Delta F/\Delta R$ was used as the measure of telomerase activity. **Fig. 3.16** show that upon increasing the concentration of mitoxantrone from 0.01 μM to 10 μM the relative fluorescence intensity $\Delta F/\Delta R$ decreases. At 1 μM concentration MTX shows ~30 % inhibition of telomerase activity and at 10 μM the percentage of inhibition increases to 60 %. It shows IC_{50} value of 2 - 4 μM . The result of the TRAP assay confirms dose dependent telomerase inhibition by mitoxantrone, which is owing to its binding and stabilization of G-quadruplex structure. Its telomerase inhibition activity is greater than many of the known anthraquinone derivatives (Cairns *et al.*, 2002). Thus we conclude that MTX can be promising G4 ligand with implications towards G-quadruplex mediated telomerase inhibition for anticancer therapy.

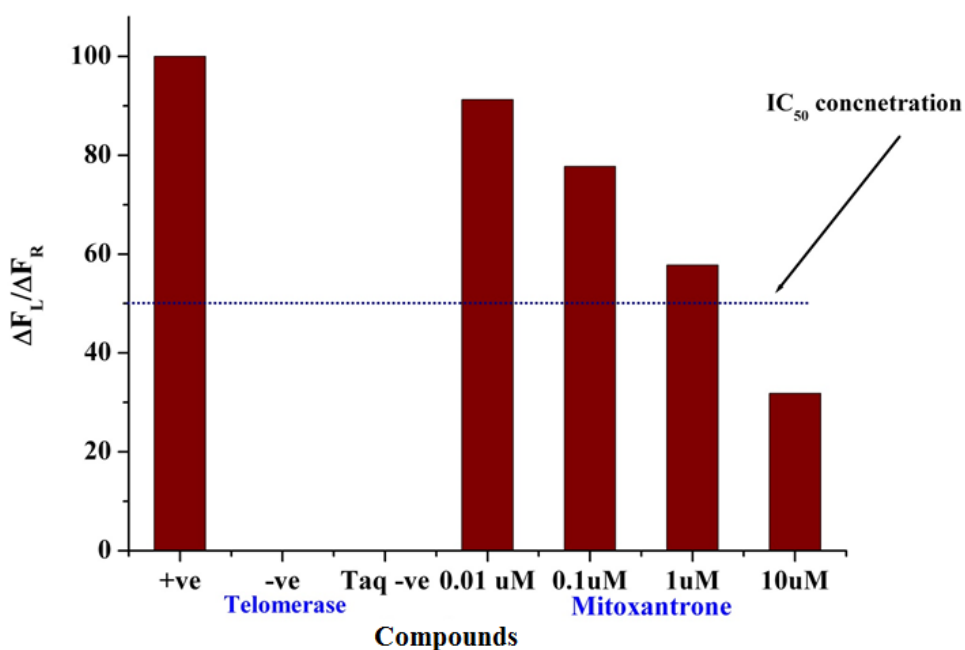


Fig. 3.16: Inhibitory effect of MTX on telomerase activity determined by TRAP assay.

3.2 Conclusion

Formation of G-quadruplex in the telomeric region of human chromosome followed by its stabilization with small ligands is the prominent strategy for telomerase inhibition. Anthraquinone and its derivatives constitute a major class of anti-cancer agents. One such compound of this class is MTX, which is well known for its anticancer properties. Several studies have been carried out on the interaction of mitoxantrone with duplex DNA and RNA, but there is no report on its interaction with G-quadruplex DNA. In order to gain insights into its mechanism of action with G-quadruplex structures, I have characterized the interaction of MTX with human G-quadruplex sequence using multiple optical spectroscopic and thermodynamic techniques. The absorption studies show hypochromicity and red shift in both the visible band of MTX i.e. 609 nm and 659 nm. There are apparently two binding modes- one at higher D/N ratios which is marked by an isobestic point at 677 nm and hypochromicity and second at lower D/N ratios that lack isobestic point and shows hyperchromicity. The binding constant in case of higher D/N ratios is in the range of 3.04×10^6 and that of lower D/N is $2.35 \times 10^5 \text{ M}^{-1}$. Fluorescence studies also show a dual mode of interaction similar to that observed in absorption experiments with high binding affinity and a stoichiometry of both 1:1 and 2:1. This stoichiometry was further strengthened by Job plot. Life time studies also confirm the existence of two species with an increase in a fluorescence life time value compared to that of free MTX. Presence of induced negative CD (ICD) band within the absorption range of MTX molecule, gives a clear proof of the formation of bound complex of MTX-d-(TTAGGGT)₄. This binding leads to thermal stabilization of G-quadruplex with an increase in T_m of 13°C. DSC studies also showed that MTX forms a stable complex with quadruplex sequence d-(TTAGGGT)₄, which is responsible for the enhanced stability of complex compared to that of uncomplexed quadruplex. Finally, TRAP assay reactions were carried out to assess the ability of MTX towards telomerase inhibition, which in turn can throw light on its anticancer property. TRAP assay shows dose dependent telomerase inhibition through G-quadruplex stabilization. In a nutshell we can say that MTX can be a promising G4 ligand with implications towards G-quadruplex mediated telomerase inhibition for anticancer therapy.

NMR Structure of Mitoxantrone bound to human G-quadruplex DNA

Formation of G-quadruplex in the telomeric region of human chromosome followed by its stabilization with small ligands is the prominent strategy for telomerase inhibition. This has led to structure-based drug designing of molecules specific to G-quadruplex that can act as a potential target for broad-spectrum anticancer therapies. Several ligands are evaluated for telomerase inhibition but lack of structural data of G-quadruplex-ligand complexes has restricted therapeutic applications. Anthraquinone derivative is one of the most important classes of G4 ligands but till date there is not a single X-ray crystal/NMR structure available on G-quadruplex structures with anthraquinone derivatives. The present chapter presents deep insights into the structural interactions of human G-quadruplex forming telomere single repeat sequence d-(TTAGGGT) with mitoxantrone (a synthetic anthraquinone derivative). Structural elucidation of MTX-d-(TTAGGGT)₄ complex was done using Nuclear Magnetic Resonance (NMR) techniques followed by restrained Molecular Dynamics (rMD) simulations. Following sets of experiments were done for the assignment of various resonances in uncomplexed and complexed states.

- 1D ¹H and ¹³C NMR and 2D ¹H-¹H ROESY and ¹H-¹³C HSQC of MTX in 90% H₂O and 10% D₂O.
- 1D ¹H and ³¹P NMR of d-(TTAGGGT)₄ over a range of temperature between 278-348 K in 90% H₂O and 10% D₂O.
- 2D ¹H-¹H NOESY at 298 K using mixing time $\tau_m = 100, 200, 250$ ms in 90% H₂O/10% D₂O.
- 2D ¹H-¹H COSY and ¹H-¹³C HSQC at 298 and 318 K, respectively in 90% H₂O/10% D₂O.
- 1D ¹H and ³¹P NMR of MTX-d-(TTAGGGT)₄ complex at various D/N ratios of 0.25, 0.5, 0.75, 1.0, 1.25, 1.5, 1.75 and 2.0 over a range of temperature between 278-318 K in 90% H₂O/10% D₂O.
- 2D ¹H-¹H NOESY at D/N = 1.0 and 2.0 using mixing time $\tau_m = 100, 200, 250$ ms at 278, 298, 308 and 318 K in 90% H₂O/10% D₂O.
- 2D ¹H-¹H COSY at D/N = 1.0 and 2.0 at 298 and 318 K in 90% H₂O/10% D₂O.
- 2D ¹H-¹³C HSQC at D/N = 2.0 at 318 K in 90% H₂O/10% D₂O.
- Restrained molecular dynamics studies on the solution structure for the complex of mitoxantrone with d-(TTAGGGT)₄ in D/N ratio of 2:1 using inter-proton distances obtained from 2D NOESY 200 ms as restraints.

4.1: Results and Discussion

4.1.1 Resonance assignment of mitoxantrone

The complete unambiguous assignment of all proton and carbon resonances of mitoxantrone (Table 4.1) were done using standard NMR techniques of ^1H 1D NMR, ^{13}C NMR and two dimensional ^1H - ^{13}C HSQC, ^1H - ^{13}C HMBC, ^1H - ^1H ROESY, techniques. Analysis of the proton NMR spectrum of mitoxantrone (Fig 4.1) shows eight proton resonances which constitute both the aromatic and aliphatic protons. The two singlets resonating at 6.71 and 6.82 ppm are due to aromatic ring protons, 2H/3H and 6H/7H. Mitoxantrone is a C_2 -symmetry molecule, hence the aromatic resonances 2H and 3H is expected to give a single resonance, the same behavior is expected for other aromatic resonance 6H and 7H and side chains protons. Four triplets resonating in the region 3.2–4.0 ppm are attributed to four sets of methylene protons. Among the spin–spin coupled pairs of methylene protons, 14CH_2 – 13CH_2 and 11CH_2 – 12CH_2 , the 14CH_2 and 11CH_2 protons are expected to be downfield shifted, being attached to 14OH and 11NH protons, respectively. The amino proton coupled to 11CH_2 protons is assigned to 11NH. All methylene protons are assigned accordingly. The resonance at 13.23 ppm has been assigned to 1OH/4OH being the maximum downfield shifted protons.

MTX Protons	Proton Chemical shift δ (ppm)	MTX Carbon	Carbon Chemical shift δ (ppm)	Lown <i>et al.</i> , 1985	Varani <i>et al.</i> , 2009	Dogra <i>et al.</i> , 2013
11NH	9.68					
6/7H	6.82	6C/7C	123.25	7.02	7.12	6.69
2/3H	6.71	2C/3C	124.58	7.12	6.92	6.48
1,4OH	13.23					
11CH ₂	3.53	11C	41.91	3.78	3.69	3.49
12CH ₂	3.24	12C	49.14	3.39	3.35	3.27
13CH ₂	3.21	13C	52.44	3.28	3.23	3.25
14CH ₂	3.88	14C	60.05	3.90	3.86	3.89

Table 4.1: Proton and carbon chemical shift assignments of MTX at 298 K.

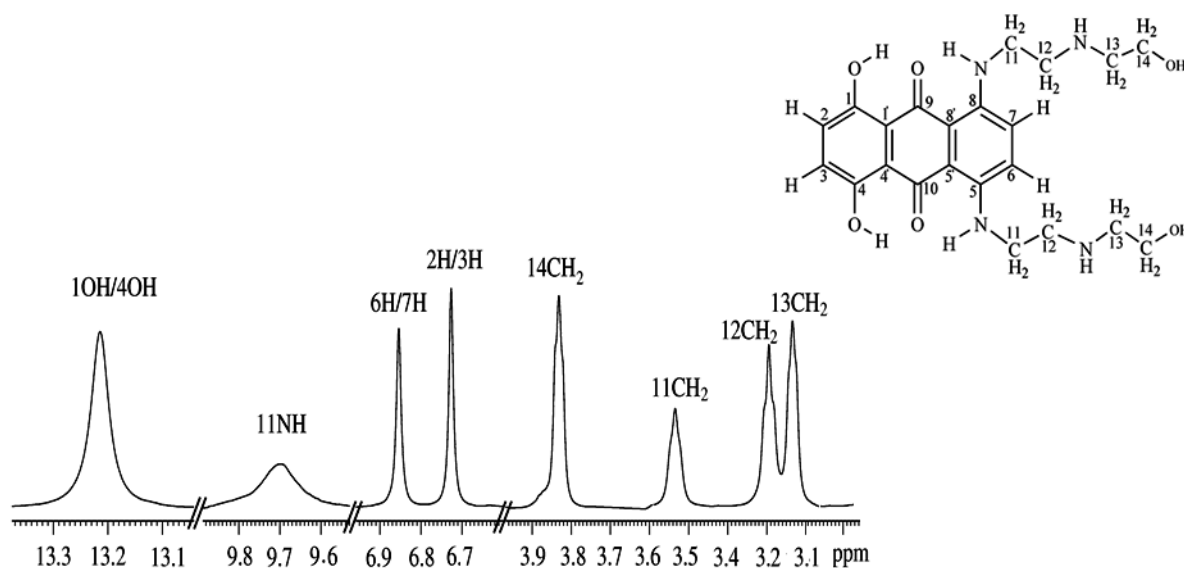


Fig. 4.1: Proton NMR spectra of 10 mM MTX in KBPES buffer at 298 K.

The ^1H - ^{13}C HSQC spectra (**Fig. 4.2**) show six protons that were directly coupled to their respective carbon atoms. Four methylene carbons i.e. 11C, 12C, 13C and 14C resonates in the aliphatic region of 40–60 ppm while that of aromatic carbons (6C/7C and 2C/3C) resonates between 126–128 ppm.

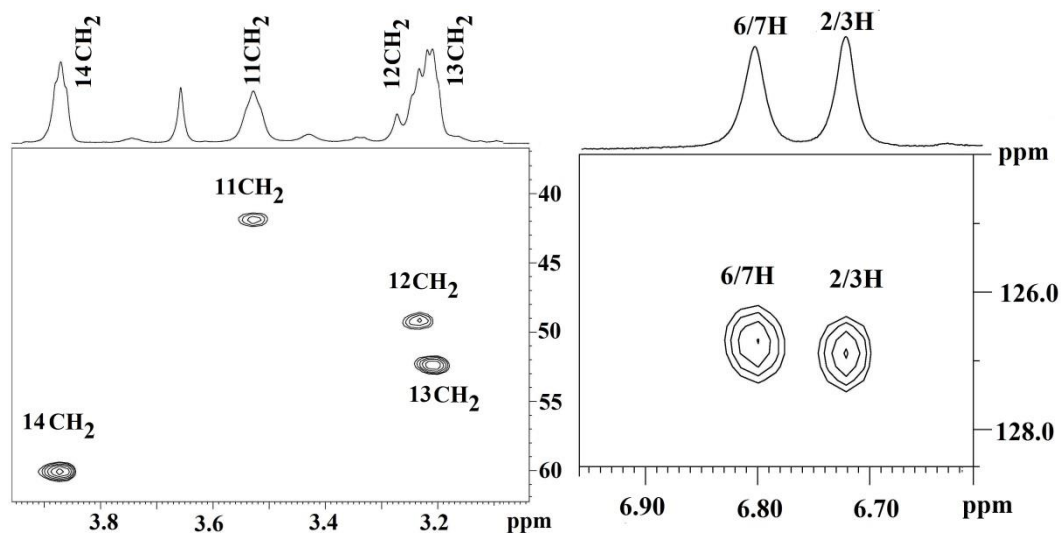


Fig. 4.2: ^1H - ^{13}C HSQC spectra of mitoxantrone showing resonances of methylene and aromatic protons.

4.1.2 Resonance assignment of uncomplexed sequence d-(TTAGGGT)₄

We have chosen an oligonucleotide sequence d-(TTAGGGT)₄ (**Fig. 4.3**), which is a single repeat sequence of human telomere with an extra thymine at the 3' position to prevent the aggregation of end stacking of G-tetrads. Sequence with longer G tracts exists in different forms, which coexist in solution in equilibrium making the interpretation of ligand-quadruplex interactions difficult. Shorter sequence capable of forming G-quadruplex can be an ideal model

for the easier interpretation of ligand-quadruplex interactions. Oligonucleotide sequence d-(TTAGGGT), form a right handed parallel stranded G-quadruplex in presence of K⁺ ion (100 mM) and that was independently proved by CD spectroscopy (Chapter 3 section 3.3.1).

The complete unambiguous assignment of the non-exchangeable and exchangeable protons of d-(TTAGGGT)₄ have been accomplished by a combination of analysis of both 1D ¹H and ³¹P and 2D ¹H-¹H NOESY, COSY, and ¹H-¹³C HSQC NMR experiments. The sugar protons were assigned by COSY experiments and the bases were assigned based on the sequential NOEs connectivities of base GH8/TH6 with H1', H2', H2'' protons.

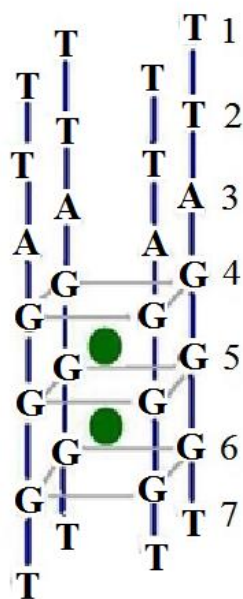


Fig. 4.4: Schematic representation of parallel-stranded G-quadruplex structure formed by oligonucleotide sequence d-(TTAGGGT)₄.

Proton NMR spectrum of d-(TTAGGGT)₄ at 25°C (**Fig. 4.5a**) shows the formation of a single predominant quadruplex structure with three well resolved imino (NH) peaks resonating between 10.5 to 12 ppm region. The number of the imino resonances present is directly related to the number of G residue participated in G-tetrad formation.

Thus the presence of three NH peaks, which corresponds to three G residues, i.e. G4:G4:G6 indicates the formation of three G-tetrads. The upfield shift of these imino resonances is due to the stacking arrangement of G-tetrads that shows Hoogsteen type H-bonding (NH...O). On contrary to this the imino resonances of duplex DNA shift downfield (Keniry, 2001; Webba da Silva, 2007). All the four strands associate to form a tetramolecular quadruplex structure, having a C₄ symmetry in which all the strands are equivalent and orient in the same 5' to 3'direction.

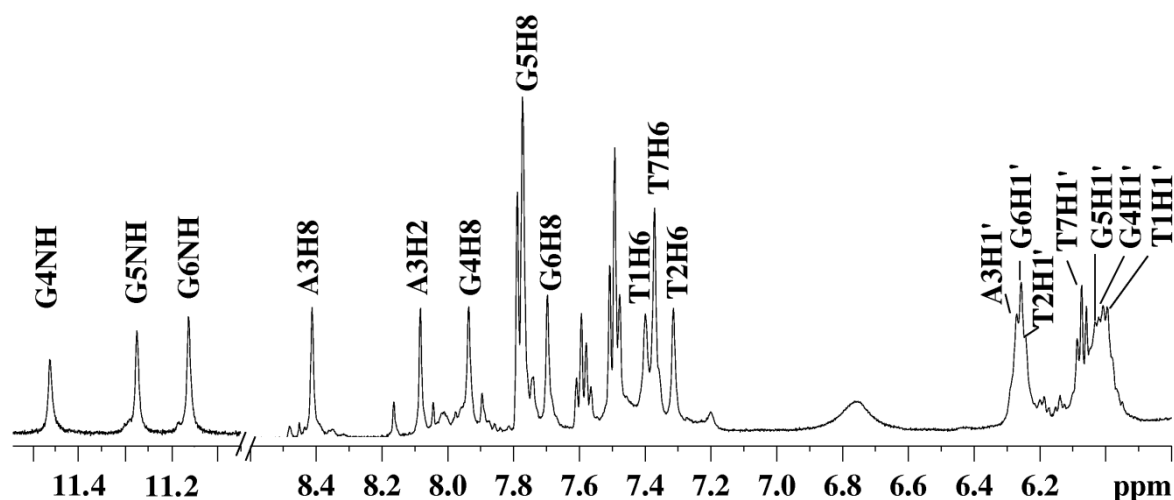


Fig. 4.5: (a) 1D proton spectrum of uncomplexed quadruplex sequence $d\text{-(TTAGGGT)}_4$ showing exchangeable and non-exchangeable resonances.

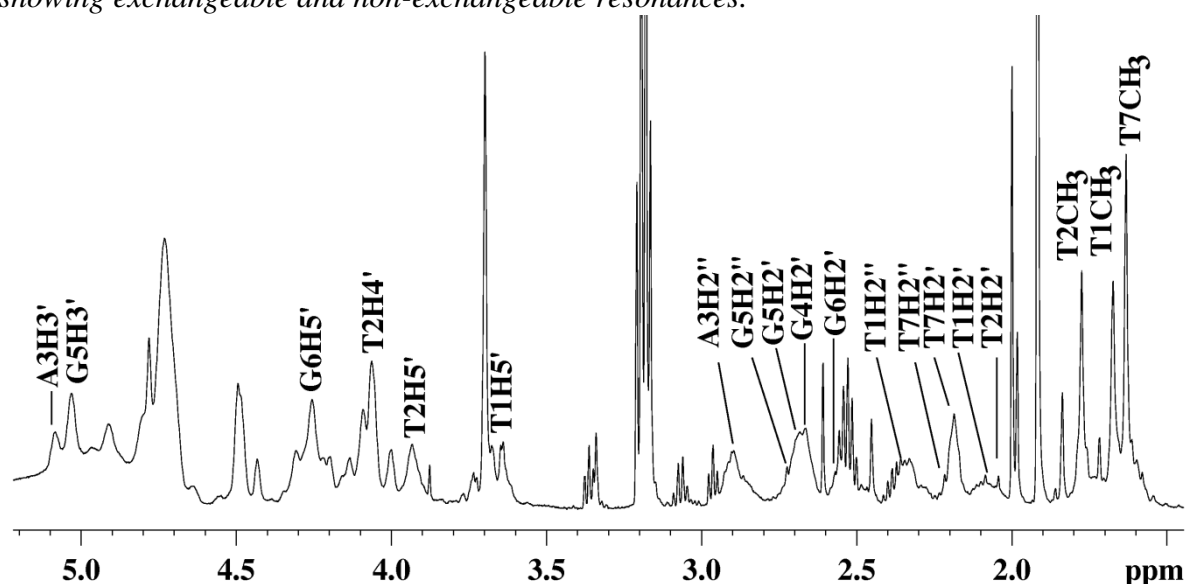


Fig. 4.5 (b): 1D proton spectrum of uncomplexed quadruplex sequence $d\text{-(TTAGGGT)}_4$ showing sugar and methyl resonances.

We have not observed the imino protons of T (thymine) owing to its fast exchange with solvent. Apart from the major dominant resonances some minor resonances were also observed that corresponds to the single stranded components. The imino proton resonances were sharp and are unaffected by increase in temperature, which persist till 55°C. This sharp resonance clearly indicates that these protons are in slow exchange with surrounding water molecules in NMR time scale. Two distinct sets of amino resonances were observed for each guanine. One was involved in hydrogen bonding hence appeared downfield while that of the other was

exposed to solvent, results in an upfield position. The non-exchangeable resonances (**Fig. 4.5b**) (bases and sugar) cover a major portion between 1.5-8.5 ppm.

NOESY spectra also give evidence for G-tetrad formation (**Fig. 4.6**) due to the presence of NH-NH NOE connectivity that exist between adjacent NH protons in the sequence G4-G5-G6 (**Fig. 4.7a**) and the presence of interstrand NOEs between guanine imino proton to its own and its 5' flanking base protons in A3-G4-G5-G6 segment of d-(TTAGGGT)₄ sequence (**Fig. 4.7b**) (Wang and Patel, 1992). Such long range NOE cannot be possible within same strand. The observed NH and base protons connectivities showed a good stacking interaction that persists not only between G-tetrads but also to some extent to adenine (A3).

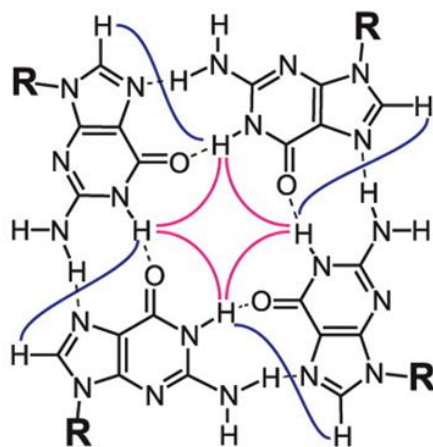


Fig. 4.6: G-tetrad showing NH-NH and NH-H8 connectivities that can be observable in NOESY experiments.

Classical sequential assignment used for nucleic acid was employed for the assignment of the nonexchangeable protons of quadruplex (Wuthrich, 1986), which were done by observing NOE connectivities between base H8/H6 protons to its own and its 5' flanking H1'/H2'/H2'' sugar protons (**Fig. 4.8 a, b**). This hereby indicates the presence of right handed helical geometry similar to that observed in B-DNA. 5'-anti-3'-anti conformation was determined by observing the connectivity of base H8/H6-H1' whose distance was in the range of 3.5-3.7 Å.

The structure of the uncomplexed sequence d-(TTAGGGT)₄ is consistent with that reported in the literature (Gavathiotis and Searle, 2003; Wang and Patel, 1993).

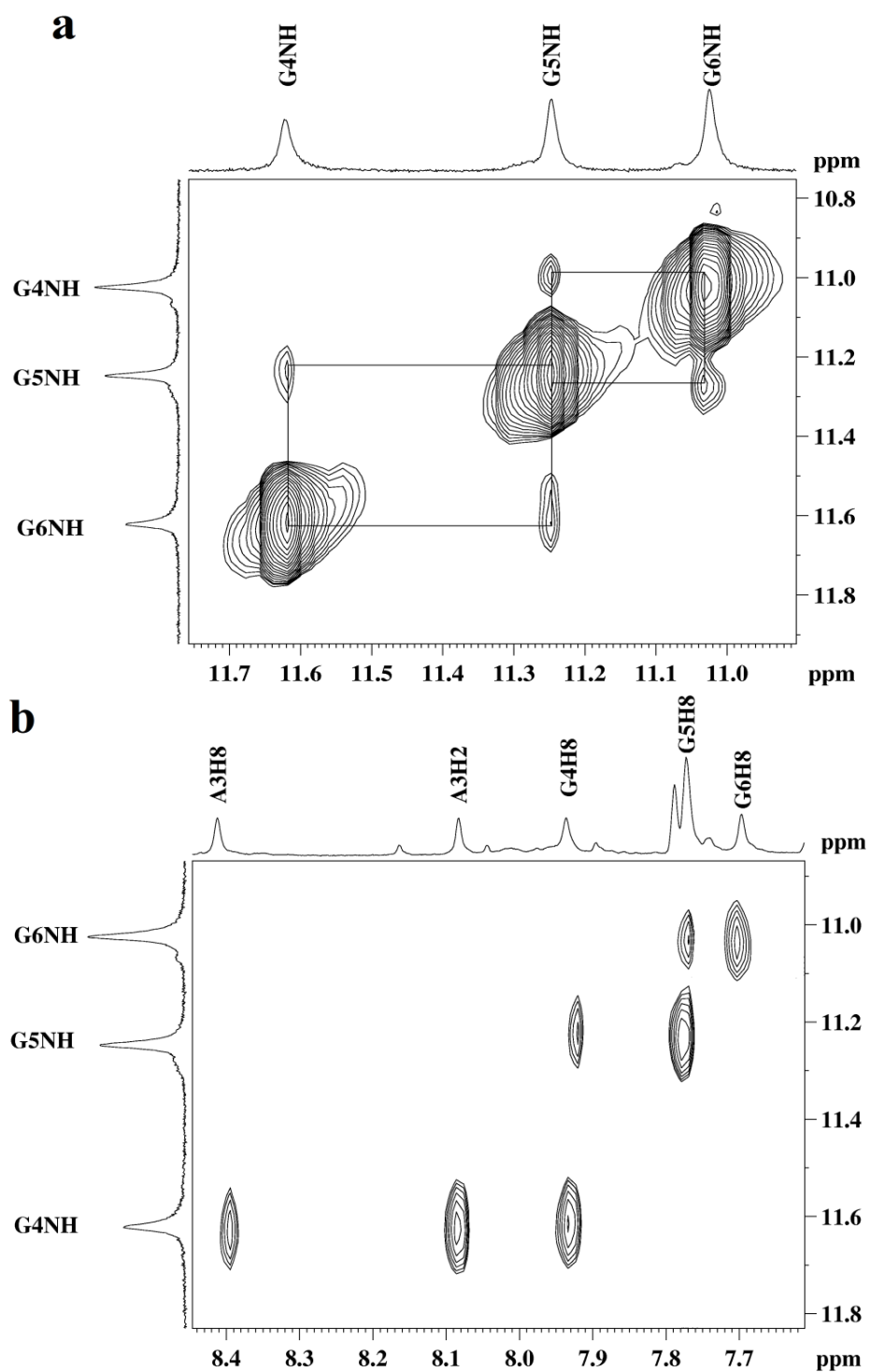


Fig. 4.7: Expansion of the NOESY spectra of uncomplexed quadruplex sequence d -(TTAGGGT)₄ at 298 K showing (a) NH-NH connectivity between adjacent imino protons. (b) Interstrand guanine NH connectivities with its own and 5' flanking base protons in A3-G4-G5-G6 segment.

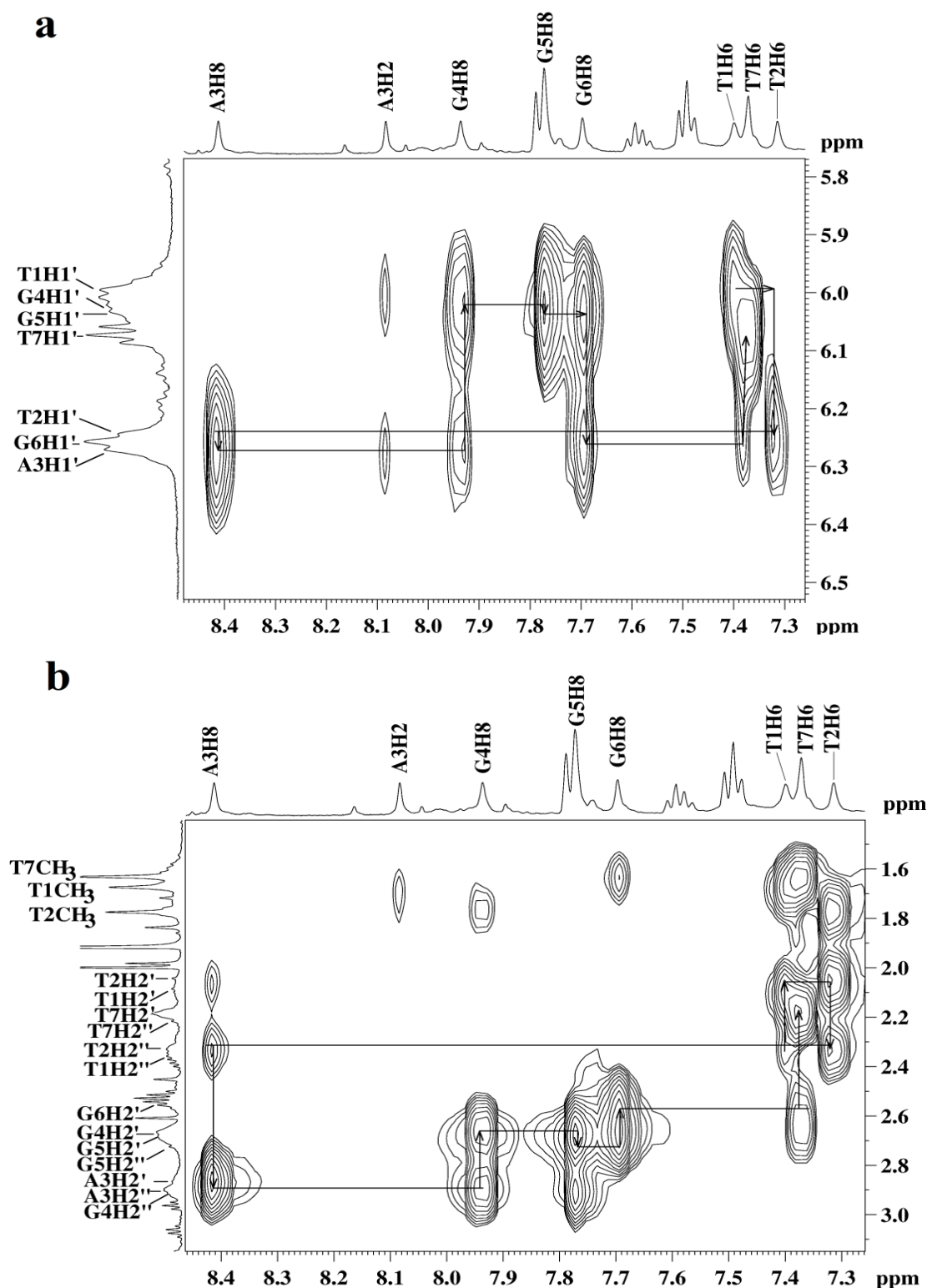


Fig. 4.8: Expansion of the NOESY spectra of uncomplexed quadruplex sequence $d\text{-(TTAGGGT)}_4$ at 298 K showing (a) intrastrand base H8/H6-H1' sequential connectivity. (b) Intrastrand base H8/H6-H2'H2'' sequential connectivity in T1-T2-A3-G4-G5-G6-T7 segment.

4.1.3 Resonance assignment of MTX- $d\text{-(TTAGGGT)}_4$ complex

To examine the binding interaction of mitoxantrone with quadruplex sequence $d\text{-(TTAGGGT)}_4$ increasing concentration of mitoxantrone was titrated to the quadruplex solution to reach the

desired D/N ratios of 0.25, 0.5, 0.75, 1.0, 1.25, 1.5, 1.75 and 2.0. The changes were continuously monitored by ^1H and ^{31}P NMR at different temperatures. Only one set of DNA signals was seen at all D/N values, during the course of titration (except at D/N=2.0 at 278 K, as discussed below) indicating that the binding was fast in NMR time scale. The complete unambiguous resonances assignment of MTX-d-(TTAGGGT)₄ complex were done by using various one dimensional and two dimensional NMR experiments besides comparing them with that of uncomplexed DNA and MTX. The NH-NH NOE connectivity between adjacent imino protons and interstrand guanine NH connectivities to its own and 5' flanking base protons in A3-G4-G5-G6 segment indicate that G-quartets were intact and there was no loss of original fourfold symmetry of the quadruplex in MTX-d-(TTAGGGT)₄ complex (**Figs. 4.9 a, b**). As for DNA, resonances within deoxyribose were identified by COSY as well as ^1H - ^{13}C HSQC in view of overlap with MTX signals. Analysis of sequential NOEs among base and H1'/H2'/H2'' protons allowed assignment of all base protons. All bases have classical H8/H2'-H2'' sequential connectivities to neighbouring 5'-end bases indicating that the four strands were involved in the formation of helical structure in the complex. The entire pattern of NOEs indicates that the backbone conformation closely resembles that of uncomplexed d-(TTAGGGT)₄ possessing a right handed B-form helix structure. The presence of all sequential base GH8/H6-H1'/H2'/H2'' NOEs (**Figs. 4.10a, b**), indicates that there was no opening of base pairs at any step, hence excluding intercalation of drug chromophore between base pairs.

A single set of MTX signals was present in the spectra of complex at 298 K and was assigned unambiguously. The 11NH proton resonating at 9.58 ppm does not overlap with any of DNA protons and grows gradually during progressive addition of MTX. The side chain aliphatic 11CH₂, 12CH₂, 13CH₂, 14CH₂ protons resonates at 3.1-3.8 ppm show expected COSY and NOESY connectivities among themselves. There was no ambiguity in the assignment of MTX due to overlap with H2'/H2'' or H5'/H5'' on either side of proton spectra, as ^{13}C signals of MTX methylene groups resonate in the region 38-58 ppm, while that of 7 sets of H2'/H2'' and H5'/H5'' protons belonging to nucleotide bases resonate at 35-38 and 64-66 ppm, respectively (**Fig 4.11a, b**).

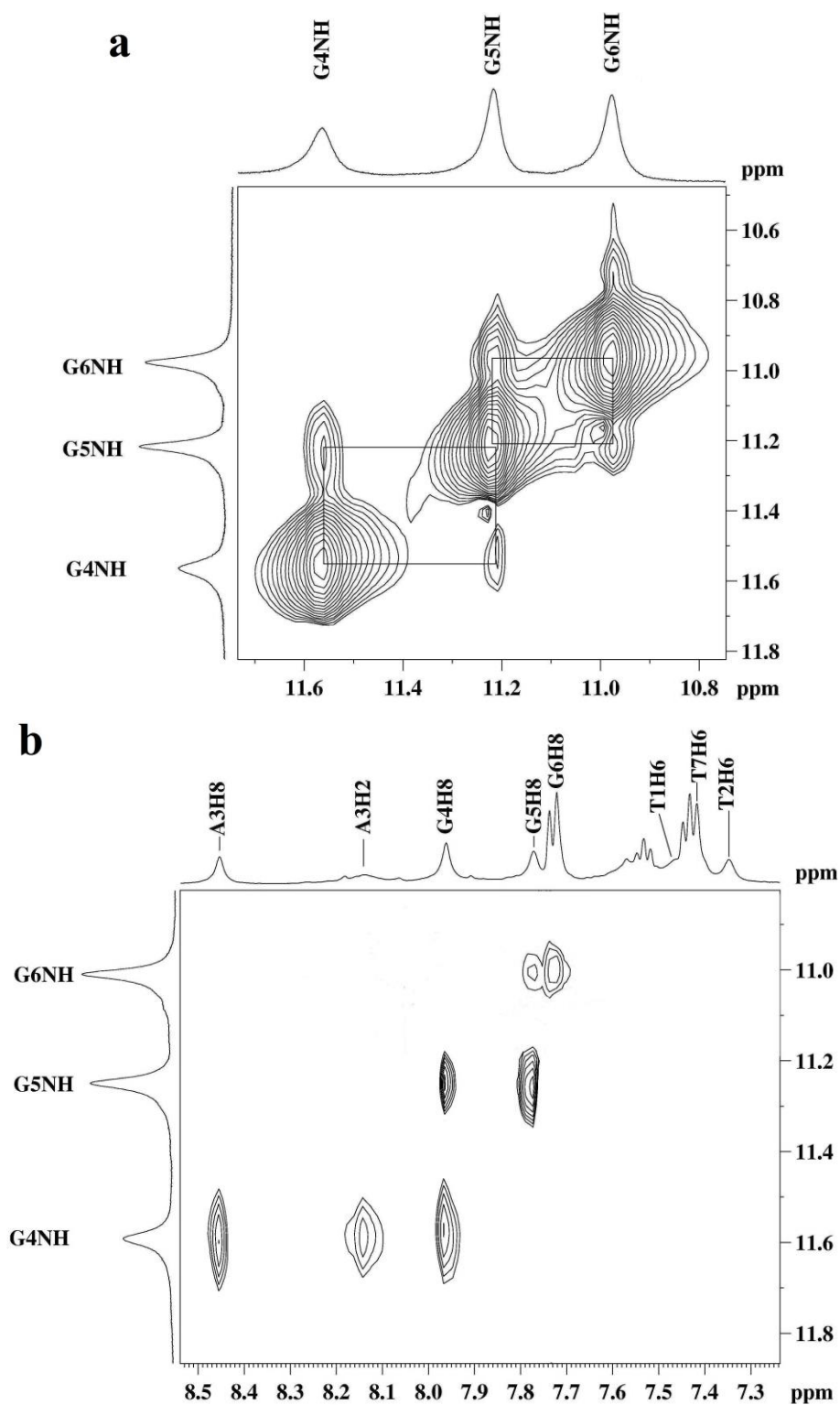


Fig. 4.9: Expansion of the NOESY spectra of MTX-d-(TTAGGGT)₄ complex at 298 K, $D/N=2.0$ showing (a) NH-NH connectivity between adjacent imino protons. (b) Interstrand guanine NH connectivities to its own and 5' flanking base protons in A3-G4-G5-G6 segment.

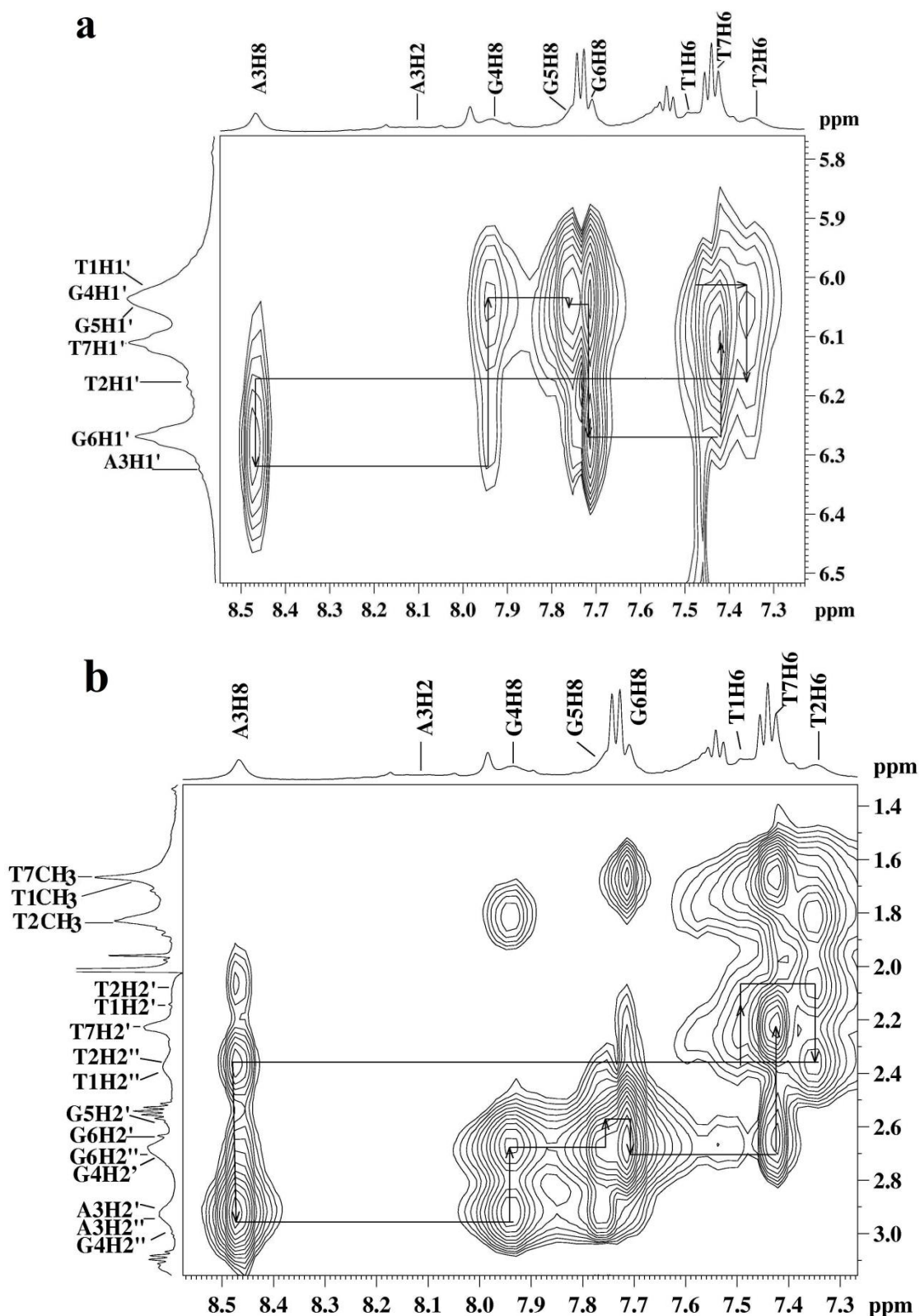


Fig. 4.10: Expansion of the NOESY spectra of MTX-d-(TTAGGGT)₄ complex at 298 K, D/N=2.0 showing (a) intrastrand base H8/H6-H1' sequential connectivity. (b) Intrastrand base H8/H6-H2'H2'' sequential connectivity in T1-T2-A3-G4-G5-G6-T7 segment.

The aromatic ring protons 6H/7H and 2H/3H overlap with G6NH₂^{nb} and deoxyribose H1' protons, but their corresponding ¹³C resonances resonate at ~122-124 ppm (region for aromatic

carbons), being well separated from that of deoxyribose H1' resonating at ~85-88 ppm. 1OH/4OH protons resonating at 13.23 ppm in free mitoxantrone are ascertained on the basis of expected NOE cross peak with 2H/3H protons.

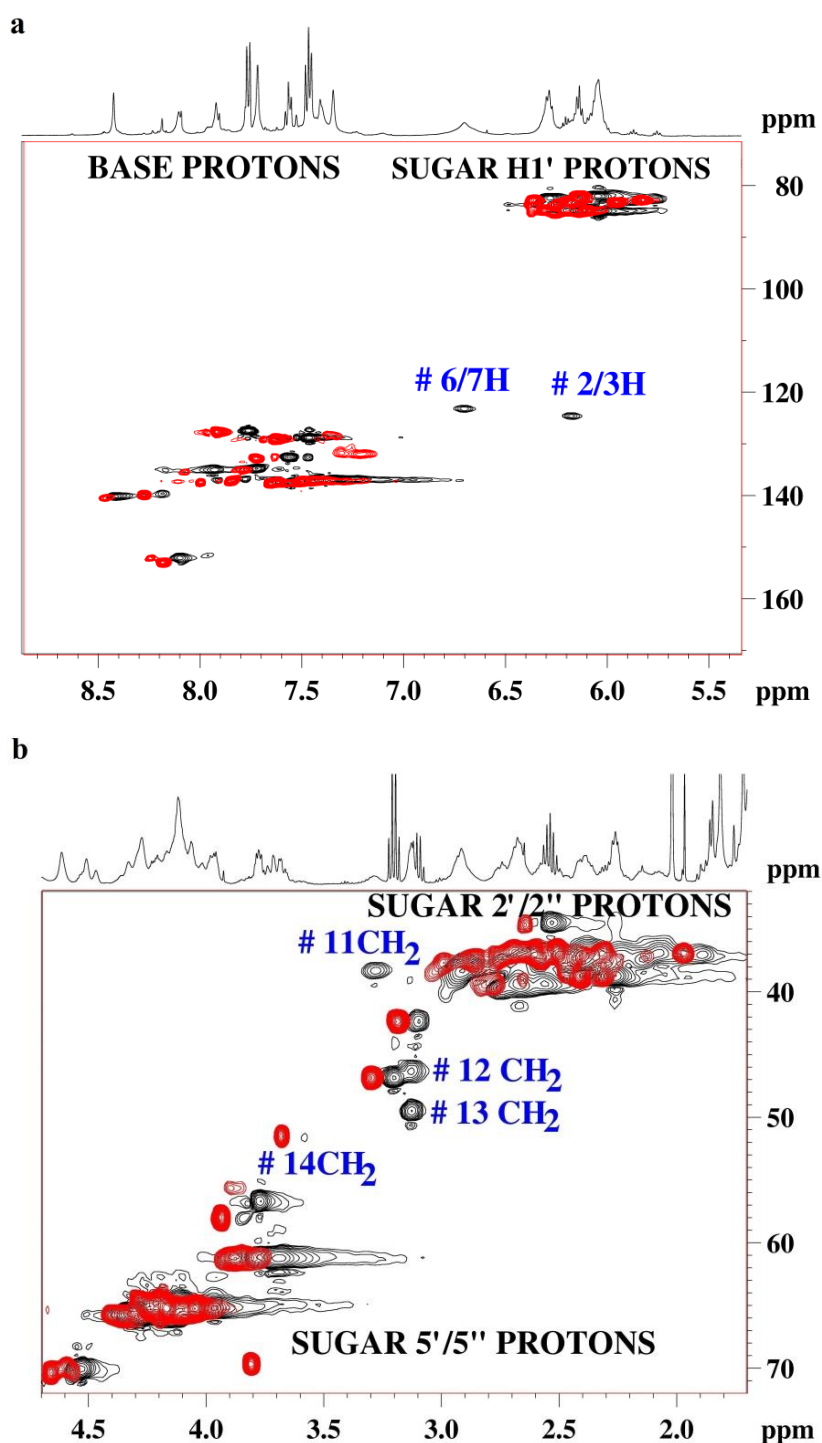
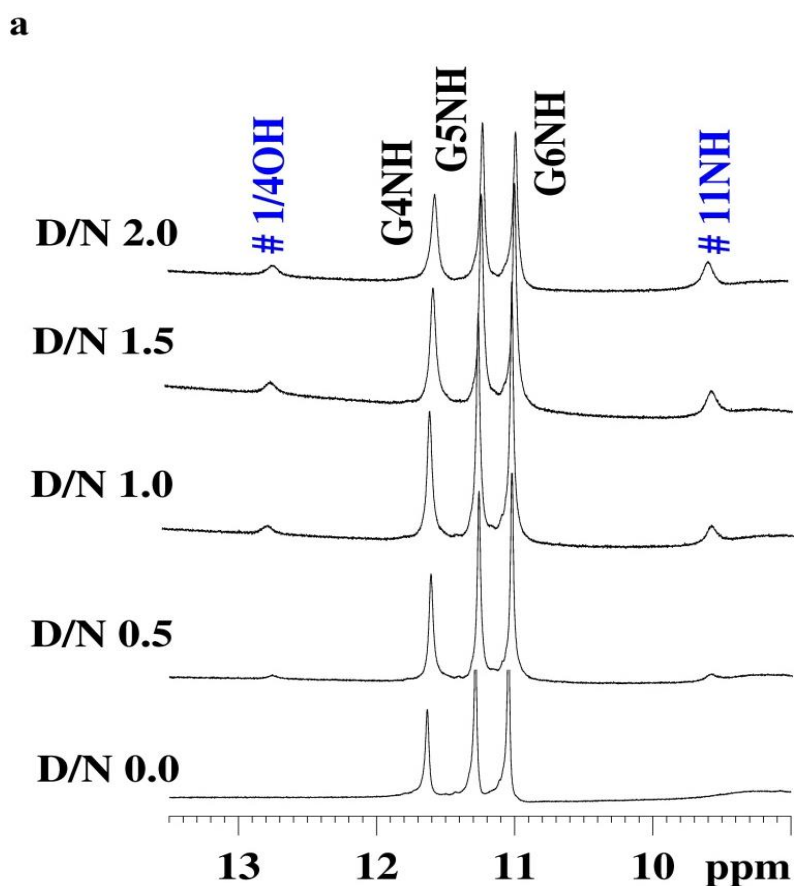


Fig. 4.11: Overlap of the uncomplex (red) and mitoxantrone complexed d -(TTAGGGT)₄ complex (black) ^1H - ^{13}C HSQC spectra at 318 K showing (a) aromatic protons of MTX. (b) Aliphatic protons of MTX.

4.1.4 Effects of titrimetric addition of MTX

Addition of 2 mol equivalent of MTX to the DNA quadruplex in steps caused broadening of T1H6, T2H6, A3H2, G4H8 protons selectively (**Figs. 4.12a, b**). In comparison, the G6H8 and T7H6 protons appear as sharp resonances at D/N = 2.0. The DNA signals shifted progressively with D/N ratio and increasing amount of DNA gets bound to MTX (**Fig. 4.12 and Table 4.2**). A downfield shift of 0.05-0.06 ppm was observed in T1H6, T2CH3 while G4H8, G4NH, G5NH and G6NH shifted upfield by 0.06 ppm (**Table 4.3**). The shift in all other DNA protons due to binding was insignificant (**Fig. 4.13a-c**). The MTX protons showed relatively large upfield shifts at D/N = 0.25 (**Table 4.4**). The largest upfield shift was observed in ring A protons, it being 0.53 and 0.49 ppm for 2/3H and 1/4OH, respectively followed by 0.26 ppm upfield shift in 11CH2 protons (**Table 4.5**). All MTX signals grew in intensity as more and more drug was added to a fixed concentration of DNA quadruplex but the signal did not shift any further upto D/N = 2.0 (**Figs. 4.12a-c; Figs. 4.14a, b**).



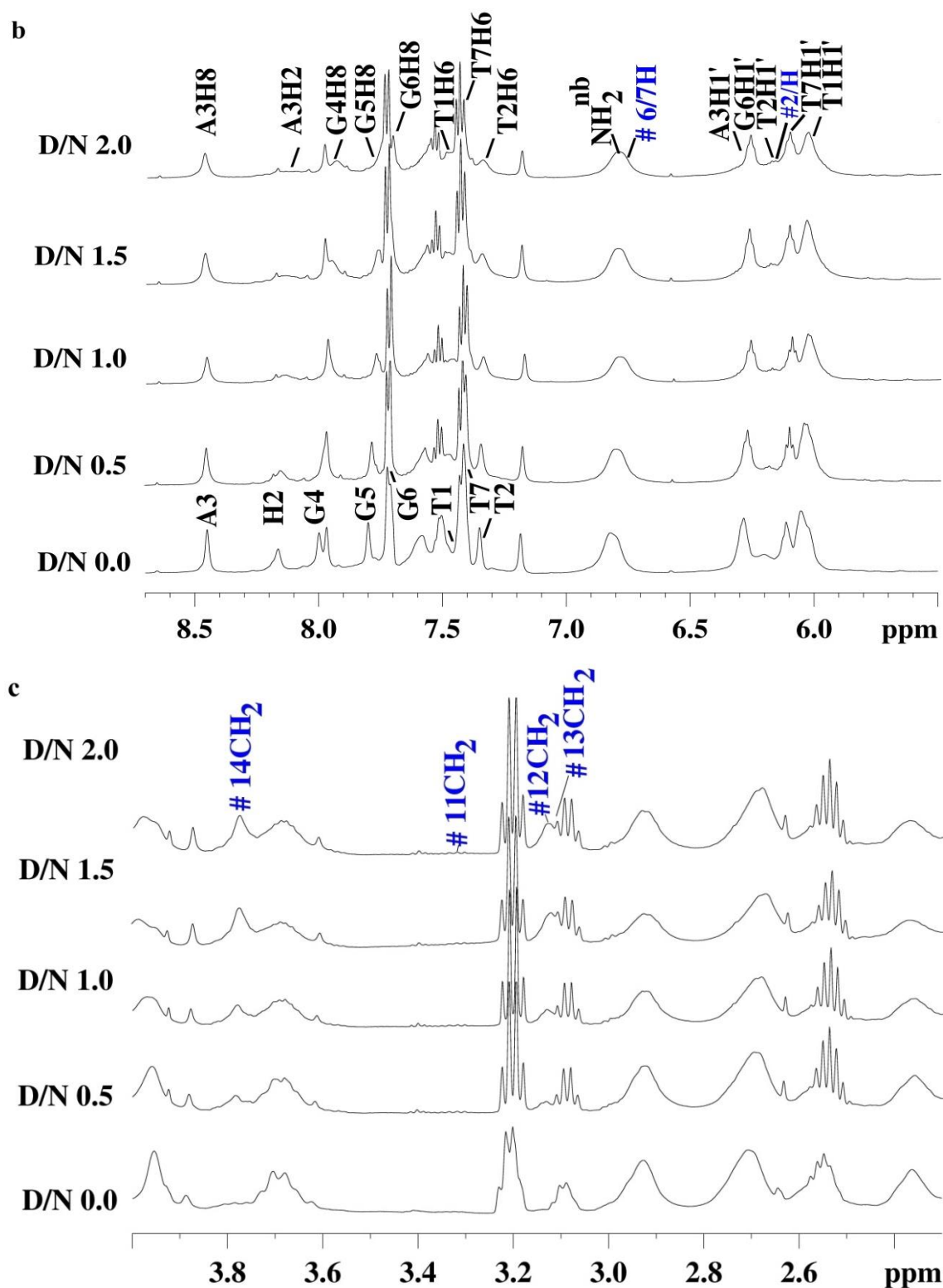


Fig. 4.12: $1D$ 1H NMR spectra of $MTX-d-(TTAGGGT)_4$ complex at 298 K showing change in the quadruplex and MTX proton resonances upon titration (a) imino proton region; (b, c) base and sugar regions.

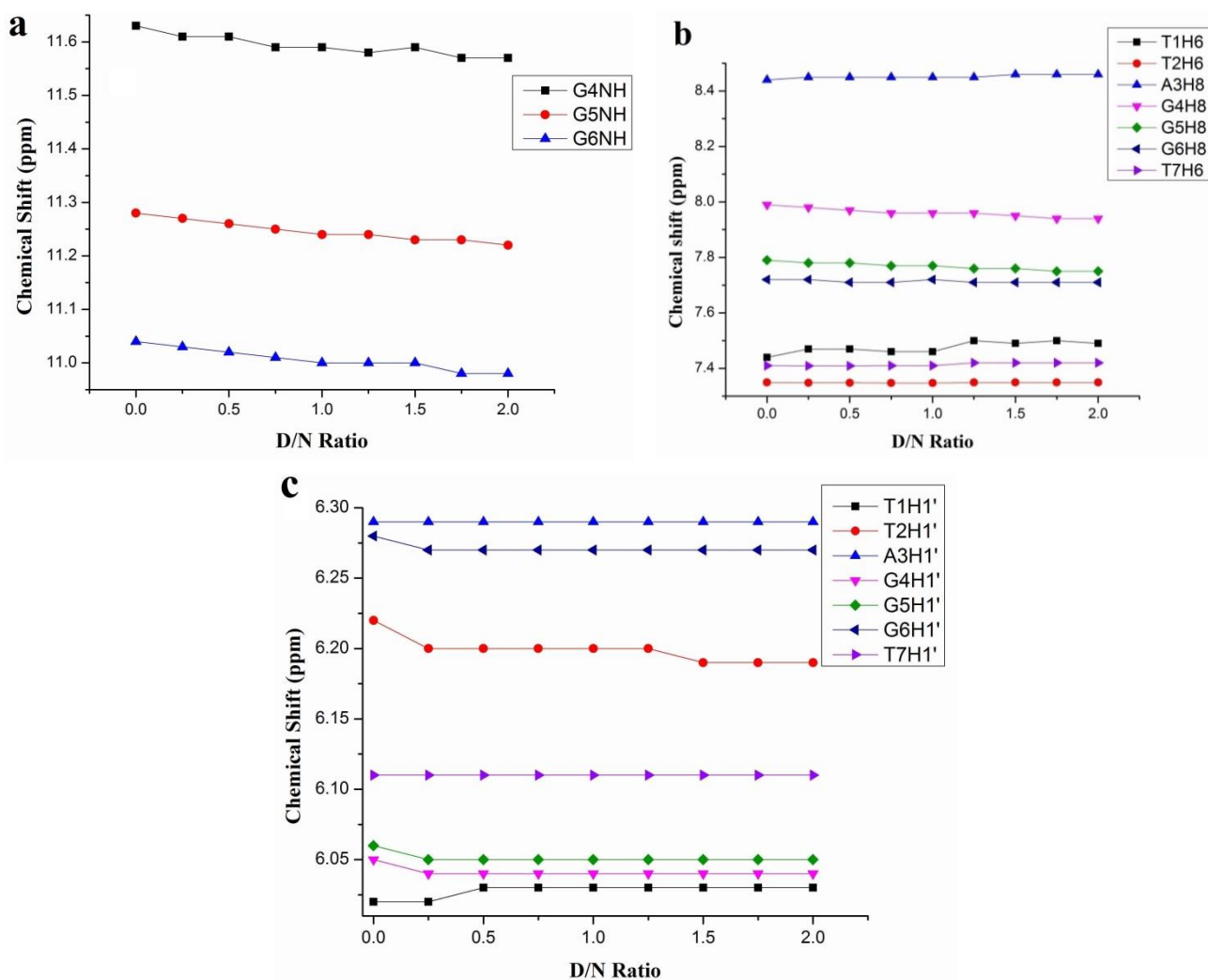


Fig. 4.13: Variation in the chemical shift of *d*-(TTAGGGT)₄ protons on increasing D/N ratios at 298 K (a-c).

D/N ratios	T1H1'	T2H1'	A3H1'	G4H1'	G5H1'	G6H1'	T7H1'	T1CH ₃	T2CH ₃	T7CH ₃	A3H2
0.0	6.02	6.22	6.29	6.05	6.06	6.28	6.11	1.68	1.77	1.67	8.16
0.25	6.02	6.20	6.29	6.04	6.05	6.27	6.11	1.68	1.78	1.67	8.15
0.5	6.03	6.20	6.29	6.04	6.05	6.27	6.11	1.68	1.78	1.67	8.15
0.75	6.03	6.20	6.29	6.04	6.05	6.27	6.11	1.68	1.79	1.67	8.14
1.0	6.03	6.20	6.29	6.04	6.05	6.27	6.11	1.68	1.8	1.67	8.14
1.25	6.03	6.20	6.29	6.04	6.05	6.27	6.11	1.68	1.8	1.67	8.14
1.5	6.03	6.19	6.29	6.04	6.05	6.27	6.11	1.68	1.81	1.67	8.12
1.75	6.03	6.19	6.29	6.04	6.05	6.27	6.11	1.68	1.81	1.67	8.12
2.0	6.03	6.19	6.29	6.04	6.05	6.27	6.11	1.68	1.83	1.67	8.12
$\Delta \delta$	0.01	-0.03	0.00	-0.01	-0.01	-0.01	0.00	0.00	0.06	0.00	-0.04

D/N ratios	T1H6	T2H6	A3H8	G4H8	G5H8	G6H8	T7H6	G4NH	G5NH	G6NH
0.0	7.44	7.349	8.44	7.99	7.79	7.72	7.41	11.63	11.28	11.04
0.25	7.47	7.348	8.45	7.98	7.78	7.72	7.409	11.61	11.27	11.03
0.5	7.47	7.348	8.45	7.97	7.78	7.71	7.409	11.61	11.26	11.02
0.75	7.46	7.347	8.45	7.96	7.77	7.71	7.41	11.59	11.25	11.01
1.0	7.46	7.347	8.45	7.96	7.77	7.72	7.41	11.59	11.24	11.00
1.25	7.5	7.349	8.45	7.96	7.76	7.71	7.42	11.58	11.24	11.00
1.5	7.49	7.349	8.46	7.95	7.76	7.71	7.42	11.59	11.23	11.00
1.75	7.5	7.349	8.46	7.94	7.75	7.71	7.42	11.57	11.23	10.98
2.0	7.49	7.349	8.46	7.94	7.75	7.71	7.42	11.57	11.22	10.98
$\Delta \delta$	0.05	0.00	0.02	-0.05	-0.04	-0.01	0.01	-0.06	-0.06	-0.06

Table 4.2: Chemical shift (ppm) of d-(TTAGGGT)₄ protons as a function D/N ratios at 298 K. Also shown here is the change in chemical shift on binding, that is, $\Delta\delta = \delta(D/N=2.0) - \delta(D/N=0.0)$.

MTX therefore exists in completely bound state at all D/N ratios suggesting that stoichiometry of MTX-d-(TTAGGGT)₄ complex is at least 2:1. It may also be inferred that since δ_b of all MTX protons remains unchanged at all D/N ratios, there exists only one bound state of MTX throughout the course of titrations. Two molecules of MTX may partially stack at the ends of the quadruplex with 2/3H and 1/4OH protons of ring A being in close proximity to base protons, which is evident by their large upfield shift while the side chain protons interact with the groove. This can be justified by the presence of intermolecular NOE connectivities between 1/4OH proton of MTX with T1, T2, and T7 bases of d-(TTAGGGT)₄ that will be discussed later in the section 4.1.6 of this chapter. Furthermore the presence of red shift along with hypochromicity observed in the absorption band of MTX and appearance of induced negative CD band also support the finding of stacking, which was already discussed in chapter 3. Binding of MTX at two sites was also observed in the case of its interaction with Tau SRE RNA (Zheng *et al.*, 2009). The result shows that MTX with the help of its aromatic chromophore partially intercalates in the bulge region of RNA, while the second interaction take place near grooves.

Protons	T1			T2			A3			G4		
	δ_b	δ_f	$\Delta\delta$	δ_b	δ_f	$\Delta\delta$	δ_b	δ_f	$\Delta\delta$	δ_b	δ_f	$\Delta\delta$
H8/H6	7.49	7.44	0.05	7.35	7.35	0.00	8.46	8.44	0.02	7.94	7.99	-0.05
H1'	6.03	6.02	0.01	6.19	6.22	-0.03	6.29	6.29	0.00	6.04	6.05	-0.01
H2'	2.14	2.13	0.01	2.08	2.08	0.00	2.89	2.86	0.03	2.69	2.70	-0.01
H2''	2.38	2.38	0.00	2.37	2.36	0.01	2.92	2.92	0.00	2.93	2.94	-0.01
H3'		4.63			4.78		5.12	5.12	0.00	5.08	5.07	0.01
H4'	4.05	4.03	0.02	4.09	4.09	0.00	4.44	4.44	0.00	4.48	4.46	0.02
H5'	3.69	3.67	-0.02	3.99	3.95	0.04	4.18	4.17	0.01	4.28	4.28	0.00
H5''	3.69	3.70	-0.02	3.99	3.95	0.04	4.08	4.09	-0.01	4.28	4.28	0.00
H2/CH₃	1.68	1.68	0.00	1.83	1.77	0.06	8.12	8.16	-0.04			
NH₂^b												
NH₂^{nb}												
NH										11.57	11.63	-0.06
	G5			G6			T7					
	δ_b	δ_f	$\Delta\delta$	δ_b	δ_f	$\Delta\delta$	δ_b	δ_f	$\Delta\delta$			
H8/H6	7.75	7.79	-0.04	7.71	7.72	-0.01	7.42	7.41	0.01			
H1'	6.05	6.06	-0.01	6.27	6.28	-0.01	6.11	6.11	0.00			
H2'	2.63	2.64	-0.01	2.58	2.57	0.01	2.17	2.19	-0.02			
H2''	2.70	2.72	-0.02	2.69	2.68	0.01	2.23	2.23	0.00			
H3'	5.06	5.09	-0.03	4.96	4.96	0.00	4.53	4.50	0.02			
H4'		4.50		4.53	4.51	0.02	4.23	4.23	0.00			
H5'	4.33	4.31	0.02	4.29	4.28	0.01	4.12	4.11	0.01			
H5''	4.33	4.31	0.02	4.29	4.28	0.01	4.12	4.11	0.01			
H2/CH₃							1.67	1.67	0.00			
NH₂^b		9.25										
NH₂^{nb}		5.91										
NH	11.22	11.28	-0.06	10.98	11.04	-0.06						

$\Delta\delta$ - Positive means downfield shift, $\Delta\delta$ - Negative means Upfield shift

Table 4.3: Chemical shift (ppm) of *d*-(TTAGGGT)₄ protons in uncomplexed state (δ_f) and that bound to MTX (δ_b) at *D/N*=2.0 at 298 K. Along with the change in chemical shift on binding, that is. $\Delta\delta = \delta_b (D/N=2.0) - \delta_f (D/N=0.0)$.

Interestingly the spectra recorded at 278 K during the course of titrations revealed two sets of 1/4OH, G4NH and G5NH protons while G6NH remained as a single sharp line (**Fig. 4.15a**). Other base and MTX protons remained as a single resonance (**Figs. 4.15b**). This reconfirms the involvement of 1/4OH in binding. 1/4OH signal resonating at 12.77 and 12.97 ppm correspond to either 2 molecules of MTX binding at 2 different sites on DNA or else correspond to 1OH and 4OH signals of two MTX molecules binding at 2 identical sites on DNA. Both positions are considerably upfield shifted from their corresponding positions in free MTX. That is, ~13.23 ppm. The binding of MTX may or may not position 1OH and 4OH protons in proximity to DNA quadruplex in two different environments. The presence of the free and the bound peak of G4NH/G5 with increasing MTX concentration could be due to the interaction of MTX at two independent sites. A similar kind of behaviour was observed in the interaction of MTX with Tau SRE RNA (Zheng *et al.*, 2009).

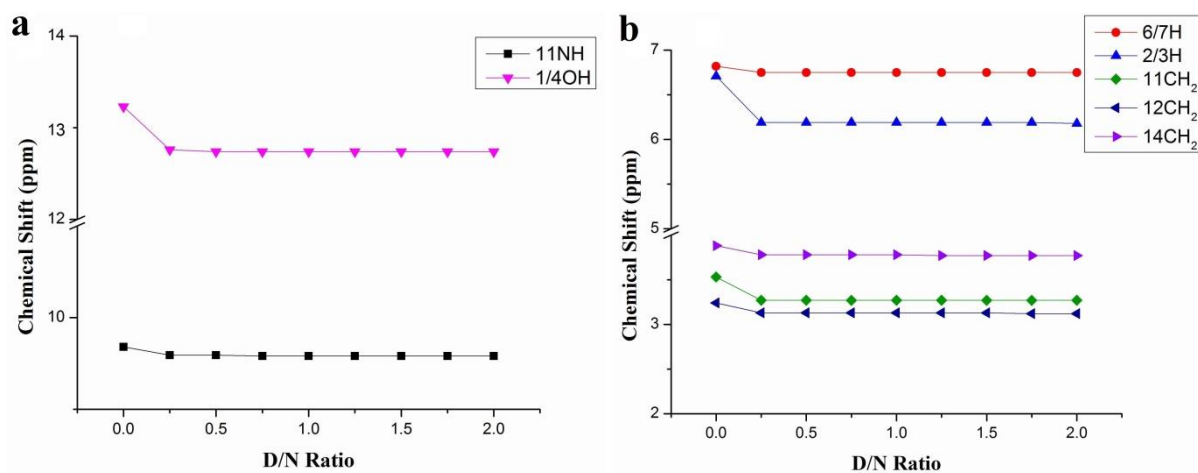


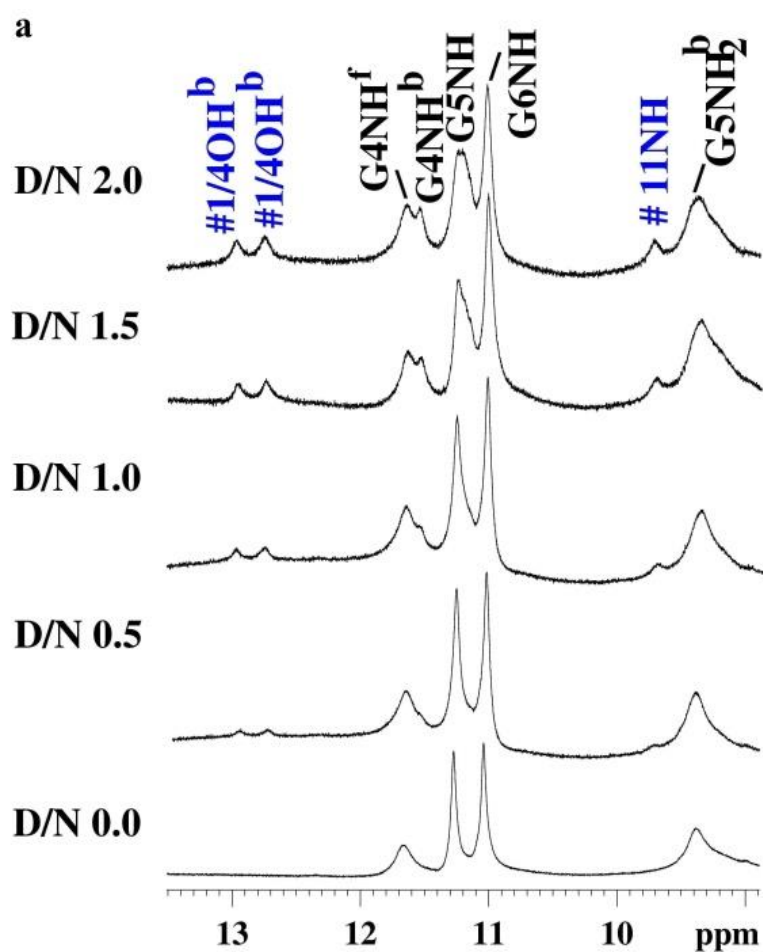
Fig. 4.14: Variation in the chemical shift of MTX protons versus increasing D/N ratios at 298 K (a, b).

D/N ratios	11NH	6/7H	2/3H	1,4OH	11CH ₂	12CH ₂	13CH ₂	14CH ₂
0.0	9.68	6.82	6.71	13.23	3.53	3.24	3.21	3.88
0.25	9.59	6.75	6.19	12.76	3.27	3.14	3.13	3.78
0.5	9.59	6.75	6.19	12.74	3.27	3.14	3.13	3.78
0.75	9.58	6.75	6.19	12.74	3.27	3.14	3.13	3.78
1.0	9.58	6.75	6.19	12.74	3.27	3.14	3.13	3.78
1.25	9.58	6.75	6.19	12.74	3.27	3.13	3.12	3.77
1.5	9.58	6.75	6.19	12.74	3.27	3.13	3.12	3.77
1.75	9.58	6.75	6.19	12.74	3.27	3.13	3.12	3.77
2.0	9.58	6.75	6.18	12.74	3.27	3.13	3.12	3.77
$\Delta\delta$	-0.10	-0.07	-0.53	-0.49	-0.26	-0.11	-0.09	-0.11

Table 4.4: Chemical shift (ppm) of MTX protons as a function of D/N ratios at 298 K. Along with the change in chemical shift on binding, that is, $\Delta\delta = \delta(D/N=2.0) - \delta(D/N=0.0)$.

MTX Protons	δ_f	δ_b D/N = 1.0	δ_b D/N = 2.0	$\Delta\delta$ D/N = 1.0 ($\Delta\delta = \delta_b - \delta_f$)	$\Delta\delta$ D/N = 2.0 ($\Delta\delta = \delta_b - \delta_f$)
11NH	9.68	9.58	9.58	-0.10	-0.10
6/7H	6.82	6.74	6.75	-0.08	-0.07
2/3H	6.71	6.19	6.18	-0.52	-0.53
1,4OH	13.23	12.74	12.74	-0.49	-0.49
11CH ₂	3.53	3.27	3.27	-0.26	-0.26
12CH ₂	3.24	3.14	3.13	-0.10	-0.11
13CH ₂	3.21	3.13	3.12	-0.08	-0.09
14CH ₂	3.88	3.78	3.77	-0.10	-0.11

Table 4.5: Chemical shift (ppm) of MTX protons from NOESY spectra of free MTX (δ_f) and MTX-d-(TTAGGGT)₄ complex (δ_b) at D/N=1.0, 2.0 at 298 K.



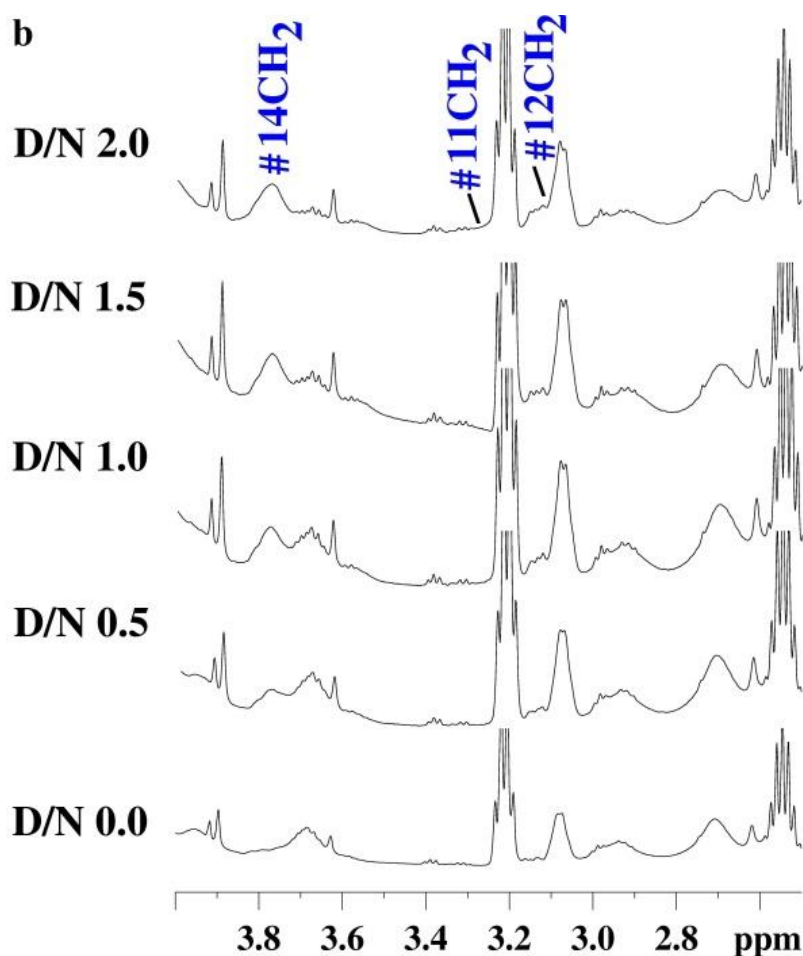


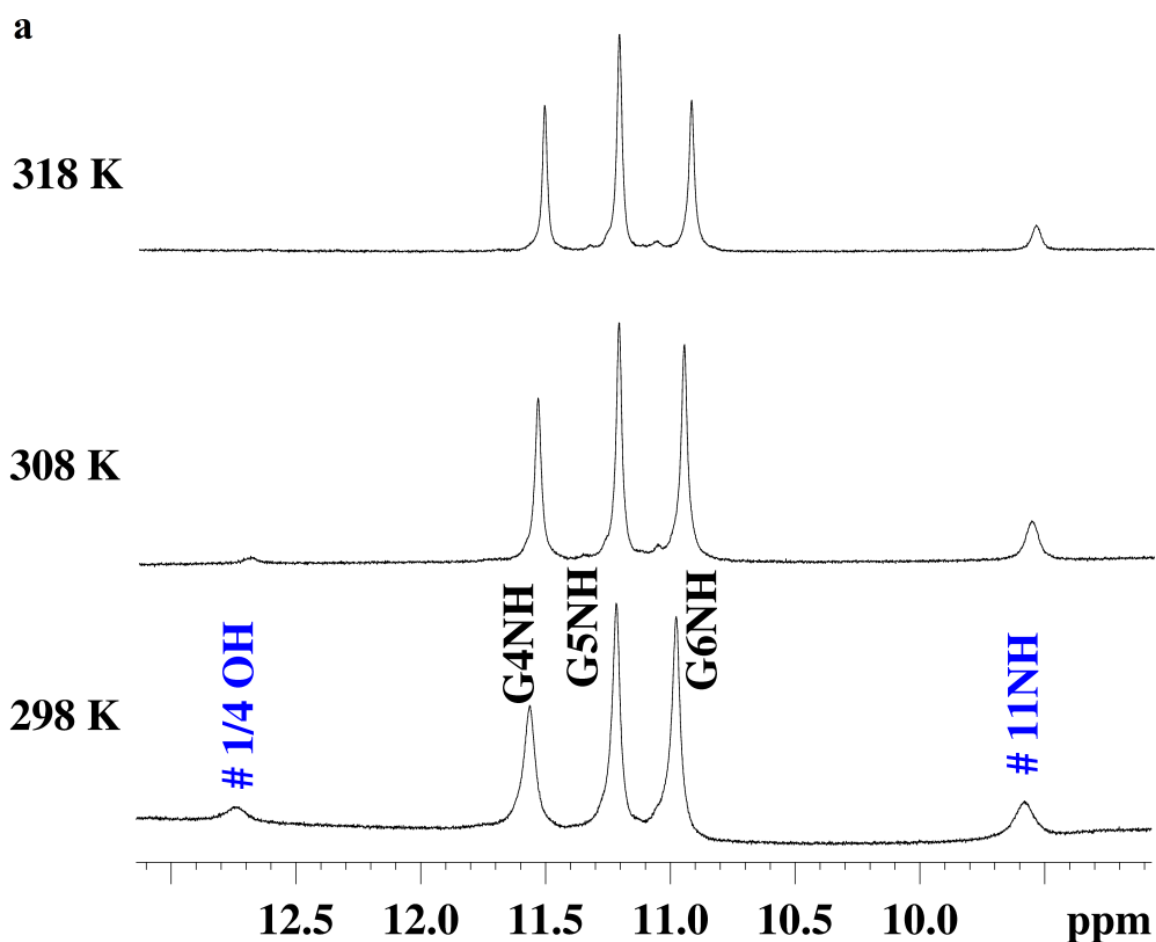
Fig. 4.15: $1D$ 1H NMR spectra of MTX-d-(TTAGGGT) $_4$ complex at 278 K showing change in the quadruplex and MTX proton resonances upon titration (a) imino proton region; (b) sugar region.

4.1.5 Temperature dependent studies revealing the stability of MTX-d-(TTAGGGT) $_4$ complex

The NMR spectra were recorded as a function of temperature. Both the quadruplex and MTX resonances were sharp and well-resolved at higher temperature, especially at 318 K (**Figs. 4.16a-c**). There was no significant shift in the quadruplex resonances while in case of MTX there was a shift in the resonances of 11NH, 6/7H and 1/4OH (**Table 4.6 and Table 4.7**). The MTX resonances were present even at higher temperature along with the imino resonances of quadruplex, which showed that the complex was fairly stable and MTX was in bound state even at higher temperature. Presence of guanine imino signals resonating between 10.0-11.5 ppm is indicative of the formation of G-quadruplex structure.

Increase in temperature results in decrease in intensity of these signals, which eventually disappear at higher temperature due to the disruption of hydrogen bonds holding the G quartet

structure. The disappearance and persistence of these imino signals in the absence and presence of a ligand with increase in temperature may be used as a measure of thermal stability of ligand-quadruplex structure. The melting profile of GNH protons was observed at 278-363 K (**Figs. 4.17**). The G4NH, G6NH and G5NH signals disappear at 328 and 333 K, respectively for uncomplexed DNA. Whereas they can all be observed at even 358 K in complex. This clearly indicates significant stabilization by about 25 K, which has independently been monitored by CD spectroscopy and Differential scanning calorimetry discussed earlier in chapter 3.



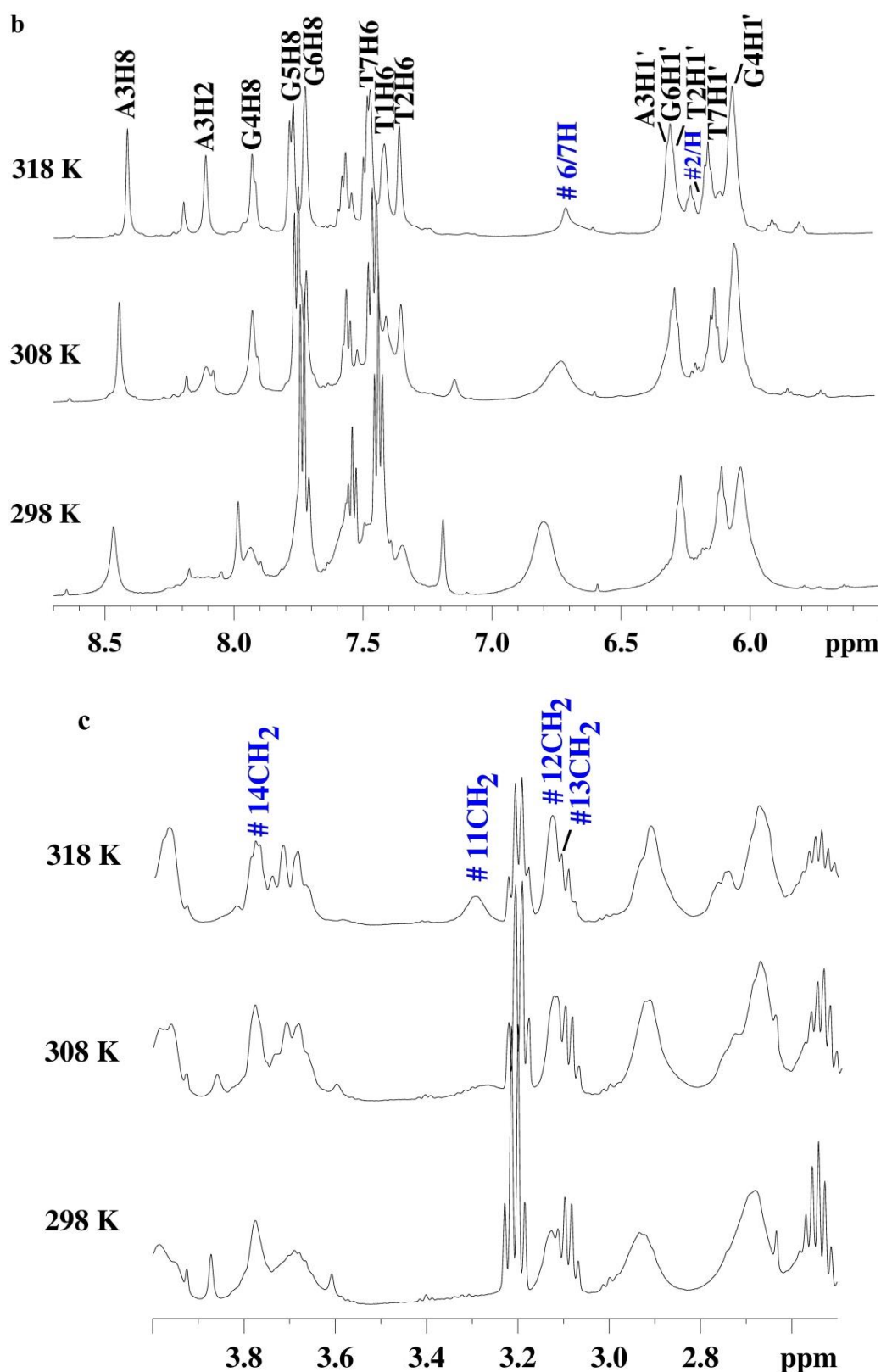


Fig. 4.16: 1D ^1H NMR spectra of MTX-d-(TTAGGGT) $_4$ complex as a function of temperature at $D/N=2.0$ showing change in the quadruplex and MTX proton resonances (a) imino proton region; (b-c) base and sugar regions.

Temp. (K)	T1H6	T2H6	A3H8	G4H8	G5H8	G6H8	T7H6	G4NH	G5NH	G6NH
278	7.45	7.25	8.50	7.98	7.83	7.71	7.40	11.54,11.65	11.25,11.20	11.01
283	7.46		8.50	7.98	7.82	7.71	7.39	11.54,11.63	11.22	11.00
288	7.47		8.48	7.98	7.81	7.71	7.40	11.60	11.22	10.99
293	7.48	7.35	8.47	7.95	7.77	7.71	7.41	11.58	11.22	10.98
298	7.49	7.35	8.46	7.94	7.75	7.71	7.42	11.57	11.21	10.97
303	7.40	7.35	8.45	7.93	7.79	7.71	7.43	11.56	11.22	10.97
308	7.40	7.34	8.44	7.92	7.78	7.71	7.45	11.54	11.21	10.95
313	7.40	7.34	8.42	7.92	7.77	7.71	7.45	11.53	11.21	10.94
318	7.40	7.34	8.41	7.92	7.76	7.71	7.46	11.52	11.21	10.93
323	7.40	7.34	8.41	7.92	7.76	7.71	7.46	11.52	11.21	10.92
328	7.41	7.35	8.40	7.92	7.77	7.72	7.46	11.50	11.21	10.91
333	7.41	7.35	8.38	7.92	7.77	7.72	7.47	11.49	11.21	10.89
338	7.41	7.35	8.37	7.92	7.78	7.73	7.47	11.47	11.20	10.86
343	7.42	7.36	8.35	7.92	7.78	7.74	7.48	11.45	11.19	10.84
348	7.42	7.37	8.34	7.92	7.78	7.74	7.48	11.43	11.18	10.81
353	7.42	7.37	8.33	7.92	7.79	7.74	7.48	11.40	11.17	10.77
358	7.43	7.38	8.31	7.93	7.79	7.75	7.49	11.38	11.16	10.75
363	7.43	7.40	8.35	7.97	7.84	7.79	7.47			
$\Delta \delta$	0.06	0.15	-0.15	-0.01	0.01	0.08	0.07	-0.16	-0.09	-0.26

Temp. (K)	T1H6	T2H6	A3H8	G4H8	G5H8	G6H8	T7H6	G4NH	G5NH	G6NH
278	7.45	7.25	8.50	7.98	7.83	7.71	7.40	11.54,11.65	11.25,11.20	11.01
283	7.46		8.50	7.98	7.82	7.71	7.39	11.54,11.63	11.22	11.00
288	7.47		8.48	7.98	7.81	7.71	7.40	11.60	11.22	10.99
293	7.48	7.35	8.47	7.95	7.77	7.71	7.41	11.58	11.22	10.98
298	7.49	7.35	8.46	7.94	7.75	7.71	7.42	11.57	11.21	10.97
303	7.40	7.35	8.45	7.93	7.79	7.71	7.43	11.56	11.22	10.97
308	7.40	7.34	8.44	7.92	7.78	7.71	7.45	11.54	11.21	10.95
313	7.40	7.34	8.42	7.92	7.77	7.71	7.45	11.53	11.21	10.94
318	7.40	7.34	8.41	7.92	7.76	7.71	7.46	11.52	11.21	10.93
323	7.40	7.34	8.41	7.92	7.76	7.71	7.46	11.52	11.21	10.92
328	7.41	7.35	8.40	7.92	7.77	7.72	7.46	11.50	11.21	10.91
333	7.41	7.35	8.38	7.92	7.77	7.72	7.47	11.49	11.21	10.89
338	7.41	7.35	8.37	7.92	7.78	7.73	7.47	11.47	11.20	10.86
343	7.42	7.36	8.35	7.92	7.78	7.74	7.48	11.45	11.19	10.84
348	7.42	7.37	8.34	7.92	7.78	7.74	7.48	11.43	11.18	10.81
353	7.42	7.37	8.33	7.92	7.79	7.74	7.48	11.40	11.17	10.77
358	7.43	7.38	8.31	7.93	7.79	7.75	7.49	11.38	11.16	10.75
363	7.43	7.40	8.35	7.97	7.84	7.79	7.47			
$\Delta \delta$	-0.05	-0.04	-0.09	-0.06	-0.07	0.00	0.06	-0.02	0.01	-0.08

Table 4.6: Chemical shift (ppm) of *d*-(TTAGGGT)₄ protons in MTX-*d*-(TTAGGGT)₄ complex at *D/N*=2.0 as a function of temperature along with the net change in chemical shift with temperature, that is, $\Delta\delta = \delta(363\text{ K}) - \delta(278\text{ K})$; $\delta(318\text{ K}) - \delta(278\text{ K})$.

Similar kind of stabilization was observed in the case of RHPS4 ($T_m = 20^\circ\text{C}$), which stacks at ApG and GpT steps. On the other hand 9-amino acridines interact with H-telo by intercalating/stacking at ApG step that induces the stabilization of quadruplex complexes by 5-10 °C (Mazzini *et al.*, 2013). Thus we can infer that the stability of MTX-*d*-(TTAGGGT)₄ complex is probably due to the binding of MTX molecules.

Temp. (K)	11NH	6/7H	2/3H	1,4OH	11CH ₂	12CH ₂	13CH ₂	14CH ₂
278	9.72	6.92	6.18	12.77,12.97	3.27	3.14	3.12	3.77
283	9.70	6.88	6.18	12.73,12.94	3.27	3.14	3.12	3.77
288	9.68	6.85	6.18	12.74,12.88	3.27	3.13	3.12	3.77
293	9.60	6.81	6.18	12.74	3.27	3.13	3.12	3.77
298	9.58	6.75	6.18	12.74	3.27	3.13	3.12	3.77
303	9.58	6.75	6.18	12.74	3.27	3.13	3.11	3.77
308	9.56	6.71	6.17	12.70	3.27	3.13	3.11	3.77
313	9.55	6.70	6.17	12.67	3.28	3.13	3.11	3.77
318	9.54	6.70	6.17	12.66	3.29	3.13	3.11	3.77
323	9.54	6.70	6.17	12.66	3.30	3.13	3.12	3.78
328	9.54	6.70	6.17		3.31	3.14	3.12	3.78
333	9.54	6.70	6.17		3.33	3.14	3.13	3.79
338	9.54	6.71	6.17		3.35	3.15	3.14	3.80
343	9.55	6.73	6.17		3.38	3.16	3.17	3.80
348	9.58	6.77	6.17		3.43	3.18	3.19	3.81
353	9.54	6.84	6.17		3.51	3.18	3.19	3.81
358	9.54	6.94	6.17		3.60	3.18	3.19	3.81
363	9.58	7.09	6.17		3.75	3.22	3.23	3.82
$\Delta \delta$	-0.14	0.17	-0.01	-0.11	0.48	0.10	0.11	0.05

Temp. (K)	11NH	6/7H	2/3H	1,4OH	11CH ₂	12CH ₂	13CH ₂	14CH ₂
278	9.72	6.92	6.18	12.77,12.97	3.27	3.14	3.12	3.77
283	9.70	6.88	6.18	12.73,12.94	3.27	3.14	3.12	3.77
288	9.68	6.85	6.18	12.74,12.88	3.27	3.13	3.12	3.77
293	9.60	6.81	6.18	12.74	3.27	3.13	3.12	3.77
298	9.58	6.75	6.18	12.74	3.27	3.13	3.12	3.77
303	9.58	6.75	6.18	12.74	3.27	3.13	3.11	3.77
308	9.56	6.71	6.17	12.70	3.27	3.13	3.11	3.77
313	9.55	6.70	6.17	12.67	3.28	3.13	3.11	3.77
318	9.54	6.70	6.17	12.66	3.29	3.13	3.11	3.77
$\Delta \delta$	-0.18	0.22	-0.01	-0.11	0.02	-0.01	-0.01	0.00

Table 4.7: Chemical shift (ppm) of MTX protons in MTX-d-(TTAGGGT)₄ complex at D/N=2.0 as a function of temperature along with the net change in chemical shift with temperature, that is, $\Delta\delta = \delta(363\text{ K}) - \delta(278\text{ K})$; $\delta(318\text{ K}) - \delta(278\text{ K})$.

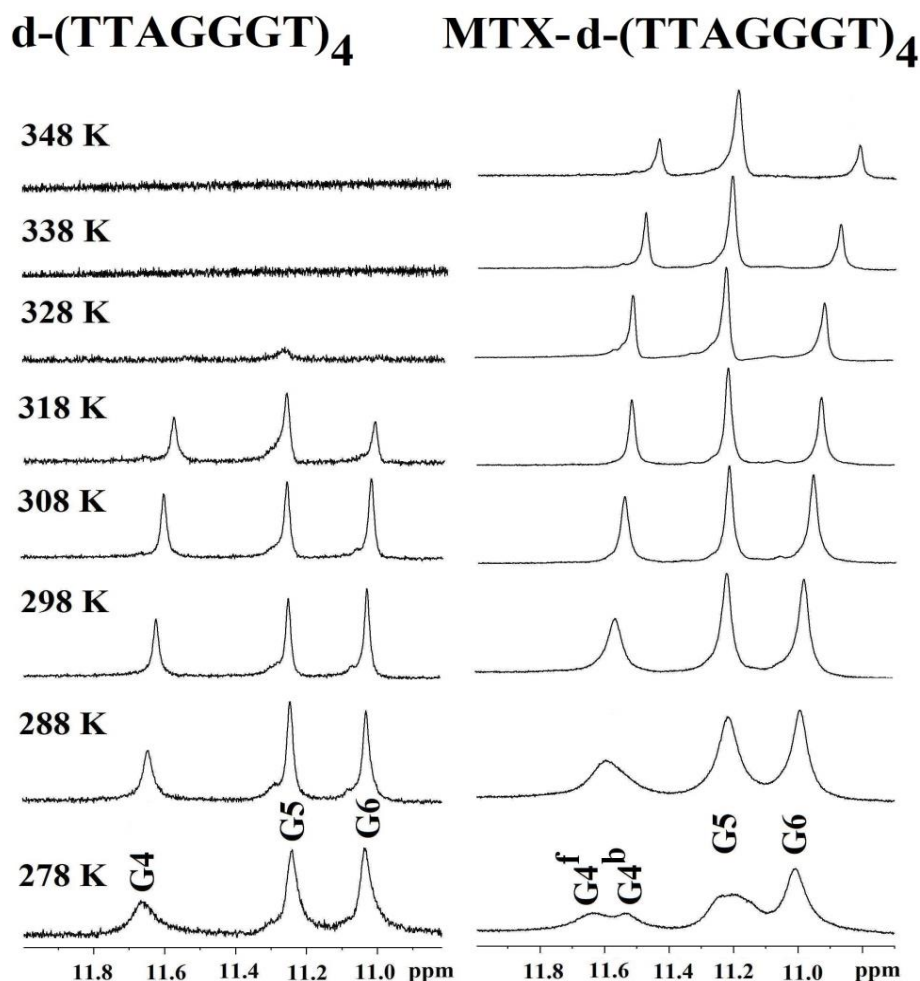


Fig. 4.17: 1D ^1H NMR spectra of imino protons region of $d\text{-(TTAGGGT)}_4$ and $\text{MTX-}d\text{-(TTAGGGT)}_4$ complex revealing the stability of complex with temperature.

4.1.6 Phosphorous-31 NMR studies of $\text{MTX-}d\text{-(TTAGGGT)}_4$ complex

The phosphorus-31 NMR spectra of unbound and bound $d\text{-(TTAGGGT)}_4$ were recorded at different temperature (278-318 K) during the course of titrations with MTX (**Figs. 4.18a, b**). The phosphorus signals were assigned using standard strategies by $^1\text{H-}^{31}\text{P}$ HMBC spectra, that is, T1pT2 shows ^3J coupling with T1H3', T2H5'/5'' and ^4J coupling with T2H4' and so on for other ^{31}P signals. These assignments were in agreement with the one that was done earlier in our lab (Amit, 2009). On progressive addition of MTX the ^{31}P signals showed minor sequence dependent shifts upto D/N = 2.0 (**Table 4.8**). Although the drift in signals is clear, particularly at D/N = 1.0, 1.5 at 298 K. Downfield shift is observed for resonances of T1pT2, G4pG5 and G5pG6 step, while A3pG4 and G6pT7 step ^{31}P resonances show upfield shift. Resonance of T1pT2 step shows maximum downfield shift of $\Delta\delta$ 0.09 ppm, followed by G4pG6 and G5pT2 ^{31}P resonance, which shows shift of 0.03 and 0.02 ppm, respectively. A3pG4 step ^{31}P resonance shows upfield shift by 0.05 ppm. The T2pA3 signal does not drift at all. The magnitudes of

shifts were insignificant. Since the maximum shift was observed for T1pT2 resonance this shows that T1pT2 is most probably involved in binding. At higher temperature the resonances cannot be assigned due to the presence of some extra signals apart from the six original ones. This might be either due to the presence of some single strand resonance which is more prominent at higher temperature or due to the flexibility of TTA bases.

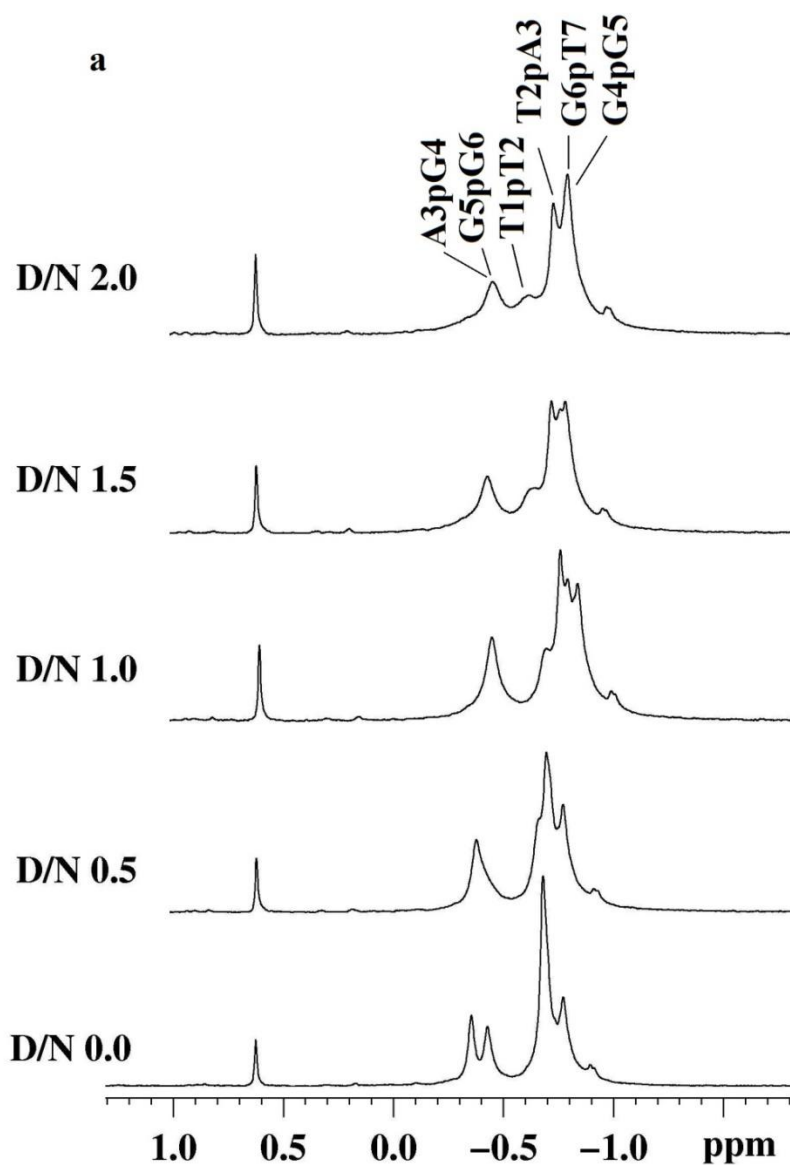


Fig. 4.18a: Proton decoupled ^{31}P NMR spectra of $d\text{-(TTAGGGT)}_4$ in uncomplexed state and complexed with MTX with increasing D/N ratios at 298 K.

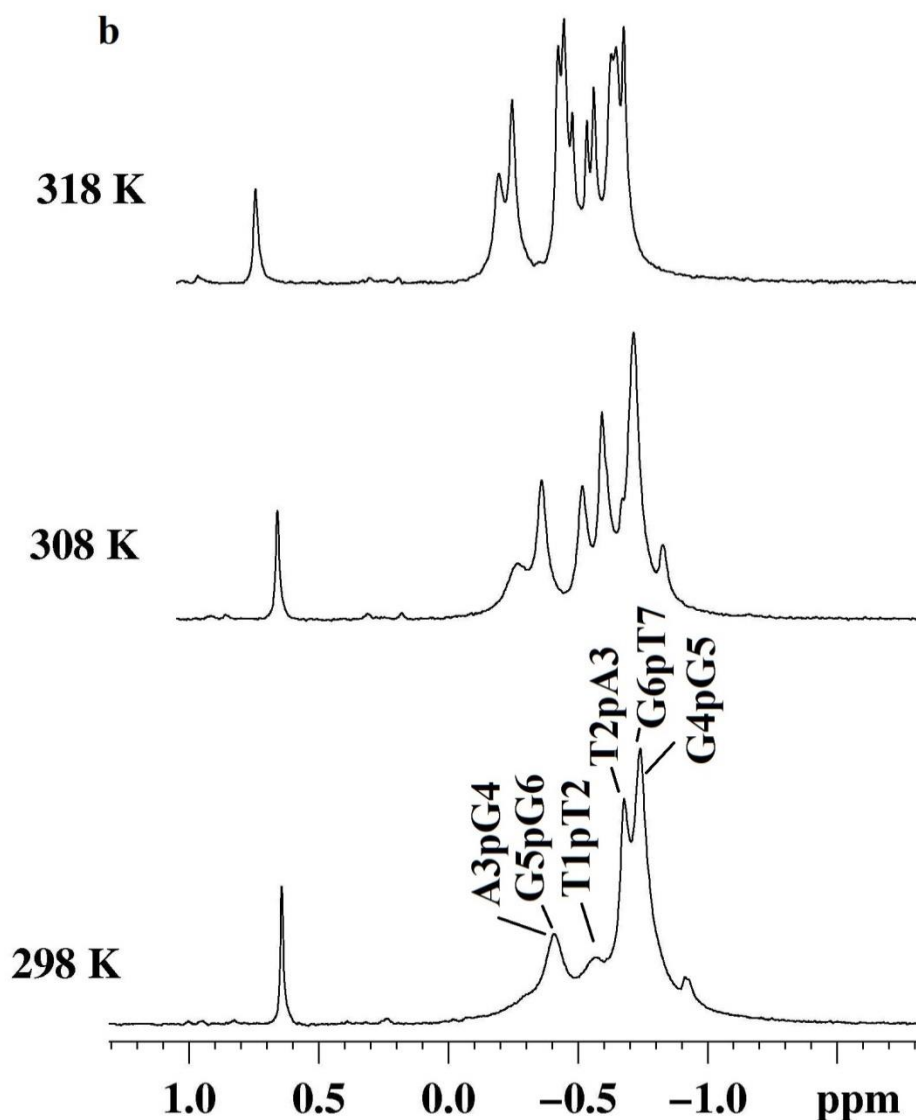


Fig. 4.18: Proton decoupled ^{31}P NMR spectra of MTX-d-(TTAGGGT)_4 as a function of temperature at $D/N=2.0$.

	DN=0	DN=0.5	DN=1.0	DN=1.5	DN=2	$\Delta\delta$
T1pT2	-0.65	-0.65	-0.61	-0.59	-0.56	0.09
T2pA3	-0.67	-0.69	-0.67	-0.68	-0.67	0.00
A3pG4	-0.35	-0.37	-0.37	-0.39	-0.40	-0.05
G4pG5	-0.77	-0.77	-0.75	-0.74	-0.74	0.03
G5pG6	-0.42	-0.41	-0.37	-0.39	-0.40	0.02
G6pT7	-0.73	-0.70	-0.70	-0.72	-0.74	-0.01

Table 4.8: Chemical shift of ^{31}P resonances of the phosphate groups of $d\text{-(TTAGGGT)}_4$, in MTX-d-(TTAGGGT)_4 complex at 298 K with increasing D/N ratios.

We have not observed any cross peaks due to exchange between the bound and free phosphate resonances in the 2D ^{31}P NMR exchange spectrum of MTX-d-(TTAGGGT)_4 complex and a single set of resonances were present. This clearly shows that ^{31}P signals from the bound

quadruplex were in fast exchange with the corresponding signals from free quadruplex on the NMR time scale.

Small upfield shifts are generally caused by electrostatic interactions between drug and duplex DNA (Patel, 1979; Wilson and Jones, 1982) while minor upfield/downfield shifts are expected on widening/narrowing of O-P-O ester bond angle (Gorenstein and Kar, 1975; Gorenstein, 1984). The observed shifts rule out opening of base pairs to permit intercalation of MTX chromophore which is expected to result in large downfield shifts ~ 1.6 - 2.6 ppm (Gorenstein 1992; Patel and Canuel, 1976). To the best of my knowledge till date, there is no literature available for changes in ^{31}P resonance positions upon interaction of ligands with quadruplex DNA.

4.1.6 Structural studies of MTX-d-(TTAGGGT)₄ complex

NOESY spectra recorded with variable mixing times τ_m 100, 200, 250 ms were analyzed at D/N=1:1 and D/N=2:1. The NOESY spectra of complex contain several intramolecular NOE connectivities within quadruplex and MTX in addition to intermolecular connectivities between quadruplex and MTX. The presence of all sequential connectivities between base-H1'/H2'', H2'' and NH-NH protons, indicate that all G-quartets were intact and quadruplex adopts a right hand helical structure with no opening of base pairs at any step. Thus exclude the possibility of intercalation of MTX chromophore between base pairs. **Table 4.9** shows the intramolecular NOE connectivities observed within the MTX molecule in the MTX-d-(TTAGGGT)₄ complex at D/N=1.0 and D/N=2.0. These connectivities also persist at different temperature. It was observed that 11NH is close to 11CH₂, 12CH₂/13CH₂ (overlap) protons as compared to 6H/7H protons. Also the ring protons 6H/7H are close to 11CH₂, 12CH₂/13CH₂ protons, as expected. This showed the rigid behavior of side chains on complex formation, which is responsible for efficient NOE transfer. Absence of intermolecular NOEs between 11 NH-2/3 H, 11 CH₂-2/3 H, 6/7 H-2/3 H reveal that MTX does not exist as dimer (Davies et al., 2001) in the complex, instead exist as monomer.

A total of 31 intermolecular NOE connectivities were observed between MTX protons and quadruplex but only non-overlapped peaks (**Table 4.10 and 4.11**) were used for distance calculation and for building model. Most of the Intermolecular NOE connectivities between MTX protons 11 NH, 1/4 OH and 6/7 H were observed with sugar (H1', H2'/H2'', H4') and CH₃ protons of T1, T2, and T7 bases of DNA (**Figs 4.19a-h**).

Intermolecular connectivities involving 2/3H proton of MTX were observed at D/N 1.0 only with G6pT7 step, but due to overlap with sugar H1' of the quadruplex it was not assigned unambiguously at D/N 2.0. These contacts were also present at D/N 1.0 but with increasing the

D/N ratios, both the intensity as well contacts increased due to more and more binding of MTX to quadruplex. Since one MTX proton cannot give peak with both T1 and T7 bases simultaneously, we can infer that two molecules of MTX (one at T1pT2 step and second at G6pT7 step) bind to one molecule of d-(TTAGGGT)₄. The two molecules of MTX may partially stack at the ends of the quadruplex with ring A 2/3H and 1/4OH protons being in close proximity to base protons, which is evident by their large upfield shift while the side chain protons interact with the groove. This was justified independently by Job plot and fluorescence studies, which gave a stoichiometry of 2:1 for MTX-d-(TTAGGGT)₄ complex (discussed in chapter 3). In order to get the clear picture of the interactions, the structure of MTX-d-(TTAGGGT)₄ complex was calculated by using restrained molecular dynamics simulation.

SI No.	MTX	MTX	DN 1.0 (298K)	DN 2.0 (298K)			DN 2.0 (308K)	DN 2.0 (318K)		
			250ms	250ms	200ms	100ms	250ms	250ms	200ms	100ms
D1	11NH	11CH ₂	+	+	+	+	+	+	+	+
D2	11NH	12CH ₂	+	+	+	+	+	+	+	+
D3	11NH	6/7H	+	+	+		+	+	+	
D4	1/4OH	11NH	+	+	+		+			
D5	6/7H	11CH ₂	+	+	+	+	+	+	+	+
D6	6/7H	12CH ₂	+	+	+	+	+	+	+	+
D7	6/7H	11NH	+	+	+		+	+	+	
D8	12CH ₂	11CH ₂	+	+	+	+	+	+	+	+
D9	12CH ₂	14CH ₂	+	+	+	+	+	+	+	+
D10	12CH ₂	6/7H	+	+	+	+	+	+	+	+
D11	12CH ₂	11NH	+	+	+	+	+	+	+	+
D12	11CH ₂	11NH	+	+	+	+	+	+	+	+
D13	11CH ₂	12CH ₂	+	+	+	+	+	+	+	+
D14	11CH ₂	6/7H	+	+	+	+	+	+	+	+
D15	14CH ₂	12CH ₂	+	+	+	+	+	+	+	+

Table 4.9: Interproton NOE connectivities within MTX molecule in MTX-d-(TTAGGGT)₄ complex at D/N=1.0 and 2.0 with different τ_m at 298 K, 308 K and 318 K. +sign indicates the presence of NOE connectivities.

Proton (δ ppm)	NOE	NOE	NOE	NOE	NOE	NOE	NOE	NOE	NOE	NOE
11NH (9.58)	T1H2'	T1H2''	T1H4'	T1CH ₃	T2H1'	G6H2''	T7H1'			
1/4OH (12.74)	T1H2'	T1H2''	T1H4'	T1H 5'/5''	T2H6	T2CH ₃	G6H8	T7CH ₃	T7H1'	T7H2''
6/7 H (6.75)	T1H2'	T1H2''	T1CH ₃	T2H2''	G6H2''					
12CH₂ (3.12)	T1CH ₃	T2H1'	G6H1'	T7H 5'/5''						

Table 4.10: Intermolecular NOE connectivities between MTX molecule and *d*-(TTAGGGT)₄ in MTX-*d*-(TTAGGGT)₄ complex at 2.0 at 298 K.

Intermolecular Connectivities	rMD Distance (Å)
11NH – T1CH ₃	4.2
1/4OH – T2CH ₃	4.5
1/4OH – T1H2'	3.0
1/4OH – T1H2''	3.1
1/4OH – T2H6	4.4
1/4OH – T7CH ₃	4.5
1/4OH – T2H4'	3.5
1/4OH – T7H1'	3.0

Table 4.11: Intermolecular NOE connectivities and rMD distances between MTX molecule and *d*-(TTAGGGT)₄ in MTX-*d*-(TTAGGGT)₄ complex at 2.0 at 298 K.

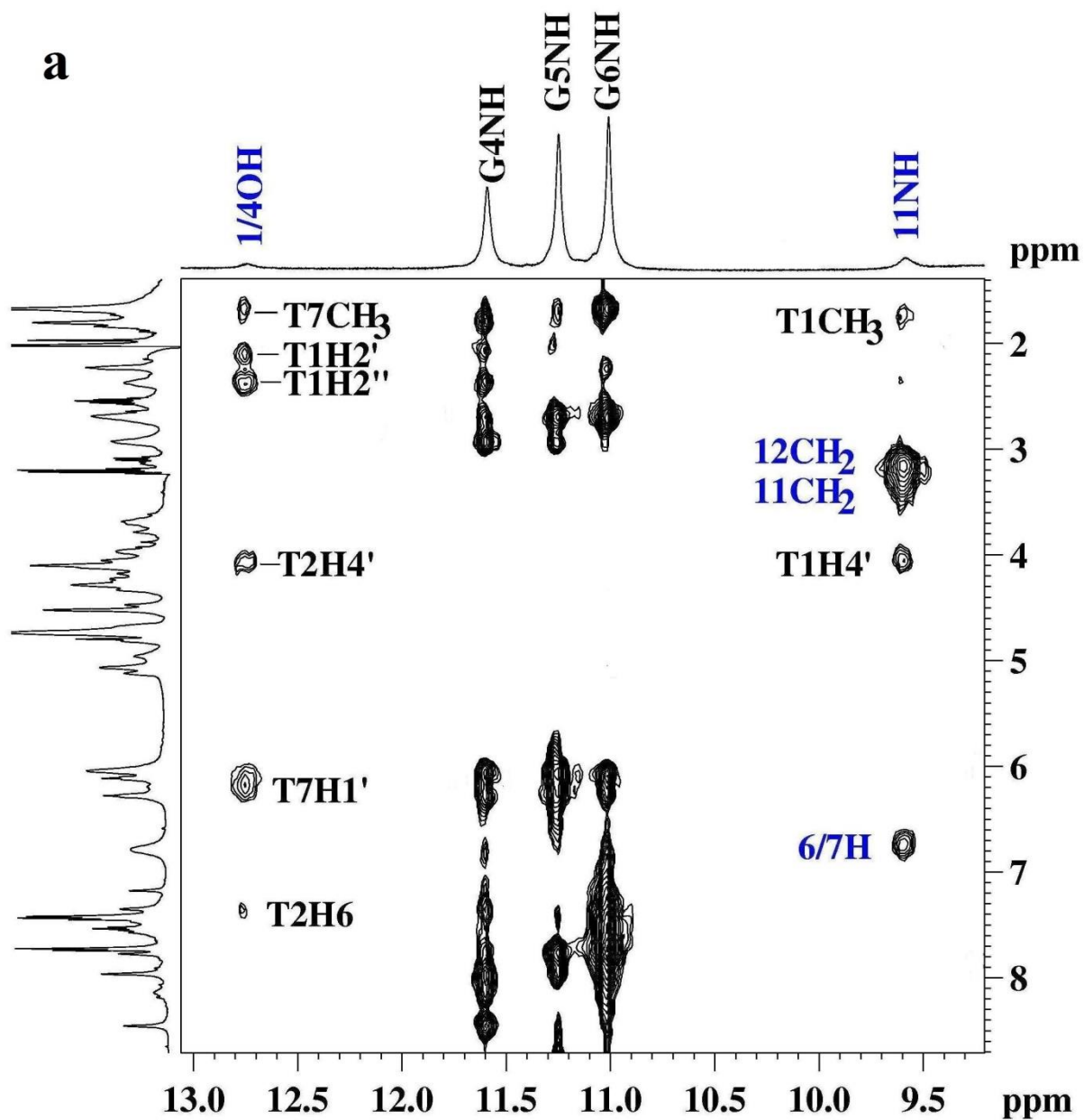


Fig. 4.19a: NOESY spectrum of MTX-d-(TTAGGGT)₄ complex at D/N=1.0 at 298 K showing intermolecular NOE connectivities between 1/4OH and 11NH protons of MTX molecule and d-(TTAGGGT)₄.

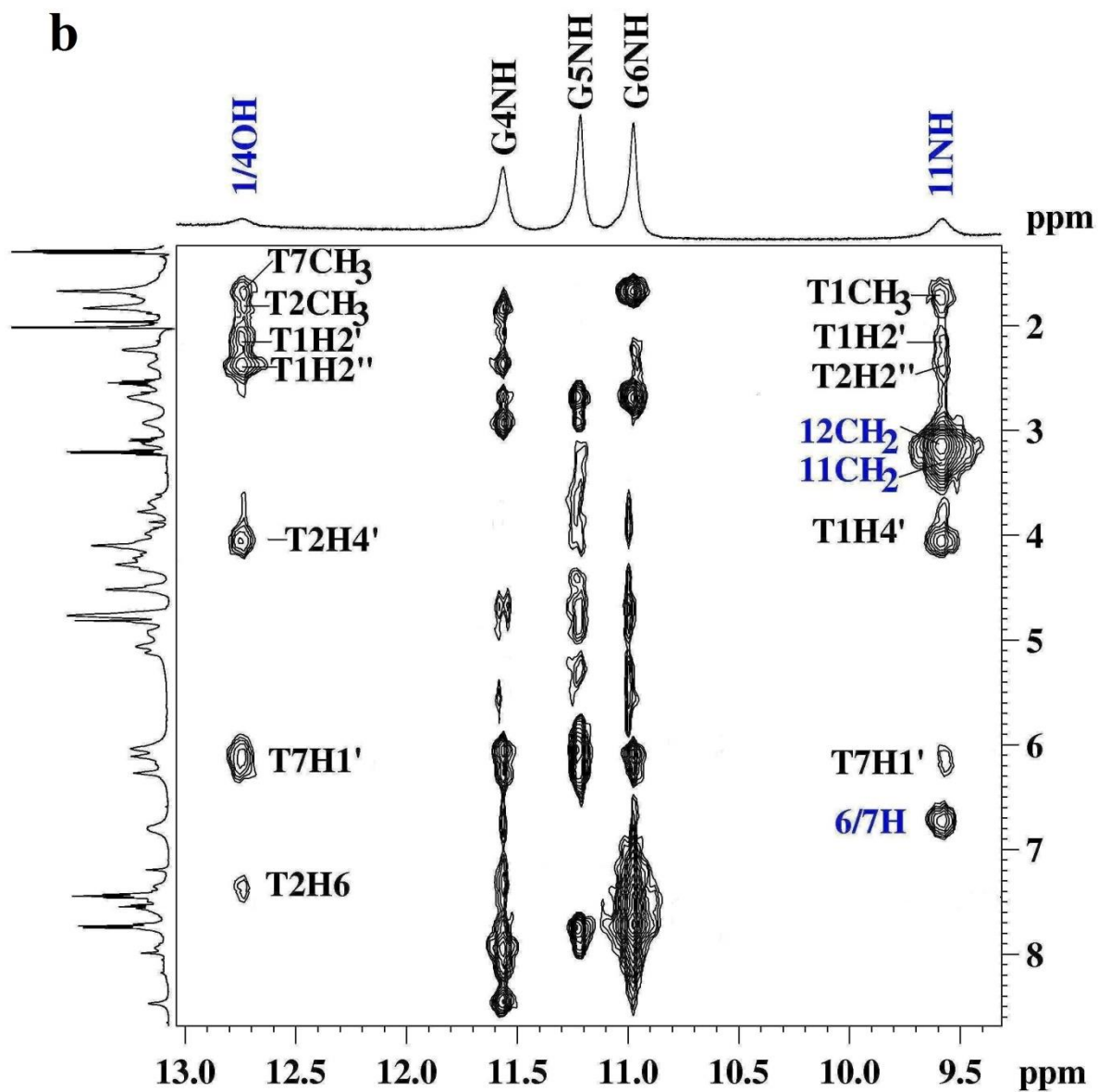


Fig. 4.19b: NOESY spectrum of MTX-d-(TTAGGGT)₄ complex at D/N=2.0 at 298 K showing intermolecular NOE connectivities between 1/4OH and 11NH protons of MTX molecule and d-(TTAGGGT)₄.

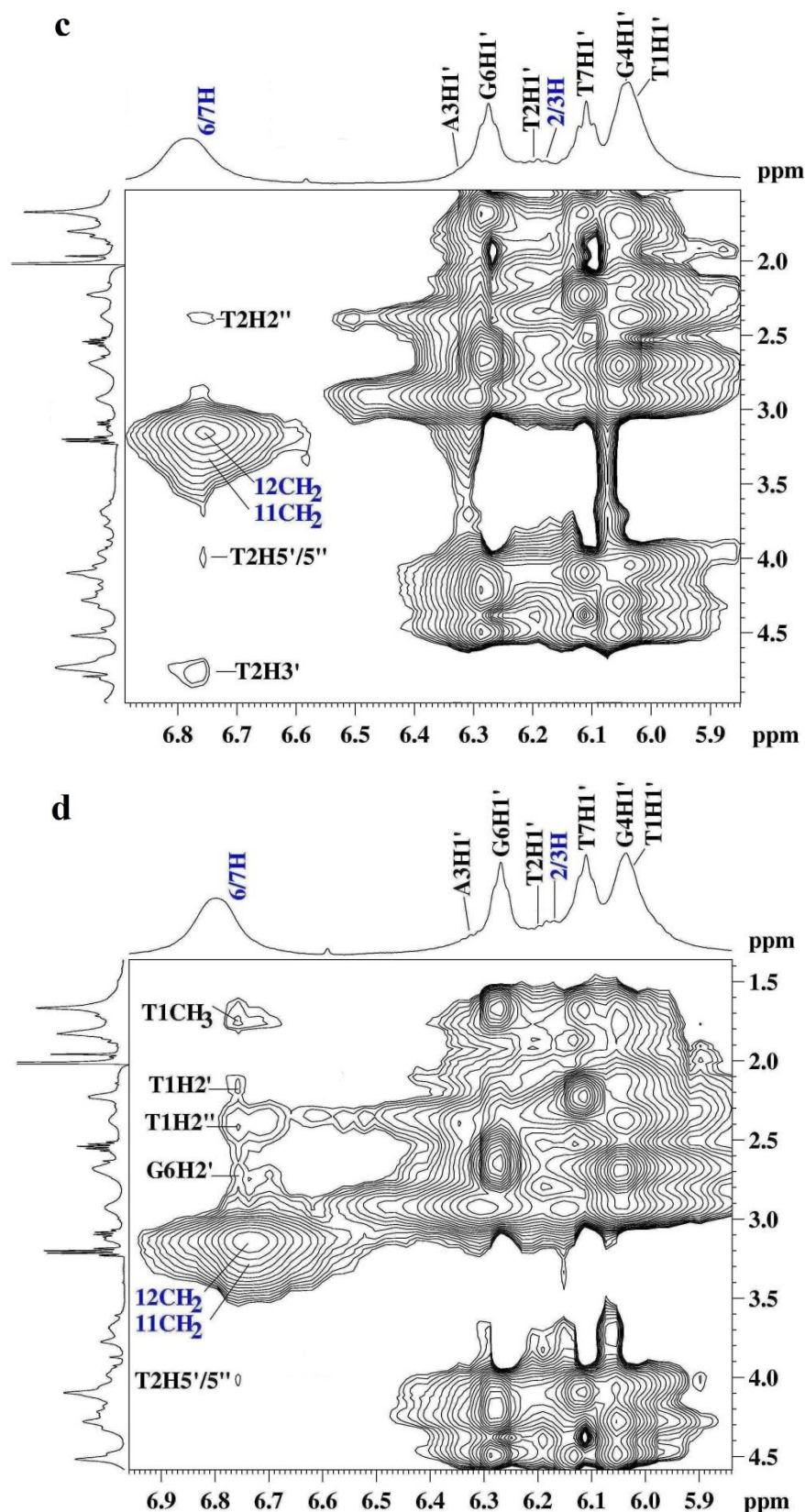


Fig. 4.19: NOESY spectra of MTX-*d*-(TTAGGGT)₄ complex at 298 K showing intermolecular NOE connectivities between 6/7H proton of MTX molecule and *d*-(TTAGGGT)₄ at (c) *D/N*=1.0 and (d) *D/N*=2.0.

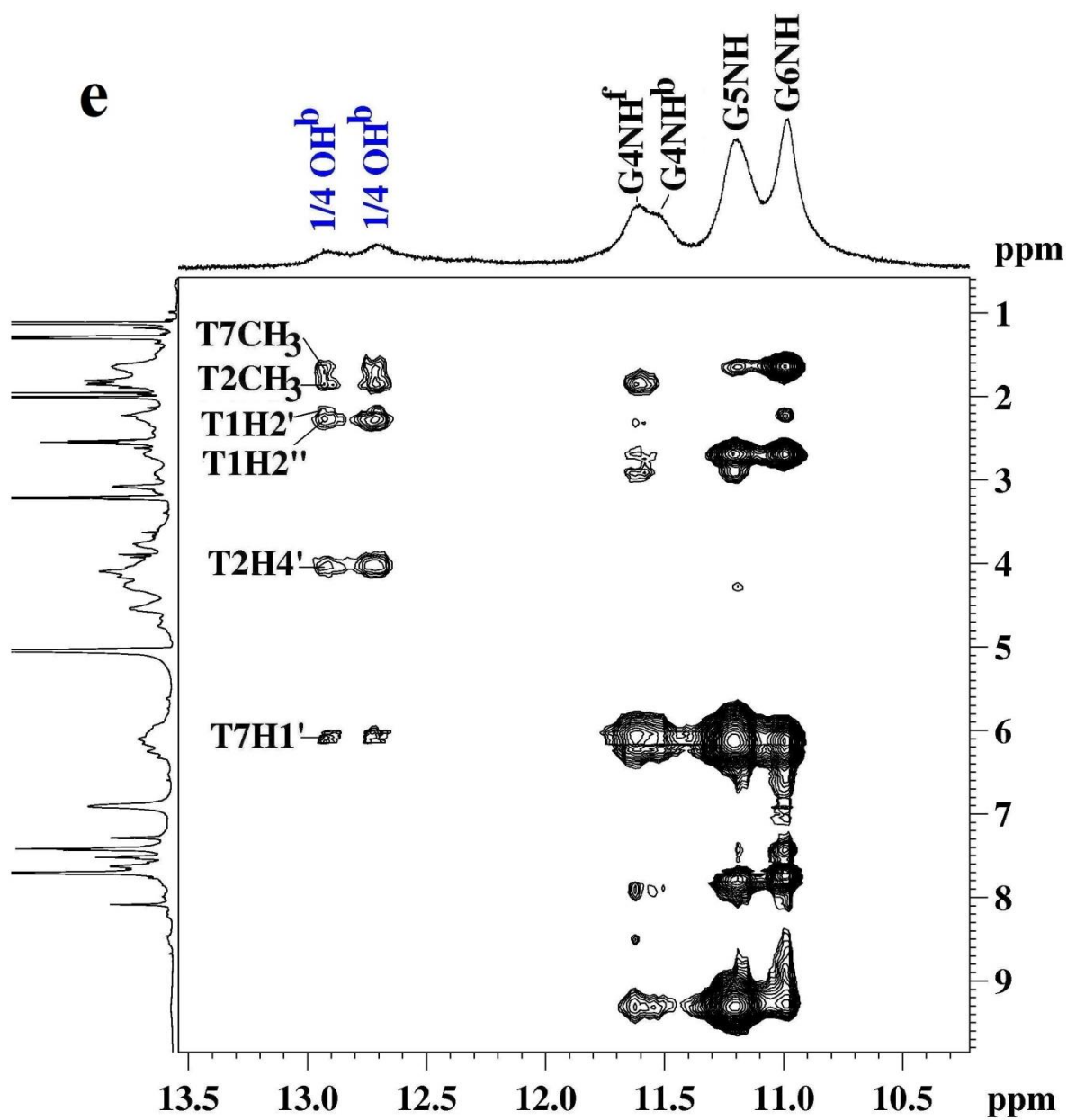


Fig. 4.19e: NOESY spectra of MTX-*d*-(TTAGGGT)₄ complex at *D/N*=2.0 at 278 K showing NOE connectivities between 1/4OH proton of MTX with *d*-(TTAGGGT)₄.

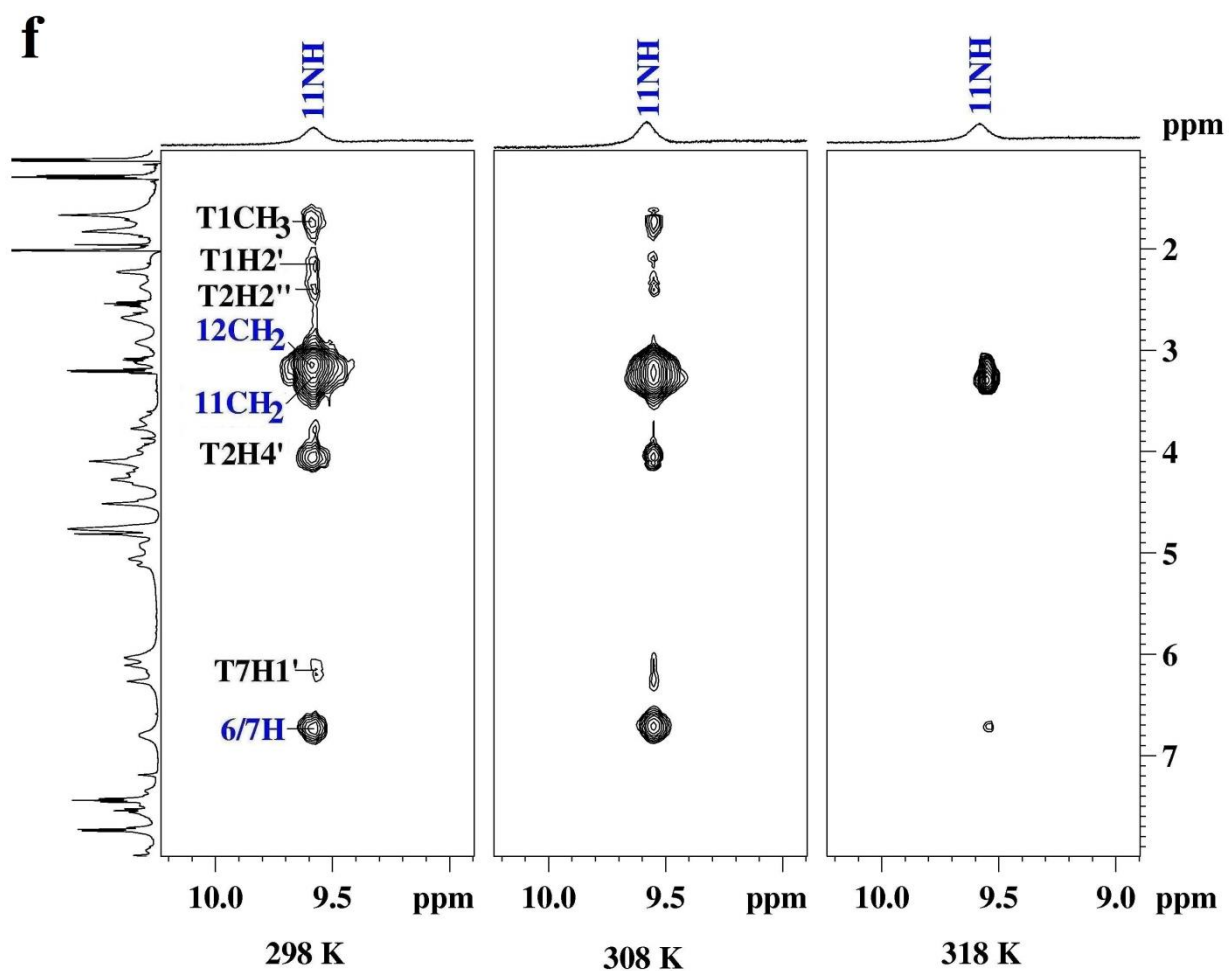


Fig. 4.19f: NOESY spectra of MTX-*d*-(TTAGGGT)₄ complex at *D/N*=2.0 showing intermolecular NOE connectivities between 1/4OH proton of MTX molecule and *d*-(TTAGGGT)₄ as a function of temperature.

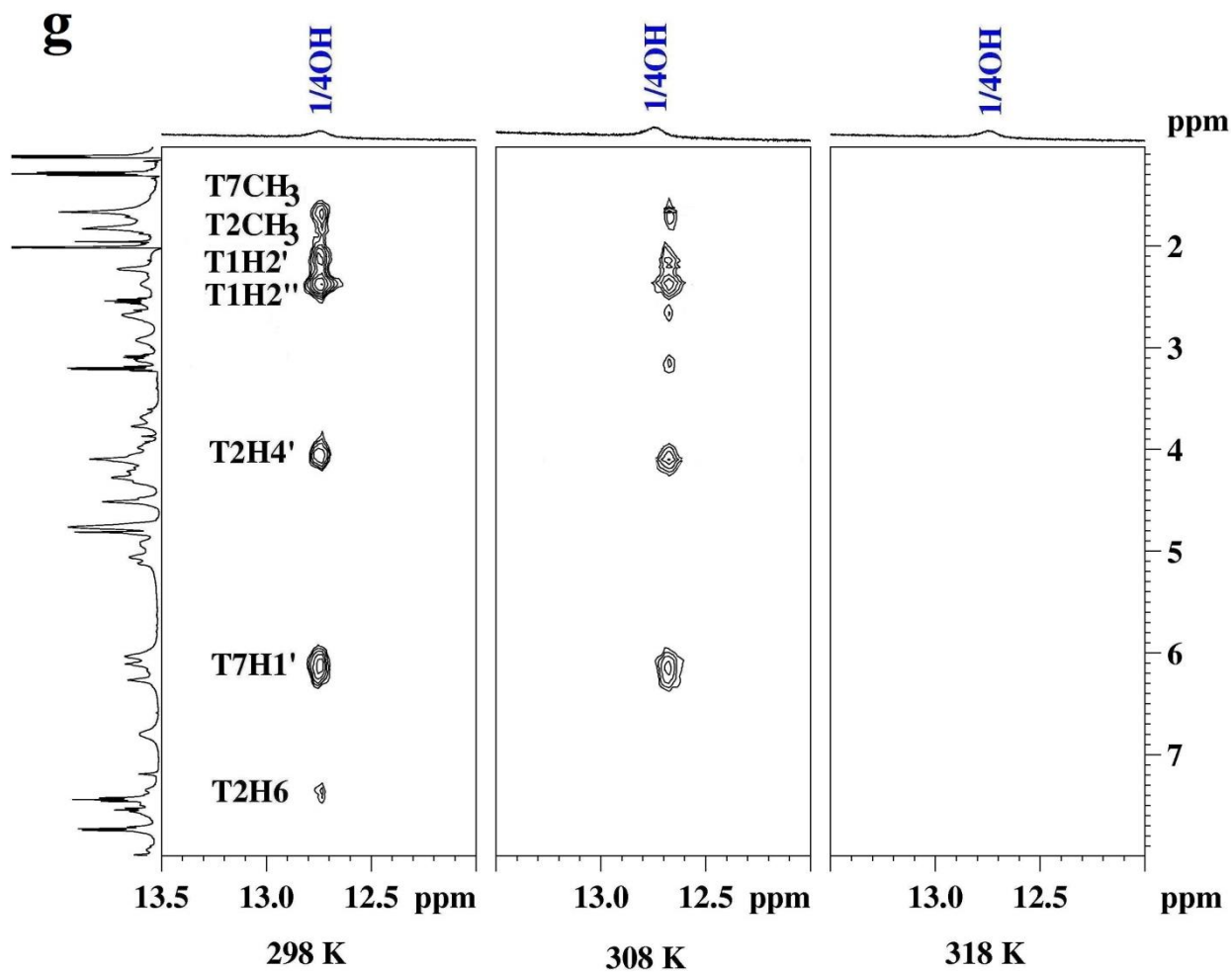


Fig. 4.19g: NOESY spectra of MTX-d-(TTAGGGT)₄ complex at D/N=2.0 showing intermolecular NOE connectivities between 11NH proton of MTX molecule and d-(TTAGGGT)₄ as a function of temperature.

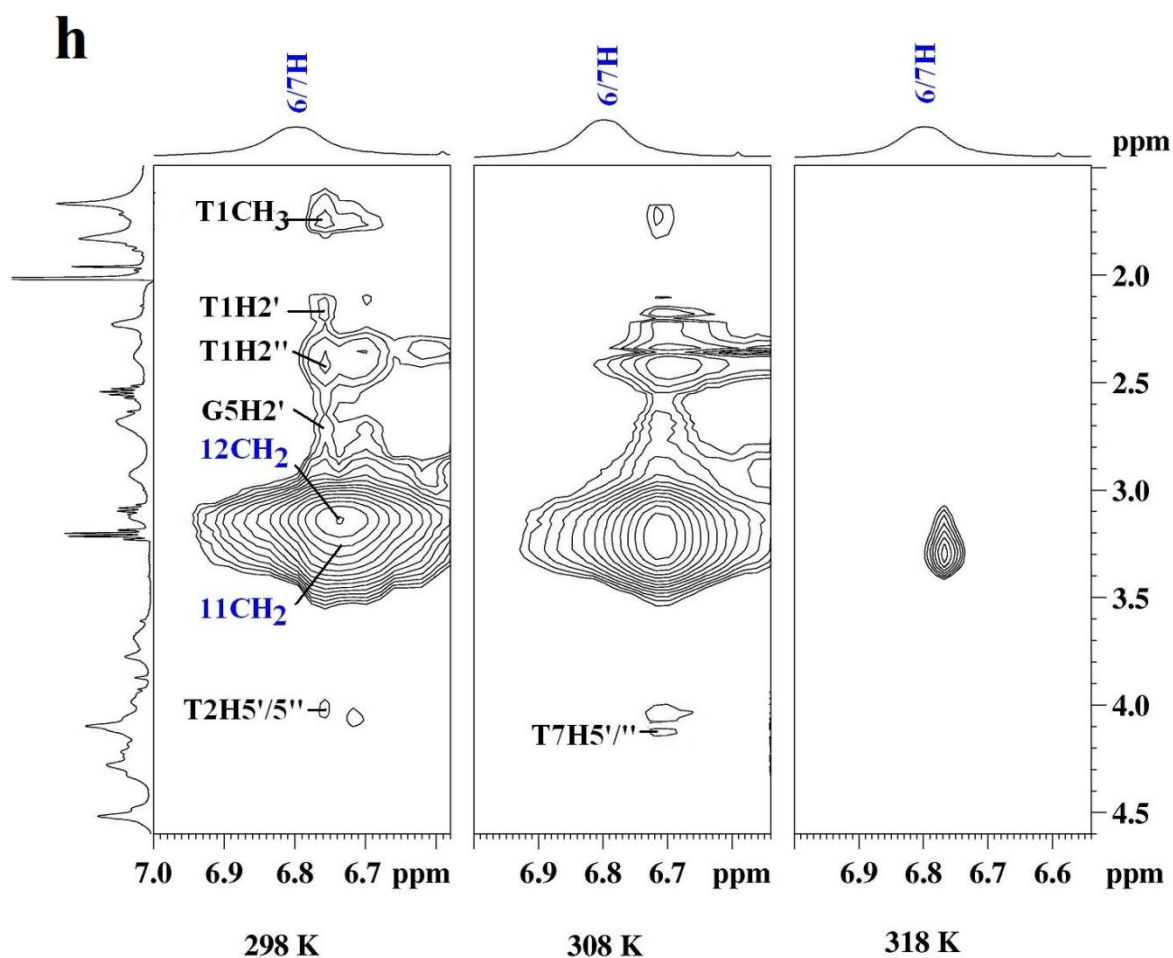


Fig. 4.19h: NOESY spectrum of MTX-d-(TTAGGGT)₄ complex at D/N=2.0 showing intermolecular NOE connectivities between 6/7H proton of MTX molecule and d-(TTAGGGT)₄ as a function of temperature.

4.1.7 Restrained Molecular dynamics studies of MTX-d-(TTAGGGT)₄ complex

To obtain final structure of MTX-d(TTAGGGT)₄ complex, distance restraints obtained from 2:1 complex NOESY ($\tau_m = 200$ ms) at 298 K were used. The NOE peaks were integrated using SPARKY software (T.D Goddard DGK, University of California, San Francisco, USA 2004) and distances obtained were calculated using the methodology given in chapter 2 section 2.5.2.4.4. The inter and intra molecular distances obtained in MTX-d-(TTAGGGT)₄ complex were of three types, i) intermolecular distances between MTX and d-(TTAGGGT)₄ protons, ii) intra molecular distances obtained between protons of MTX molecule and iii) intra molecular distances between protons of d-(TTAGGGT)₄. These distances were used as NOE restraints to build the final structure using restrained molecular dynamics simulation protocol.

The PDB structure 1NP9 (Gavathiotis and Searle, 2003) was used as the initial structure for tetramolecular quadruplex d-(TTAGGGT)₄ and was minimized. The initial structure of MTX was built using the builder module of INSIGHT II, version 2005 (Accelrys Inc., San Diego,

California) on Silicon Graphics Fuel (SGI) workstation and was minimized. The different types of restraints used before energy minimization and simulated annealing were given in **Table 4.12**. Based on the set of 12 MTX-quadruplex NOEs, the MTX molecule was placed in the T1pT2 and G6pT7 steps of the quadruplex DNA such that all constraints were compiled satisfactorily. Once the MTX molecules were placed in the binding site all the restraints were incorporated using the generic distance option of the Discover module with a force constant of 25, 15, 10 Kcal mol⁻¹ Å⁻² for strong, medium and weak interactions, respectively. The structure was energy minimized for 1000 steps using CVFF1 (consistent valence force field) force field, and restrained simulations were carried out for 25 ps using steepest descent protocol.

The assessment of refined structures after equilibration at the end of 25 ps in terms of energetics including restraint violation energies and root mean square derivative of energy with respect to atomic coordinates, given in **Table 4.13** were found to be in reasonable limits. The simulation results are in accordance with the conclusion drawn from intermolecular NOEs connectivities. There was no significant change in the conformation of quadruplex DNA upon MTX binding. Most of the MTX contacts were centred at T1pT2 and G6pT7 steps (**Fig. 4.20**). Close analysis of **Fig. 4.21** shows that the interaction between MTX and d-(TTAGGGT)₄ was stabilized by π - π stacking interaction between aromatic ring of MTX and aromatic ring of T1, T2, G6, T7 bases. The stacking interaction was partial and the extent of stacking was more in T1pT2 step than that of G6pT7 step. This interaction may be the dominant driving force for the complex formation. Furthermore the electrostatic interaction and H-bonding between the amino-alkyl side chains of MTX and quadruplex DNA also contributes to the stabilization of MTX-d-(TTAGGGT)₄ complex. The MTX molecule present at T1pT2 steps form two H-bonds that occur between 1'OH and 14OH of MTX and o1 of T2 sugar. Similarly the MTX molecule present at G6pT7 step also forms H-bonds that result between 1'OH and 12N and 3' o of T7 sugar, respectively.

The rMD results clearly shows that the binding of MTX to quadruplex structure occur via somewhat threading intercalation mode, in which the aromatic ring partially end-stacked while the side chains occupy the groove of quadruplex.

Experimental Restraints	
Intramolecular	
MTX-MTX	12
Quadruplex-Quadruplex	236
Intermolecular	
MTX-quadruplex	16
CVFF energy (kcal mol ⁻¹) of the minimized structures	
Total	2578
Non-bonded	-224
Restraint	336
Average rmsd	0.72Å
Restraint Violations	
Distance (>0.25Å)	16

Table 4.12: Experimental restraints and structure statistics of the final structure.

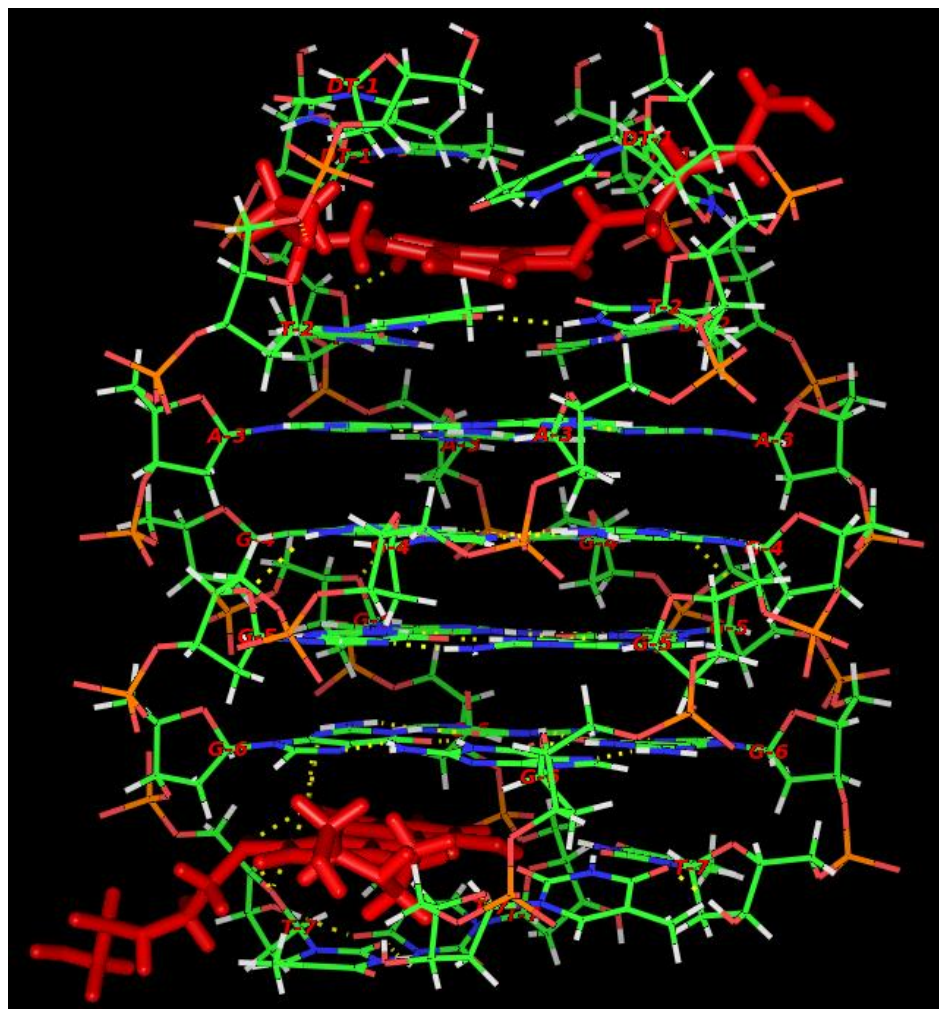


Fig. 4.20: Front view of the final structure of MTX-d-(TTAGGGT)₄ complex obtained by restrained molecular dynamics simulations.

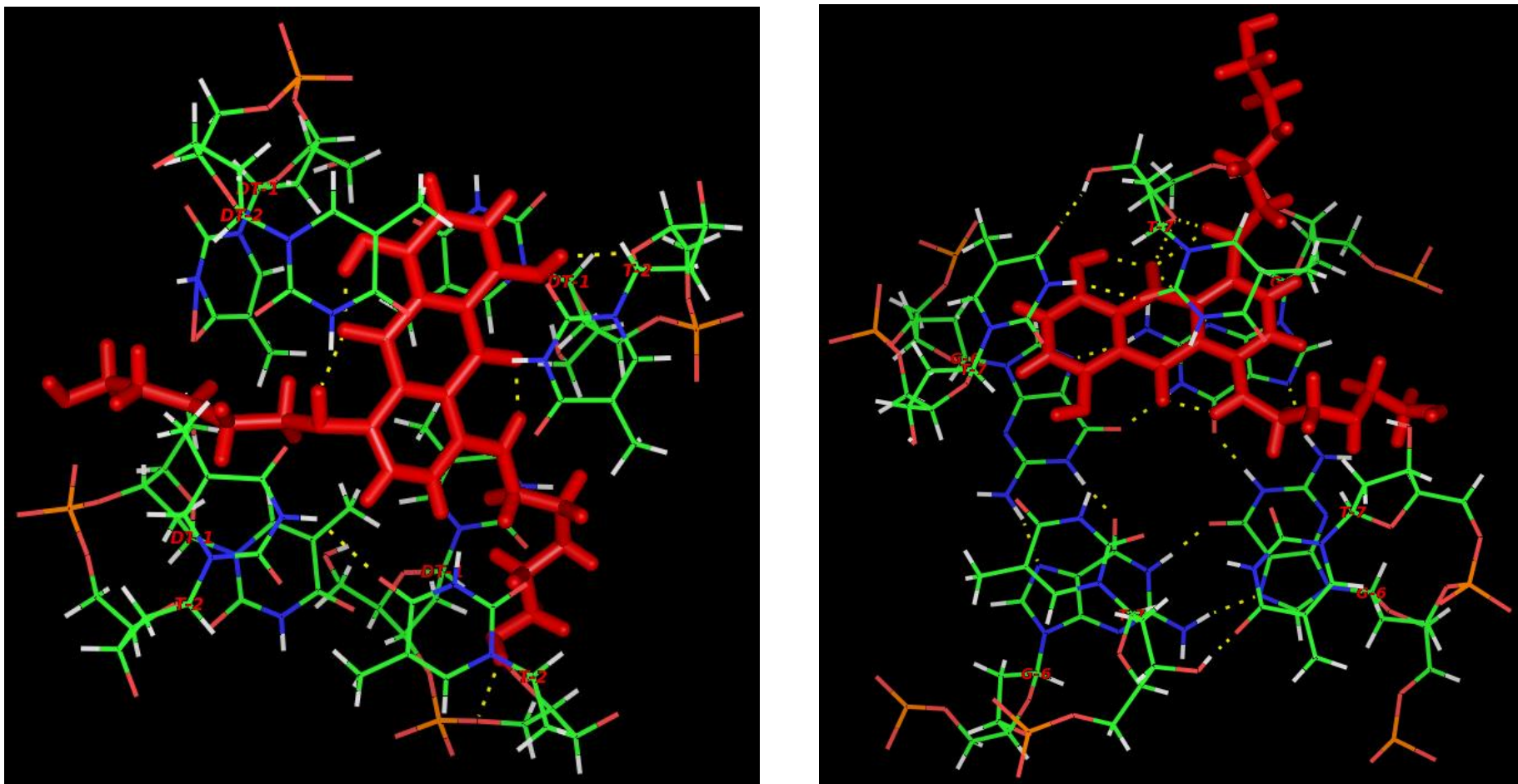


Fig. 4.21: Close-up view of the MTX-d-(TTAGGGT)₄ interaction at T1pT2 and G6pT7 binding sites.

4.2: Conclusion

In order to know the exact mode of binding and forces involved in the interaction of MTX with quadruplex sequence d-(TTAGGGT)₄ NMR techniques followed by restrained Molecular Dynamics (rMD) simulations were employed. Oligonucleotide sequence d-(TTAGGGT), form a right handed parallel stranded G-quadruplex in presence of K⁺ ion, with C₄ symmetry in which all the four strands are equivalent. Presence of three well resolved imino (NH) peaks resonating between 10.5 to 12 ppm region along with NH-NH and NH-H8 NOE connectivities showed the formation of three G-tetrad. The existence of all sequential connectivities between base H8/H6-H1'/H2'/H2" sugar protons indicates the presence of right handed helical geometry similar to that observed in B-DNA. The above mentioned connectivities were also observed in the complex d-(TTAGGGT)₄, which inferred that the G-quartets were intact and there was no opening of base pairs at any step in the complex structure. Thus, there was no loss of original fourfold symmetry of the quadruplex in MTX-d-(TTAGGGT)₄ complex. Only a single set of MTX and quadruplex protons resonances were seen at all D/N ratios, during the course of titration indicating that the binding is fast in NMR time scale. Addition of MTX to d-(TTAGGGT)₄ did not induce significant chemical shift variation of phosphate and proton signals. A maximum upfield shift of 0.06 ppm is observed in all NH protons of quadruplex on binding while MTX protons 2/3 H, 1/4 OH and 11 CH₂ shift upfield by 0.53 ppm, 0.48 ppm and 0.31 ppm, respectively. The stability of complex was assessed by monitoring the melting profile of imino signals, which is indicative of formation of G-quadruplex structure. The result showed that the NH signals of uncomplexed d-(TTAGGGT)₄ disappear at 60°C while that of complexed DNA persist even at 85°C, This clearly indicates significant stabilization of G-quadruplex by about 25°C on binding to MTX.

There was no significant shift in ³¹P resonances a maximum downfield shift of 0.09 ppm was observed in case of T1pT2 step. Absence of significant downfield shift of ³¹P resonances (> 1.5 ppm) excludes the possibility of opening of base pair at any step to permit intercalative mode of binding. Most of the Intermolecular NOE connectivities between MTX protons 11NH, 1/4OH and 6/7H were observed with sugar (H1', H2'/H2", H4') and CH₃ protons of T1, T2, and T7 bases of DNA. Since one MTX proton cannot give peak with both T1 and T7 bases simultaneously, we can infer that probably two molecules of MTX (one at T1pT2 step and second at G6pT7 step) may partially stack at ends of the quadruplex with ring A 2/3H and 1/4OH protons being in close proximity to base protons, which is evident by their large upfield shift while the side chain protons interact with the groove of d-(TTAGGGT)₄. The rMD results are in accordance with the

conclusion drawn from intermolecular NOEs connectivities, which clearly shows that two molecules of the MTX bind to the quadruplex structure. There exist two binding sites one at T1pT2 and other at G6pT7 steps on the quadruplex. The aromatic ring of MTX is partially end-stacked while the side chains occupy the groove of quadruplex. The binding is stabilized by both partial stacking as well as H-bonding and electrostatic interaction.

NMR analysis of luteolin interaction with human and *Tetrahymena* G-quadruplex DNA

Luteolin, 3', 4', 5, 7-tetrahydroxyflavone is a best known flavonoid, which has shown anticancer activity both *in vitro* and *in vivo*. Apart from its anticancer property it also exhibits antioxidant, anti-inflammation and anti-allergy properties. Its interaction with biomolecules occurs due to the presence of aromatic rings and hydrogen bonding capabilities. Till date there is no report on the structural detail of flavonoid-G-quadruplex complex. The present chapter deals with the structural studies of luteolin complexed with two G-quadruplex sequences d-(TTAGGGT)₄ and d-(TTGGGGT)₄, which occur in human and *Tetrahymena* telomeres, respectively and differ at third base position. The structural analysis was done using Nuclear Magnetic Resonance (NMR) techniques followed by restrained Molecular Dynamics (rMD) simulations. Following sets of experiments were done for the assignment of various resonances in uncomplexed and complexed states.

- 1D ¹H and ¹³C NMR and 2D ¹H-¹H ROESY TOCSY, COSY, ¹H-¹³C HSQC and ¹H-¹³C HMBC of luteolin in DMSO-d₆ at 298 K.
- 1D ¹H and ³¹P NMR of d-(TTAGGGT)₄ and d-(TTAGGGT)₄ over a range of temperature between 278-348 K in 90% H₂O and 10% D₂O.
- 2D ¹H-¹H NOESY at 298 K using mixing time $\tau_m = 100, 200, 250$ ms in 90% H₂O/10% D₂O.
- 2D ¹H-¹H COSY and ¹H-¹³C HSQC at 298 and 308 K, respectively in 90% H₂O/10% D₂O.
- 1D ¹H and ³¹P NMR of luteolin-d-(TTAGGGT)₄ complex at various drug D/N ratios of 0.25, 0.5, 0.75, 1.0, 1.25, 1.5, 1.75 and 2.0 over a range of temperature between 278-318 K in 90% H₂O/10% D₂O.
- 1D ¹H and ³¹P NMR of luteolin-d-(TTGGGGT)₄ complex at various drug D/N ratios of 0.25, 0.5, 0.75 and 1.0 over a range of temperature between 278-318 K in 90% H₂O/10% D₂O.
- 2D ¹H-¹H NOESY of luteolin-d-(TTAGGGT)₄ at D/N = 1.0 and 2.0 using mixing time $\tau_m = 100, 200, 250$ ms at 278, 298, 308 and 318 K in 90% H₂O/10% D₂O.
- 2D ¹H-¹H NOESY of luteolin-d-(TTGGGGT)₄ at D/N = 1.0 using mixing time $\tau_m = 100, 200, 250$ ms at 278, 298, 308 and 318 K in 90% H₂O/10% D₂O.

- 2D ^1H - ^1H NOESY of luteolin-d-(TTGGGGT)₄ at D/N = 1.0 using mixing time $\tau_m = 100, 200, 250$ ms at 278, 298, 308 and 318 K in 90% H₂O/10% D₂O.
- 2D ^1H - ^1H COSY at D/N = 1.0 and 2.0 at 298 and 318 K in 90% H₂O/10% D₂O.
- 2D ^1H - ^{13}C HSQC at D/N = 2.0 at 308 K in 90% H₂O/10% D₂O.
- Restrained molecular dynamics studies on the solution structure for the complex of luteolin with d-(TTAGGGT)₄ and d-(TTAGGGT)₄ in D/N ratio of 2:1 and 1:1 using inter-proton distances obtained from 2D NOESY at 200 ms as restraints.

5.1: Results and Discussion

5.1.1 Resonance assignment of luteolin

Complete unambiguous assignment of all proton (**Table 5.1**) and carbon (**Table 5.2**) resonances of luteolin were done using standard NMR techniques of ^1H 1D NMR (**Fig 5.1**), ^{13}C NMR (**Fig 5.2**) and two dimensional ^1H - ^{13}C HSQC, ^1H - ^{13}C HMBC, ^1H - ^1H ROESY, ^1H - ^1H TOCSY, ^1H - ^1H COSY techniques. Analysis of the proton NMR spectrum of luteolin (**Fig 5.1**) shows ten proton resonances which are classified into aromatic and hydroxyl ring protons. The aromatic protons (6-7.5 ppm) are directly attached to the benzene nucleus and experience more ring current effect and hence appear up-field to the hydroxyl protons which are attached to an electron withdrawing oxygen atom. The aromatic region of proton NMR spectra consists of a singlet assigned to be H3 (6.67 ppm). Rest aromatic protons show characteristic splitting patterns (**Table 5.1**). The appearance of doublet of a doublet peak at 7.40 ppm was assigned to be H6' proton, it shows the presence of both ortho ($J=1-2$ Hz) and meta ($J=8-9$ Hz) coupling. H6' proton shows a doublet due to the presence of H5' meta proton ($J=8.6$ Hz). This doublet was further splits by ~ 1.9 Hz, giving a characteristic doublet of a doublet appearance. This splitting is attributed to the presence of ortho proton H2' in the ring B. The other aromatic protons H6, H8 and H2' show ortho effect ($J=1.9$ Hz) and appear as weak doublets. Protons H8 and H6 are attached to the ring A. The hydroxyl protons resonate downfield to that of aromatic protons owing to the electronegative character of the oxygen atom. All the four -OH resonances appeared as singlets and showed no correlation to the carbon resonances in the 2D ^1H - ^{13}C HSQC (**Fig 5.3**) experiment. The unambiguous assignment of OH protons were achieved by 2D ^1H - ^{13}C HMBC experiment (**Fig 5.4**), which revealed the long range coupling of OH signals to the nearby coupled carbon atoms (**Table 5.3**). The 12.96 ppm peak, which is > 2 ppm downfield from other OH protons was assigned to be 5OH signal owing to the formation of an intramolecular hydrogen bond with -CO(4).

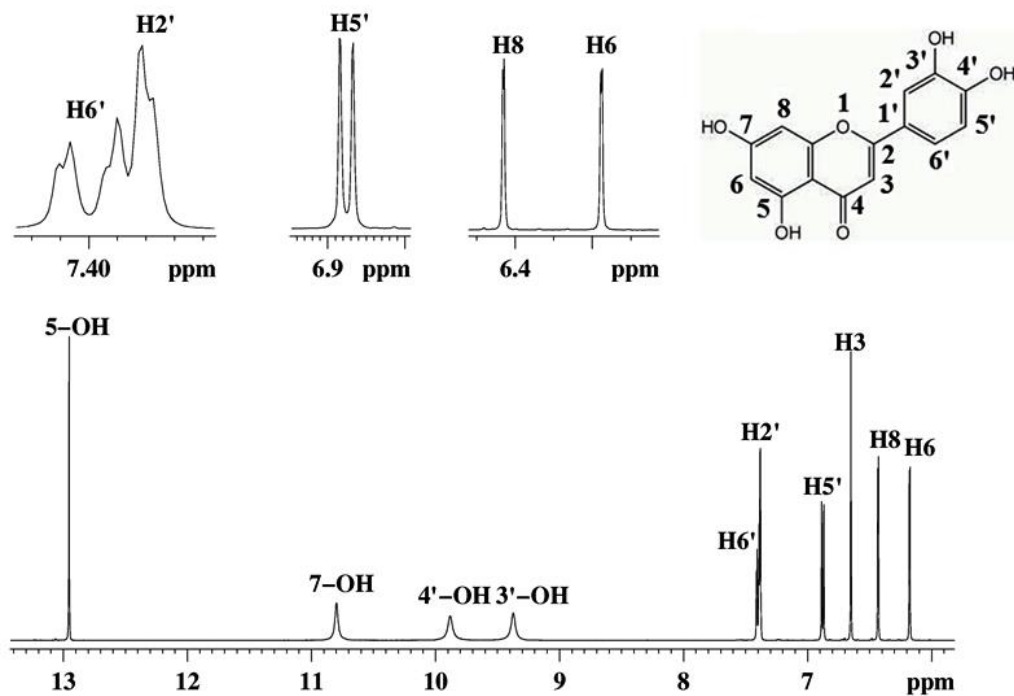


Fig. 5.1: Proton NMR spectra of luteolin in DMSO- d_6 at 298 K.

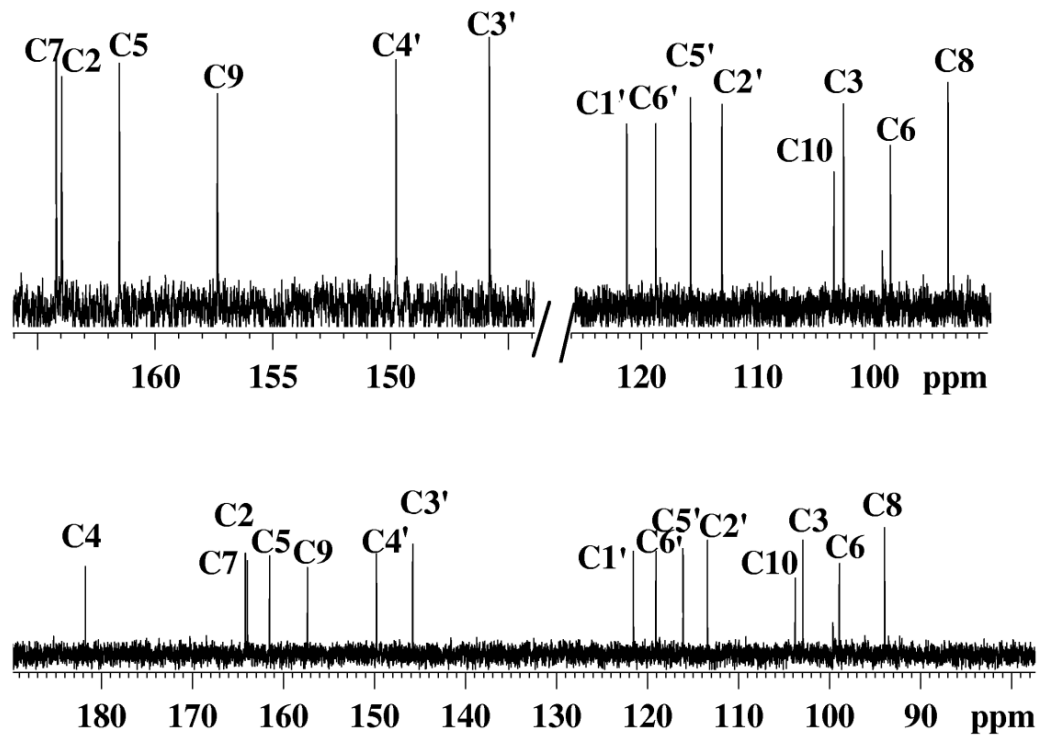


Fig. 5.2: Carbon NMR spectra of luteolin in DMSO- d_6 at 298 K.

Luteolin Protons	Present work (DMSO-d ₆)	<i>J</i> coupling (Hz)	Rietjens 2002 (DMSO-d ₆)	Owen et al. 2003 (3:1CD ₃ OD/DMSO-d ₆)	Nissler et al. 2004 (DMSO-d ₆)	Park et al. 2007 (DMSO-d ₆)	Wang et al. 2008 (MeOH-d ₄)	E.J.Lee et al. 2010 (DMSO-d ₆)	S.Lee et al. 2012 (DMSO-d ₆)
H3	6.67		6.63	6.58	6.65	6.65	6.59	6.66	6.67
H6	6.18	1.9 (d, <i>J</i> H6-H8)	6.14	6.21	6.18	6.18	6.31	6.18	6.18
H8	6.44	1.9 (d, <i>J</i> H8-H6)	6.40	6.45	6.43	6.43	6.62	6.43	6.37
H2'	7.38	1.9 (d, <i>J</i> H2'-H6')	7.35	7.39	7.38	7.39	7.59	7.38	7.39
H5'	6.88	8.3 (d, <i>J</i> H5'-H6')	6.84	6.91	6.88	6.89	7.10	6.88	6.88
H6'	7.40	1.9 (dd, <i>J</i> H6'-H2') 8.3(<i>J</i> H6'-H5')	7.37	7.39	7.40	7.40	7.51	7.40	7.40
5-OH	12.96		-	-	-	12.97	12.97	13.00	12.97
7-OH	10.90		-	-	-	10.80	-	-	-
3'-OH	9.48		-	-	-	9.40	-	-	-
4'-OH	9.97		-	-	-	9.90	-	-	-

Table 5.1: Proton chemical shift (ppm) of luteolin in DMSO-d₆ of present work and its comparison with results reported in literature

Luteolin Carbon No.	Present work (DMSO-d ₆)	Kumari et al. 1986 (DMSO-d ₆)	Wawer et al. 2001 (DMSO-d ₆)	Owen et al. 2003 (3:1CD ₃ OD/DMSO-d ₆)	Nissler et al. 2004 (DMSO-d ₆)	Park et al. 2007 (DMSO-d ₆)	Wang et al. 2008 (MeOH-d ₄)	E.J.Lee et al. 2010 (DMSO-d ₆)	S.Lee et al. 2012 (DMSO-d ₆)
C2	163.95	164.5	163.9	165.44	164.4	163.9	164.94	164.1	163.9
C3	102.91	103.3	102.5	103.88	103.3	102.9	104.25	103.0	102.9
C4	181.73	182.2	182.5	183.11	182.1	181.7	183.10	181.8	181.6
C5	161.51	162.1	161.8	162.70	161.9	161.5	163.39	161.7	161.4
C6	98.88	99.2	98.7	99.74	99.3	98.9	99.72	99.0	98.8
C7	164.17	164.7	164.8	165.30	164.5	164.1	165.19	164.3	164.1
C8	93.92	94.2	93.6	94.75	94.3	93.9	94.74	94.0	93.8
C9	157.34	157.9	158.0	158.81	157.7	157.3	158.81	157.5	157.3
C10	103.74	104.2	103.9	104.98	104.2	103.8	105.39	103.9	103.7
C1'	121.53	122.1	122.3	123.22	122.0	121.6	123.79	121.7	119.0
C2'	113.38	113.8	112.8	114.04	113.8	113.4	114.20	113.5	113.4
C3'	145.78	146.2	145.6	146.65	146.2	145.8	146.51	145.9	145.7
C4'	149.75	150.2	149.6	150.51	150.1	149.7	150.16	149.9	149.7
C5'	116.06	116.4	115.4	116.74	116.5	116.1	116.66	116.2	116.0
C6'	119.06	119.3	118.9	119.96	119.4	119.0	120.15	119.2	121.5

Table 5.2: Carbon chemical shift (ppm) of luteolin in DMSO-d₆ of present work and its comparison with results reported in literature.

The 5OH of luteolin is more shielded than that of flavonols (e.g. quercetin) due to the absence of 3OH, which decreases the strength of this hydrogen bonding. It appeared as sharp resonance above ambient temperature due to the inaccessibility to the surrounding solvent molecules. On the other hand the rest of the OH protons, that is, 7OH, 4'OH and 3'OH form intermolecular hydrogen bonding with the surrounding solvent, hence appeared as broad signal at and above room temperature, owing to the fast exchange on NMR time scale (**Fig. 5.5**).

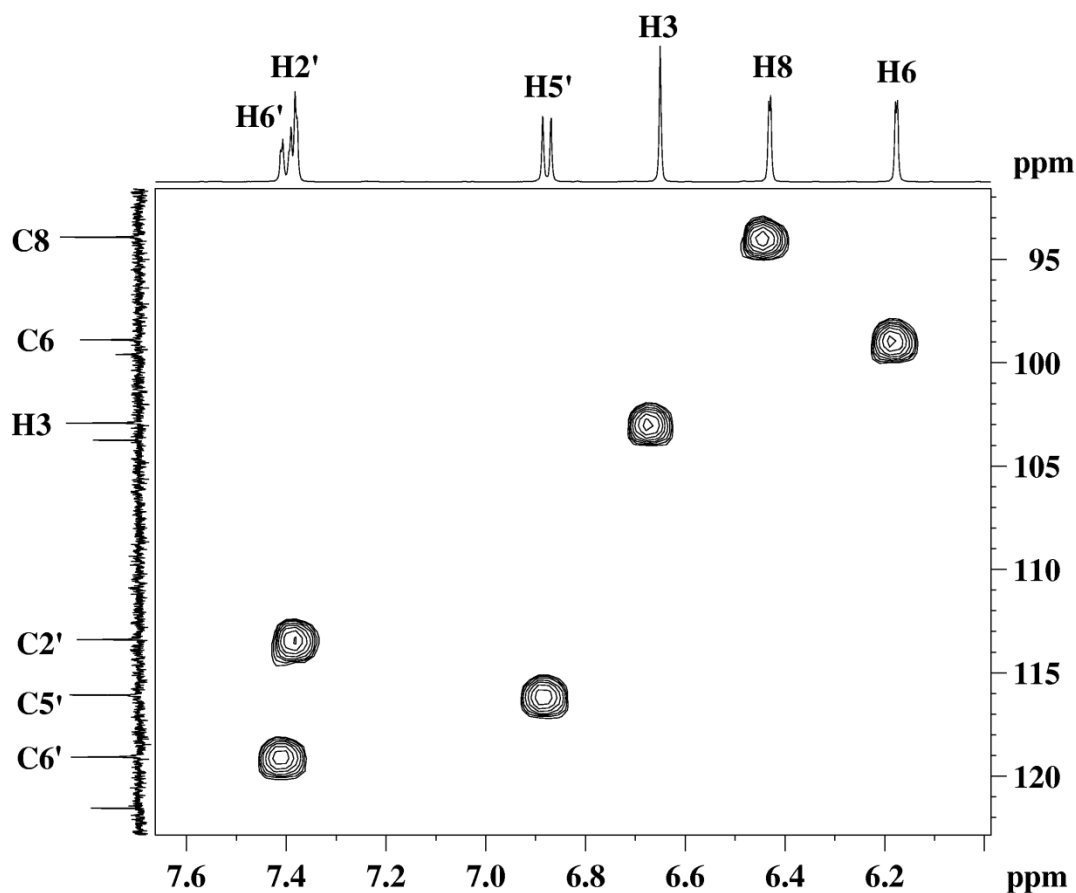


Fig. 5.3: ^1H - ^{13}C HSQC spectrum of luteolin showing directly coupled aromatic protons resonance.

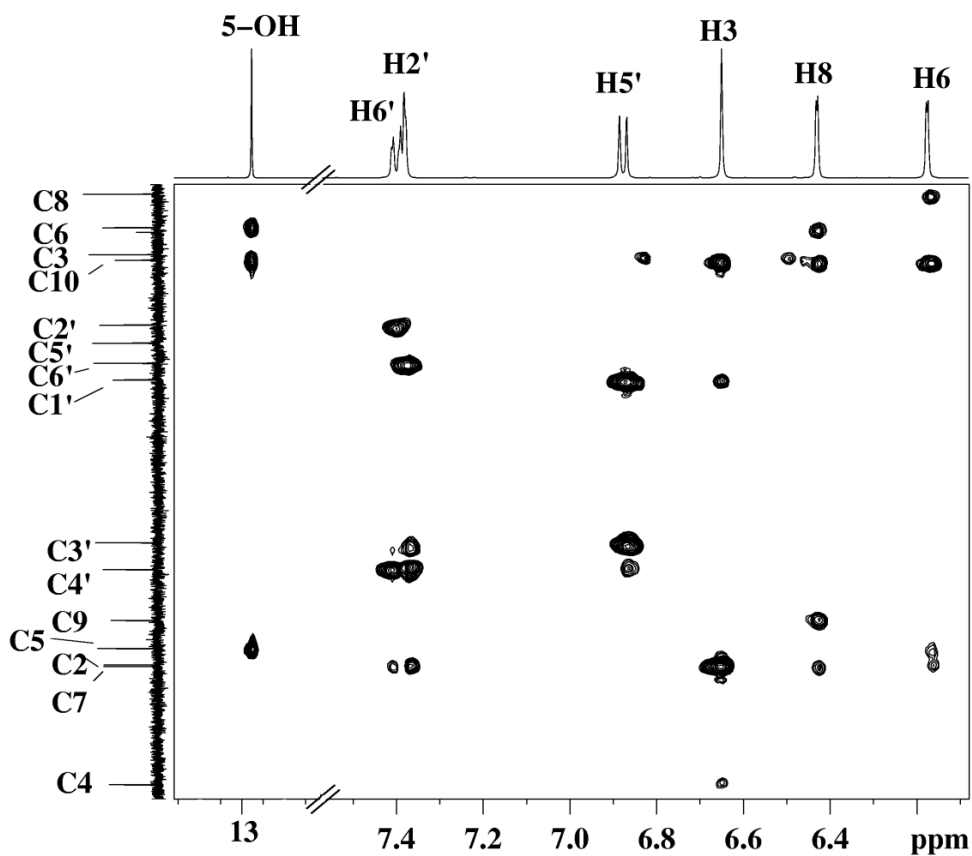


Fig. 5.4: ^1H - ^{13}C HMBC spectrum of luteolin showing long ranged coupling.

5X

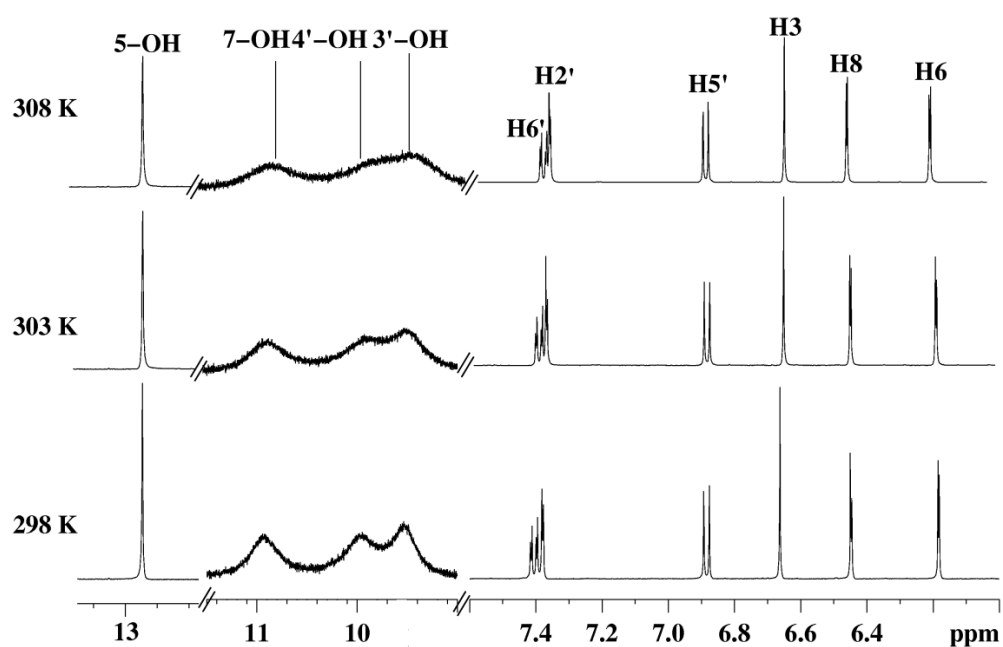


Fig. 5.5: ^1H NMR spectra of luteolin as a function of temperature showing the exchange of OH signals.

As carbon atoms are shielded from the outer environment, chemical shift of the carbons were largely determined by the electron density at that particular carbon atom. Thus the carbon resonating at the lowest field was attributed to the carbonyl at position 4, followed by hydroxylated aromatic carbons.

Fig. 5.6 shows the ^1H - ^1H TOCSY spectrum of luteolin, which helps in the identification of spin systems present in the molecule. The aromatic proton H2' shows a weak correlation with both H6' and H5' protons. The meta-coupled protons H5' and H6' shows a very intense peak, which is expected for a three bond coupled protons. The most shielded aromatic proton H6 gives a weak TOCSY correlation with H8 proton. This confirms the presence of aromatic protons attached to two separate spin systems (ring A and B). H2', H5', H6' protons are attached to aromatic B and H6 and H8 protons to another aromatic ring A. Rings A and B are separated by the heterocyclic ring C. The presence of meta coupled proton was also confirmed by the presence of intense cross peak between H6' and H5' in the magnitude mode COSY spectra (**Fig. 5.7**).

LUTEOLIN CARBON NO.	LUTEOLIN PROTON NO.	COSY	TOCSY	HSQC (C-H Single bond correlation)	HMBC (C-H multiple bond correlation)
C2					2J (H3); 3J (H2', H6'), 4J (H8)
C3	H3			C3-H3	1J (H3)
C4					2J (H3); 4J (H6, H8)
C5	5-OH				2J (H6, 5OH); 4J (H3, H8)
C6	H6	4J H8-H6	4J H6-H8	C6-H6	1J (H6); 3J (H8, 5OH)
C7	7-OH				2J (H6, H8)
C8	H8		4J H8-H6	C8-H8	1J (H8); 3J (H6)
C9					2J (H8); 4J (H6)
C10					3J (H3,H6,H8, 5OH)
C1'					2J (H2', H6'); 3J (H5', H3)
C2'	H2'		4J H2'-H6'	C2'-H2'	1J (H2'); 3J (H6'); 4J (H5')
C3'	3'-OH				2J (H2'); 3J (H5'); 4J (H6')
C4'	4'-OH				2J (H5'); 3J (H2', H6')
C5'	H5'	3J H5'-H6'	3J H5'-H6'	C5'-H5'	1J (H5'); 2J (H6')
C6'	H6'	3J H6'-H5'	3J H6'-H5' 4J H6'-H2'	C6'-H6'	1J (H6'); 2J (H5'); 3J (H2')

Table 5.3: The complete assignments of the ^1H and ^{13}C chemical shift correlation of luteolin.

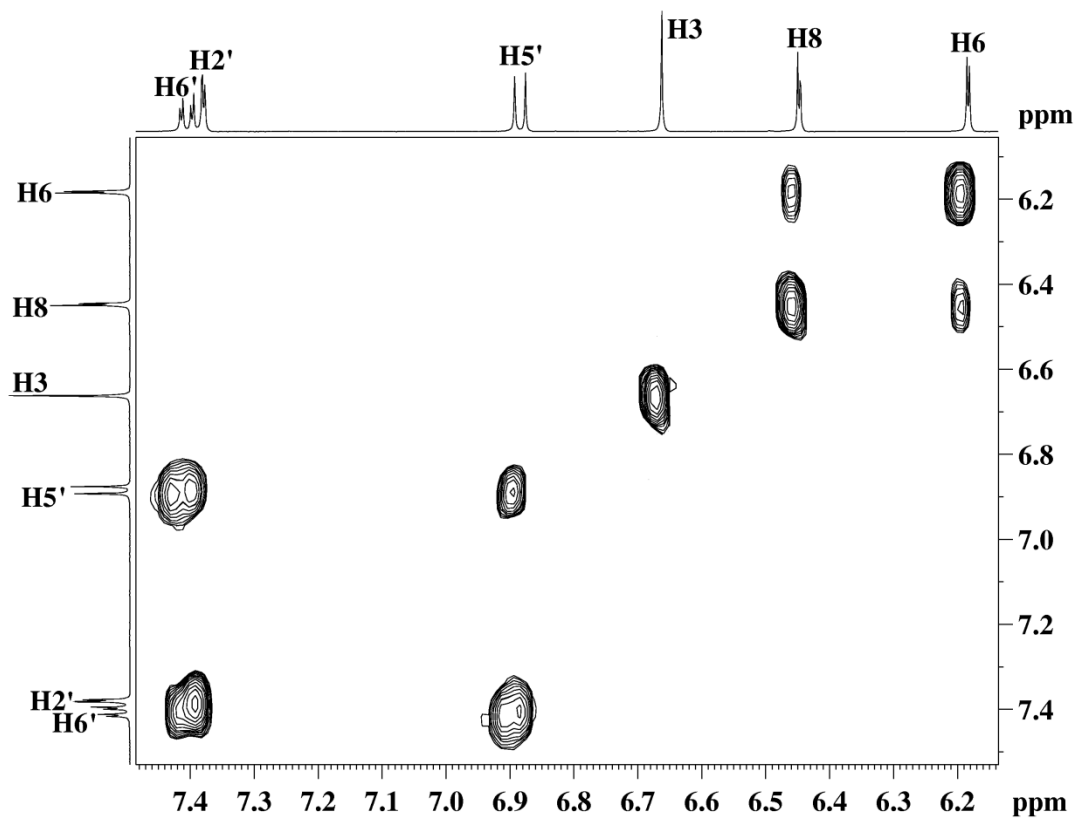


Fig. 5.6: TOCY spectrum of luteolin.

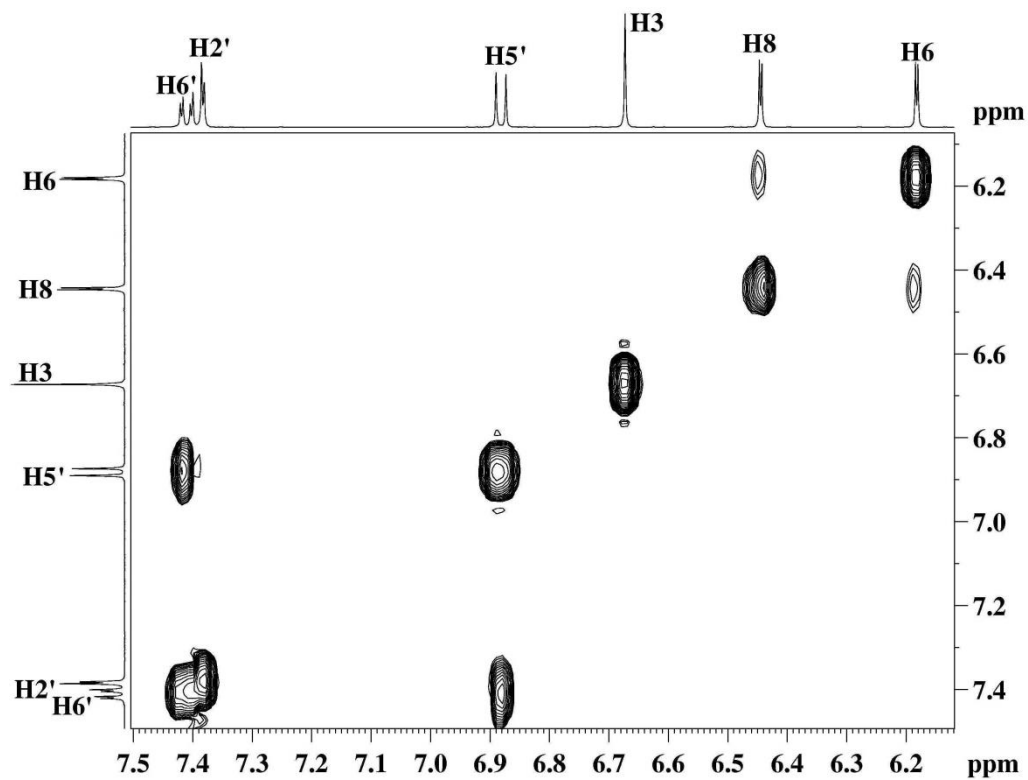
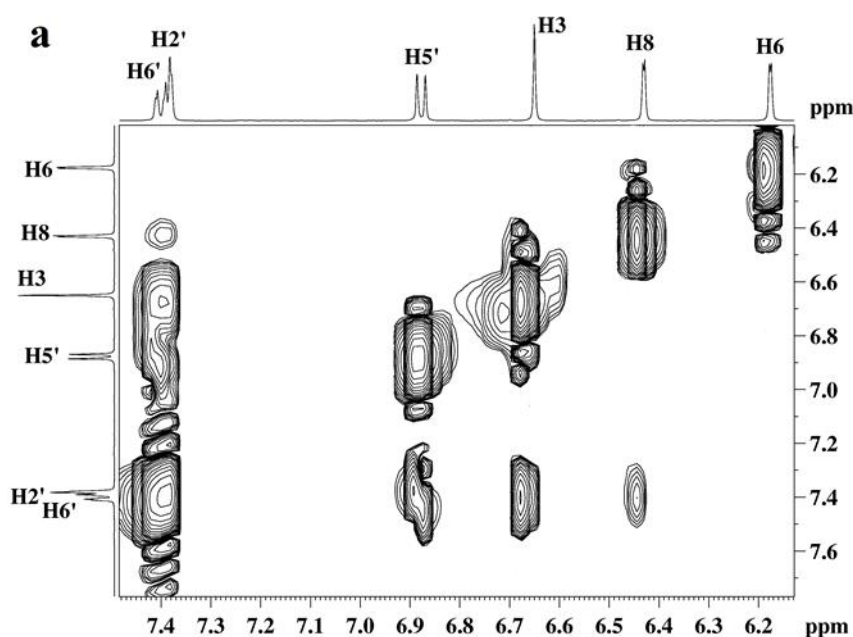


Fig. 5.7: COSY spectrum of luteolin.

To obtain three dimensional structure of luteolin ^1H - ^1H ROESY experiment was used. **Fig 5.8a, b** shows the ROESY spectra (200 ms) of luteolin at 298 K. Meta coupled protons H5'-H6' shows a strong cross peak, and apart from this, cross peaks were also observed for H8 with H2', OH7 with H8 and H6, OH4'-H5', OH3'-H2'. These cross peak volumes were integrated to get distance and used in the energy minimization and restrained molecular dynamics to get final minimized structure. **Table 5.4** shows the ROESY cross peaks, distance obtained from ROESY experiment and distances after energy minimization of luteolin molecule using rMD (**Fig. 5.9**).

S. No.	Connectivities	Insight (Å)	Interproton distances (ROESY) (Å)	Distances in rMD structure (Å)
1	H3-H6'	2.56	2.64	2.07
2	H3-H2'	4.43	O	-
3	H5'-H6'	2.44	2.44	2.27
4	H5'-H2'	4.95	O	-
5	H2'-H8	4.66	4.04	3.89
6	H2'-H6'	4.31	O	-
7	5-OH-H3	4.28	4.80	4.49
8	5-OH-H6	3.51	4.11	3.60
9	7-OH-H8	2.25	4.03	3.90
10	7-OH-H6	3.55	4.77	4.40
11	4'-OH-H5'	3.55	4.02	3.92
12	3'-OH-H2'	2.20	4.05	3.94

Table 5.4: Connectivities and interproton distances (Å) from ROESY spectra of luteolin used in restrained molecular dynamics. The corresponding distances obtained from optimized rMD are also shown.



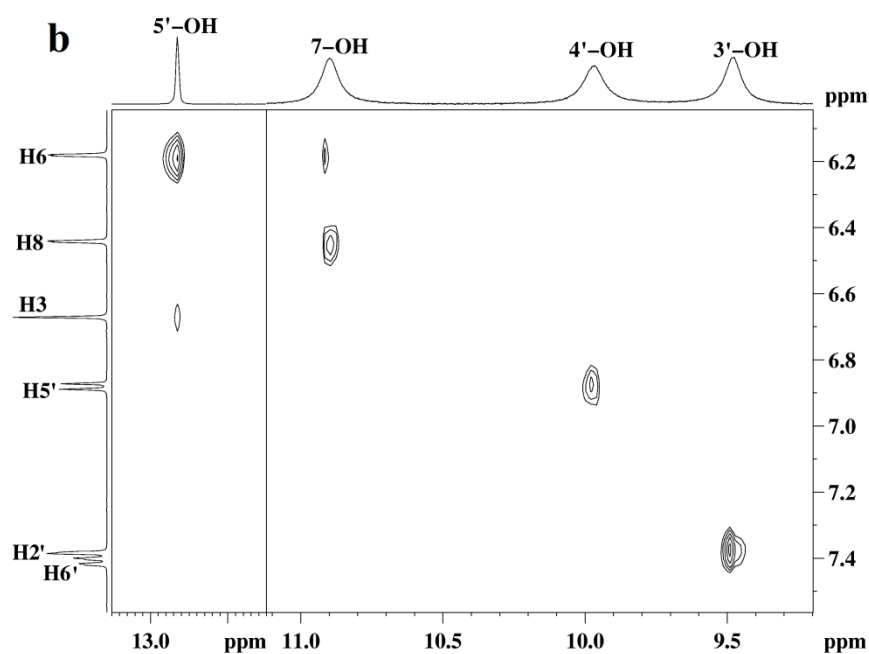


Fig. 5.8: ROESY spectra of luteolin showing the intramolecular connectivities (a) of the aromatic protons and (b) of hydroxyl protons.

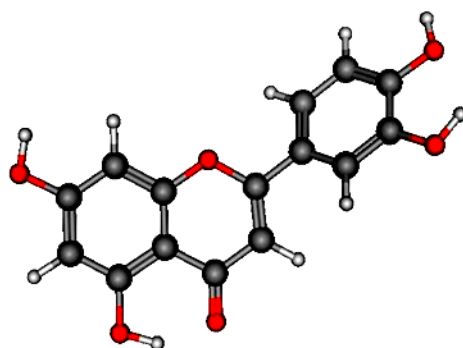


Fig. 5.9: Minimized solution structure of luteolin by rMD.

5.1.2 Resonance assignment of uncomplexed sequence d-(TTAGGGT)₄

The resonance assignment of uncomplexed sequence d-(TTAGGGT)₄ have already been covered in chapter 4 section 4.1.2. But for the sake of new titration the assignment of uncomplexed sequence was achieved. There were no significant changes in the spectra of both the uncomplexed sequences. All the sequential connectivities between base and G-tetrads were present. Hereby, confirming the formation of parallel-stranded G-quadruplex structure.

5.1.3 Resonance assignment of luteolin-d-(TTAGGGT)₄ complex

To examine the binding interaction of luteolin with quadruplex sequence d-(TTAGGGT)₄ increasing concentration of luteolin was titrated to the quadruplex solution to reach the desired D/N ratios of 0.25, 0.5, 0.75, 1.0, 1.25, 1.5, 1.75 and 2.0. The changes were continuously monitored by ¹H and ³¹P NMR at different temperatures. Only one set of DNA signals was seen at all D/N values, during the course of titration, indicating that the binding was fast in NMR time scale. A complete assignment of all non-exchangeable and exchangeable protons of the complex had been accomplished by means of a combination of 2D NMR experiments besides comparing them with that of uncomplexed DNA and luteolin. The NH-NH NOE connectivity between adjacent imino protons and interstrand guanine NH connectivities to its own and 5' flanking base protons in A3-G4-G5-G6 segment indicate that G-quartet were intact and there was no loss of original fourfold symmetry of the quadruplex in MTX-d-(TTAGGGT)₄ complex (**Figs. 5.10 a, b**). As for DNA, resonances within deoxyribose were identified by COSY as well as ¹H-¹³C HSQC in view of overlap with luteolin signals. Analysis of sequential NOEs among base and H1'/H2'/H2'' protons allowed assignment of all base protons. All bases have classical H8/H2'-H2'' sequential connectivities to neighboring 5'-end bases indicating that the four strands were involved in the formation of helical structure in the complex. The entire pattern of NOEs indicates that the backbone conformation closely resembles that of uncomplexed d-(TTAGGGT)₄ possessing a right handed B-form helix structure. The presence of all sequential base GH8/H6-H1'/H2'/H2'' NOEs (**Figs. 5.11a, b**), indicates that there was no opening of base pairs at any step, hence excluding intercalation of drug chromophore between base pairs.

A single set of signals of luteolin protons was present in the spectra of complex at 298 K and was assigned unambiguously. The meta coupled protons H5' and H6' of luteolin was easily identified in the COSY spectra (**Fig. 5.12**) while rest of the luteolin aromatic protons were identified in the HSQC spectra. The aromatic protons H5' and H3 overlap with deoxyribose H1' protons, but their corresponding ¹³C resonances resonate at ~100-116 ppm (region for aromatic carbons), being well separated from that of deoxyribose H1' resonating at ~85-88 ppm (**Fig 5.13a, b**).

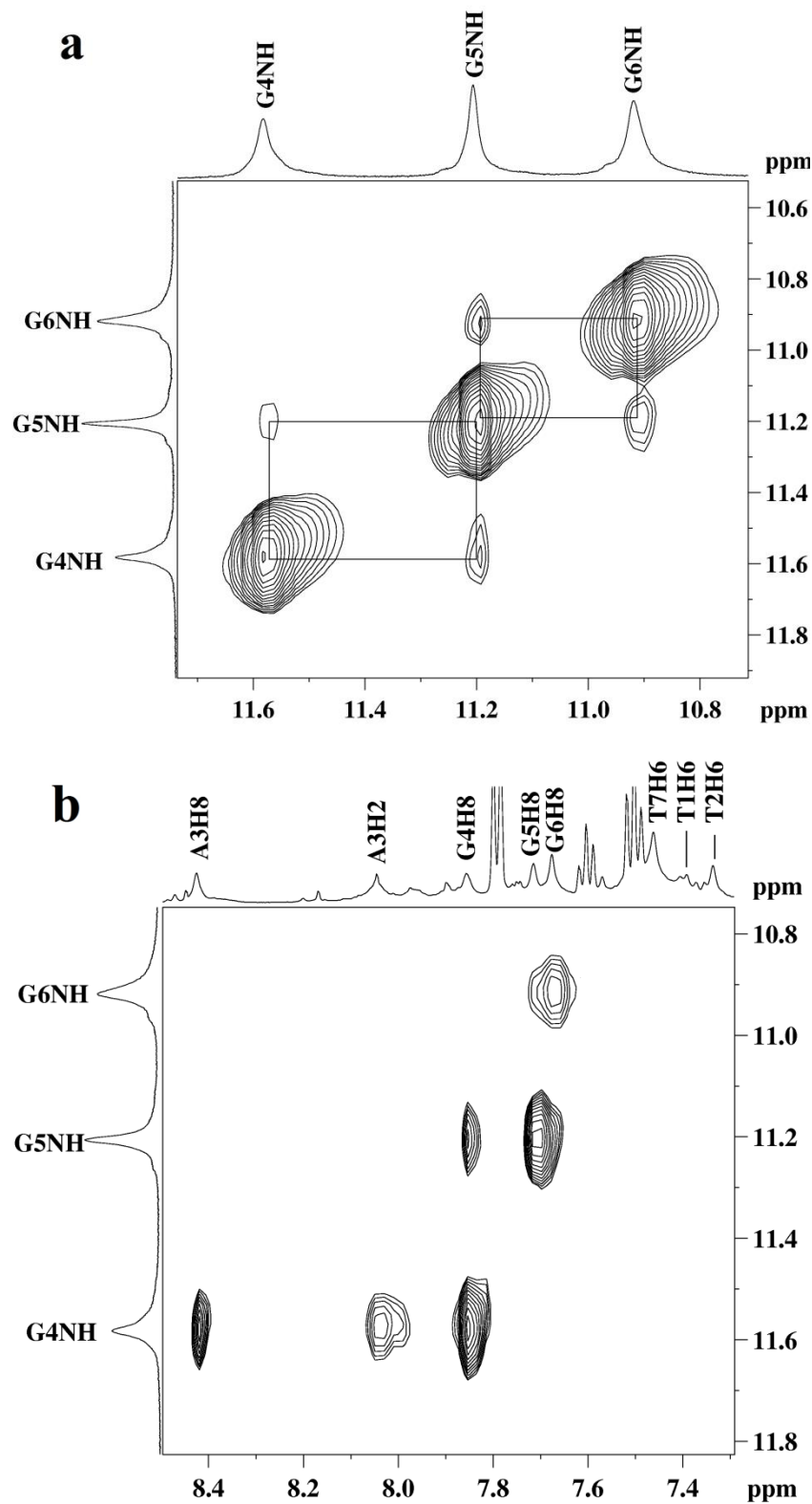


Fig. 5.10: Expansion of the NOESY spectra of luteolin-*d*-(TTAGGGT)₄ complex at 298 K, *D/N*=2.0 showing (a) NH-NH connectivity between adjacent imino protons. (b) Interstrand guanine NH connectivities to its own and 5' flanking base protons in A3-G4-G5-G6 segment.

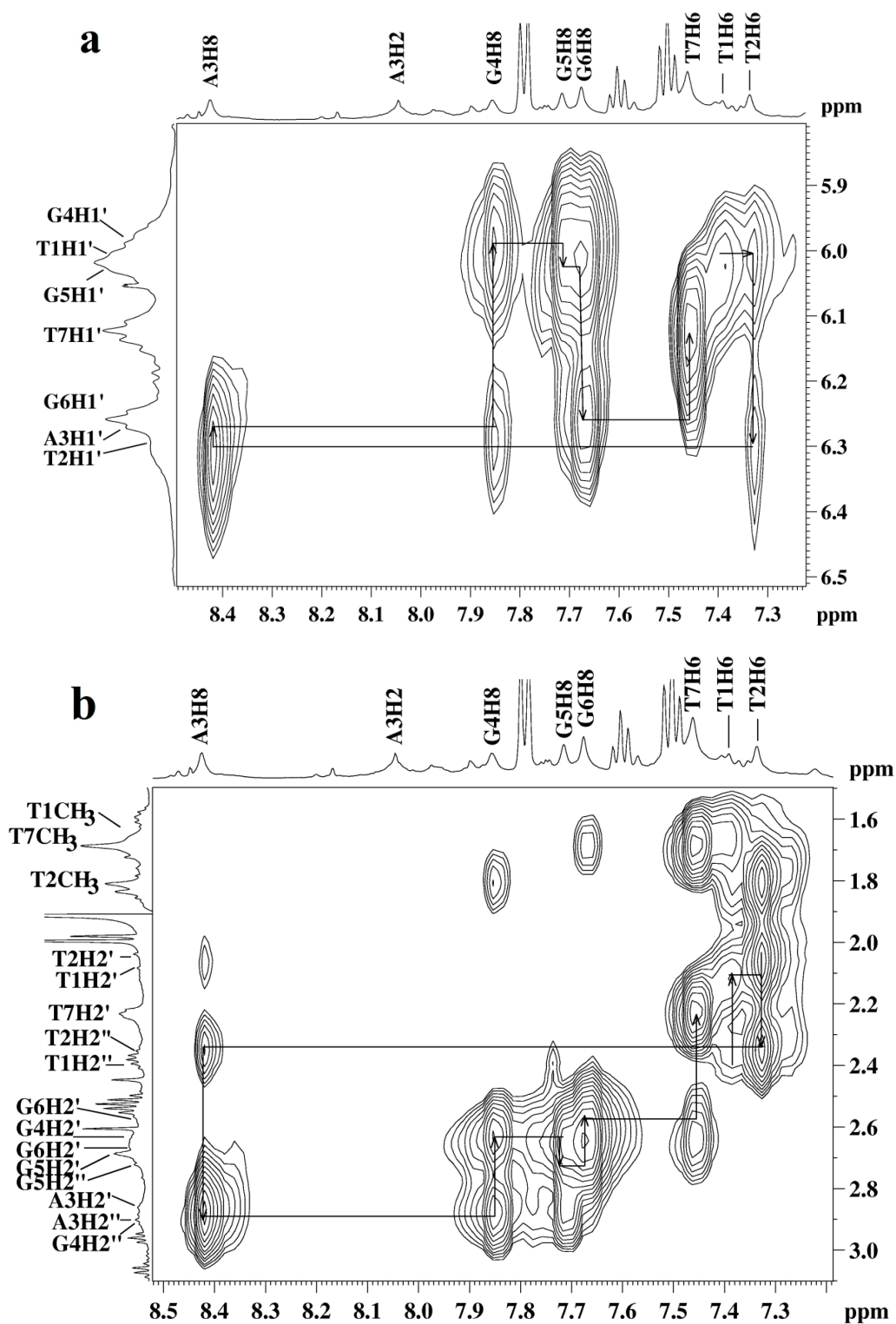


Fig. 5.11: Expansion of the NOESY spectra of luteolin-d-(TTAGGGT)₄ complex at 298 K, $D/N=2.0$ showing (a) intrastrand base H8/H6-H1' sequential connectivity. (b) Intrastrand base H8/H6-H2'H2'' sequential connectivity in T1-T2-A3-G4-G5-G6-T7 segment.

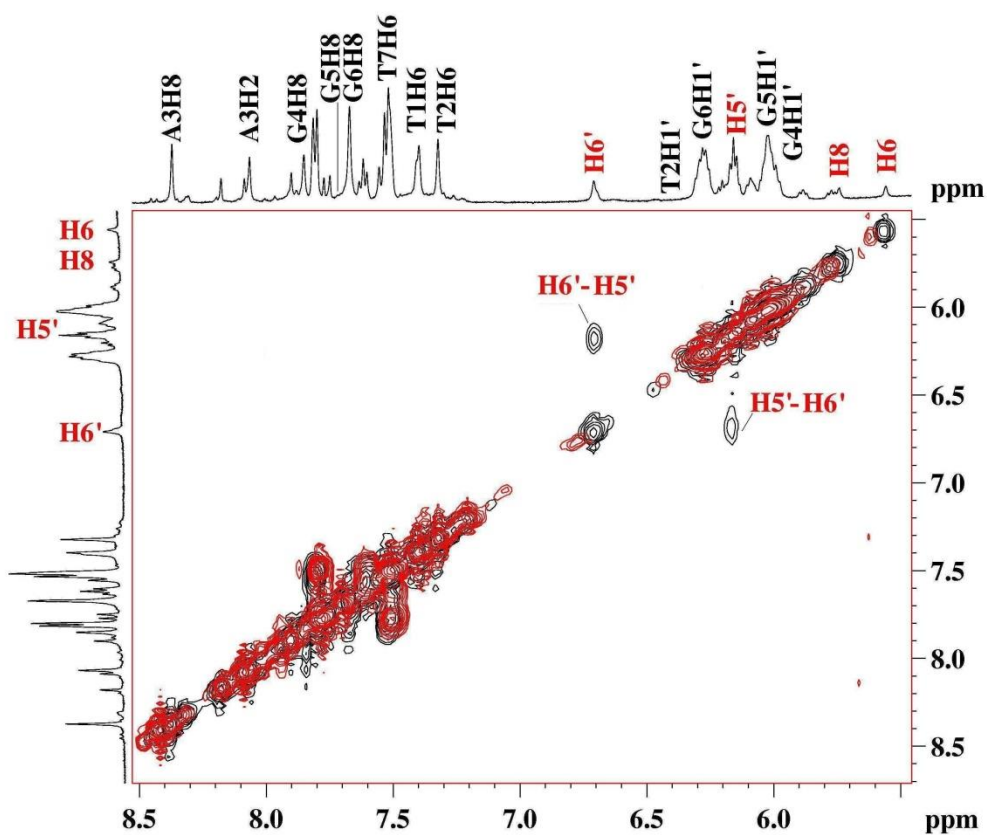
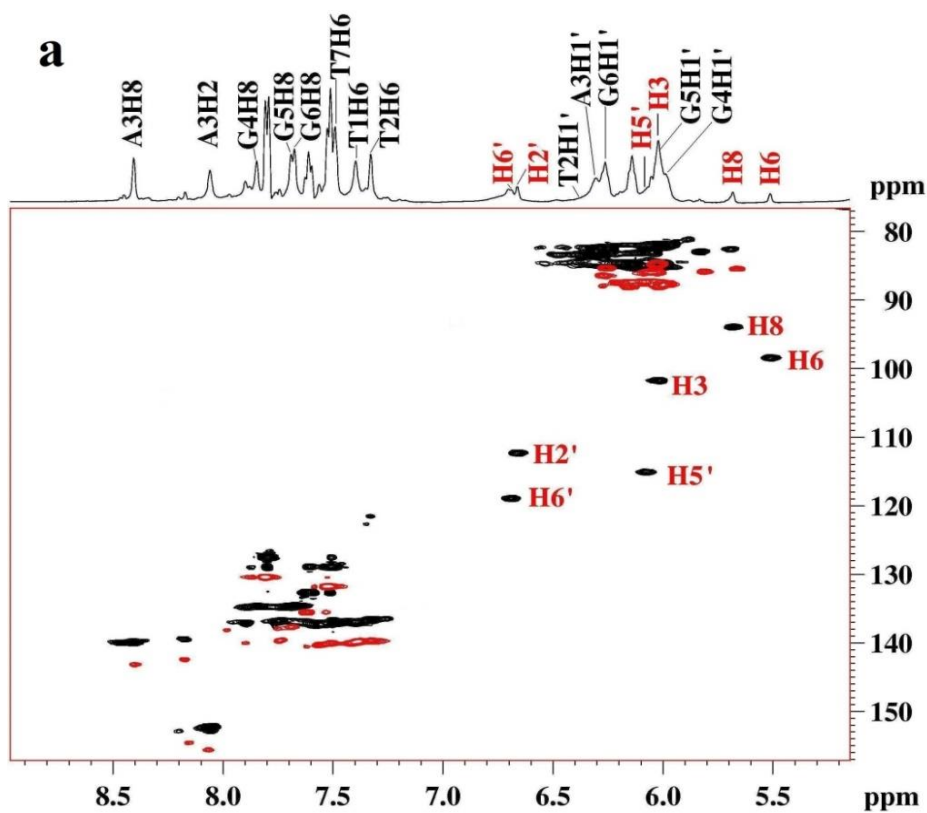


Fig. 5.12: *Overlap of the uncomplex (red) and luteolin-d-(TTAGGGT)₄ complex(black) ¹H-¹H COSY spectra at 308 K showing meta coupled protons H5' and H6' of luteolin.*



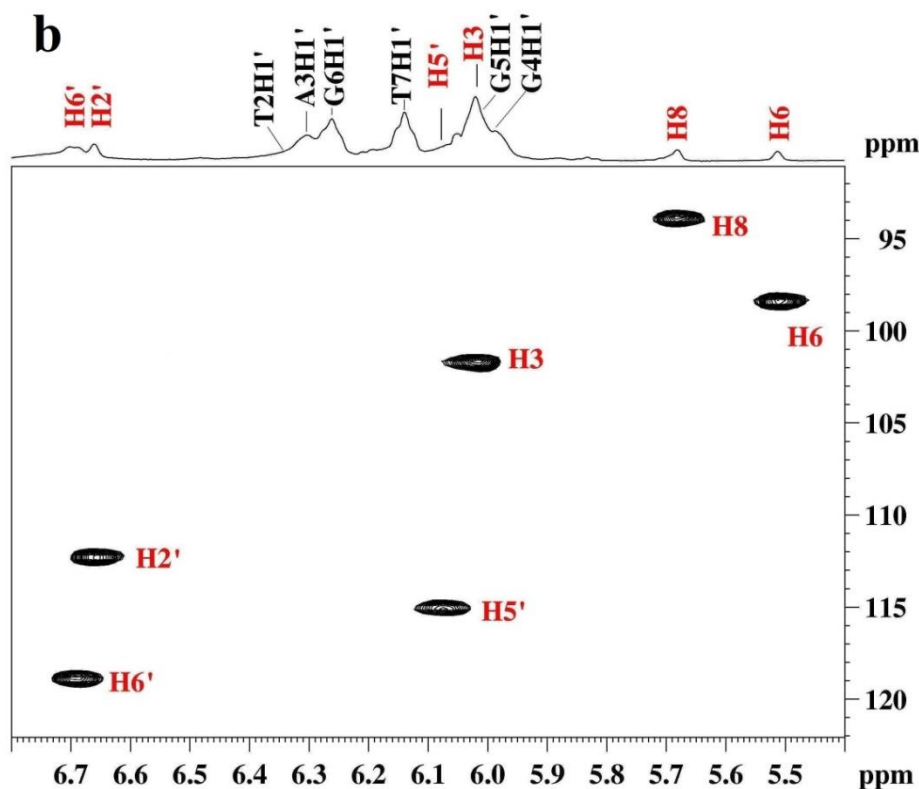


Fig. 5.13: Overlap of the uncomplex (red) and luteolin complexed $d\text{-(TTAGGGT)}_4$ (black) ^1H - ^{13}C HSQC spectra at 308 K showing (a) aromatic protons of luteolin. (b) expansion of luteolin protons.

5.1.4 Effects of titrimetric addition of luteolin

On addition of luteolin to $d\text{-(TTAGGGT)}_4$, new proton signals appeared in the aromatic region of the spectrum, which corresponds to luteolin. Intensity of these signals increases with increase in the D/N ratios. The quadruplex signals shifted progressively with D/N ratio, as more and more quadruplex binds to the luteolin. With increase in the luteolin concentration the intensity of T1H6, T1CH₃ signals decreased followed by significant broadening (**Fig. 5.14b**). Maximum upfield shift of 0.11 ppm was observed for G6NH (**Fig. 5.14a**) while the T7H6, T7CH₃ showed a downfield shift (**Table 5.5**). There were no significant shifts in rest of the quadruplex resonances. With further increase in the luteolin concentration, i.e., at D/N=2.0 there were significant shifts in the resonances of G4NH, T7H6 and T7CH₃ (**Fig. 5.14d**; **Table 5.6** and **Table 5.7**). The T7H6 signal becomes sharp. This shows that there may be probably two binding sites. At lower D/N ratio there is broadening in the T1pT2 while at higher D/N ratio there is more shift in the G6pT7 step.

Such kind of upfield shift were earlier reported for G-quadruplex ligands which stack to G-tetrads through π - π stacking interaction, which leads to the upfield shift in imino protons (Fedoroff *et al.*, 1998; Gavathiotis *et al.*, 2003; Mita *et al.*, 2006).

The intensity of luteolin protons H6, H8, H2', H6' grows gradually as D/N increases (**Fig. 5.14c**). There was no further noticeable shift at $D/N > 0.25$ (**Table 5.8**) and apparently the luteolin was completely bound at all D/N ratios. The upfield shifts in its protons are fairly large being 0.66-0.81 ppm (**Table 5.9**), which might be probably due to stacking of luteolin. None of the four OH protons were visible at any D/N ratio. This shows that the OH protons are in fast exchange on NMR time scale.

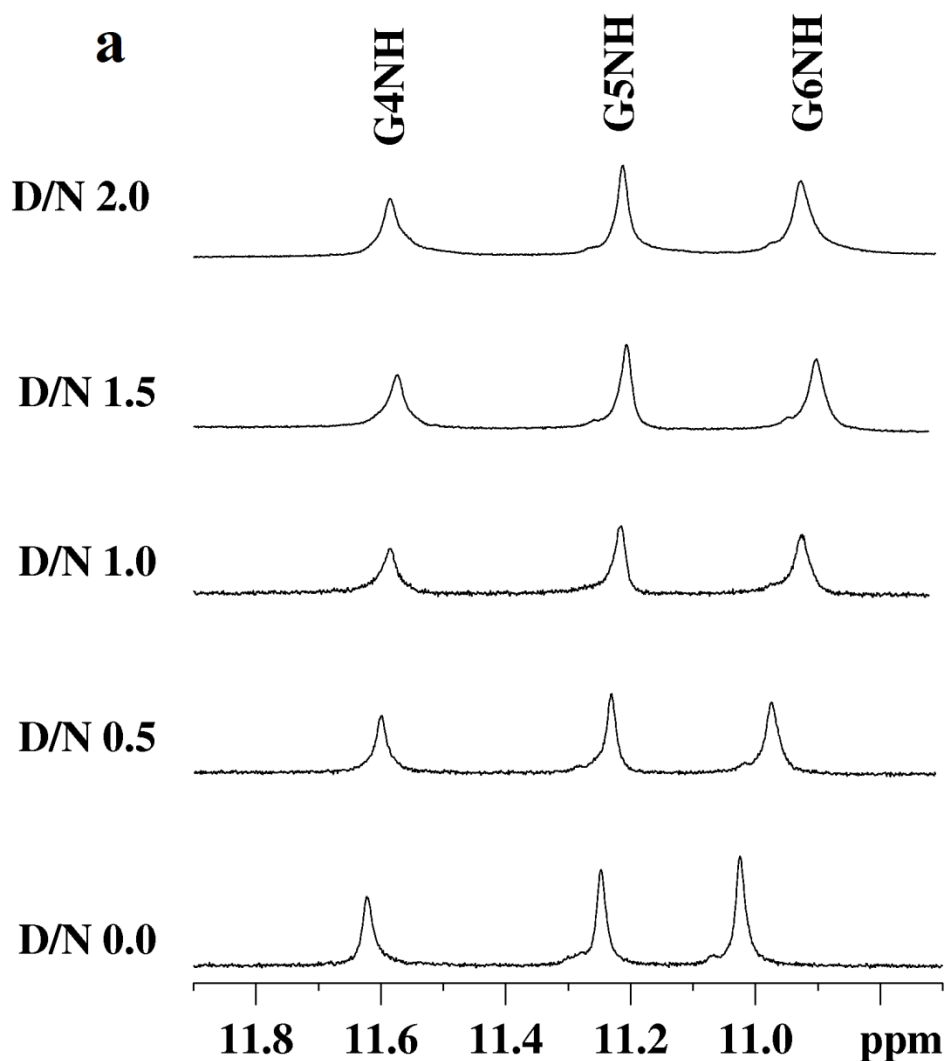


Fig. 5.14a: $1D$ 1H NMR spectra of luteolin- d -(TTAGGGT) $_4$ complex at 298 K showing change in the imino proton resonances of quadruplex upon titration.

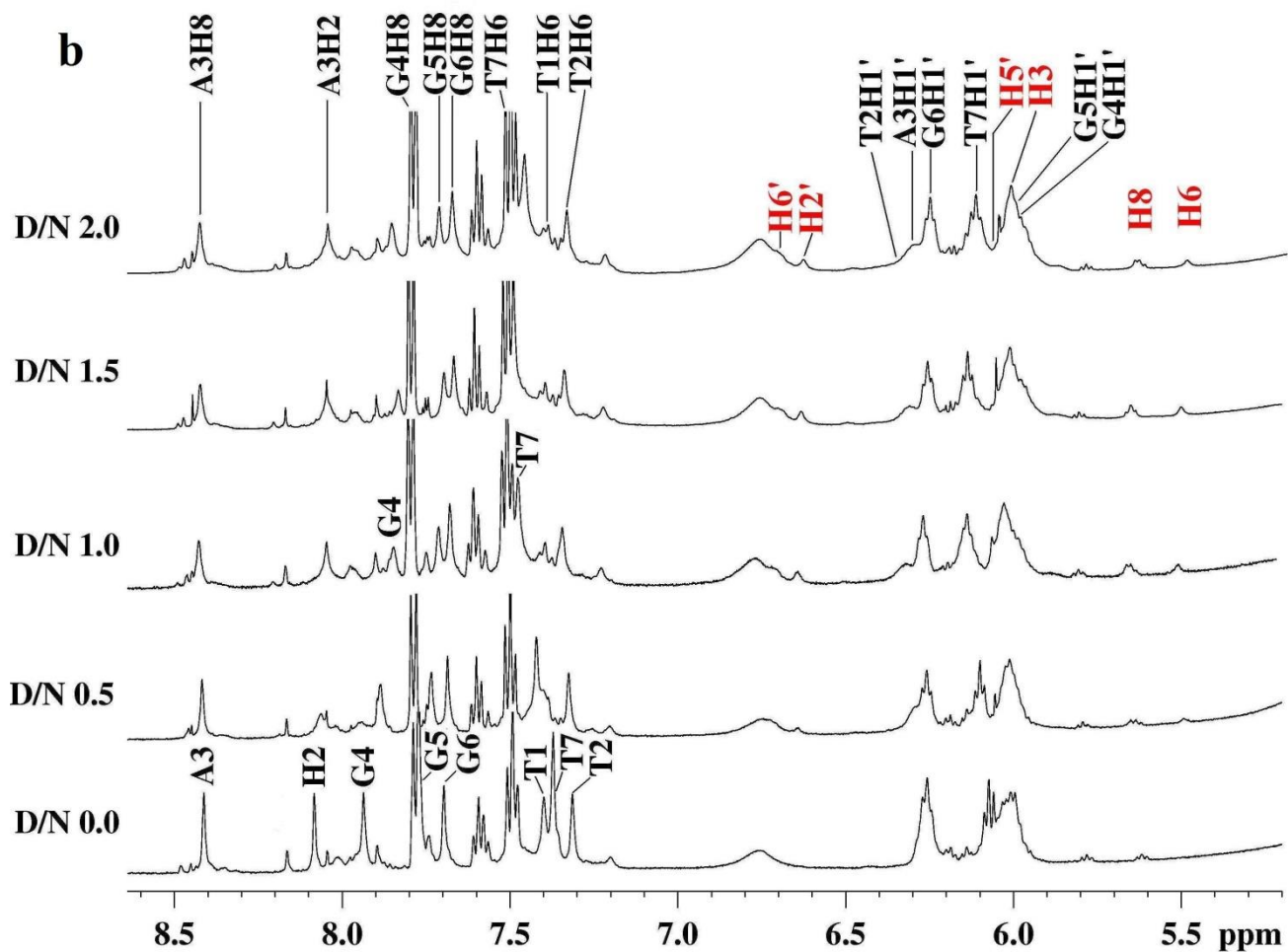


Fig. 5.14b: $1D$ 1H NMR spectra of luteolin- d -(TTAGGGT) $_4$ complex at 298 K showing change in the quadruplex and luteolin proton resonances upon titration.

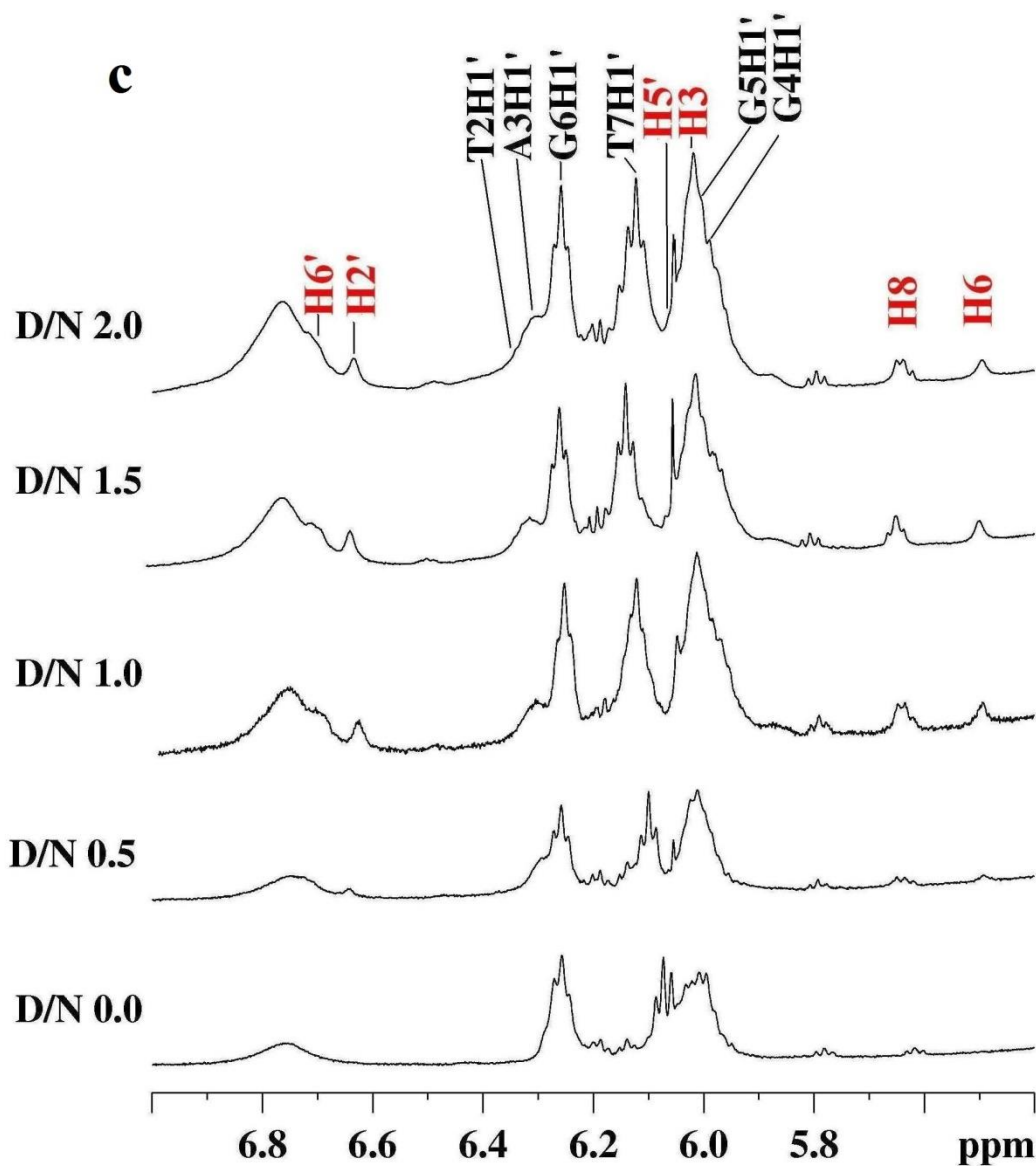


Fig. 5.14c: $1D$ 1H NMR spectra of luteolin-d-(TTAGGGT) $_4$ complex at 298 K showing change in the quadruplex and luteolin proton resonances upon titration.

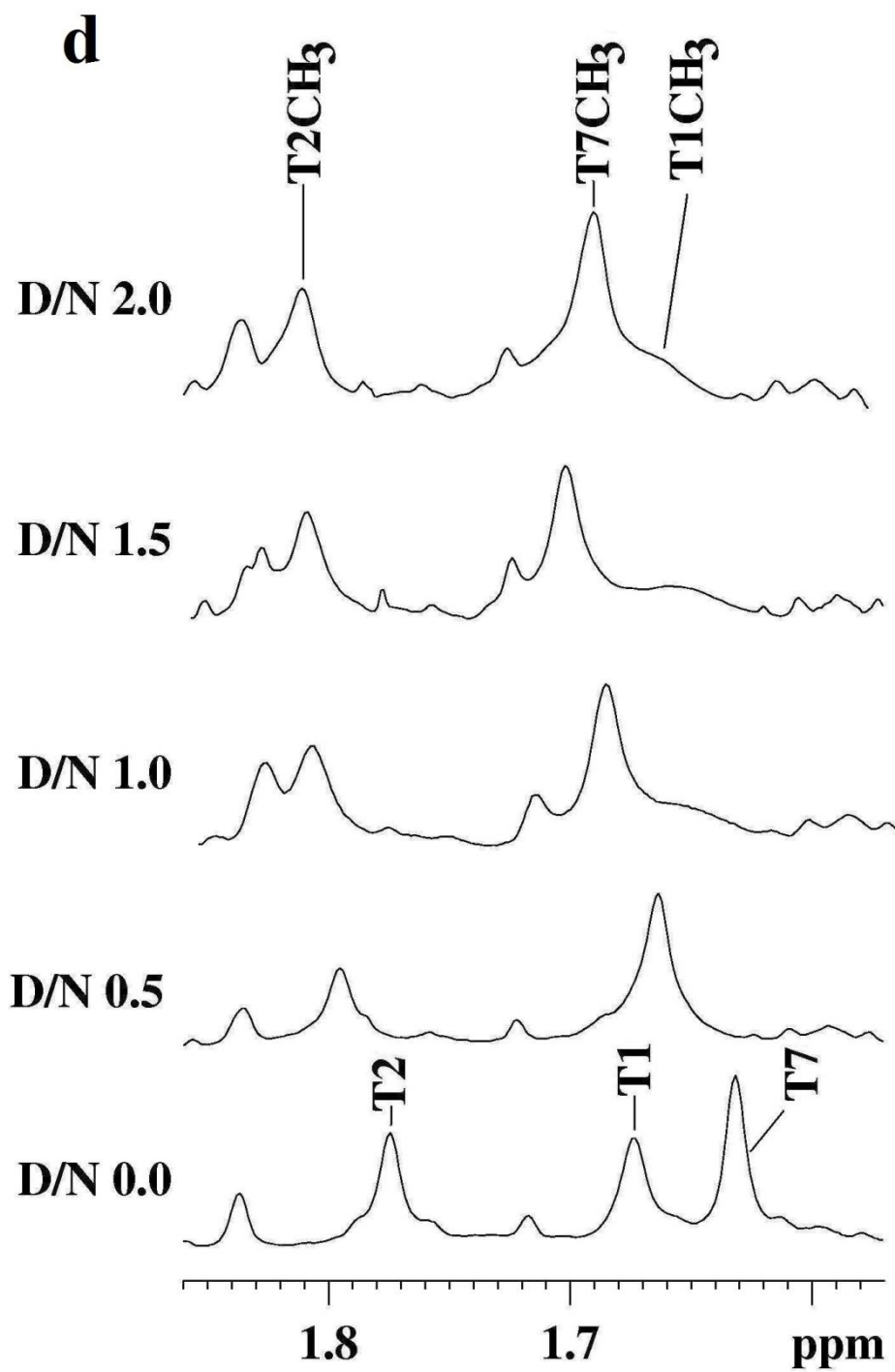


Fig. 5.14: $1D$ 1H NMR spectra of luteolin- d -(TTAGGGT) $_4$ complex at 298 K showing change in the methyl proton resonances of quadruplex upon titration.

Protons	T1			T2			A3			G4		
	δ_b	δ_f	$\Delta\delta$	δ_b	δ_f	$\Delta\delta$	δ_b	δ_f	$\Delta\delta$	δ_b	δ_f	$\Delta\delta$
H8/H6	7.39	7.39	0.00	7.33	7.31	0.02	8.42	8.41	0.01	7.84	7.93	-0.07
H1'	6.01	5.99	0.02	6.30	6.24	0.06	6.29	6.27	0.02	5.98	6.02	-0.04
H2'	2.12	2.09	0.03	2.06	2.06	0.00	2.86	2.86	0.00	2.63	2.66	-0.03
H2''	2.36	2.34	0.02	2.34	2.34	0.00	2.90	2.90	0.00	2.91	2.91	0.00
H3'	4.66	4.64	0.02	4.78			5.09	5.10	-0.01	5.04	5.06	-0.02
H4'		4.00	-	4.05	4.06	-0.01	4.43	4.43	0.00	4.45	4.47	-0.02
H5'	3.64	3.65	-0.01	3.96	3.93	0.03	4.14	4.14	0.00	4.24	4.25	0.01
H5''	3.64	3.65	-0.01	3.96	3.93	0.03	4.08	4.06	0.02	4.24	4.25	0.01
H2/CH₃	1.66	1.67	-0.01	1.80	1.77	0.03	8.04	8.08	-0.04			
NH₂^b												
NH₂^{nb}												
NH										11.58	11.62	-0.04
	G5			G6			T7					
	δ_b	δ_f	$\Delta\delta$	δ_b	δ_f	$\Delta\delta$	δ_b	δ_f	$\Delta\delta$			
H8/H6	7.71	7.77	-0.06	7.67	7.69	-0.02	7.46	7.37	0.09			
H1'	6.03	6.03	0.00	6.25	6.25	0.00	6.11	6.07	0.04			
H2'	2.68	2.68	0.00	2.57	2.55	0.02		2.18	-			
H2''	2.72	2.72	0.00	2.66	2.67	-0.01	2.22	2.21	0.01			
H3'	5.01	5.03	-0.02	4.94	4.91	0.03	4.49	4.49	0.00			
H4'	4.47	4.49	-0.02	4.51	4.50	0.01	4.19	4.20	-0.01			
H5'	4.29	4.30	0.01	4.25	4.25	0.00	4.09	4.06	0.03			
H5''	4.29	4.30	0.01	4.25	4.25	0.00	4.09	4.06	0.03			
H2/CH₃							1.68	1.63	0.05			
NH₂^b												
NH₂^{nb}												
NH	11.20	11.24	-0.04	10.91	11.02	-0.11						

Table 5.5: Chemical shift (ppm) of *d*-(TTAGGGT)₄ protons in uncomplexed state (δ_f) and that bound to luteolin (δ_b) at $D/N=1.0$ at 298 K along with the change in chemical shift on binding, that is. $\Delta\delta=\delta_b(D/N=1.0)-\delta_f(D/N=0.0)$.

D/N ratios	G4NH	G5NH	G6NH	T1CH3	T2CH3	T7CH3	A3H2
0.00	11.62	11.24	11.02	1.67	1.77	1.63	8.08
0.25	11.61	11.23	11.00	1.67	1.78	1.64	8.07
0.50	11.59	11.22	10.96	1.67	1.79	1.66	8.06
0.75	11.59	11.21	10.94	1.66	1.80	1.67	8.04
1.0	11.58	11.20	10.91	1.66	1.81	1.68	8.04
1.25	11.58	11.20	10.93	1.65	1.80	1.67	8.04
1.50	11.57	11.19	10.88	1.65	1.81	1.70	8.04
1.75	11.56	11.18	10.86	1.65	1.81	1.71	8.04
2.0	11.56	11.18	10.85	1.65	1.81	1.72	8.04
$\Delta\delta=(\delta_b-\delta_f)$	-0.06	-0.06	-0.17	-0.02	0.04	0.09	-0.04

D/N ratios	T1H6	T2H6	A3H8	G4H8	G5H8	G6H8	T7H6
0.00	7.39	7.31	8.41	7.93	7.77	7.69	7.37
0.25	7.38	7.32	8.41	7.89	7.74	7.69	7.39
0.50	7.38	7.32	8.41	7.89	7.73	7.68	7.42
0.75	7.38	7.33	8.42	7.87	7.72	7.68	7.43
1.0	7.39	7.33	8.42	7.84	7.71	7.67	7.46
1.25	7.39	7.33	8.42	7.84	7.71	7.67	7.47
1.50	7.39	7.33	8.42	7.83	7.69	7.66	7.47
1.75	7.39	7.34	8.42	7.82	7.68	7.66	7.51
2.0	7.40	7.34	8.42	7.81	7.67	7.65	7.51
$\Delta\delta=(\delta_b-\delta_f)$	0.01	0.03	0.01	-0.12	-0.10	-0.04	0.14

Table 5.6: Chemical shift (ppm) of *d*-(TTAGGGT)₄ protons as a function D/N ratios at 298 K along with the change in chemical shift on binding, that is, $\Delta\delta = \delta(D/N=2.0) - \delta(D/N=0.0)$.

Protons	T1			T2			A3			G4		
	δ_b	δ_f	$\Delta\delta$	δ_b	δ_f	$\Delta\delta$	δ_b	δ_f	$\Delta\delta$	δ_b	δ_f	$\Delta\delta$
H8/H6	7.40	7.39	0.01	7.34	7.31	0.03	8.42	8.41	0.01	7.81	7.93	-0.12
H1'	6.01	5.99	0.02	6.33	6.24	0.09	6.31	6.27	0.04	5.98	6.02	-0.04
H2'	2.12	2.09	0.03	2.07	2.06	0.01	2.85	2.86	-0.01	2.63	2.66	-0.03
H2''	2.39	2.34	0.05	2.36	2.34	0.02	2.91	2.90	0.01	2.92	2.91	0.01
H3'		4.64					5.10	5.10	0.00	5.05	5.06	-0.01
H4'	3.98	4.00	-0.02	4.07	4.06	0.01	4.45	4.43	0.02	4.42	4.47	-0.05
H5'	3.67	3.65	0.02	3.99	3.93	0.06	4.16	4.14	0.02	4.24	4.25	-0.01
H5''	3.67	3.65	0.02	3.99	3.93	0.06	4.10	4.06	0.04	4.24	4.25	-0.01
H2/CH₃	1.65	1.67	-0.02	1.81	1.77	0.04	8.04	8.08	-0.04			
NH₂^b												
NH₂^{nb}												
NH										11.56	11.62	-0.06
	G5			G6			T7					
	δ_b	δ_f	$\Delta\delta$	δ_b	δ_f	$\Delta\delta$	δ_b	δ_f	$\Delta\delta$			
H8/H6	7.67	7.77	-0.10	7.65	7.69	-0.04	7.51	7.37	0.14			
H1'	6.00	6.03	-0.03	6.25	6.25	0.00	6.15	6.07	0.08			
H2'	2.68	2.68	0.02	2.55	2.55	0.00		2.18				
H2''	2.71	2.72	-0.01	2.64	2.67	-0.03	2.26	2.21	0.05			
H3'	5.02	5.03	-0.01	4.99	4.91	0.08	4.53	4.49	0.04			
H4'	4.46	4.49	-0.03	4.48	4.50	-0.02	4.20	4.20	0.00			
H5'	4.29	4.30	-0.01	4.25	4.25	0.00	4.12	4.06	0.06			
H5''	4.29	4.30	-0.01	4.25	4.25	0.00	4.12	4.06	0.06			
H2/CH₃								1.63	0.08			
NH₂^b												
NH₂^{nb}												
NH	11.18	11.24	-0.06	10.85	11.02	-0.17						

Table 5.7: Chemical shift (ppm) of *d*-(TTAGGGT)₄ protons in uncomplexed state (δ_f) and that bound to luteolin (δ_b) at *D/N*=2.0 at 298 K along with the change in chemical shift on binding, that is. $\Delta\delta = \delta_b (D/N=1.0) - \delta_f (D/N=0.0)$.

298	H6'	H2'	H5'	H3	H8	H6
Luteolin	7.40	7.38	6.88	6.67	6.44	6.18
D/N 0.25	6.70	6.64	6.06	6.01	5.63	5.49
D/N 0.50	6.70	6.64	6.06	6.01	5.63	5.49
D/N 0.75	6.70	6.63	6.06	6.01	5.63	5.49
D/N 1.0	6.70	6.63	6.06	6.01	5.63	5.49
D/N 1.25	6.70	6.63	6.06	6.01	5.63	5.49
D/N 1.50	6.69	6.63	6.06	6.01	5.65	5.50
D/N 1.75	6.69	6.63	6.06	6.00	5.65	5.50
D/N 2.0	6.69	6.63	6.06	6.00	5.65	5.51
$\Delta\delta$	-0.71	-0.75	-0.82	-0.67	-0.79	-0.67

Table 5.8: Chemical shift (ppm) of luteolin protons as a function of D/N ratios at 298 K along with the change in chemical shift on binding, that is, $\Delta\delta = \delta(D/N=2.0) - \delta(D/N=0.0)$.

Luteolin Protons	δ_f	δ_b D/N = 1.0	δ_b D/N = 2.0	$\Delta\delta$ D/N = 1.0 ($\Delta\delta = \delta_b - \delta_f$)	$\Delta\delta$ D/N = 2.0 ($\Delta\delta = \delta_b - \delta_f$)
H3	6.67	6.01	6.00	-0.66	-0.67
H6	6.18	5.49	5.51	-0.69	-0.67
H8	6.44	5.63	5.65	-0.81	-0.79
H2'	7.38	6.63	6.63	-0.75	-0.75
H5'	6.88	6.06	6.06	-0.82	-0.82
H6'	7.40	6.70	6.69	-0.70	-0.71

Table 5.9: Chemical shift (ppm) of luteolin protons from NOESY spectra of free luteolin (δ_f) and luteolin-d-(TTAGGGT)₄ complex (δ_b) at D/N=1.0, 2.0 at 298 K.

5.1.5 Temperature dependent studies revealing the stability of luteolin-d-(TTAGGGT)₄ complex

The NMR spectra were recorded as a function of temperature (**Fig. 5.15**). Both the quadruplex and luteolin resonances were sharp and well-resolved at higher temperature. With increase in the temperature G4NH, G6NH shifted further upfield from their position in bound state (**Fig. 5.16**) and that of T7H6, T7CH₃ shifted downfield (**Table 5.10**). The trend was same at D/N 2.0. The luteolin proton H6' was more prominent at higher temperature and there was gradual downfield shift in all the luteolin protons (**Table 5.11**). There were no abrupt shifts indicating that the complex is fairly stable and quadruplex is in bound state even at 353 K. This was also evident from GNH protons which persist at higher temperature > 318 K (**Fig. 5.16**). Presence of guanine imino signals resonating between 10.0-11.5 ppm is indicative of the formation of G-quadruplex structure.

Their intensity decreases with temperature and they eventually disappear at higher temperature due to disruption of hydrogen bonds holding the G-quartet structure. It was observed that G4NH and G6NH disappeared at 353 K while G5NH disappeared at 358 K (**Fig. 5.16**). On the other hand, the melting profiles of uncomplexed quadruplex (**Fig. 5.16**) that the G4NH, G6NH and G5NH signals disappear at 328 and 333 K, respectively. These findings clearly indicate stabilization by about 25 K. The result was similar to that observed in the case of binding of MTX to d-(TTAGGGT)₄. This probably indicates that the mode is probably similar in case of both the ligands. These results were consistent to that reported in literature for the ligands, which stack at the end of G-quadruplex structure (Gavathiotis *et al.*, 2003; Mazzini *et al.*, 2013).

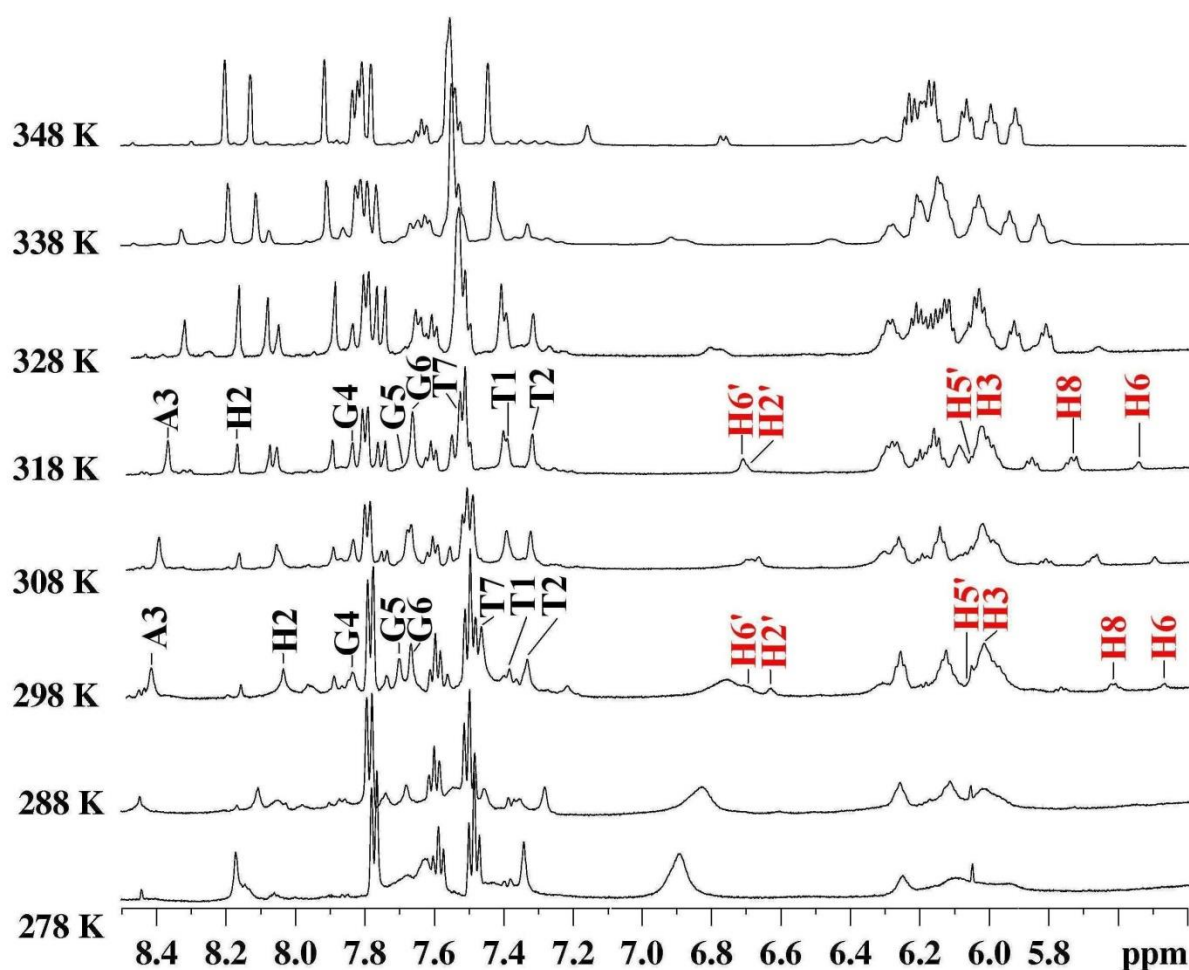


Fig. 5.15: 1D ¹H NMR spectra of luteolin-d-(TTAGGGT)₄ complex as a function of temperature at D/N=2.0 showing change in the quadruplex and luteolin proton resonances.

Temp. (K)	T1H6	T2H6	A3H8	G4H8	G5H8	G6H8	T7H6	G4NH	G5NH	G6NH
278	7.39	7.36	8.44	7.84	7.72	7.67	7.45	11.61	11.21	10.97
283	7.38	7.35	8.44	7.84	7.72	7.67	7.45	11.62	11.21	10.96
288	7.38	7.35	8.44	7.84	7.72	7.67	7.45	11.61	11.21	10.94
293	7.38	7.34	8.44	7.84	7.72	7.67	7.45	11.59	11.20	10.92
298	7.39	7.33	8.42	7.84	7.71	7.67	7.46	11.57	11.20	10.90
303	7.39	7.33	8.41	7.84	7.69	7.67	7.48	11.56	11.20	10.89
308	7.39	7.32	8.40	7.84	7.68	7.67	7.49	11.55	11.20	10.87
313	7.39	7.32	8.39	7.84	7.68	7.67	7.51	11.53	11.19	10.85
318	7.39	7.32	8.37	7.84	7.68	7.67	7.51	11.52	11.19	10.83
323	7.39	7.32	8.36	7.84	7.68	7.66	7.52	11.51	11.19	10.82
328	7.40	7.32	8.34	7.85	7.68	7.66	7.52	11.49	11.18	10.80
333	7.40	7.32	8.34	7.85	7.68	7.66	7.52	11.49	11.18	10.80
338	7.40	7.32	8.32	7.86	7.68	7.66	7.52	11.47	11.18	10.78
343	7.41	7.33	8.30	7.86	7.68	7.66	7.52	11.46	11.18	10.77
348	7.41	7.33	8.29	7.86	7.68	7.66	7.52	11.44	11.18	10.76
353	7.41	7.34	8.28	7.86	7.68	7.66	7.52		11.18	
$\Delta \delta$	0.02	-0.02	-0.16	0.02	-0.04	-0.01	0.07	-0.17	-0.03	-0.21

Temp.(K)	T1CH ₃	T2CH ₃	T7CH ₃
278	1.63	1.81	1.64
283	1.63	1.81	1.64
288	1.63	1.81	1.65
293	1.65	1.81	1.67
298	1.66	1.81	1.68
303	1.66	1.81	1.71
308	1.67	1.80	1.72
313	1.67	1.80	1.74
318	1.68	1.79	1.75
323	1.69	1.78	1.76
328	1.69	1.79	1.77
333	1.70	1.80	1.77
338	1.71	1.80	1.78
343	1.72	1.80	1.78
348	1.72	1.81	1.79
353	1.73	1.81	1.79
$\Delta \delta$	0.10	0.00	0.15

Table 5.10: Chemical shift (ppm) of *d*-(TTAGGGT)₄ protons in luteolin-*d*-(TTAGGGT)₄ complex at *D/N*=1.0 as a function of temperature along with the net change in chemical shift with temperature, that is, $\Delta\delta = \delta(353\text{ K}) - \delta(278\text{ K})$.

Temp.(K)	H6'	H2'	H5'	H3	H8	H6
278						
283						
288	6.71	6.60				
293	6.71	6.62	6.06	6.01	5.60	5.48
298	6.70	6.63	6.06	6.01	5.63	5.49
303	6.69	6.64	6.06	6.02	5.67	5.50
308	6.69	6.66	6.07	6.02	5.69	5.52
313	6.68	6.68	6.07	6.02	5.72	5.54
318	6.71	6.70	6.07	6.02	5.76	5.57
323	6.75	6.72	6.09	6.03	5.79	5.61
328	6.80	6.77	6.11	6.03	5.82	5.67
333	6.82	6.78	6.12	6.03	5.83	5.69
338	6.91	6.87	6.14	6.03	5.85	5.79
343	7.03	6.99	6.14	6.03	5.88	
348	7.14		6.14	6.03	5.89	
353	7.23		6.14	6.04	5.91	
$\Delta \delta$	0.52	0.39	0.08	0.03	0.31	0.31

Table 5.11: Chemical shift (ppm) of luteolin protons in luteolin-d-(TTAGGGT)₄ complex at D/N=1.0 as a function of temperature along with the net change in chemical shift with temperature, that is, $\Delta\delta = \delta(353\text{ K}) - \delta(288\text{ K})$.

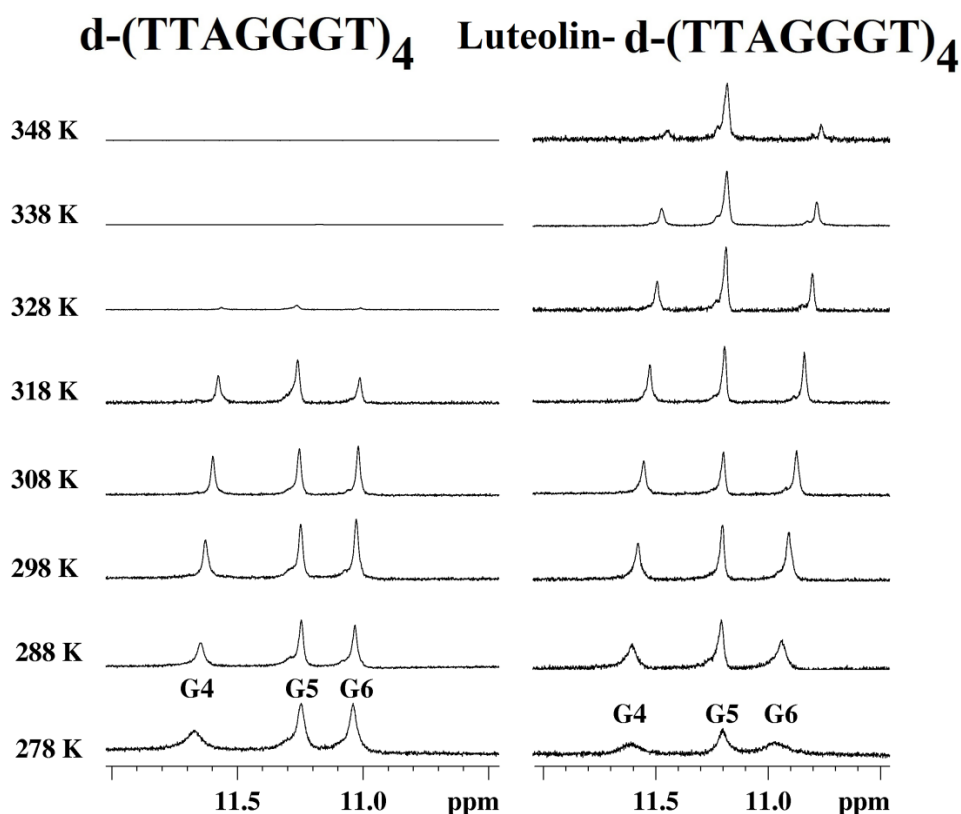


Fig. 5.16: 1D ¹H NMR spectra of imino protons region of d-(TTAGGGT)₄ and luteolin-d-(TTAGGGT)₄ complex revealing the stability of complex with temperature.

5.1.6 Phosphorous-31 NMR studies of luteolin-d-(TTAGGGT)₄ complex

The phosphorus-31 NMR spectra of unbound and bound d-(TTAGGGT)₄ were recorded at different temperature (278-328 K) during the course of titrations with luteolin (**Figs. 5.17a, b**). The phosphorus signals were assigned using standard strategies by ¹H-³¹P HMBC spectra, that is, T1pT2 shows ³J coupling with T1H3', T2H5'/5" and ⁴J coupling with T2H4' and so on for other ³¹P signals. On progressive addition of luteolin, the ³¹P NMR signals showed minor sequence dependent shifts (**Table 5.12**). The A3pG4 signal does not drift at all while rest of the ³¹P signals shifted downfield. The luteolin-d-(TTAGGGT)₄ complex also showed a maximum downfield shift (0.12 ppm) in T1pT2 step similar to that observed for MTX-d-(TTAGGGT)₄ complex. This result also confirmed that the binding of MTX and luteolin with this sequence is somewhat similar. It can be justified because both the ligands are having planar aromatic rings, which help in their stacking to G-quadruplex structure. Further increase in the luteolin concentration also caused a gradual downfield shift similar to that observed at D/N=1.0. At higher temperature (**Fig. 5.18**) the resonances cannot be assigned due to the presence of some extra signals apart from the six original ones. This might be either due to the presence of some single strand resonance which is more prominent at higher temperature or due to the flexibility of TTA bases.

We have not observed any cross peaks due to exchange between the bound and free phosphate resonances in the 2D ³¹P NMR exchange spectrum of luteolin-d-(TTAGGGT)₄ complex and a single set of resonances were present. This clearly shows that ³¹P signals from the bound quadruplex were in fast exchange with the corresponding signals from free quadruplex on the NMR time scale.

Small upfield shifts are generally caused by electrostatic interactions between drug and duplex DNA (Patel, 1979; Wilson and Jones, 1982) while minor upfield/downfield shifts are expected on widening/narrowing of O-P-O ester bond angle (Gorenstein and Kar, 1975; Gorenstein, 1984). The observed shifts rule out opening of base pairs to permit intercalation of luteolin chromophore which is expected to result in large downfield shifts ~ 1.6-2.6 ppm (Gorenstein 1992; Patel and Canuel, 1976). To the best of my knowledge till date, there is no literature available for changes in ³¹P resonance positions upon the interaction of ligands with quadruplex DNA.

	D/N = 0	D/N = 1.0	$\Delta\delta$ D/N 1.0	D/N = 2.0	$\Delta\delta$ D/N 2.0
T1pT2	-0.66	-0.54	0.12	-0.41	0.25
T2pA3	-0.69	-0.64	0.05	-0.48	0.21
A3pG4	-0.37	-0.37	0.00	-0.35	0.02
G4pG5	-0.73	-0.69	0.04	-0.58	0.15
G5pG6	-0.66	-0.60	0.06	-0.47	0.19
G6pT7	-0.69	-0.66	0.06	-0.52	0.17

Table 5.12: Chemical shift of ^{31}P resonances of the phosphate groups of $d\text{-(TTAGGGT)}_4$, in luteolin- $d\text{-(TTAGGGT)}_4$ complex at 298 K with increasing D/N ratios.

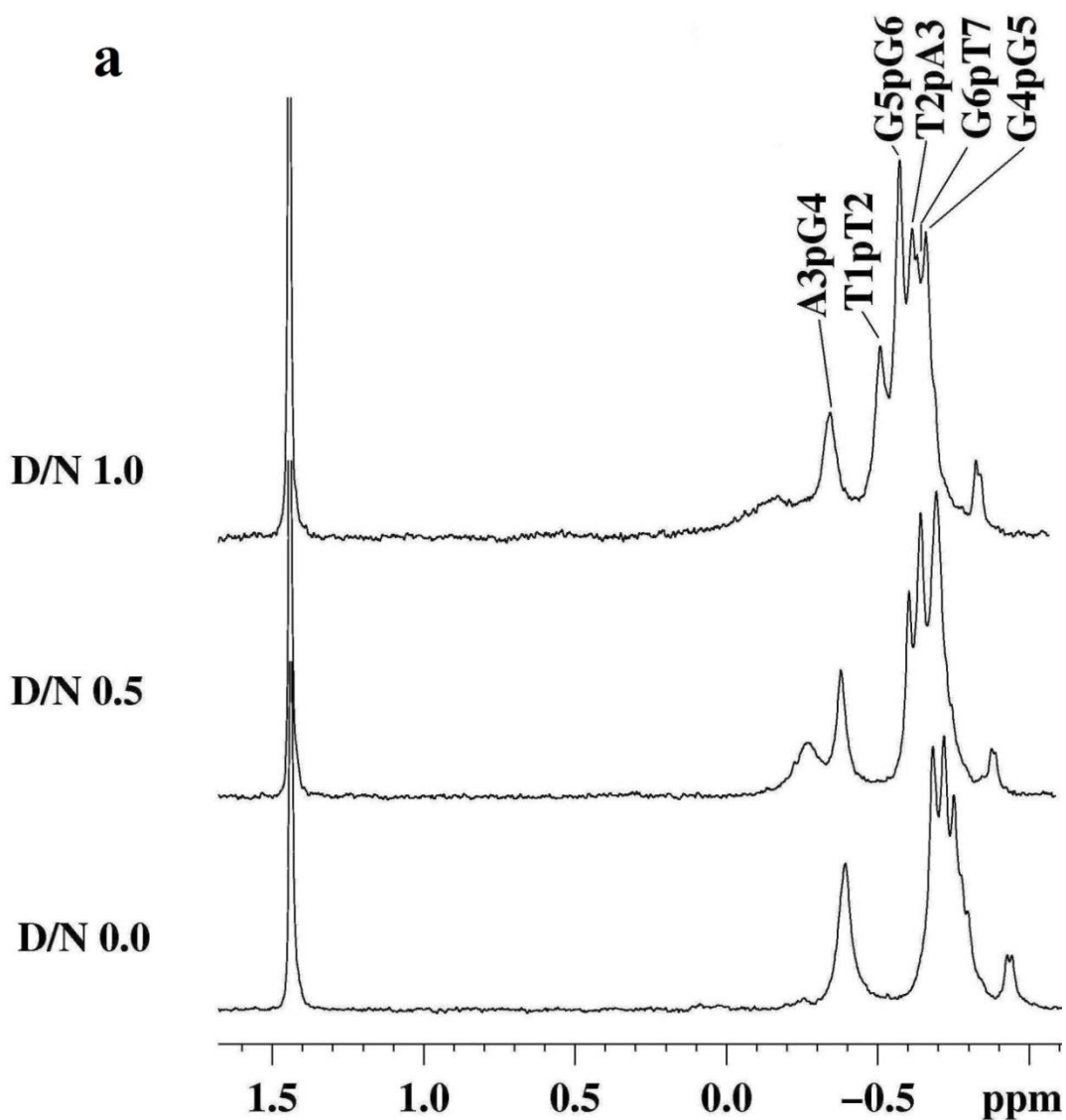


Fig. 5.17a: Proton decoupled ^{31}P NMR spectra of $d\text{-(TTAGGGT)}_4$ in uncomplexed state and complexed with luteolin with increasing D/N ratios at 298 K.

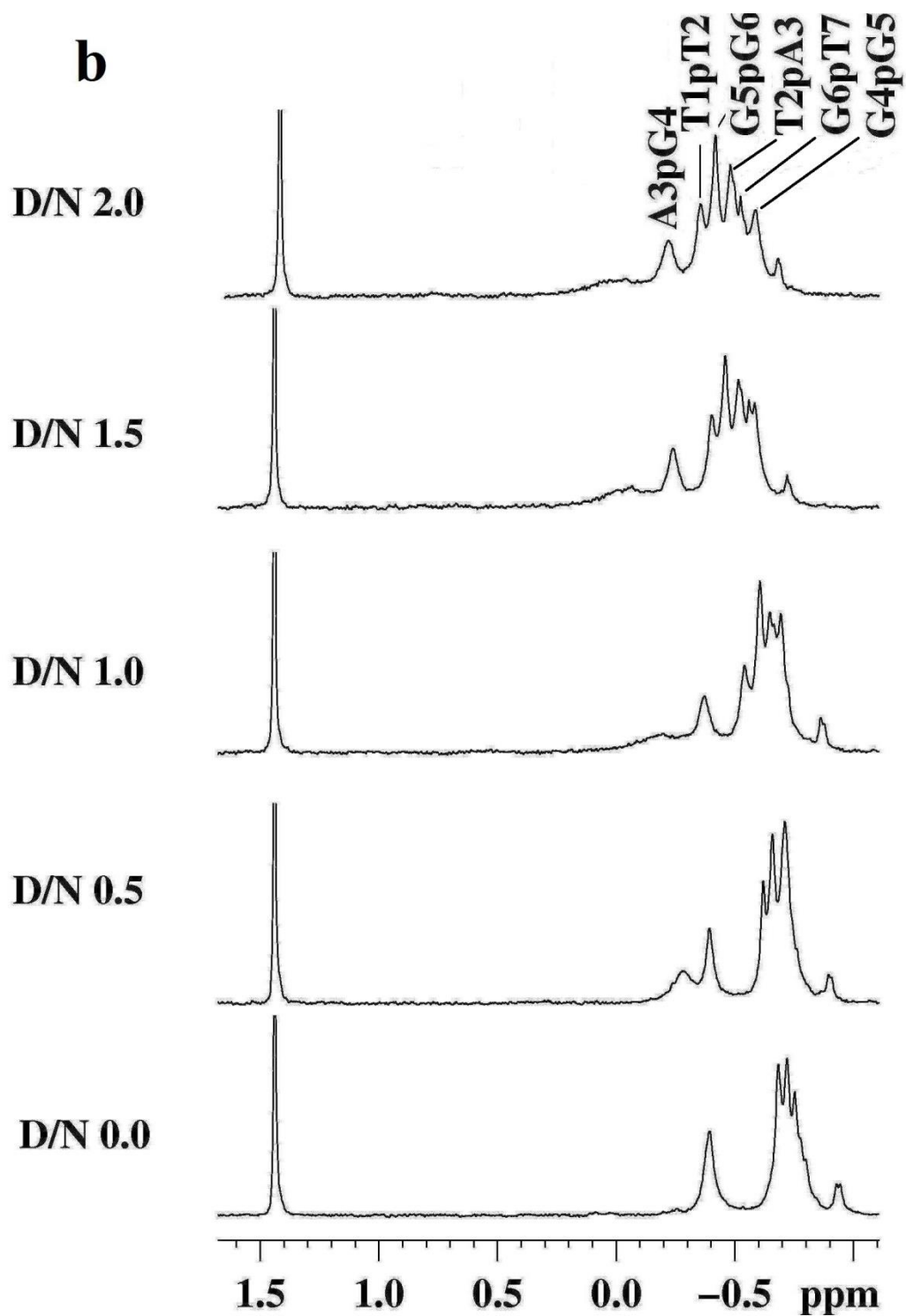


Fig. 5.17b: Proton decoupled ^{31}P NMR spectra of $d\text{-(TTAGGGT)}_4$ in uncomplexed state and complexed with luteolin with increasing D/N ratios at 298 K.

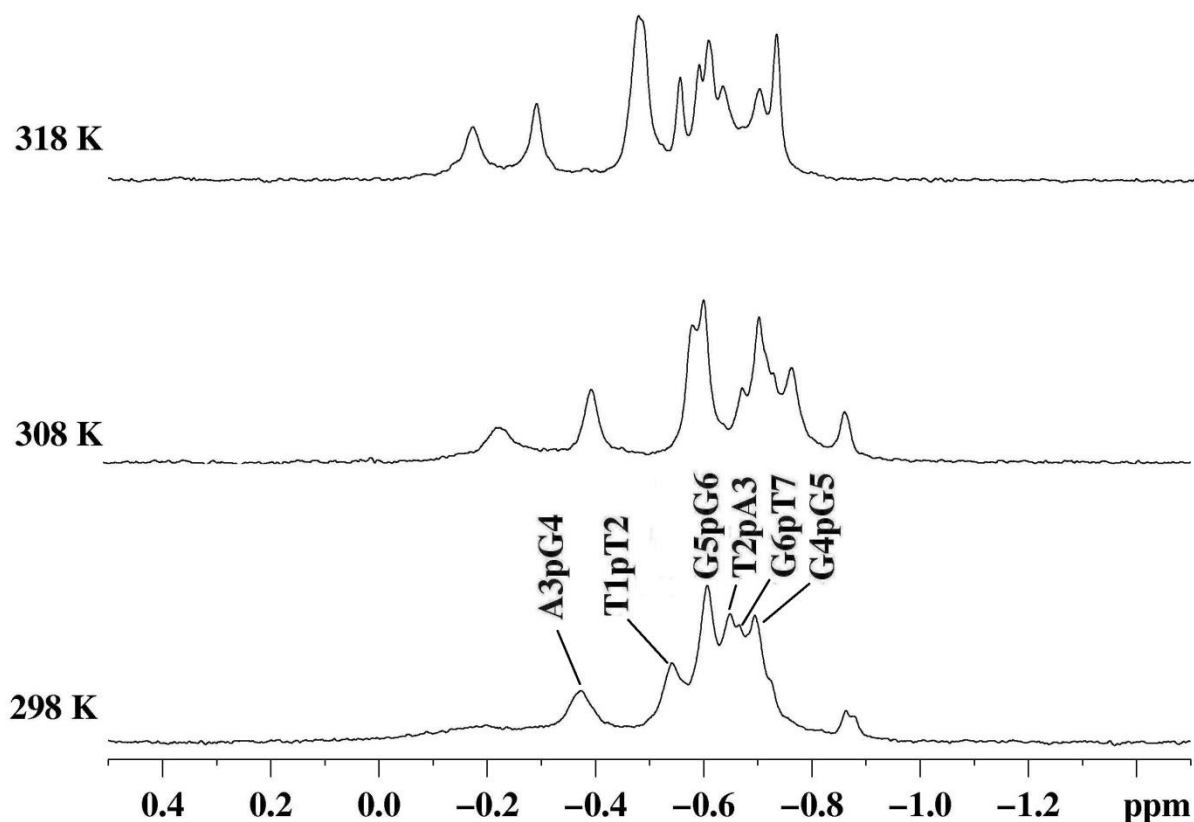


Fig. 5.18: Proton decoupled ^{31}P NMR spectra of luteolin-d-(TTAGGGT) $_4$ as a function of temperature at $D/N=1.0$.

5.1.7 Structural studies of luteolin-d-(TTAGGGT) $_4$ complex

NOESY spectra recorded with variable mixing times τ_m 100, 200, 250 ms were analyzed at $D/N=1:1$ and $D/N=2:1$. The NOESY spectra of complex contain several intramolecular NOE connectivities within quadruplex and luteolin in addition to intermolecular connectivities between quadruplex and luteolin. The presence of all sequential connectivities between base-H1'/H2'', H2'' and NH-NH protons, indicate that all G-quartets were intact and quadruplex adopts a right hand helical structure with no opening of base pairs at any step. Thus exclude the possibility of intercalation of luteolin chromophore between base pairs. **Table 5.13** shows the intramolecular NOE connectivities observed within the luteolin molecule in the luteolin-d-(TTAGGGT) $_4$ complex at $D/N=1.0$ and $D/N=2.0$. The meta coupled proton H6', H5', which was clearly observable in the COSY spectra was not clearly evident in NOESY spectra due to overlapped signals. It was observed that H6' proton was close to H3 proton compared to H2'.

Sl No.	Intramolecular connectivities
1	H3-H6'
2	H3-H2'
3	H6'-H5'
4	H2'-H8

Table 5.13: Interproton NOE connectivities within luteolin molecule in luteolin-*d*-(TTAGGGT)₄ complex at *D/N*=1.0 and 2.0 at 298 K.

Proton	ppm	NOE	NOE	NOE	NOE	NOE	NOE	NOE
H6'	6.70	T1H2'	T1H2''	T2H4'	G6H1'	G6NH	T7CH ₃	
H2'	6.63	T1H2'	T1H2''	T2H1'	T2H4'	T7H1'	G6NH	T7CH ₃
H8	5.63	T1H2'	T1H2''	T2H1'	T2H4'	T7CH ₃		
H6	5.49	T1CH ₃	G6H2''					
H3	6.01	G6NH						

Table 5.14: Intermolecular NOE connectivities between luteolin molecule and *d*-(TTAGGGT)₄ in luteolin-*d*-(TTAGGGT)₄ complex at *D/N*=1.0 and 2.0 at 298 K.

A total of 22 intermolecular NOE connectivities were observed between luteolin protons and quadruplex but only non-overlapped peaks (**Table 5.14 and 5.15**) were used for distance calculation and for building model. Most of the Intermolecular NOE connectivities between luteolin protons H6', H2', H8 and H6 were observed with sugar (H1', H2'/H2'', H4') and CH₃ protons of T1, T2, and T7 bases of quadruplex (**Figs 5.19a-e**). The intensity of these intermolecular connectivities increased due to more and more binding of luteolin to quadruplex. The connectivities of H2' and H8 protons of luteolin with quadruplex were same, because they lie in the same plane. Since one luteolin proton cannot give peak with both T1 and T7 bases simultaneously, we can infer that probably two molecules of luteolin (one at T1pT2 step and second at G6pT7 step) bind to one molecule of *d*-(TTAGGGT)₄. Similarly the connectivities were selectively with T1, T2, G6, T7, which in turn confirm the binding of luteolin in these 2 steps. Similar contacts were observed with both the ligands (MTX and luteolin) except for the G6NH protons. This shows that probably one binding site was common for both the ligand. The exact mode of binding can be revealed after the rMD simulations. But one mode of binding is probably stacking, which results into a large upfield shift in G6NH proton.

Intermolecular Connectivities	rMD Distance (Å)
H8-T1H2''	3.51
H8-T2H1'	3.02
H8-T2H2'	3.59
H8-T2H2''	3.62
H8-T2H4'	2.90
H8-G6NH	2.91
H8-T7CH ₃	4.50
H6'-T2H2''	2.95
H6'-T2H4'	3.24
H6'-G6HI'	4.30
H6'-G6NH	3.88
H6'-T7CH ₃	4.35
H2'-T2H2'	3.23
H2'-T2H2''	3.19
H2'-T2H4'	3.24
H2'-G6HI'	2.36
H2'-G6NH	3.18
H2'-T7CH ₃	3.65

Table 5.15: Intermolecular NOE connectivities and rMD distances between luteolin molecule and *d*-(TTAGGGT)₄ in luteolin-*d*-(TTAGGGT)₄ complex at 2.0 at 298 K.

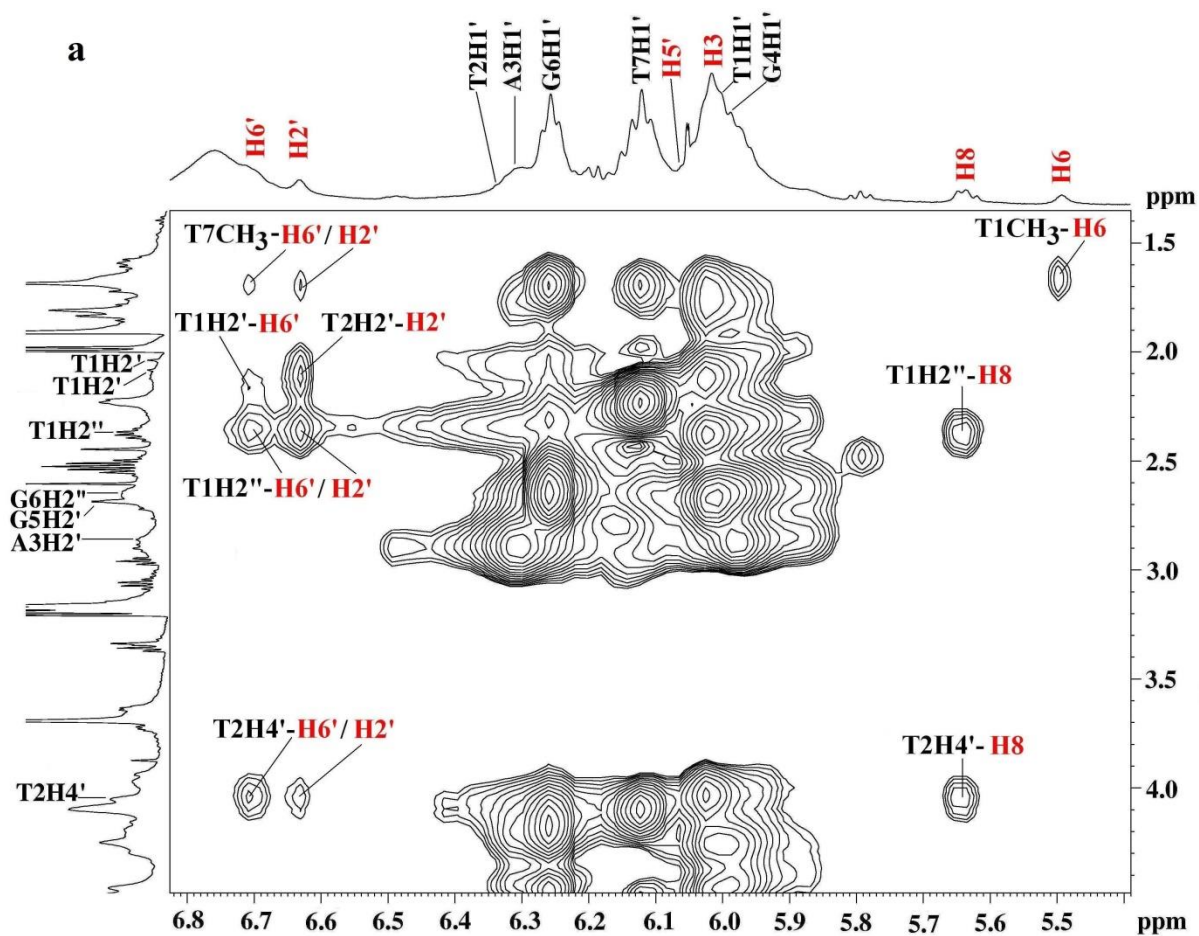


Fig. 5.19a: NOESY spectrum of luteolin-*d*-(TTAGGGT)₄ complex at *D/N*=1.0 at 298 K showing intermolecular NOE connectivities between H6', H2', H8 and H6 protons of luteolin molecule and *d*-(TTAGGGT)₄.

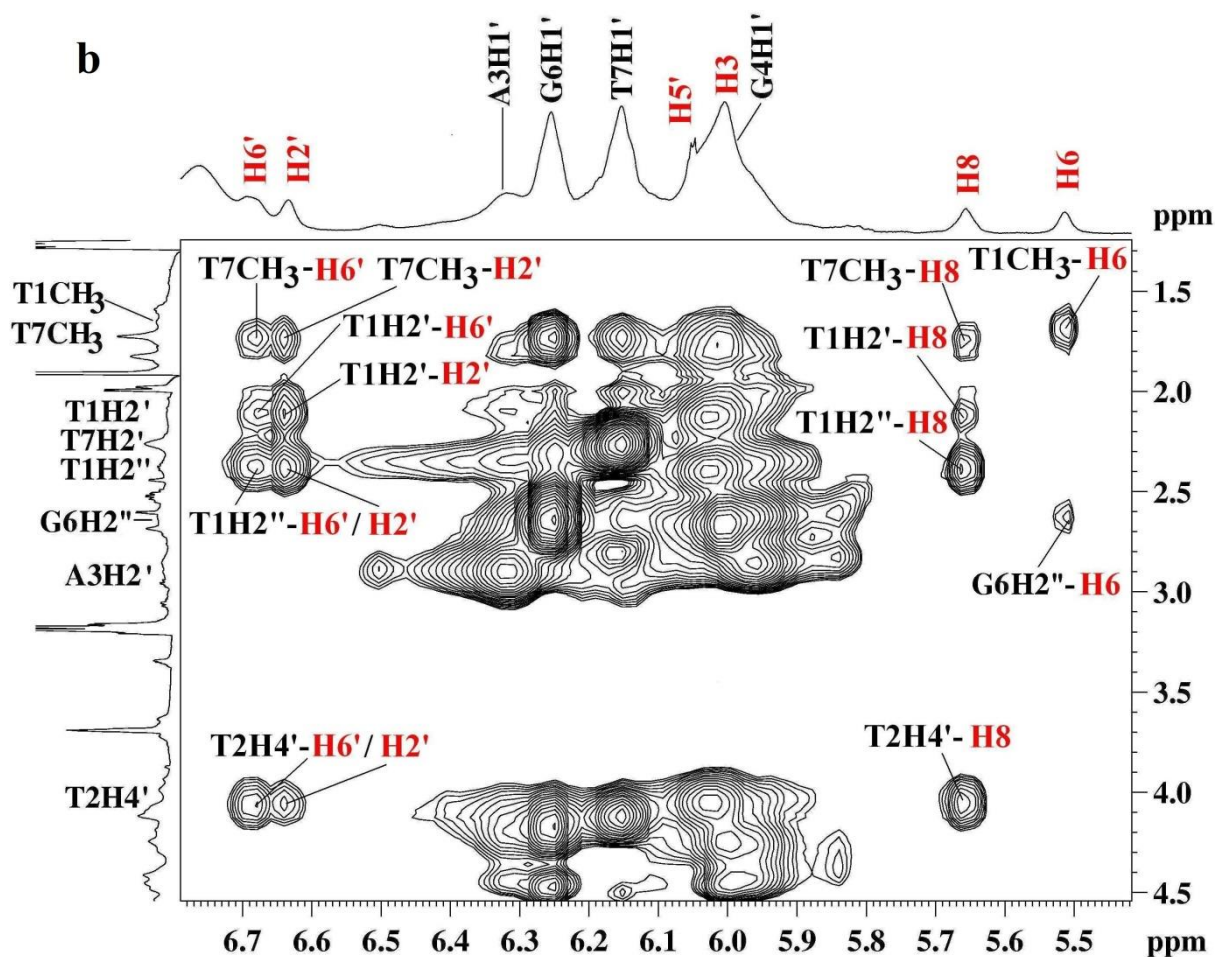
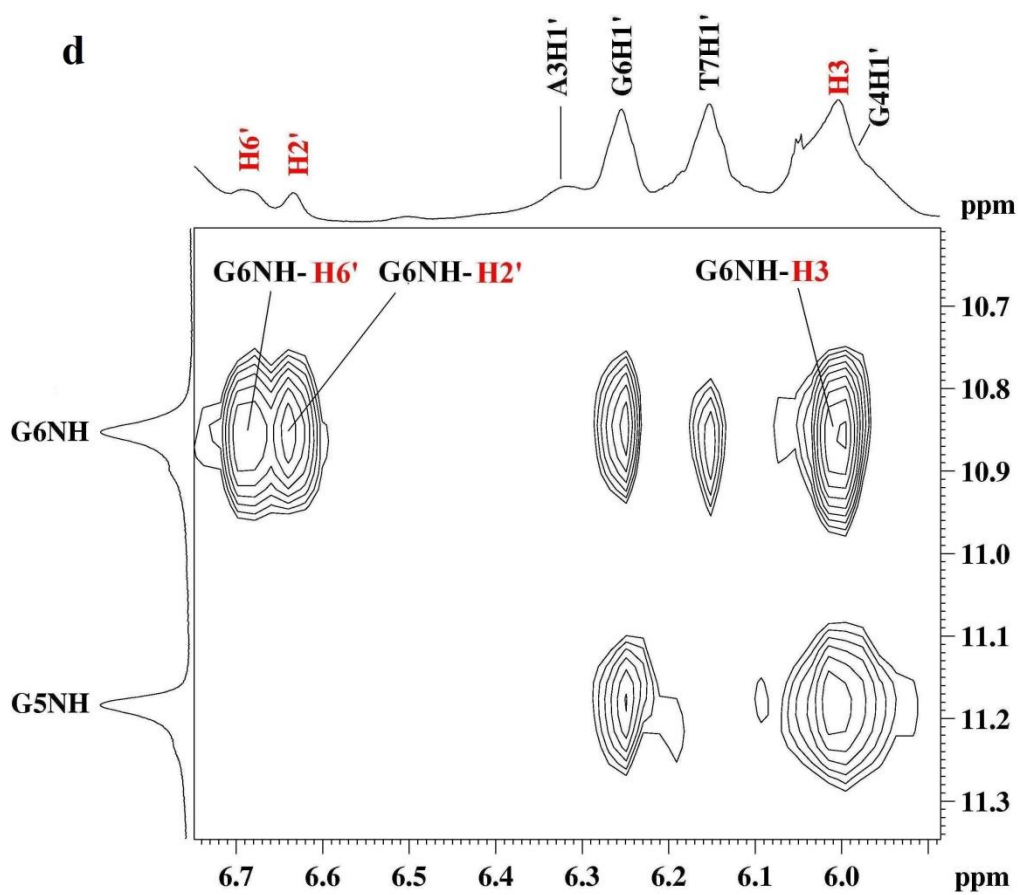
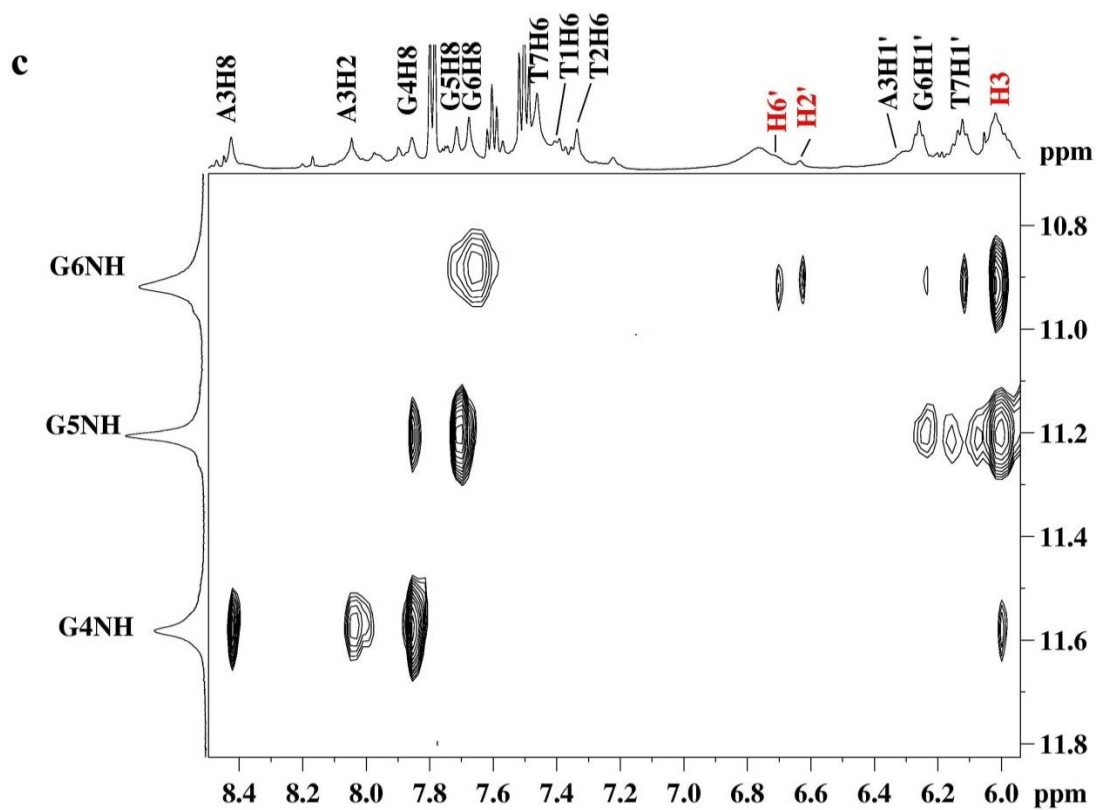


Fig. 5.19b: NOESY spectrum of luteolin- d -(TTAGGGT) $_4$ complex at $D/N=2.0$ at 298 K showing intermolecular NOE connectivities between $\text{H6}'$, $\text{H2}'$, H8 and H6 protons of luteolin molecule and d -(TTAGGGT) $_4$.



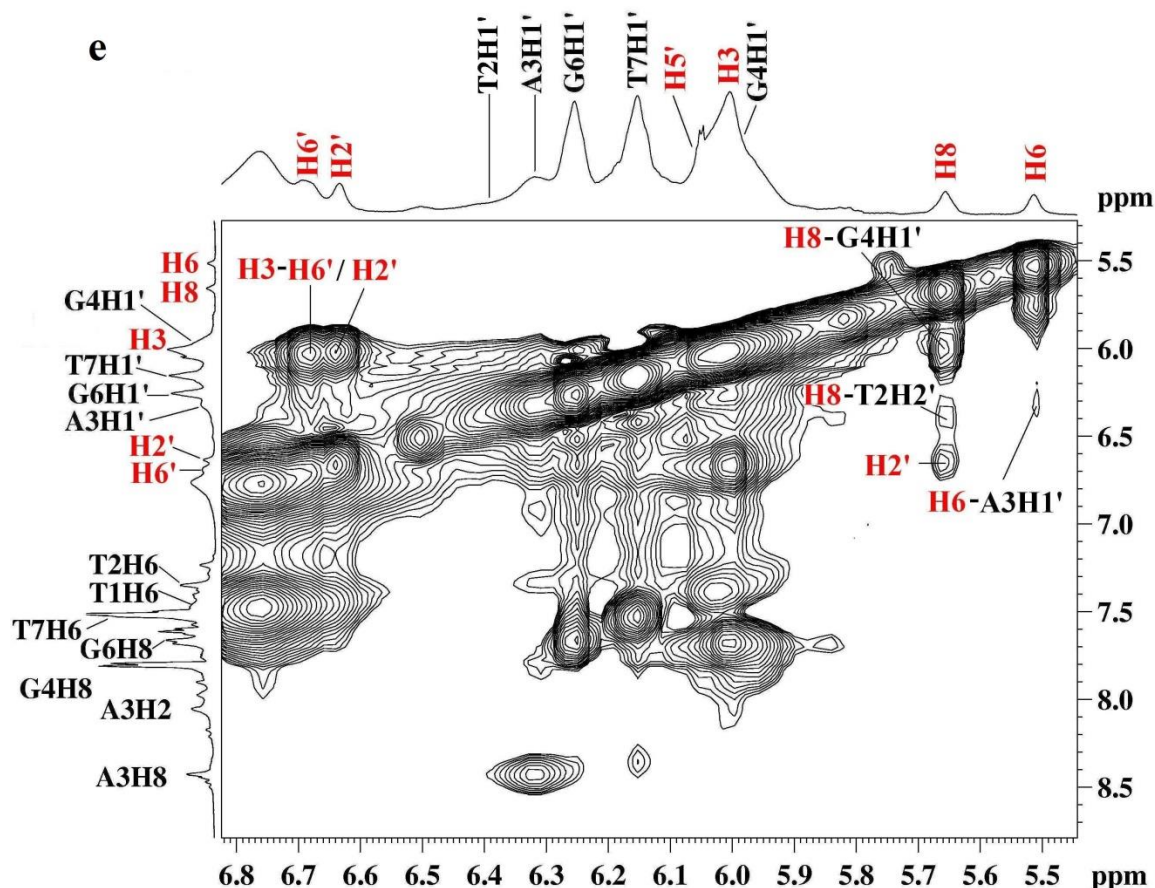


Fig. 5.19: NOESY spectra of luteolin-d-(TTAGGGT)₄ complex at 298 K showing intermolecular NOE connectivities between luteolin molecule and d-(TTAGGGT)₄ (C) at D/N=1.0 and (d-e) D/N=2.0.

5.1.8 Restrained Molecular dynamics studies of luteolin-d-(TTAGGGT)₄ complex

To obtain final structure of luteolin-d(TTAGGGT)₄ complex, distance restraints obtained from 2:1 complex NOESY ($\tau_m = 200$ ms) at 298 K were used. The NOE peaks were integrated using SPARKY software (T.D Goddard DGK, University of California, San Francisco, USA 2004) and distances obtained were calculated using the methodology given in chapter 2 section 2.5.2.4.4. The inter and intra molecular distances obtained in luteolin-d-(TTAGGGT)₄ complex were of three types, i) intermolecular distances between luteolin and d-(TTAGGGT)₄ protons, ii) intra molecular distances obtained between protons of luteolin molecule and iii) intra molecular distances between protons of d-(TTAGGGT)₄. These distances were used as NOE restraints to build the final structure using restrained molecular dynamics simulation protocol.

The PDB structure 1NP9 (Gavathiotis and Searle, 2003) was used as the initial structure for tetramolecular quadruplex d-(TTAGGGT)₄ and was minimized. The initial structure of luteolin

was built using the builder module of INSIGHT II, version 2005 (Accelrys Inc., San Diego, California) on Silicon Graphics Fuel (SGI) workstation and was minimized. The different types of restraints used before energy minimization and simulated annealing were given in **Table 5.16**. Based on the set of 19 luteolin-quadruplex NOEs, the luteolin molecule was placed in the T1pT2 and G6pT7 steps of the quadruplex DNA such that all constraints were compiled satisfactorily. Once the luteolin molecules were placed in the binding site all the restraints were incorporated using the generic distance option of the Discover module with a force constant of 25, 15, 10 Kcal mol⁻¹ Å⁻² for strong, medium and weak interactions, respectively. The structure was energy minimized for 1000 steps using CVFF1 (consistent valence force field) force field, and restrained simulations were carried out for 25 ps using steepest descent protocol.

The assessment of refined structures after equilibration at the end of 25 ps in terms of energetics including restraint violation energies and root mean square derivative of energy with respect to atomic coordinates, given in **Table 5.16** were found to be in reasonable limits. The simulation results are in accordance with the conclusion drawn from intermolecular NOEs connectivities. There was no significant change in the conformation of quadruplex DNA upon luteolin binding. Most of the luteolin contacts were centred at T1pT2 and G6pT7 steps (**Fig. 5.20**). Close analysis of **Fig. 5.21** shows that the interaction between luteolin and d-(TTAGGGT)₄ occurs both via partial stacking and groove binding. The first luteolin molecule occupies the groove of T1pT2 step while the second luteolin molecule partially stacked at G6pT7 step. This result is somewhat different to that observed in case of MTX-d-(TTAGGGT)₄ complex, where both MTX molecules were partially stacked. This difference in binding is probably due to the lack of side chains in luteolin molecule. The binding is stabilized by both partial stacking and electrostatic interactions. Dual mode of binding was earlier reported by Gai *et al.*, for the interaction of a cyanine dye with d-(TGGGGT)₄. But on contrary to our results the dye binds as monomer at one site and as dimer at second site. The rMD results clearly show that the luteolin shows a dual mode of interaction with quadruplex DNA. This binding results in the stabilization of quadruplex structure, which probably leads to telomerase inhibition.

Experimental Restraints	
Intramolecular	
Luteolin-Luteolin	8
Quadruplex-Quadruplex	236
Intermolecular	
Luteolin-quadruplex	22
CVFF energy (kcal mol ⁻¹) of the minimized structures	
Total	369.7
Non-bonded	-106
Restraint	250
Average rmsd	0.48Å
Restraint Violations	
Distance (>0.25Å)	8

Table 5.16: *Experimental restraints and structure statistics of the final structure.*

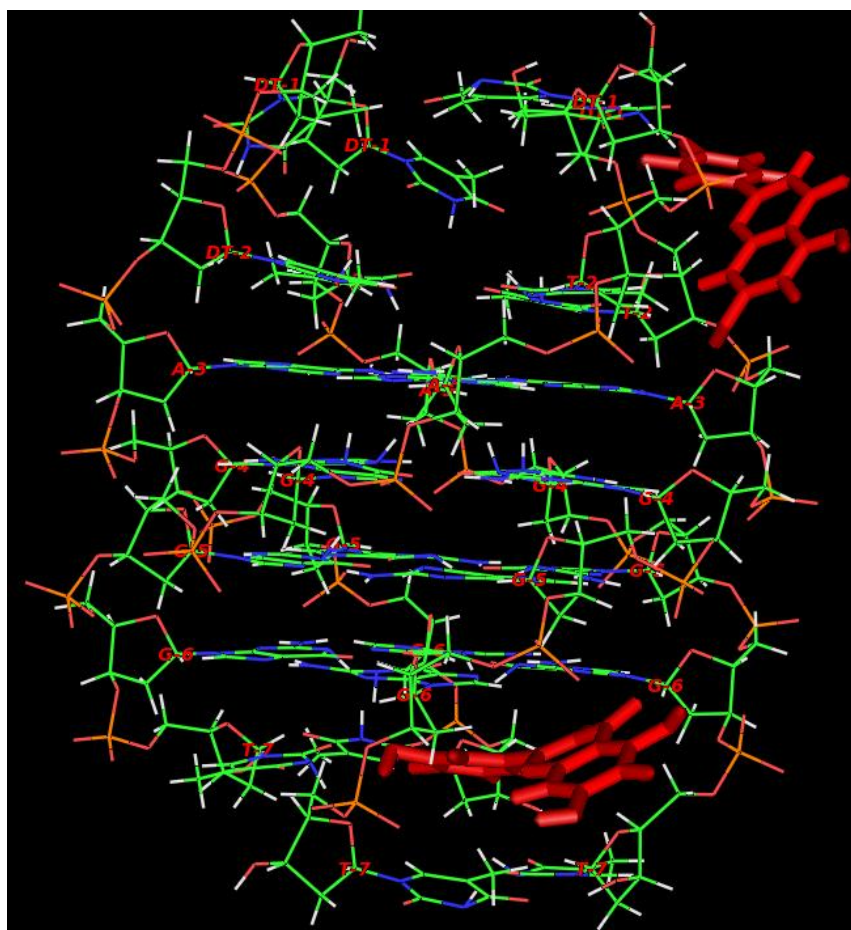


Fig. 5.20: Front view of the final structure of luteolin-d-(TTAGGGT)₄ complex obtained by restrained molecular dynamics simulations.

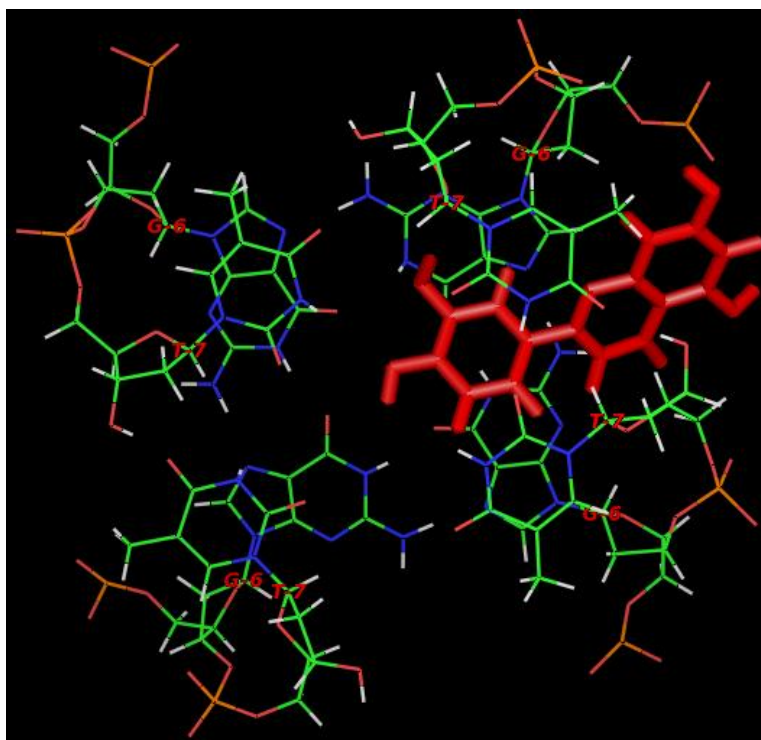
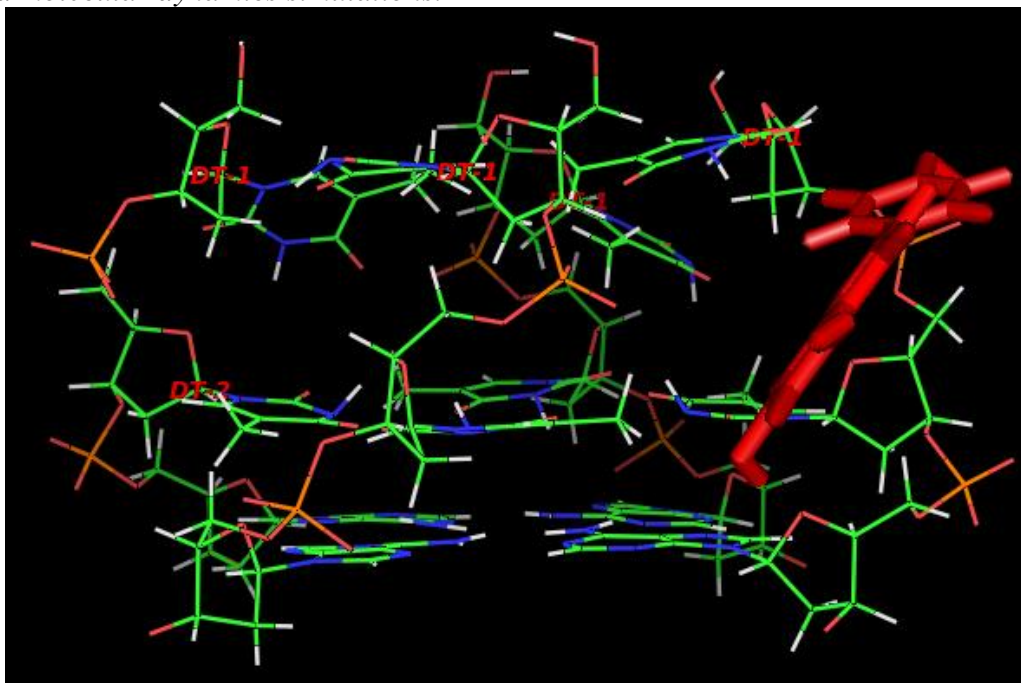


Fig. 5.21: Close-up view of the luteolin-d-(TTAGGGT)₄ interaction at T1pT2 and G6pT7 binding sites.

5.1.9 Resonance assignment of uncomplexed sequence d-(TTGGGGT)₄

Oligonucleotide sequence d-(TTGGGGT)₄ (**Fig. 5.22**), is a single repeat sequence of *the Tetrahymena telomere* with an extra thymine at the 3' position to prevent the aggregation of end stacking of G-tetrads. It also forms a parallel stranded G-quadruplex similar to that of human single repeat sequence. 1D ¹H and 2D ¹H-¹H NOESY, ¹H-¹H COSY experiments were used to determine the structural conformation of d-(TTGGGGT)₄ sequence. Proton NMR spectrum of d-(TTGGGGT)₄ (**Fig. 5.23a**) at 100mM KCl containing buffer in 10 % D₂O and 90 % H₂O at 25°C shows the four well resolved NH peaks resonating between 10.5 to 12 ppm region. This confirms the formation of single predominant stable structure by the TTGGGGT oligonucleotide sequence in present experimental conditions. These four NH resonances corresponds to the four guanines in the sequence d-(TTGGGGT)₄, that is G3:G4:G5:G6. The G3 imino proton resonates downfield of the spectrum followed by G4 and G5 imino resonances, whereas G6 imino proton resonates in the upfield region. This observation is consistent with the results of alone parallel tetramolecular structures formed by sequence d-(TTAGGGT)₄ and d-(TTGGGGT)₄ reported previously (Gravathiotis and Searle, 2003; Wang and Patel, 1993). The upfield shift of these imino resonances is due to the stacking arrangement of G-tetrads that shows Hoogsteen type H-bonding (NH...O). On contrary to this the imino resonances of duplex DNA shift downfield (Keniry, 2001; Webba da Silva, 2007). Similar kind of upfield shift in the imino protons of guanine was also observed in the Wobble G-T pairs, in which guanine imino proton hydrogen bonds with the carbonyl group (Patel *et al.*, 1982). Observance of only four NH resonances indicates the formation of tetramolecular quadruplex structure by the association of four identical strands of d-(TTGGGGT) and also confirms the C₄ symmetry of the G-quartet structure formed (Lu *et al.*, 1992). In C₄ symmetric G-quartet structures, all the Gs are structurally equivalent, and present in an identical environment. Apart from the major dominant resonances some minor resonances were also observed that corresponds to the single stranded components.

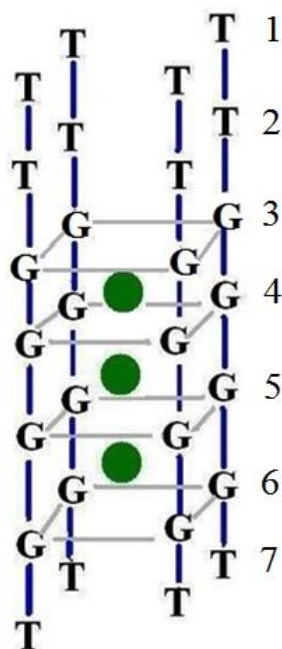


Fig. 5.22: Schematic representation of parallel-stranded G-quadruplex structure formed by oligonucleotide sequence $d\text{-(TTGGGGT)}_4$.

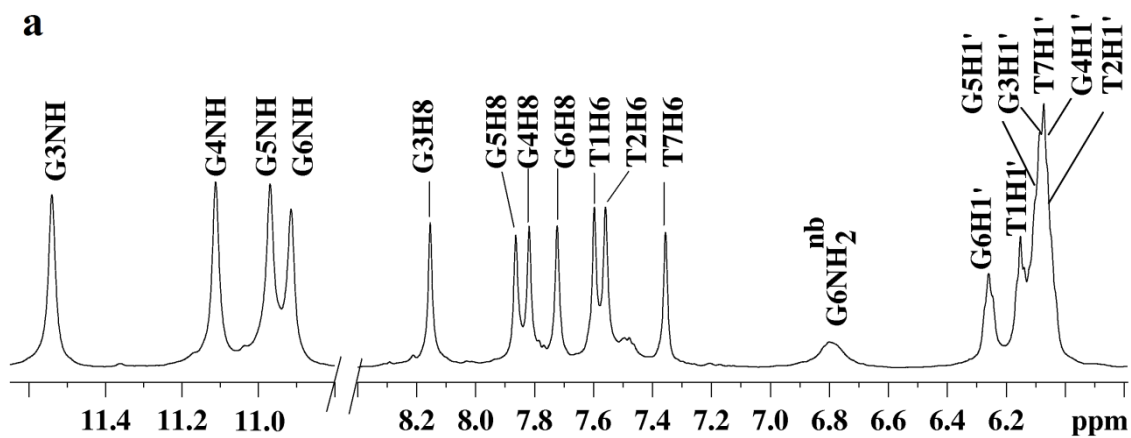


Fig. 5.23a: 1D proton spectrum of uncomplexed quadruplex sequence $d\text{-(TTGGGGT)}_4$ showing exchangeable and non-exchangeable resonances.

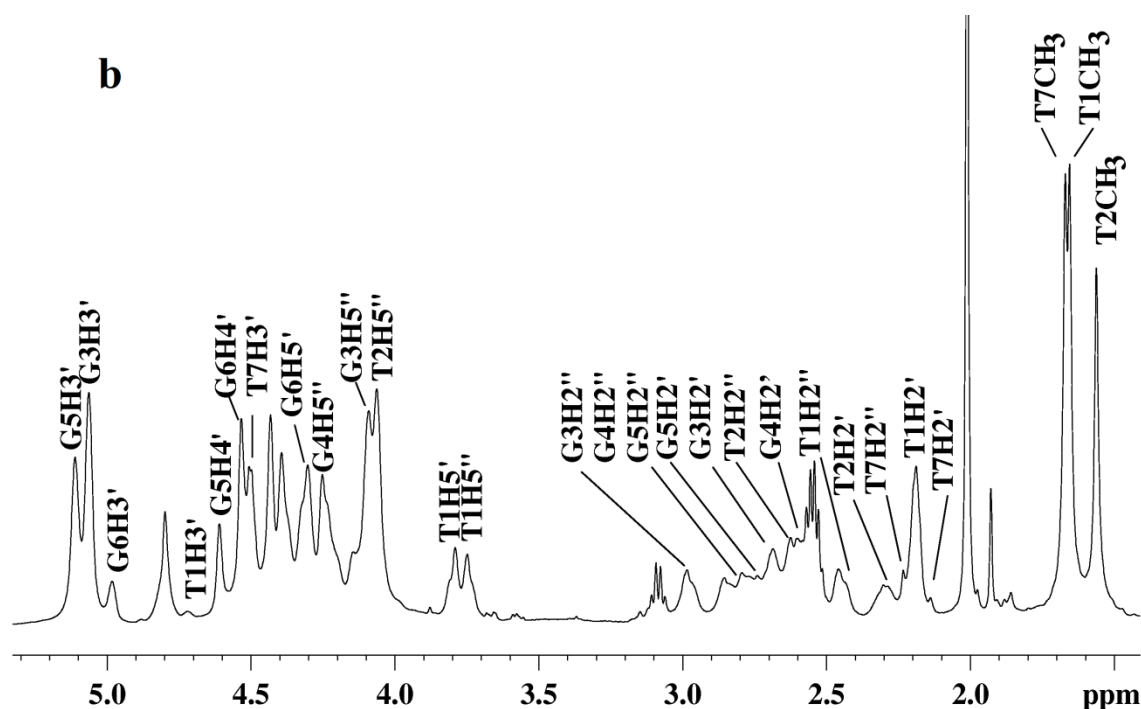


Fig. 5.23b: 1D proton spectrum of uncomplexed quadruplex sequence $d\text{-(TTGGGGT)}_4$ showing exchangeable and non-exchangeable resonances.

The ^1H spectrum of $d\text{-(TTGGGGT)}_4$ recorded at 278 K exhibits the well resolved exchangeable imino and amino resonances. The imino proton resonances were sharp and are unaffected by increase in temperature, till 248 K. The two resonances present in most up field and most downfield region among for imino protons start to disappear upon increase in temperature. This may be attributed to the breakdown of G-quartet structure which results in the exchange of Hoogsteen H-bonded imino protons to exchange with solvent water molecules. The central G-quartet core is unperturbed at this temperature and hence shows stable imino resonances in this region. Appearance of sharp resonances clearly indicates that the protons are in slow exchange with surrounding water molecules in NMR time scale. The non-exchangeable resonances (**Fig. 5.23b**) (bases and sugar) cover a major portion between 1.5-8.7 ppm.

NOESY spectra also give evidence for G-tetrad formation (**Fig. 5.24**) due to the presence of NH-NH NOE connectivity between adjacent imino protons in the sequence G3-G4-G5-G6 (**Fig. 5.25a**) and the presence of interstrand NOEs between guanine imino proton to its own and its 5'flanking base protons in G3-G4-G5-G6 segment of $d\text{-(TTGGGGT)}_4$ sequence (**Fig. 5.25b**) (Wang and Patel, 1992). Such long range NOE is not possible within same strand.

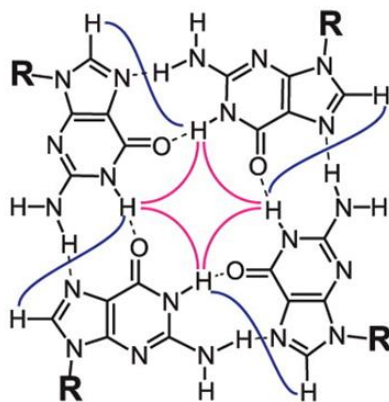
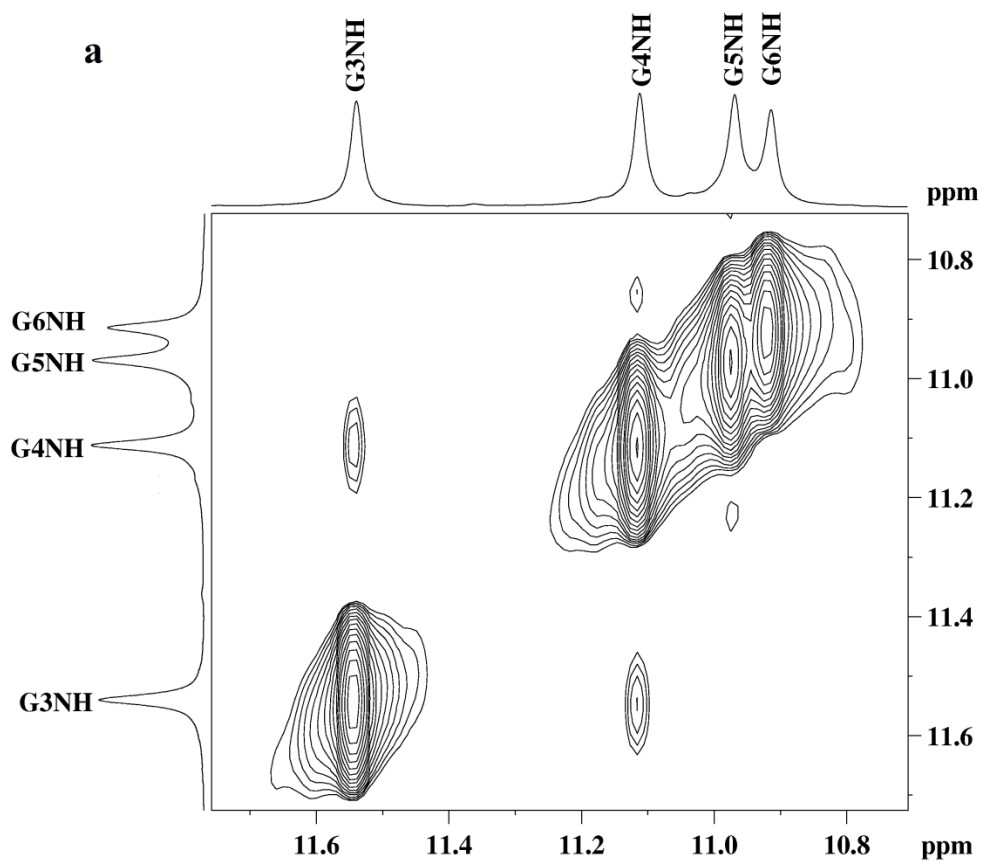


Fig. 5.24: G-tetrad showing NH-NH and NH-H8 connectivities that can be observable in NOESY experiments.



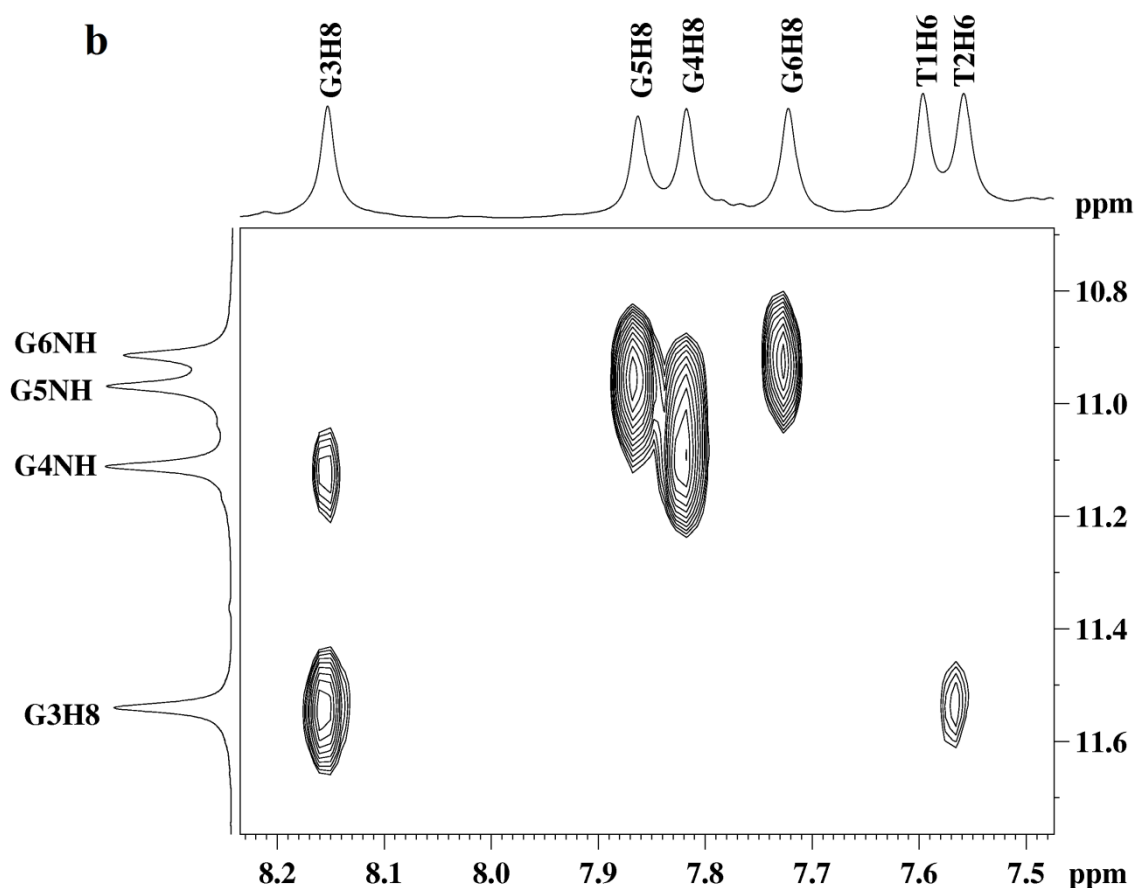


Fig. 5.25: Expansion of the NOESY spectra of uncomplexed quadruplex sequence $d\text{-}(TTGGGGT)_4$ at 298 K showing (a) NH-NH connectivity between adjacent imino protons. (b) Interstrand guanine NH connectivities to its own and 5' flanking base protons in G3-G4-G5-G6 segment.

Classical sequential assignment used for nucleic acid was employed for the assignment of the nonexchangeable protons of quadruplex (Wuthrich, 1986), which were done by observing NOE connectivities between base H8/H6 protons to its own and its 5' flanking H1'/H2'/H2'' sugar protons (**Fig. 5.26 a, b**). This hereby indicates the presence of right handed helical geometry similar to that observed in B-DNA. 5'-anti-3'-anti conformation was determined by observing the connectivity of base H8/H6-H1' whose distance was in the range of 3.5-3.7 Å.

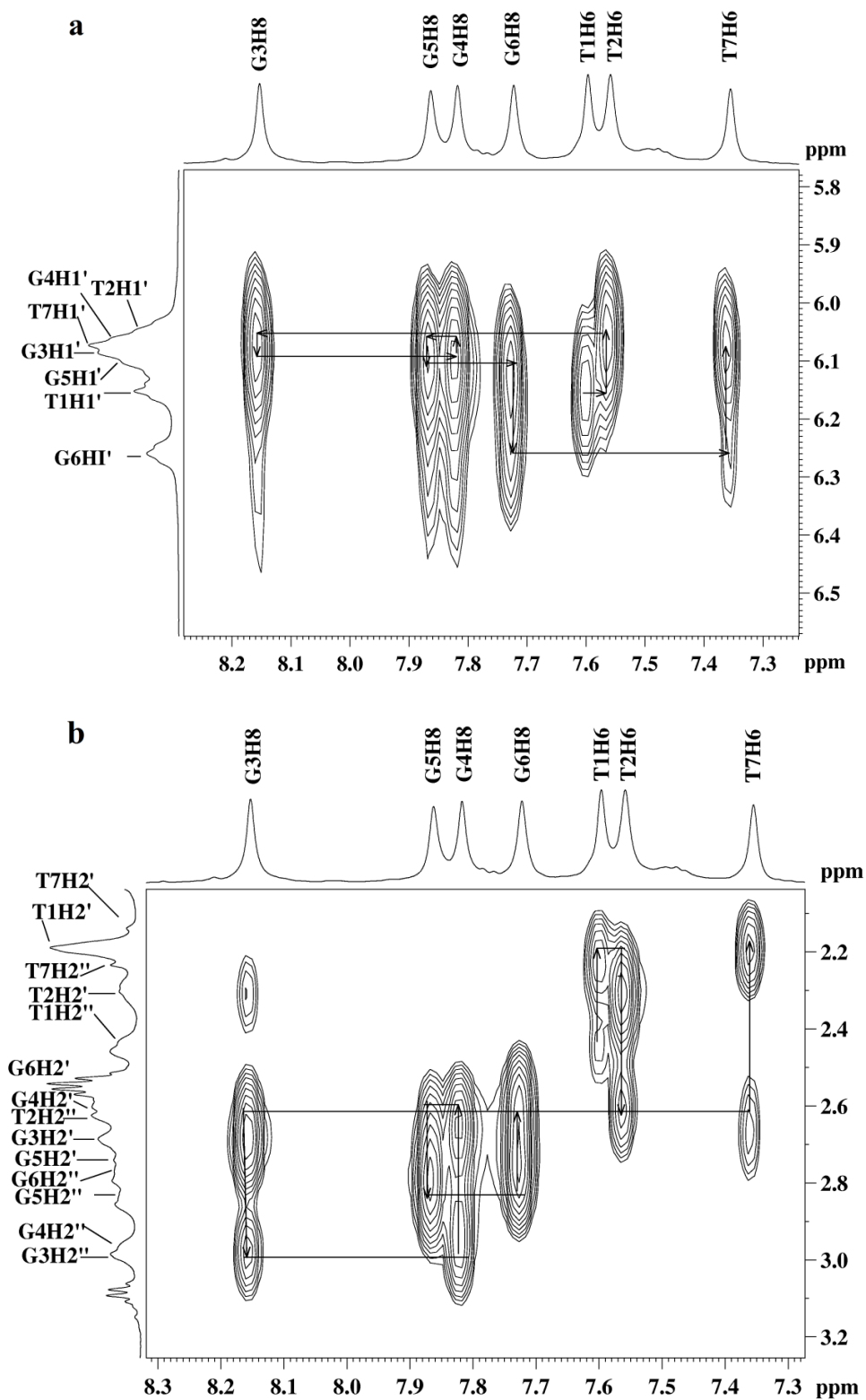


Fig. 5.26: Expansion of the NOESY spectra of uncomplexed quadruplex sequence $d\text{-(TTGGGGT)}_4$ at 298 K showing (a) intrastrand base H8/H6-H1' sequential connectivity. (b) Intrastrand base H8/H6-H2'H2'' sequential connectivity in T1-T2-G3-G4-G5-G6-T7 segment.

5.1.10 Resonance assignment of luteolin-d-(TTGGGGT)₄ complex

To examine the binding interaction of luteolin with quadruplex sequence d-(TTGGGGT)₄ increasing concentration of luteolin was titrated to the quadruplex solution to reach the desired D/N ratios of 0.25, 0.5, 0.75, 1.0 and 2.0. The changes were continuously monitored by ¹H and ³¹P NMR at different temperatures. Only one set of DNA signals was seen at all D/N values, during the course of titration, indicating that there was no loss of original fourfold symmetry of the quadruplex in luteolin-d-(TTGGGGT)₄ complex. A complete assignment of all non-exchangeable and exchangeable protons of the complex had been accomplished by means of a combination of 2D NMR experiments besides comparing them with that of uncomplexed DNA and luteolin. The NH-NH NOE connectivity between adjacent imino protons and interstrand guanine NH connectivities to its own and 5' flanking base protons in G3-G4-G5-G6 segment indicate that G-quartet is intact in the complex (**Figs. 5.27 a, b**). As for DNA, resonances within deoxyribose were identified by COSY as well as ¹H-¹³C HSQC in view of overlap with luteolin signals. Analysis of sequential NOEs among base and H1'/H2'/H2'' protons allowed assignment of all base protons. All bases have classical H8/H2'-H2'' sequential connectivities to neighbouring 5'-end bases indicating that the four strands were involved in the formation of helical structure in the complex. The entire pattern of NOEs indicates that the backbone conformation closely resembles that of uncomplexed d-(TTGGGGT)₄ possessing a right handed B-form helix structure. The presence of all sequential base GH8/H6-H1'/H2'/H2'' NOEs (**Figs. 5.28a, b**), indicates that there was no opening of base pairs at any step, hence excluding intercalation of drug chromophore between base pairs. A single set of luteolin signals were present in the spectra of complex at 298 K and was assigned unambiguously by the strategies used in section 5.1.3.

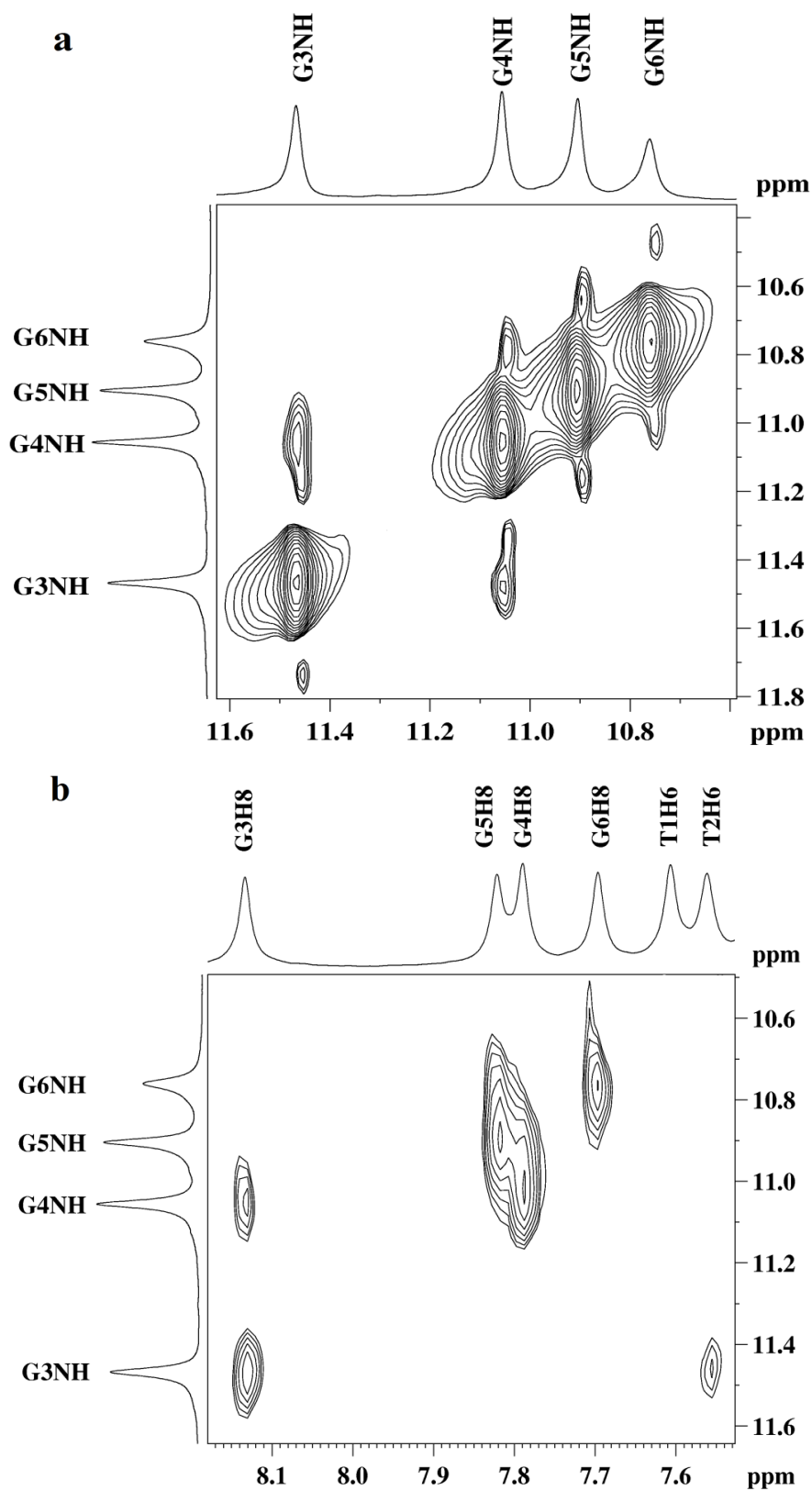


Fig. 5.27: Expansion of the NOESY spectra of luteolin-*d*-(TTGGGGT)₄ complex at 298 K showing (a) NH-NH connectivity between adjacent imino protons. (b) Interstrand guanine NH connectivities to its own and 5' flanking base protons in G3-G4-G5-G6 segment.

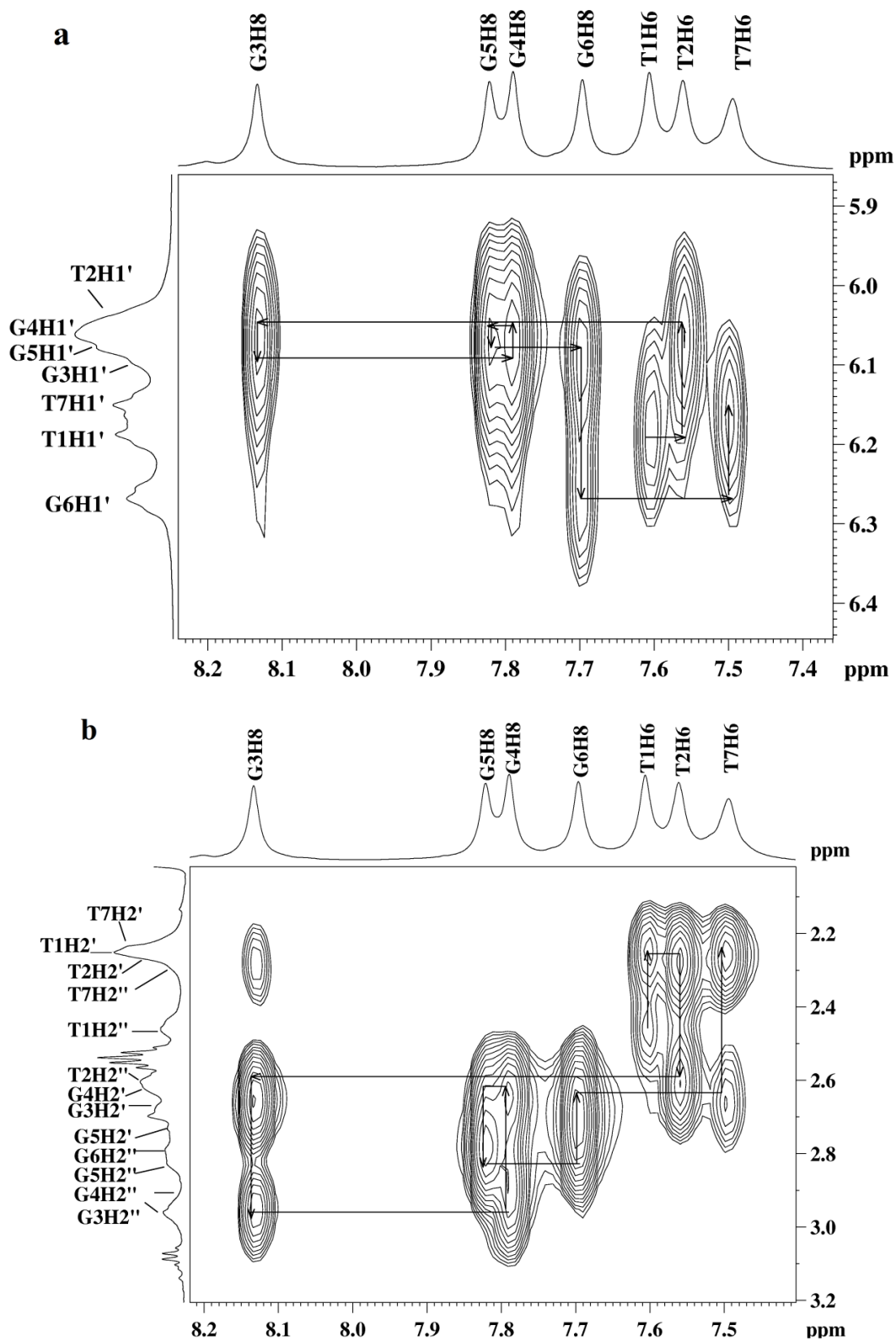


Fig. 5.28: Expansion of the NOESY spectra of luteolin-d-(TTGGGGT)₄ complex at 298 K showing (a) intrastrand base H8/H6-H1' sequential connectivity. (b) Intrastrand base H8/H6-H2'H2'' sequential connectivity in T1-T2-G3-G4-G5-G6-T7 segment.

5.1.11 Effects of titrimetric addition of luteolin

The initial addition of luteolin to the quadruplex d-(TTGGGGT)₄ caused shift in several protons which increased with D/N (**Fig. 5.30 and Table 5.17-5.18**). Except for G6NH signal, which broadened slightly as compared to other GNH signals, there was no noticeable broadening in other spectral lines (**Fig. 5.30b**). Among the NH protons, G6NH showed maximum upfield shift ~ 0.15 ppm as compared to G3NH, G5NH (~ 0.07 ppm) and G4NH (0.04 ppm). There was no significant shift in any of the base or sugar protons of T1, T2, A3, G4, G5, G6 residues. The T7 nucleotide protons shifted downfield on binding to luteolin; it being 0.14, 0.08 and 0.09 ppm for T7H6, T7H1' and T7CH₃ signals. With further increase in luteolin concentration the shifts in G6NH, T7H6 and T7CH₃ signals increased (**Fig. 5.29**). On addition of increasing concentration of luteolin to a fixed amount of DNA quadruplex, the intensity of H6, H8, H2', H5' and H6' protons grew gradually (**Fig. 5.30c**). All luteolin signals were upfield shifted from their corresponding positions in free luteolin by 0.67-0.80 ppm at D/N = 0.25. The signals do not shift any further with D/N and apparently luteolin was completely bound at all D/N ratios (**Table 5.19-5.20**). None of the OH protons were visible at any D/N ratio. The interaction of luteolin with both the telomeric sequence showed change in G6pT7 step, but the magnitude of the shift was slightly greater in case of d-(TTGGGGT)₄ (**Fig. 5.31a-d**). This showed that the binding site of luteolin is probably near G6pT7 of quadruplex.

D/N ratios	G3NH	G4NH	G5NH	G6NH	T1CH ₃	T2CH ₃	T7CH ₃
D/N 0.00	11.54	11.11	10.97	10.91	1.67	1.56	1.66
D/N 0.25	11.52	11.09	10.95	10.87	1.66	1.55	1.66
D/N 0.50	11.50	11.08	10.94	10.84	1.65	1.55	1.69
D/N 0.75	11.48	11.07	10.92	10.79	1.65	1.54	1.72
D/N 1.0	11.47	11.06	10.90	10.76	1.65	1.55	1.75
D/N 2.0	11.41	11.02	10.86	10.67	1.61	1.53	1.78
$\Delta\delta=(\delta_b-\delta_f)$	-0.13	-0.09	-0.11	-0.24	-0.06	-0.03	0.12
D/N ratios	T1H6	T2H6	G3H8	G4H8	G5H8	G6H8	T7H6
D/N 0.00	7.59	7.56	8.15	7.82	7.86	7.72	7.35
D/N 0.25	7.59	7.56	8.14	7.81	7.85	7.71	7.38
D/N 0.50	7.59	7.56	8.14	7.80	7.84	7.71	7.42
D/N 0.75	7.59	7.56	8.13	7.79	7.83	7.70	7.47
D/N 1.0	7.61	7.56	8.13	7.79	7.82	7.70	7.49
D/N 2.0	7.59	7.55	8.10	7.77	7.79	7.68	7.55
$\Delta\delta=(\delta_b-\delta_f)$	0.00	0.00	-0.05	-0.05	-0.07	-0.04	0.20

Table 5.17: Chemical shift (ppm) of d-(TTGGGGT)₄ protons as a function D/N ratios at 298 K along with the change in chemical shift on binding, that is, $\Delta\delta = \delta(D/N=2.0) - \delta(D/N=0.0)$.

Protons	T1			T2			G3			G4		
	δ_b	δ_f	$\Delta\delta$	δ_b	δ_f	$\Delta\delta$	δ_b	δ_f	$\Delta\delta$	δ_b	δ_f	$\Delta\delta$
H8/H6	7.61	7.59	0.02	7.56	7.56	0.00	8.13	8.15	-0.02	7.79	7.82	-0.03
H1'	6.19	6.15	0.04	6.05	6.05	0.00	6.09	6.08	0.01	6.06	6.06	0.00
H2'	2.25	2.21	0.04	2.27	2.30	-0.03	2.65	2.68	-0.03	2.60	2.62	-0.02
H2''	2.44	2.46	-0.02	2.60	2.62	-0.02	2.95	2.97	-0.02	2.91	2.94	-0.03
H3'	4.76	4.74	0.02	4.84	4.86	-0.02	5.05	5.06	-0.01	5.04	5.05	-0.01
H4'	4.30	4.32	-0.02	4.27	4.27	0.00	4.42	4.43	-0.01		4.43	-
H5'	3.85	3.79	0.06	4.11	4.14	-0.03	4.21	4.25	-0.04	4.35	4.34	0.01
H5''	3.76	3.75	0.01	4.05	4.05	-0.01	4.15	4.09	0.06	4.26	4.24	0.02
H2/CH₃	1.65	1.67	-0.02	1.55	1.56	-0.01	8.04					
NH₂^b							9.84	9.84	0.00	9.21	9.25	-0.04
NH₂^{nb}							6.23	6.24	-0.01	6.12	6.17	-0.04
NH							11.4 7	11.54	-0.07	11.06	11.11	-0.05
	G5			G6			T7					
	δ_b	δ_f	$\Delta\delta$	δ_b	δ_f	$\Delta\delta$	δ_b	δ_f	$\Delta\delta$			
H8/H6	7.82	7.86	-0.04	7.70	7.72	-0.02	7.49	7.35	0.14			
H1'	6.09	6.10	-0.01	6.27	6.26	0.01	6.15	6.07	0.08			
H2'	2.71	2.74	-0.03	2.60	2.53	0.07	2.22	2.14	0.08			
H2''	2.82	2.81	0.01	2.70	2.76	-0.06	2.29	2.23	0.06			
H3'	5.07	5.11	-0.04	4.98	4.97	0.01	4.55	4.51	0.04			
H4'	4.59	4.61	-0.02	4.55	4.56	-0.01	-	4.46				
H5'	4.36	4.39	-0.03	4.31	4.31	0.00	4.21	4.24	-0.03			
H5''	4.20	4.33	-0.03	4.25	4.23	0.02	4.10	4.05	0.05			
H2/CH₃							1.75	1.66	0.09			
NH₂^b	9.13	9.17	-0.04									
NH₂^{nb}	6.14	6.23	-0.09									
NH	10.90	10.97	-0.07	10.76	10.91	-0.15						

Table 5.18: Chemical shift (ppm) of *d*-(TTGGGGT)₄ protons in uncomplexed state (δ_f) and that bound to luteolin (δ_b) at $D/N=1.0$ at 298 K along with the change in chemical shift on binding, that is, $\Delta\delta=\delta_b(D/N=1.0)-\delta_f(D/N=0.0)$.

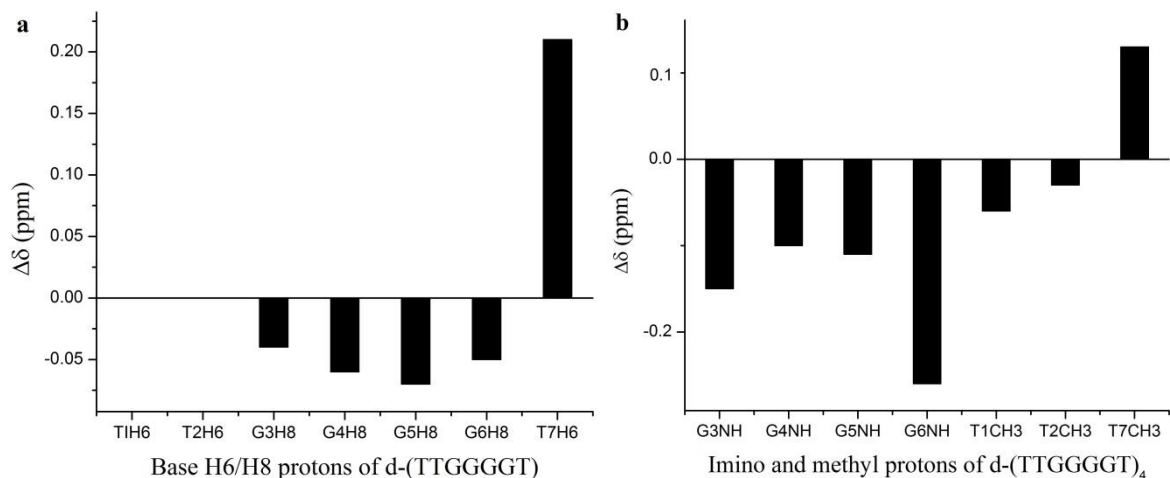


Fig. 5.29: Difference in the chemical shifts ($\Delta\delta$) of base protons on $d\text{-(TTGGGGT)}_4$ (a, b) on binding of luteolin at D/N 2.0 at 298 K.

Luteolin Protons	H6'	H2'	H5'	H3	H8	H6
LUT	7.40	7.38	6.88	6.67	6.44	6.18
D/N 0.25	-	6.66	-	-	5.66	5.49
D/N 0.50	-	6.66	-	-	5.67	5.50
D/N 0.75	-	6.66	-	-	5.67	5.51
D/N 1.0	6.68	6.66	6.08	-	5.67	5.51
D/N 2.0	6.66	6.62	-	-	5.69	5.55
$\Delta\delta$	-0.74	-0.76	-0.80	-	-0.75	-0.63

Table 5.19: Chemical shift (ppm) of luteolin protons as a function of D/N ratios at 298 K. Also shown here is the change in chemical shift on binding, that is, $\Delta\delta = \delta(D/N=1.0) - \delta(D/N=0.0)$.

Luteolin Protons	δ_f	δ_b D/N = 1.0	$\Delta\delta$ D/N = 1.0 ($\Delta\delta = \delta_b - \delta_f$)	δ_b D/N = 2.0	$\Delta\delta$ D/N = 2.0 ($\Delta\delta = \delta_b - \delta_f$)
H3	6.67	-	-	-	-
H6	6.18	5.51	-0.67	5.55	-0.63
H8	6.44	5.67	-0.77	5.69	-0.75
H2'	7.38	6.66	-0.73	6.62	-0.76
H5'	6.88	6.08	-0.80		
H6'	7.40	6.68	-0.72	6.66	-0.74

Table 5.20: Chemical shift (ppm) of luteolin protons from NOESY spectra of free luteolin (δ_f) and luteolin- $d\text{-(TTGGGGT)}_4$ complex (δ_b) at $D/N=1.0$ and 2.0 at 298 K.

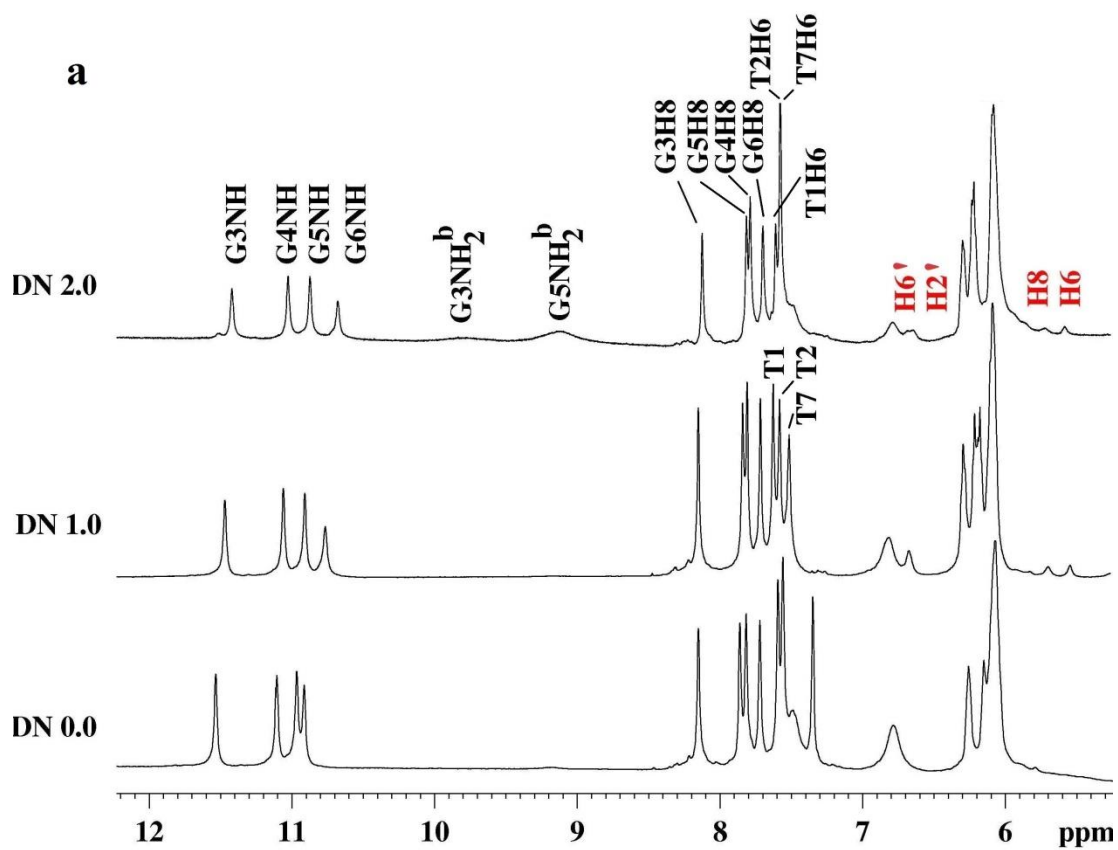
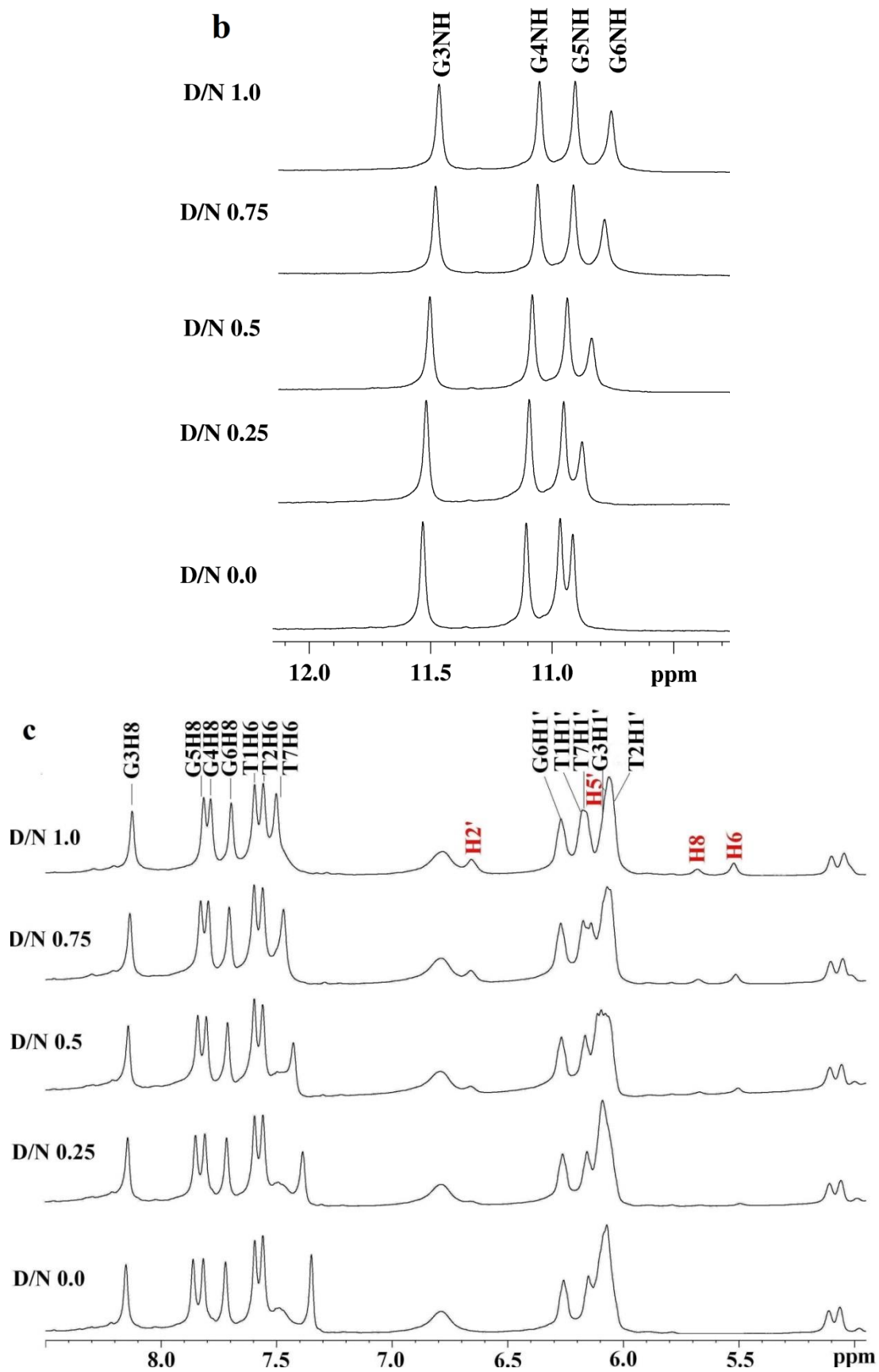


Fig. 5.30: Proton NMR spectra of uncomplexed d -(TTGGGGT)₄ and complex of luteolin with d -(TTGGGGT)₄ at 298 K.



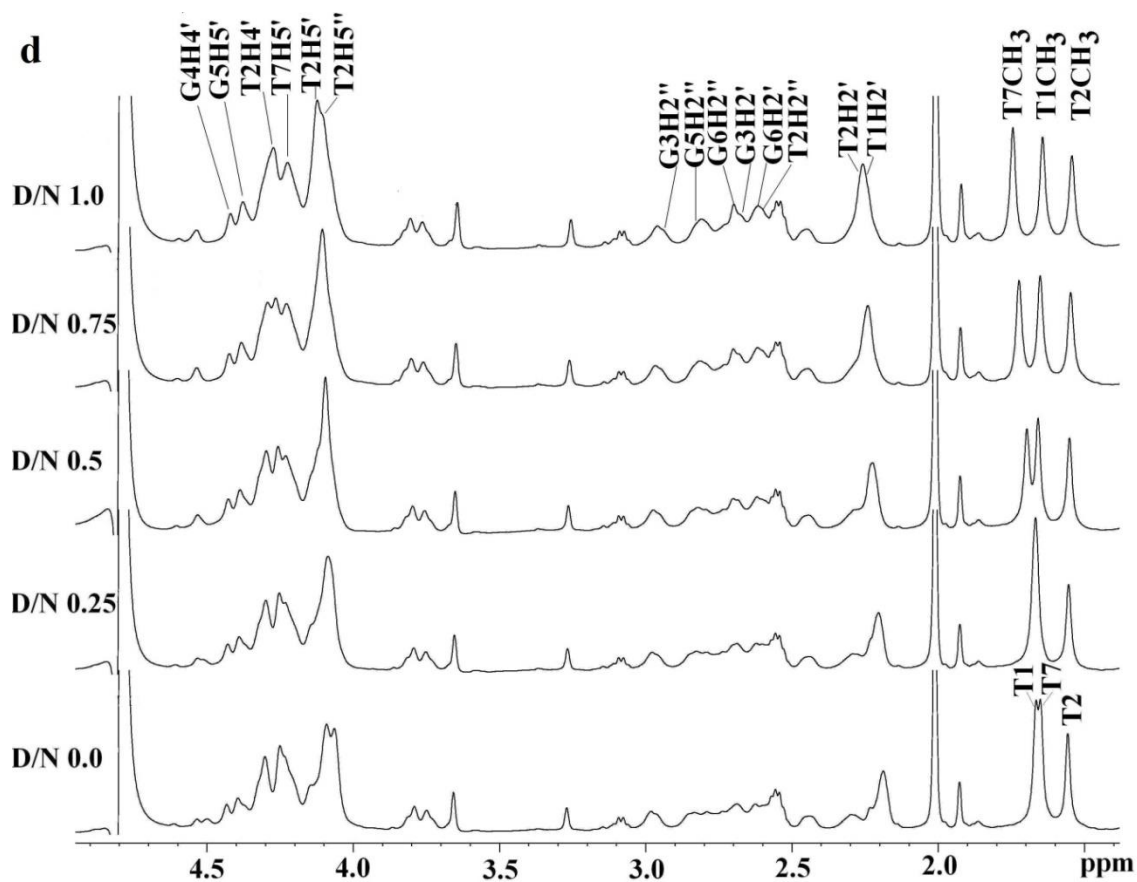


Fig. 5.30: $1\text{D } ^1\text{H}$ NMR spectra of luteolin- d -(TTGGGGT) $_4$ complex at 298 K showing change in the quadruplex and luteolin proton resonances upon titration (b) imino proton region; (c-d) base and sugar regions.

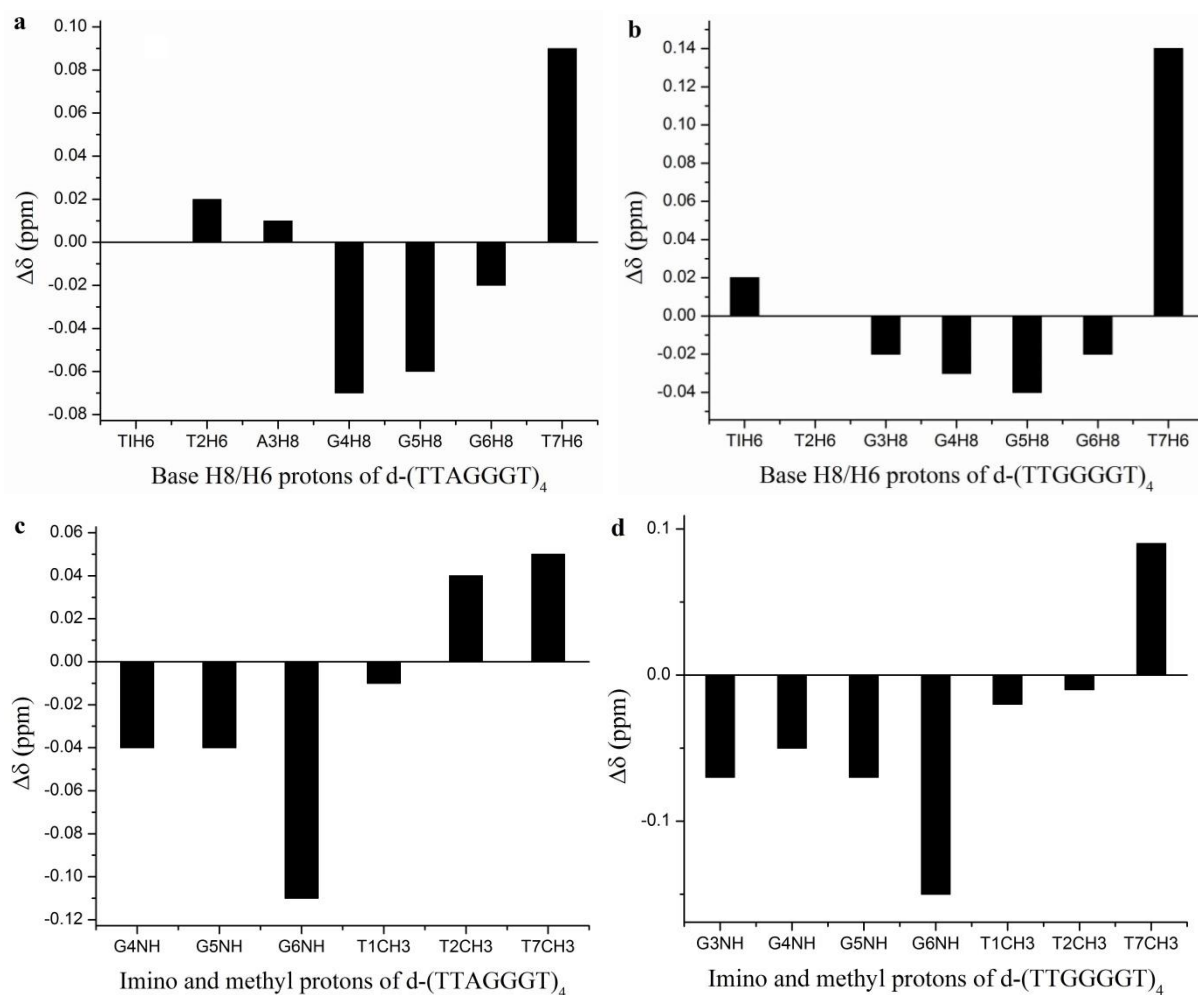


Fig. 5.31: Difference in the chemical shifts ($\Delta\delta$) of base protons on d-(TTAGGGT)₄ (a, c) and d-(TTGGGGT)₄ (b, d) on binding of luteolin.

5.1.12 Temperature dependent studies revealing the stability of luteolin-d-(TTGGGGT)₄ complex

The NMR spectra were recorded as a function of temperature (**Fig. 5.32-5.33**). The GNH protons shifted downfield by ~ 0.1 ppm while the other base H8/H6/CH₃ protons showed shift in either direction with increase in temperature (**Table 5.21-5.22**). The magnitude of shifts was less in case of G6 and T7 bases, which was probably due to the involvement of these protons in binding that in turn result into their stabilization. The luteolin protons, particularly H8 and H6 protons shifted downfield by ~ 0.2 ppm (**Table 5.23-5.24**).

However, there were no abrupt shifts in any of the DNA or luteolin protons with an increase in the temperature, indicating that bound complex is fairly stable and exists even at 353 K. The guanine

imino signals resonating between 10.0-11.5 ppm at all temperatures are indicative of the formation of G-quadruplex, which is intact in the present case after binding to luteolin. The intensity of these signals decreases with temperature and eventually disappears at higher temperatures due to disruption of hydrogen bonds holding the G-quartet structure. It was observed that G3NH and G6NH disappeared at 343 K while G4NH and G5NH were intact being part of the central G-tetrad (**Fig. 5.34**). On binding to luteolin G3NH and G6NH still persisted at 348 K. Unlike the uncomplexed quadruplex melting where the decrease in intensity of both G3 and G6NH peak were same, in the complexed quadruplex the intensity of both the peaks were different. G6NH being more stabilized than G3NH. This increase in the stabilization is due to the binding of luteolin near G6 base.

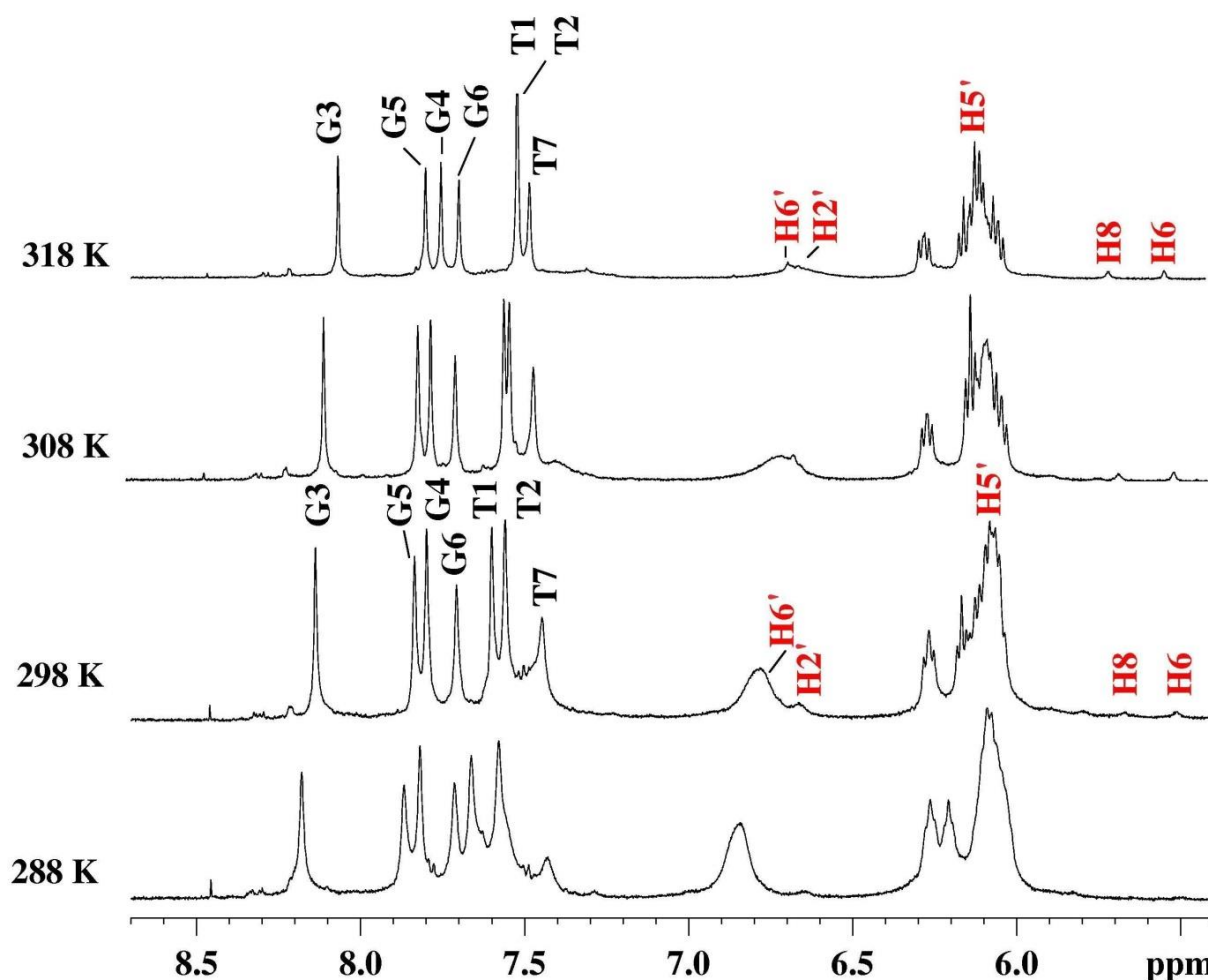


Fig. 5.32: $1D$ 1H NMR spectra of luteolin- d -(TTGGGGT) $_4$ complex as a function of temperature at $D/N=1.0$ showing change in the quadruplex and luteolin proton resonances.

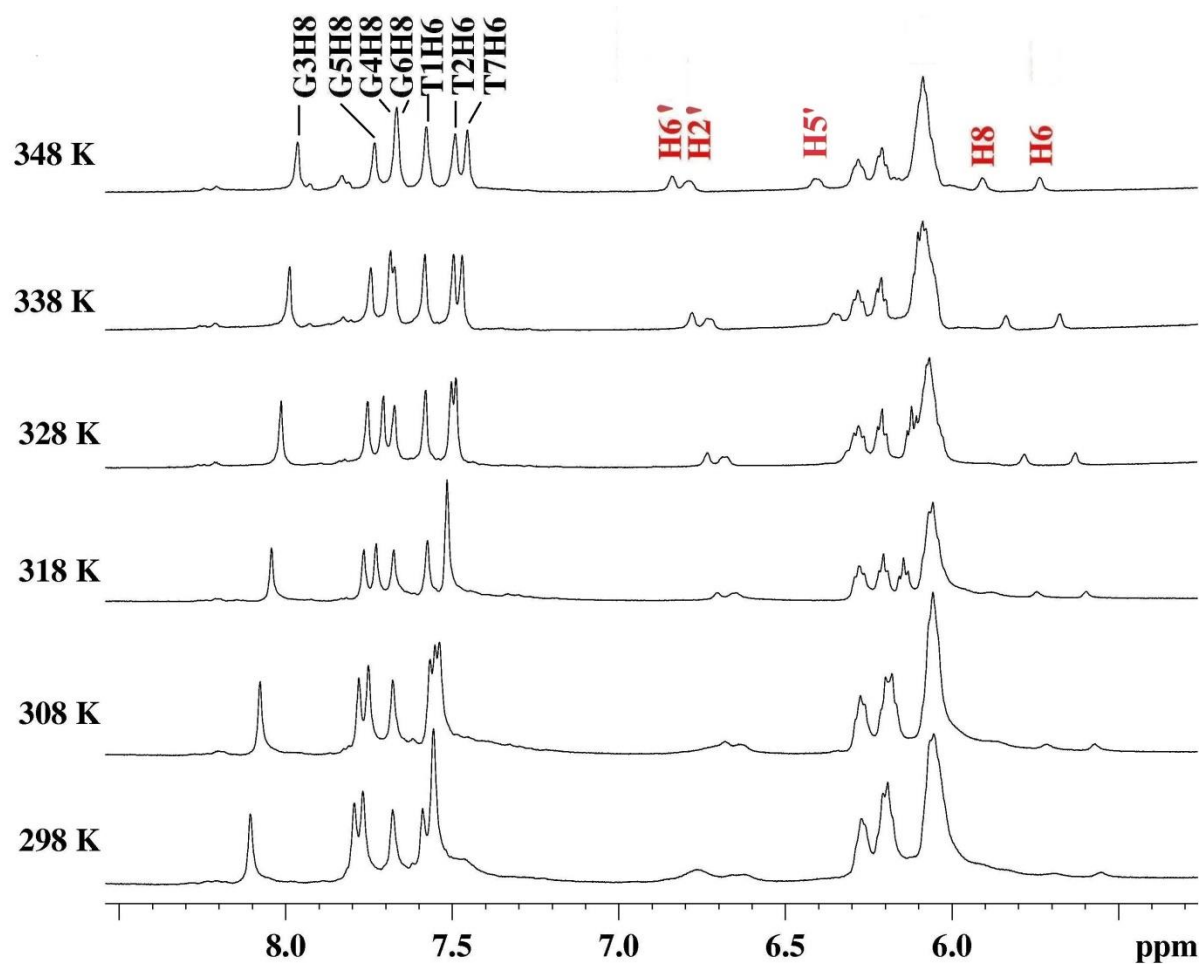


Fig. 5.33: $1D$ 1H NMR spectra of luteolin-d-(TTGGGGT) $_4$ complex as a function of temperature at $D/N=2.0$ showing change in the quadruplex and luteolin proton resonances.

Thus we can say that the structure of G-quadruplex was stabilized by about 10 K on binding to luteolin. The stabilization was less compared to that of luteolin-d-(TTAGGGT) $_4$ complex where two molecules of luteolin were involved in binding. These results are also in favor of groove binding, since end-stacking results into greater stabilization (Gavathiotis *et al.*, 2003)

Temp.(K)	G3NH	G4NH	G5NH	G6NH
278	11.49	11.09	10.88	10.76
283	11.49	11.09	10.88	10.75
288	11.51	11.09	10.92	10.83
293	11.50	11.08	10.93	10.83
298	11.50	11.07	10.93	10.83
303	11.49	11.06	10.93	10.82
308	11.49	11.06	10.93	10.82
313	11.50	11.06	10.94	10.81
318	11.50	11.06	10.94	10.81
323	11.51	11.07	10.95	10.81
328	11.53	11.09	10.97	10.86
333	11.53	11.09	10.97	10.86
338	11.54	11.09	10.97	10.86
343	11.54	11.10	10.98	10.86
348	11.54	11.10	10.98	10.86
353	11.54	11.11	10.98	10.86
358		11.11	10.98	
363		11.11	10.98	
$\Delta\delta$	0.05	0.02	0.10	0.10

Temp.(K)	T1H6	T2H6	G3H8	G4H8	G5H8	G6H8	T7H6	T1CH ₃	T2CH ₃	T7CH ₃
278	7.62	7.59	8.20	7.82	7.89	7.73	7.48	-	1.53	1.67
283	7.69	7.58	8.18	7.81	7.86	7.70	7.48	1.66	1.54	1.70
288	7.66	7.57	8.18	7.81	7.86	7.71	7.48	1.66	1.54	1.70
293	7.62	7.56	8.15	7.80	7.84	7.71	7.48	1.66	1.54	1.70
298	7.61	7.56	8.13	7.79	7.82	7.70	7.49	1.65	1.55	1.75
303	7.57	7.54	8.12	7.78	7.82	7.70	7.45	1.66	1.55	1.73
308	7.55	7.53	8.09	7.77	7.81	7.69	7.46	1.66	1.55	1.73
313	7.53	7.52	8.08	7.76	7.80	7.69	7.47	1.67	1.56	1.73
318	7.52	7.51	8.06	7.74	7.79	7.69	7.47	1.68	1.58	1.75
323	7.52	7.50	8.05	7.74	7.79	7.69	7.48	1.69	1.59	1.75
$\Delta\delta$	-0.10	-0.09	-0.15	-0.08	-0.10	-0.04	0.00	0.03	0.06	0.08

Table 5.21: Chemical shift (ppm) of *d*-(TTGGGGT)₄ protons in luteolin-*d*-(TTGGGGT)₄ complex at *D/N*=1.0 as a function of temperature along with the net change in chemical shift with temperature, that is, $\Delta\delta = \delta(363\text{ K}) - \delta(278\text{ K})$.

Temp.(K)	G3NH	G4NH	G5NH	G6NH
278	11.44	11.06	10.84	10.64
288	11.42	11.03	10.85	10.66
298	11.41	11.02	10.86	10.67
308	11.42	11.02	10.87	10.67
318	11.43	11.02	10.88	10.66
328	11.44	11.03	10.89	10.66
338	11.46	11.04	10.90	10.65
348	11.46	11.06	10.90	10.65
353	11.46	11.06	10.90	10.64
$\Delta\delta$	0.02	0.00	0.06	0.00

Temp.(K)	T1H6	T2H6	G3H8	G4H8	G5H8	G6H8	T7H6	T1CH ₃	T2CH ₃	T7CH ₃
278	7.62	7.59	8.19	7.74	7.80	7.67	7.53	1.65	1.54	1.74
288	7.64	7.57	8.14	7.78	7.81	7.68	7.54	1.62	1.53	1.76
298	7.59	7.55	8.10	7.77	7.79	7.68	7.55	1.61	1.53	1.78
308	7.56	7.55	8.07	7.75	7.78	7.68	7.54	1.62	1.54	1.79
318	7.57	7.51	8.04	7.73	7.76	7.67	7.51	1.64	1.56	1.81
328	7.58	7.50	8.01	7.70	7.75	7.67	7.49	1.66	1.59	1.81
338	7.58	7.49	7.98	7.68	7.74	7.67	7.47	1.68	1.63	1.82
348	7.57	7.49	7.96	7.66	7.73	7.65	7.45	1.70	1.66	1.83
353	7.57	7.49	7.95	7.66	7.72	7.66	7.45	1.71	1.68	1.83
$\Delta\delta$	-0.05	-0.10	-0.24	-0.08	-0.08	-0.01	-0.08	0.06	0.14	0.09

Table 5.22: Chemical shift (ppm) of *d*-(TTGGGGT)₄ protons in luteolin-*d*-(TTGGGGT)₄ complex at *D/N*=2.0 as a function of temperature along with the net change in chemical shift with temperature, that is, $\Delta\delta = \delta(353\text{ K}) - \delta(278\text{ K})$.

Temp.(K)	H6'	H2'	H5'	H3	H8	H6
278						
283						
288		6.65	6.08		5.65	5.50
293		6.65	6.08		5.66	5.50
298	6.68	6.66	6.08		5.67	5.51
303	6.68	6.66	6.08		5.67	5.51
308	6.67	6.65	6.08		5.68	5.51
313	6.67	6.65	6.08		5.69	5.52
318	6.68	6.65	6.10		5.70	5.52
323	6.69	6.65	6.10		5.70	5.51
328	6.69	6.65			5.70	5.52
333	6.69	6.66			5.71	5.53
338	6.69	6.66			5.72	5.54
343	6.70	6.67			5.73	5.55
348	6.70	6.69			5.76	5.58
353	6.73	6.71			5.78	5.60
358	6.76	6.73			5.81	5.63
363	6.82	6.73			5.88	5.69
$\Delta\delta$	0.14	0.08	0.02		0.23	0.19

Table 5.23: Chemical shift (ppm) of luteolin protons in luteolin-d-(TTGGGGT)₄ complex at D/N=1.0 as a function of temperature along with the net change in chemical shift with temperature, that is, $\Delta\delta = \delta(363\text{ K}) - \delta(278\text{ K})$.

LUT	H6'	H2'	H5'	H3	H8	H6
278		6.58				
288		6.60			5.65	5.53
298	6.66	6.62		6.05	5.69	5.55
308	6.67	6.63		6.06	5.71	5.57
318	6.70	6.65		6.06	5.74	5.59
328	6.73	6.67	6.32	6.06	5.78	5.62
338	6.78	6.72	6.34	6.07	5.83	5.67
348	6.84	6.78	6.40	6.08	5.90	5.73
353	6.87	6.82	6.44	6.08	5.94	5.77
$\Delta\delta$	0.21	0.24	0.12	0.03	0.29	0.24

Table 5.24: Chemical shift (ppm) of luteolin protons in luteolin-d-(TTGGGGT)₄ complex at D/N=2.0 as a function of temperature along with the net change in chemical shift with temperature, that is, $\Delta\delta = \delta(353\text{ K}) - \delta(278\text{ K})$.

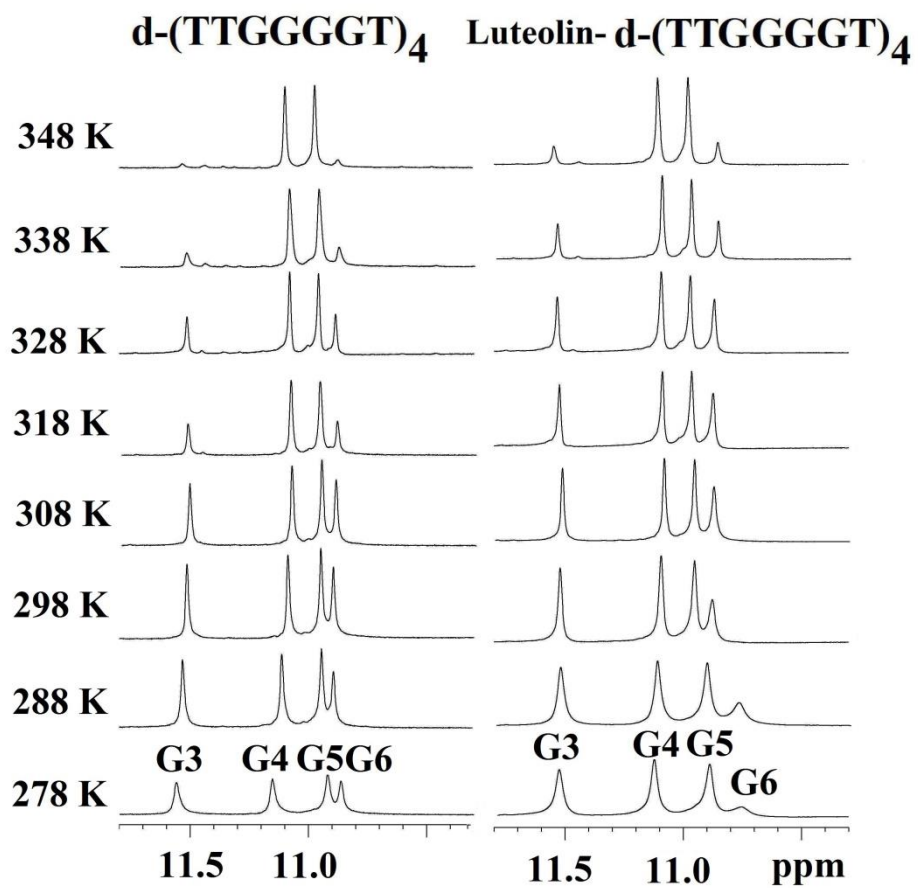


Fig. 5.34: *1D* ^1H NMR spectra of imino protons region of $d\text{-(TTGGGGT)}_4$ and luteolin- $d\text{-(TTGGGGT)}_4$ complex revealing the stability of complex with temperature.

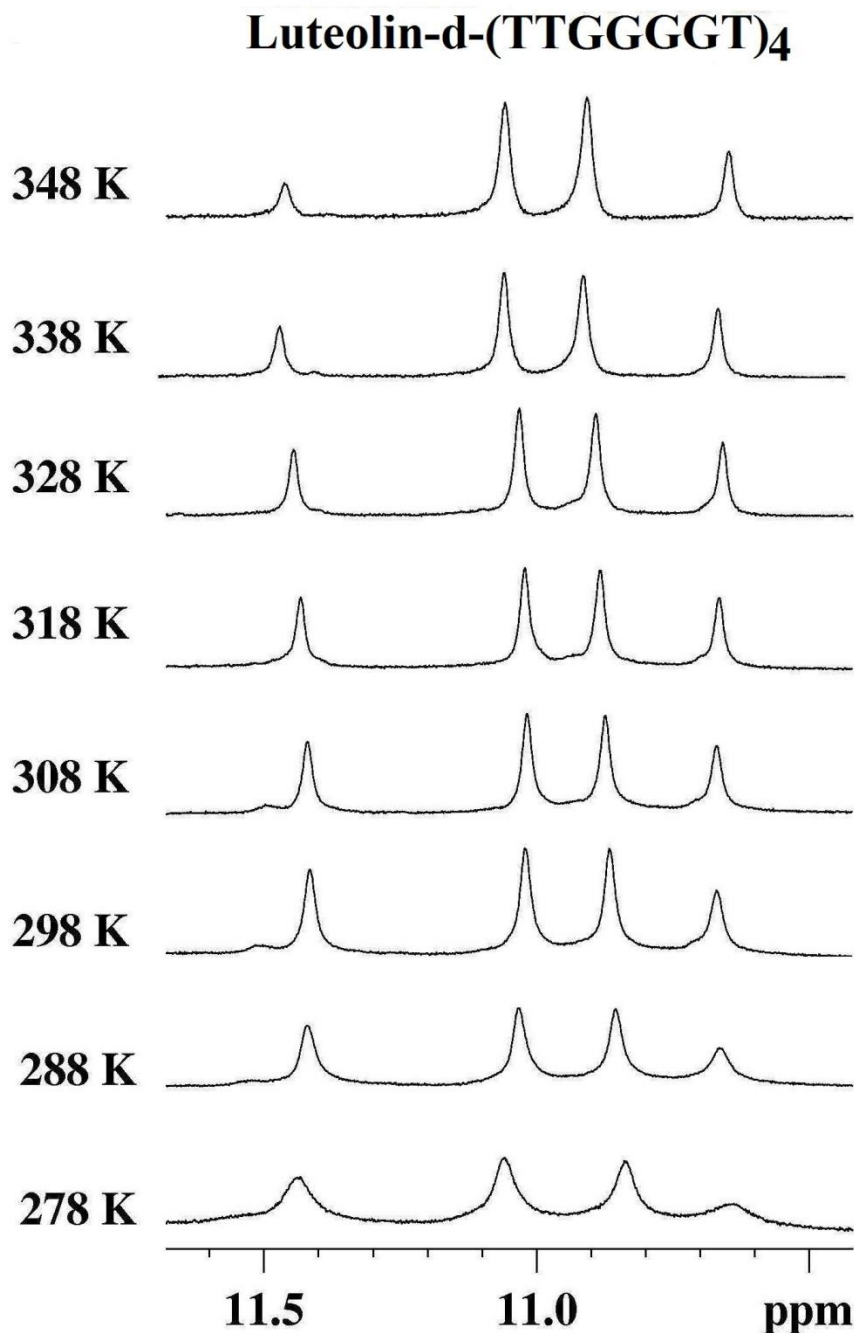


Fig. 5.34: *1D* ^1H NMR spectra of imino protons region of $d\text{-(TTGGGGT)}_4$ and MTX-d-(TTGGGGT)_4 complex revealing the stability of complex with temperature.

5.1.13 Phosphorous-31 NMR studies of luteolin-d-(TTGGGGT)₄ complex

The phosphorus signals were assigned using standard strategies by ^1H - ^{31}P HMBC spectra, that is, T1pT2 shows ^3J coupling with T1H3', T2H5'/5'' and ^4J coupling with T2H4' and so on for other ^{31}P signals (**Fig. 5.35**). This for the first time we are reporting the ^{31}P signals of uncomplexed $d\text{-(TTGGGGT)}_4$. Till date there is no literature available for changes in ^{31}P resonance positions upon

interaction of ligands with quadruplex DNA. We observe six ^{31}P signals, which corresponds to T1pT2, T2pG3, G3pG4, G5pG6 and G6pT7. These resonances were sharp when compared to that of d-(TTAGGGT) $_4$ ^{31}P resonance. The phosphorus-31 NMR spectra of unbound and bound d-(TTAGGGT) $_4$ were recorded at different temperature (278-328 K) during the course of titrations with luteolin (**Fig. 5.36**). On progressive addition of luteolin, the ^{31}P NMR signals showed minor sequence dependent shifts (**Table 5.25**). The G5pG6 signal showed upfield shift while rest of the ^{31}P signals shifted downfield. The luteolin-d-(TTGGGGT) $_4$ complex showed a maximum downfield shift (0.12 ppm) in G6pT7 step. In case of luteolin-d-(TTAGGGT) $_4$ complex similar shift was observed for T1pT2 steps. This indicates that the binding of luteolin to d-(TTGGGGT) $_4$ is slightly different to that luteolin-d-(TTAGGGT) $_4$ complex. At higher temperature (**Fig. 5.37**) the resonances were sharp and well resolved unlike that of luteolin-d-(TTGGGGT) $_4$ complex, where the resonance assignment was tedious due to the presence of extra signals. This difference in the ^{31}P signals of both the sequence is due to the difference in their structure.

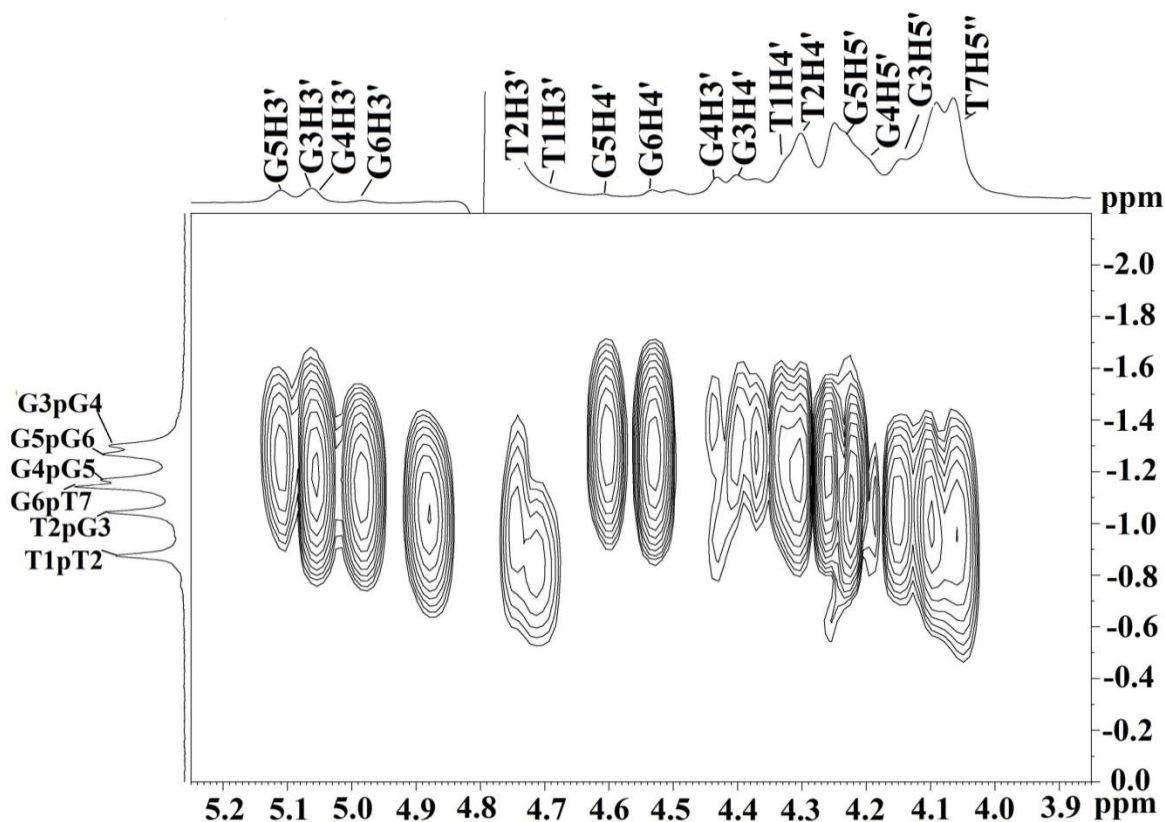


Fig. 5.35: $2D$ ^{31}P - ^1H HMBC spectrum of d-(TTGGGGT) $_4$ at 298 K.

	DN = 0	DN = 1.0	$\Delta\delta$
T1pT2	-0.88	-0.84	0.04
T2pG3	-1.11	-1.08	0.03
G3pG4	-1.20	-1.16	0.04
G4pG5	-1.35	-1.32	0.03
G5pG6	-1.30	-1.34	-0.04
G6pT7	-1.20	-1.08	0.12

Table 5.25: Chemical shift of ^{31}P resonances of the phosphate groups of $d\text{-(TTGGGGT)}_4$, in luteolin- $d\text{-(TTAGGGT)}_4$ complex at 298 K with increasing D/N ratios.

In case of $d\text{-(TTAGGGT)}_4$ sequence the 5' TTA bases are more flexible while that of $d\text{-(TTGGGGT)}_4$ sequence the T bases on both the ends are somewhat stacked due to the effect of the adjacent G-tetrads.

We have not observed any cross peaks due to exchange between the bound and free phosphate resonances in the 2D ^{31}P NMR exchange spectrum of luteolin- $d\text{-(TTGGGGT)}_4$ complex and a single set of resonances were present. This clearly shows that ^{31}P signals from the bound quadruplex were in fast exchange with the corresponding signals from free quadruplex on the NMR time scale.

Small upfield shifts are generally caused by electrostatic interactions between drug and duplex DNA (Patel, 1979; Wilson and Jones, 1982) while minor upfield/downfield shifts are expected on widening/narrowing of O-P-O ester bond angle (Gorenstein and Kar, 1975; Gorenstein, 1984). The observed shifts rule out opening of base pairs to permit intercalation of luteolin chromophore which is expected to result in large downfield shifts $\sim 1.6\text{-}2.6$ ppm (Gorenstein 1992; Patel and Canuel, 1976).

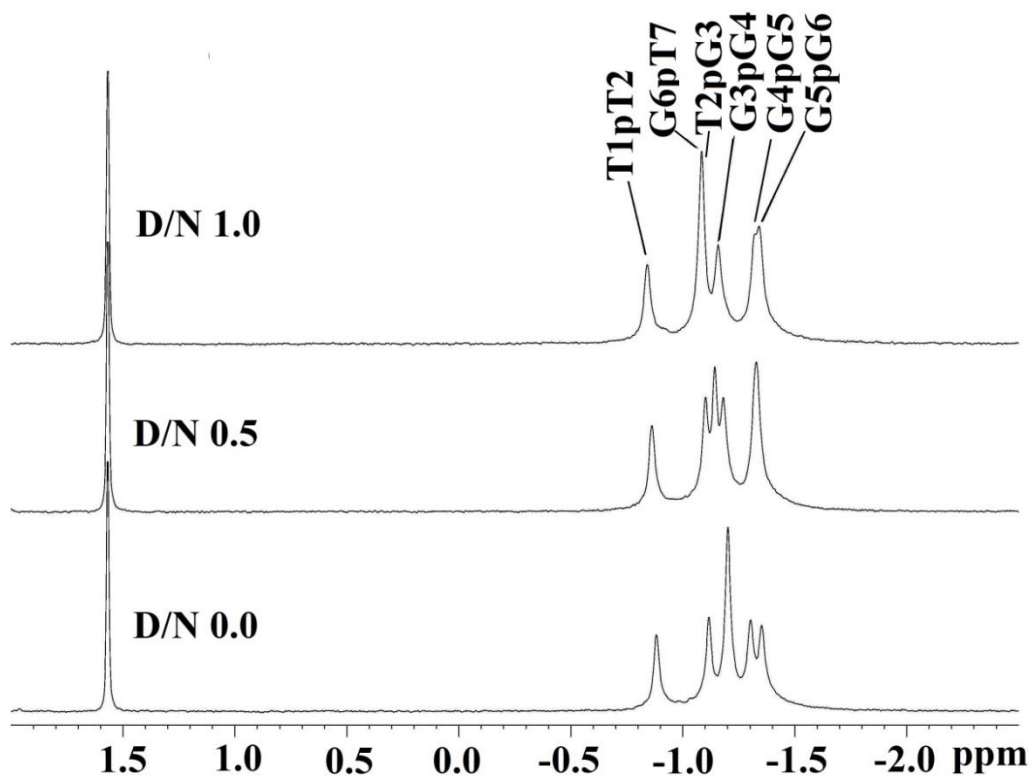


Fig. 5.36: Proton decoupled ^{31}P NMR spectra of $d\text{-(TTGGGGT)}_4$ in uncomplexed and complexed state with luteolin with increasing D/N ratios at 298 K.

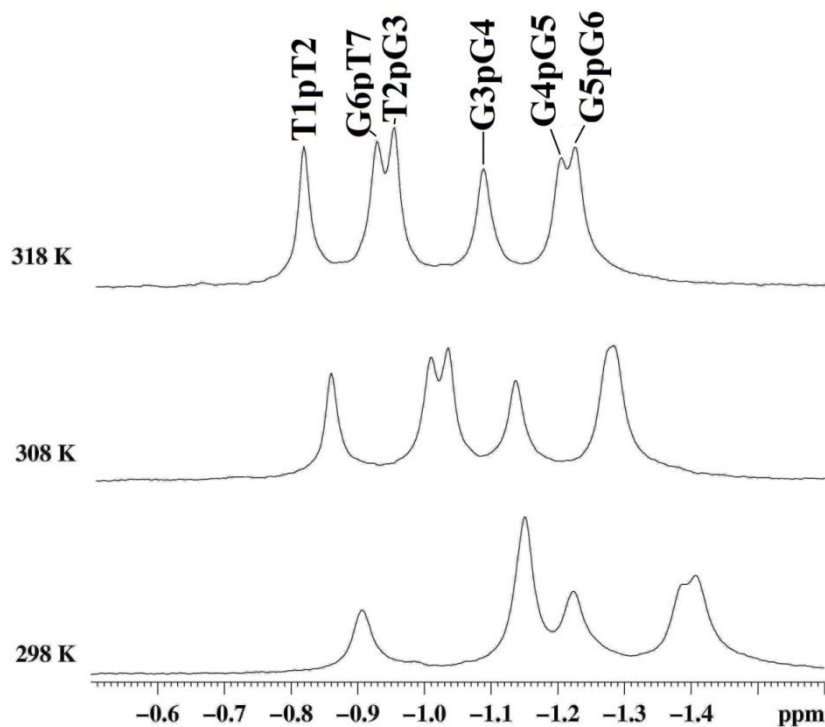


Fig. 5.37: Proton decoupled ^{31}P NMR spectra of luteolin- $d\text{-(TTGGGGT)}_4$ as a function of temperature at $D/N=1.0$.

5.1.14 Structural studies of luteolin-d-(TTGGGGT)₄ complex

NOESY spectra were recorded with variable mixing times τ_m 100, 200, 250 ms and analyzed at D/N=1:1. We observed intermolecular NOE connectivities only with G5, G6 and T7 residues unlike that observed in the case of luteolin-d-(TTAGGGT)₄ complex. This shows that luteolin probably binds at one site. The connectivities were similar at both D/N 1.0 and 2.0. Hence we have done the structural analysis at D/N 1.0. The NOESY spectra of complex contain several intramolecular NOE connectivities within quadruplex and few in luteolin in addition to intermolecular connectivities between quadruplex and luteolin. The presence of all sequential connectivities between base-H1'/H2'', H2'' and NH-NH protons, indicate that all G-quartets were intact and quadruplex adopts a right handed helical structure with no opening of base pairs at any step. This excludes the possibility of intercalation of luteolin chromophore between base pairs. **Table 5.26** shows the intramolecular NOE connectivities observed within the luteolin molecule in the luteolin-d-(TTGGGGT)₄ complex at D/N=1.0. The meta coupled proton H6', H5', which was clearly observable in COSY spectra was not clearly evident in NOESY spectra due to overlapped signals. A strong NOE connectivities were observed between luteolin protons H3 and H6' and a medium connectivities between H3 and H2' in luteolin-d-(TTAGGGT)₄ complex. These connectivities were not clearly observed in case of luteolin-d-(TTGGGGT)₄ complex, which shows that the position of luteolin is different in both the complexes.

SI No.	Intramolecular connectivities
1	H2'-H8
2	H6'-H5'

Table 5.26: *Interproton NOE connectivities within luteolin molecule in luteolin-d-(TTAGGGT)₄ complex at D/N=1.0 at 298 K.*

Proton	δ ppm	NOE	NOE	NOE	NOE	NOE
H2'	6.66	G5H1'	G6H1'	G6NH		
H8	5.67	G5H1'	G6NH			
H6	5.51	G5H3'	G6H2''	G6H8	G6NH	T7H1'

Table 5.27: *Intermolecular NOE connectivities between luteolin molecule and d-(TTGGGGT)₄ in luteolin-d-(TTGGGGT)₄ complex at D/N=1.0 at 298 K.*

A total of 10 intermolecular NOE connectivities were observed between luteolin protons and quadruplex but only non-overlapped peaks (**Table 5.27** and **Table 5.28**) were used for distance

calculation and for building model. Most of the Intermolecular NOE connectivities were observed between luteolin protons H2', H8 and H6 with sugar (H1', H2'', H3') and base (H8, NH) protons of G5, G6 and T7 bases of quadruplex (**Figs 5.38a-c**). These connectivities showed that the luteolin was most probably binding in the groove by spanning at all three bases. The intensity of these intermolecular connectivities increased due to more and more binding of luteolin to quadruplex. Unlike the luteolin-d-(TTAGGGT)₄ complex, which gave connectivities to both T1pT2 and G6pT7 steps, luteolin-d-(TTAGGGT)₄ complex gave connectivities with G5pG6 and G6pT7 steps. This shows that binding of luteolin is different in both the complexes. But one binding site in common for both the complexes. The difference in binding is probably due to differences in the structures, which is basically in the third base. Thus we can deduce that the substitution of A with G in the heptamer sequence has marked effect on the binding of luteolin.

5.1.15 Restrained Molecular dynamics studies of luteolin-d-(TTGGGGT)₄ complex

To obtain final structure of luteolin-d(TTGGGGT)₄ complex, distance restraints obtained from 1:1 complex NOESY ($\tau_m = 200\text{ms}$) at 298 K were used. Same strategy was used as mentioned in section 5.1.7 for rMD simulation except for the structure (PDB id 139D) that was used as the initial structure for tetramolecular quadruplex d-(TTGGGGT)₄. The simulation results are in accordance with the conclusion drawn from intermolecular NOEs connectivities. There was no significant change in the conformation of quadruplex DNA upon luteolin binding. Most of the luteolin contacts were centred at G5, G6, T7 bases. In fact luteolin span the groove of quadruplex structure. This result is totally opposite to what we have obtained in case of luteolin binding to d-(TTAGGGT)₄ complex. This is probably due to the difference in the base substitutions. The H2' proton of luteolin forms H-bond with G5NH₂ proton of quadruplex. The binding is stabilized by H-bonding and electrostatic interactions.

Intermolecular Connectivities	rMD Distance (Å)
H2'-G5H1'	3.5
H2'-G6H1'	4.5
H8-G5H1'	3.0
H6-G5H3'	4.0
H6-G6H2''	4.4

Table 5.28: Intermolecular NOE connectivities and rMD distances between luteolin molecule and d-(TTGGGGT)₄ in luteolin-d-(TTGGGGT)₄ complex at 1.0 at 298 K.

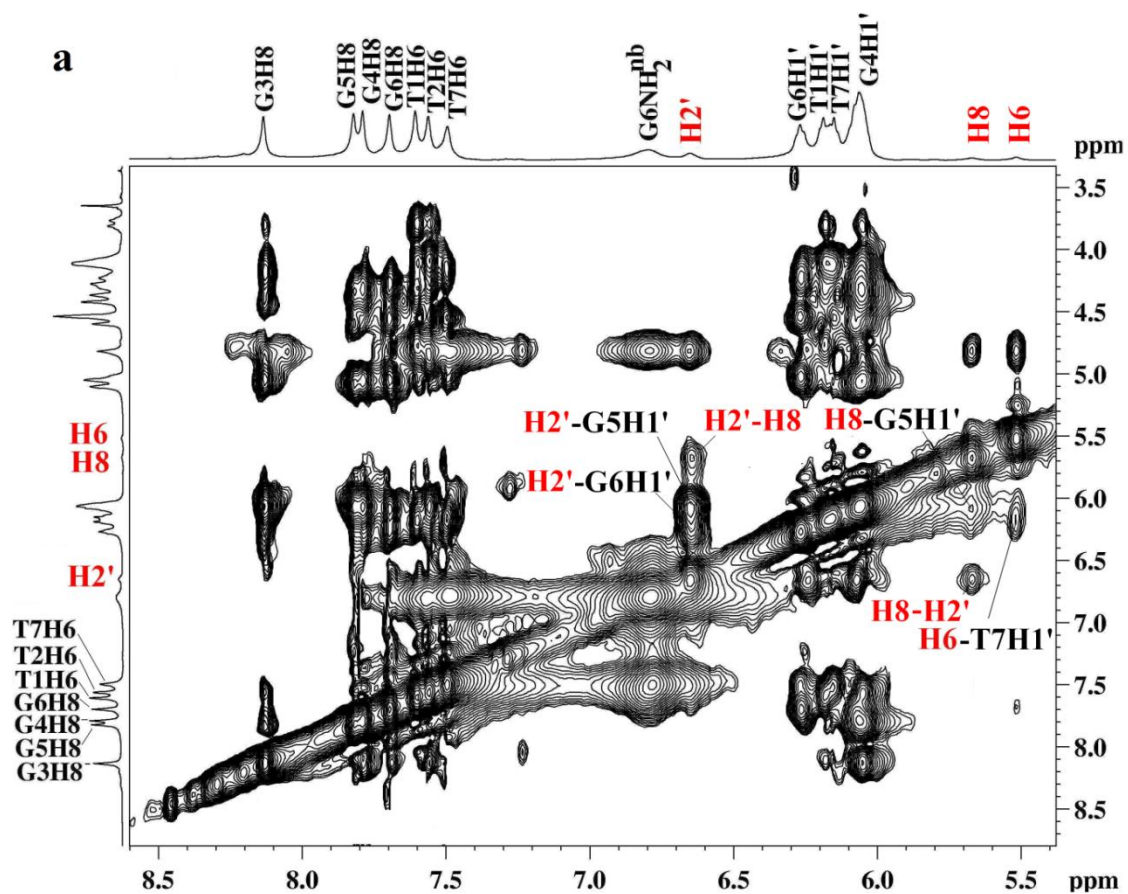


Fig. 5.38a: NOESY spectrum of luteolin-*d*-(TTGGGGT)₄ complex at *D/N*=1.0 at 298 K showing intermolecular NOE connectivities between H2', H8 and H6 protons of luteolin molecule and *d*-(TTGGGGT)₄.

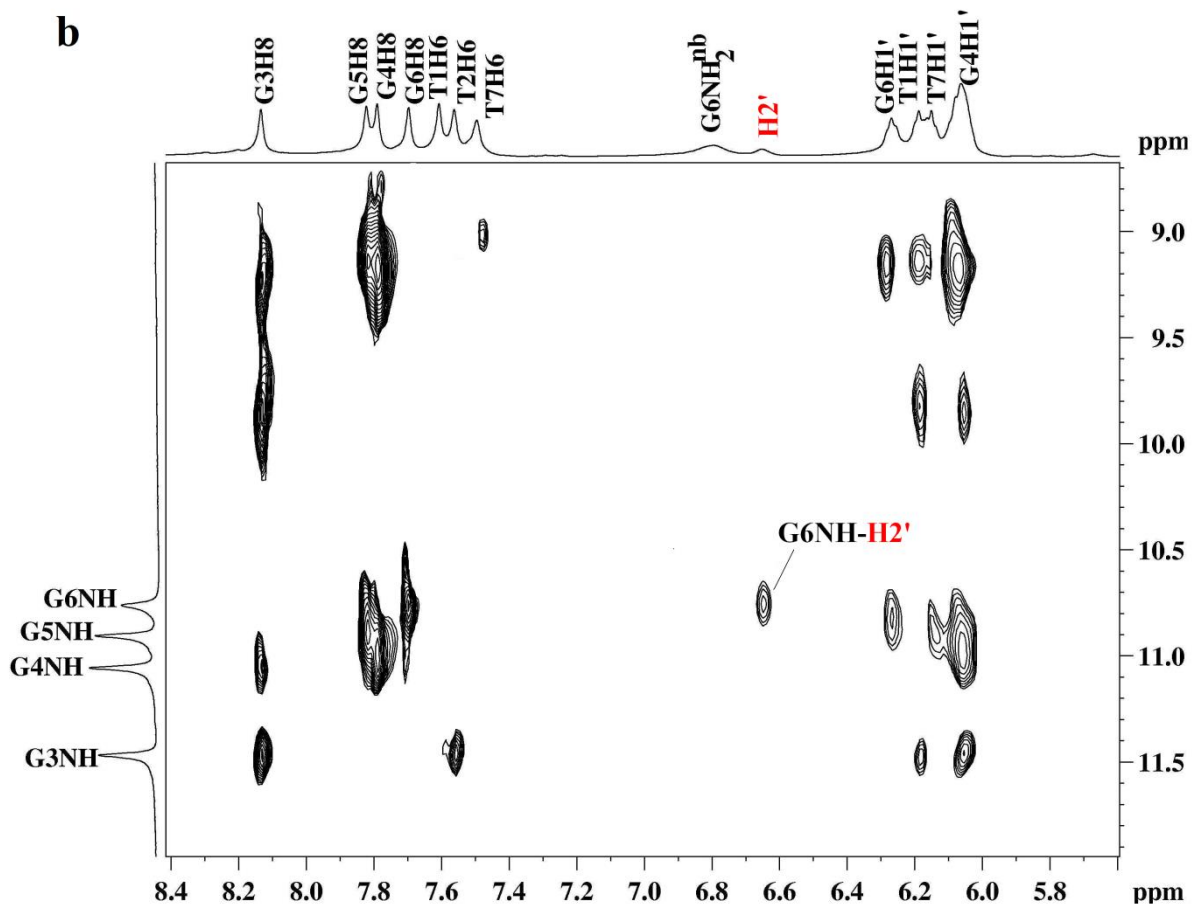


Fig. 5.38b: NOESY spectrum of luteolin-d-(TTGGGGT)₄ complex at D/N=1.0 at 298 K showing intermolecular NOE connectivity between H2' proton of luteolin molecule and G6NH proton of d-(TTGGGGT)₄.

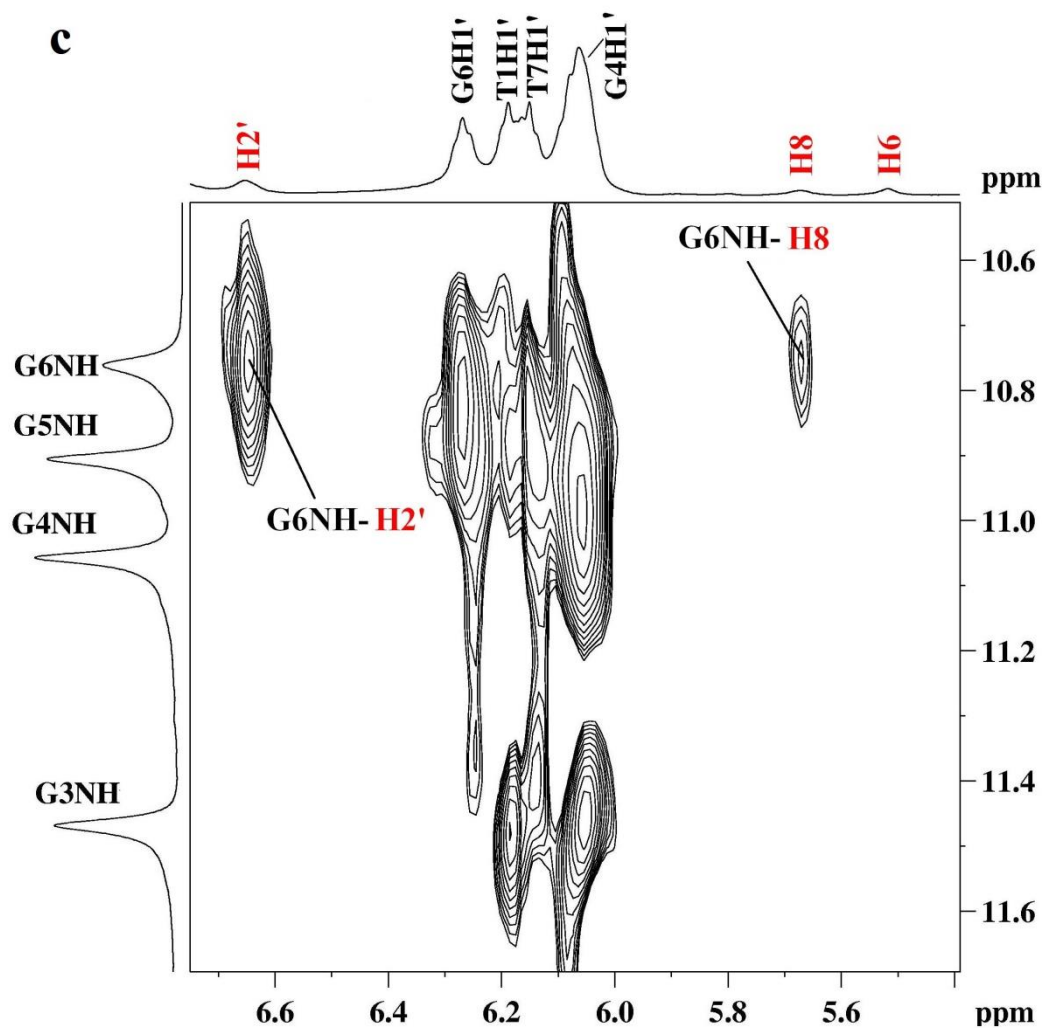
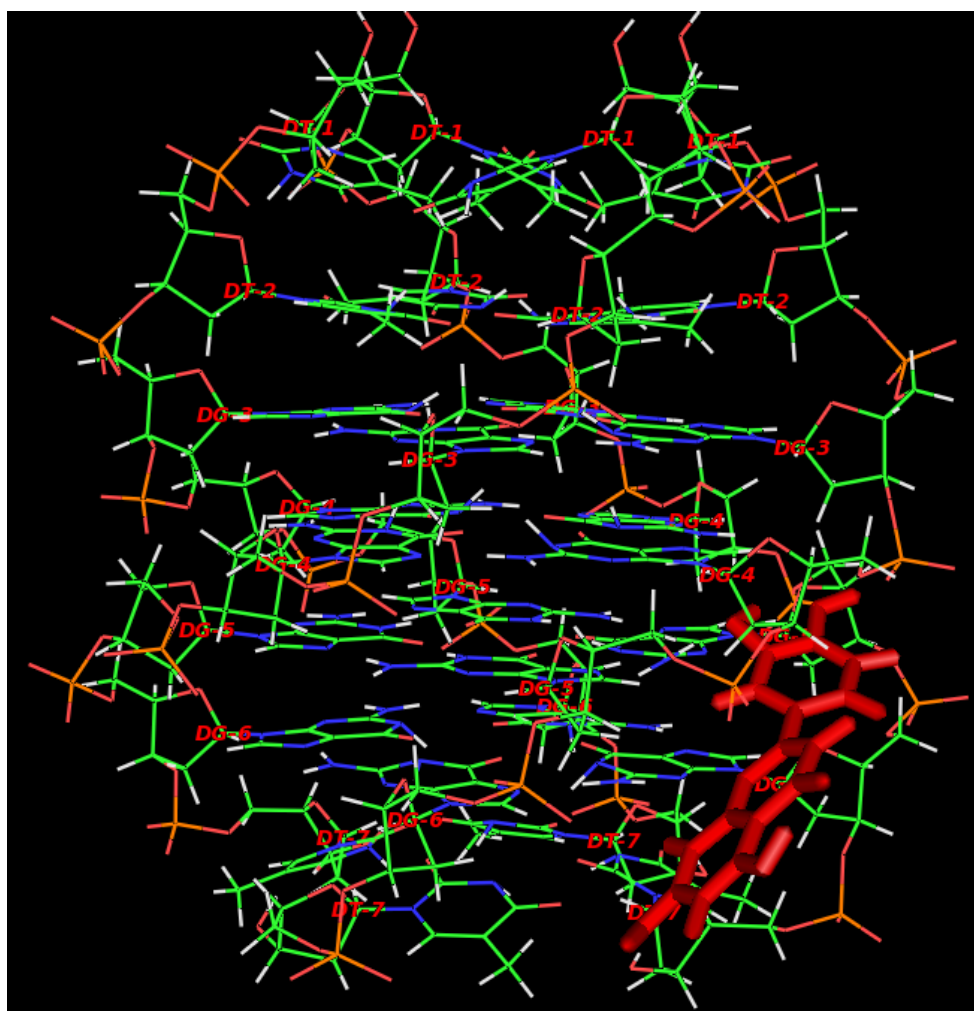


Fig. 5.38c: NOESY spectrum of luteolin- d -(TTGGGGT) $_4$ complex at $D/N=1.0$ at 298 K showing intermolecular NOE connectivities between H2' and H8 protons of luteolin molecule and d -(TTGGGGT) $_4$.

Experimental Restraints	
Intramolecular	
Luteolin-Luteolin	2
Quadruplex-Quadruplex	236
Intermolecular	
luteolin-quadruplex	5
CVFF energy (kcal mol ⁻¹) of the minimized structures	
Total	297.4
Non-bonded	-99.2
Restraint	170.2
Average rmsd	0.52Å
Restraint Violations	
Distance (>0.25Å)	5

Table 5.29: Experimental restraints and structure statistics of the final structure.



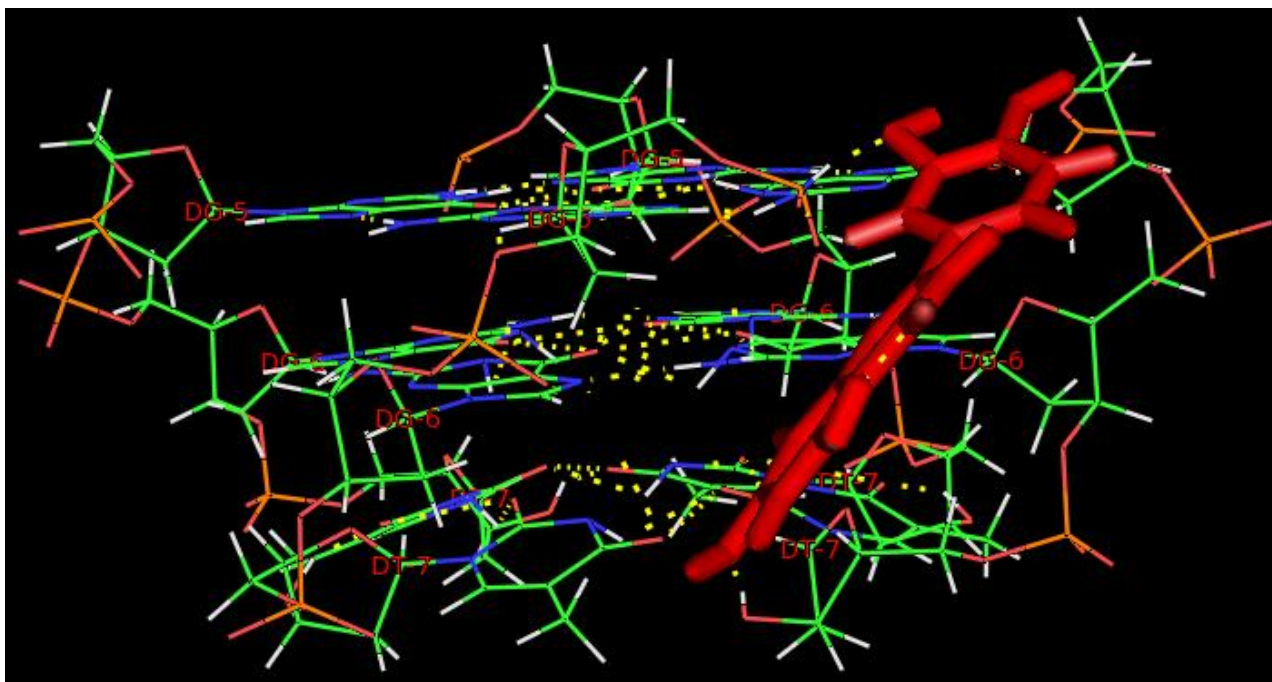


Fig. 5.39: Front and close view of the final structure of luteolin-d-(TTGGGGT)₄ complex obtained by restrained molecular dynamics simulations.

5.2 Characterizing the telomerase inhibitory effects of luteolin using TRAP Assay

Formation of G-quadruplex in the telomeric region of human chromosome followed by its stabilization with small ligands, leads to the uncapping of telomere as well as the inhibition of telomerase activity. It's a prominent strategy for anticancer therapy. So identification of G-quadruplex binding ligands have practical importance. Cancerous cells like MCF-7 have high level of telomerase activity, hence the telomerase extracted from this cell line was used as positive control. For negative control the reaction mixture was heated to inactivate telomerase activity. The telomerase inhibitory effect of luteolin was tested at increasing concentrations in the range of 0.1–100 μM . Since it's a fluorescence based assay so PCR products were directly quantified using a spectrofluorimeter. The relative fluorescence intensity $\Delta F/\Delta R$ was used as the measure of telomerase activity. **Fig. 5.36** shows that upon increasing the concentration of mitoxantrone from 0.01 μM to 100 μM the relative fluorescence intensity $\Delta F/\Delta R$ decreases. At 10 μM concentration MTX shows ~30 % inhibition of telomerase activity and at 100 μM the percentage of inhibition increases to 60 %. It shows IC_{50} value of 30 - 35 μM . The result of the TRAP assay confirms dose dependent telomerase inhibition by luteolin, which is owing to its binding and stabilization of G-quadruplex structure. The planar chromophore of flavonoid play an important role in the

interaction with DNA. Luteolin along with other flavonoids like daidzein, quercetin are known to bind to the G-quadruplex structures and in some cases they induce the formation and stabilization of G-quadruplex structure (Jin *et al.*, 2009; Jin *et al.*, 2010). The inhibition activity of luteolin is much smaller than that of MTX probably due to the lack of side chains. Presence of side chains facilitates the binding of MTX to groove apart from π - π stacking interaction of its aromatic chromophore. Thus we conclude that luteolin can be promising G4 ligands with implications towards G-quadruplex mediated telomerase inhibition for anticancer therapy.

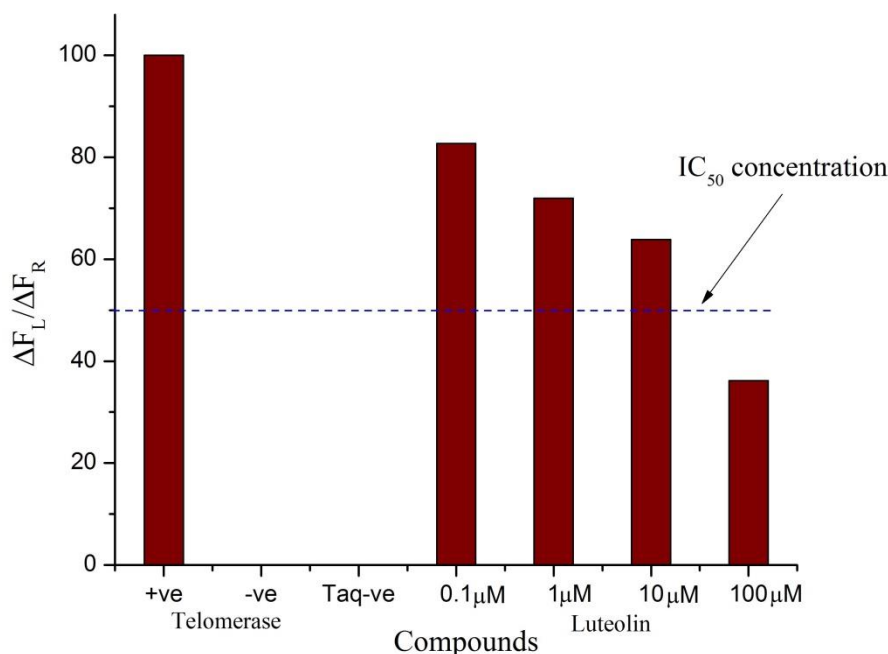


Fig. 5.40: Inhibitory effect of luteolin on telomerase activity determined by TRAP assay.

5.3: Conclusion

Luteolin a well-known flavone interact with duplex DNA in both intercalative and groove binding modes (Zhang *et al.*, 2012; Bi *et al.* 2006). These finding were based on spectroscopic studies and there was no detail structural studies reported till date, which could give a better insight into its exact binding mode. Non-canonical DNA structures like G-quadruplex gain much interest in the past few decades owing to its presence in many biologically significant regions of genome. They act as potential target for anti-cancer drug designing. We have chosen two oligonucleotide sequences d-(TTAGGGT)₄ and d-(TTGGGGT)₄ which have the ability to form quadruplex structure. In order to know the exact mode of binding and forces involved in the interaction of luteolin with G-quadruplex sequences d-(TTAGGGT)₄ and d-(TTGGGGT)₄ NMR techniques

followed by restrained Molecular Dynamics (rMD) simulations were employed. Both the sequence forms a parallel-stranded G-quadruplex structure in the presence of K⁺ ion, with C₄ symmetry in which all the four strands are equivalent. The presence of three well resolved imino (NH) peaks resonating between 10.5 to 12 ppm region along with NH-NH and NH-H8 NOE connectivities showed the formation of three G-tetrad. The existence of all sequential connectivities between base H8/H6-H1'/H2'/H2'' sugar protons indicates the presence of right handed helical geometry similar to that observed in B-DNA. The above mentioned connectivities were also observed in the complex d-(TTAGGGT)₄ and d-(TTAGGGT)₄, which inferred that the G-quartets were intact and there was no opening of base pairs at any step in the complex structures. Thus, there was no loss of original four fold symmetry of the quadruplex in both the complexes. Only a single set of luteolin and quadruplex protons resonances were seen at all D/N ratios, during the course of titration indicating that the binding was fast in NMR time scale. The interaction of luteolin with both the telomeric sequence showed change in G6pT7 step, but the magnitude of the shift was slightly greater in case of d-(TTGGGGT)₄ while there were no significant shift in the rest of the quadruplex. But in case of luteolin-d-(TTGGGGT)₄ complex there was a significant line broadening and decrease in the T1H6, T1CH₃ signals. All luteolin signals were upfield shifted from their corresponding positions in free luteolin by 0.67-0.80 ppm at D/N = 0.25. The signals do not shift any further with D/N and apparently the luteolin was completely bound at all D/N ratios in both the complexes.

The stability of complexes was assessed by monitoring the melting profile of imino signals, which is indicative of the formation of G-quadruplex structure. The result showed that the extent of stability was different for both the complexes. The luteolin-d-(TTAGGGT)₄ complex was stabilized by 25°C while that of luteolin-d-(TTGGGGT)₄ by 10°C. This difference in stability is because in case of the former two molecules of luteolin were involved in binding while in case of later only one luteolin was involved. There was no significant shift in ³¹P resonances, a maximum downfield shift of 0.12 ppm was observed in case of T1pT2 step for luteolin-d-(TTAGGGT)₄ complex. The Similar downfield shift was also observed for luteolin-d-(TTGGGGT)₄ complex but for G6pT7 step. This indicates that the binding of luteolin to d-(TTGGGGT)₄ is slightly different to that luteolin-d-(TTAGGGT)₄ complex. Absence of significant downfield shift of ³¹P resonances (> 1.5 ppm) in both the complexes excludes the possibility of opening of base pair at any step to permit intercalative mode of binding. Most of the intermolecular NOE contacts appeared between H2', H6', H6, H8 protons of luteolin and H1', H2'/H2'', CH₃ and NH of T1/T2/G6/T7 bases of d-

(TTAGGGT)₄. In case of luteolin-d-(TTGGGGT)₄ complex, same luteolin protons are involved in making short contacts with G5H1', G6H1', G6H2'', G6 NH and T7H1' protons. The rMD results showed that in case of luteolin-d-(TTAGGGT)₄ complex two molecules of luteolin bind one at T1pT2 step and other at G6pT7 step. A dual mode of interaction that is, both groove (at T1pT2 step) and partial end-stacking (at G6pT7 step) was observed. The complex was stabilized by stacking as well as electrostatic interaction. On the other hand only a single mode of binding (groove binding) occurs in case of luteolin-d-(TTGGGGT)₄ complex. The complex was stabilized by H-bonding and electrostatic interactions. The result showed that binding of luteolin is different in both the complexes. But one binding site is common for both the complexes. The difference in binding is probably due to differences in the structures, which is basically in the third base. Thus we can deduce that the substitution of A with G in the heptamer sequence has marked effect on the binding of luteolin. Luteolin shows a dose dependent telomerase inhibition, which was revealed by TRAP assay. This inhibition is due to stabilization of G-quadruplex structure on binding to luteolin. Though this inhibition is less in comparison to that of MTX but the result shows that luteolin can be a promising G4 ligand.

Conclusions and Perspectives

In recent years, telomeres and telomerase have attracted the interest of investigators due to their involvement with aging and cancer. The telomere, as the guardian of the chromosome performs essential functions that are regulated as part of the cell cycle, although many details of the events and players in telomere maintenance are as yet unclear. The only certainty is that telomerase, the key enzyme for telomere lengthening is overexpressed in about the 85% of cancer cells, thus favouring their immortalization. Hence, telomeres and telomerase represent promising targets for anti-cancer therapy. Among the strategies to target telomeres and telomerase, G-quadruplex interactive ligands appear to provide promising approaches. Several classes of molecules have been found to stabilize the folding of G-rich telomere strands into G-quadruplex structures, thereby inhibiting telomerase access. But lack of structural data of G-quadruplex-Ligand complexes has restricted their therapeutic applications. The aim of this work is to investigate the binding of both synthetic and natural ligand with G-quadruplex structure. In this respect, we have chosen two ligands from two different families; (a) mitoxantrone (MTX) - a synthetic anthraquinone derivative and (b) luteolin – a naturally occurring flavonoid. The present thesis presents deep insights into the structural interactions of human G-quadruplex forming telomere single repeat sequence d-(TTAGGGT) with luteolin and MTX, and *Tetrahymena* G-quadruplex forming telomere single repeat sequence d-(TTGGGGT) with luteolin. Both the sequences form right handed parallel stranded G-quadruplexes in presence of K⁺ ion with anti glycosidic torsion angles. Both luteolin and mitoxantrone have planar aromatic ring systems, which can easily interact with the planar surface of G-quartet and the presence of cationic side chains and hydroxyl group aid in its interaction to the grooves of quadruplexes. Till date not a single X-ray crystal/NMR structure is available on G-quadruplex structures with anthraquinone derivatives and flavonoid complexes.

The binding interactions of telomeric G-quadruplex sequences with these ligands were studied by various biophysical techniques such as; absorption, fluorescence, circular dichroism (CD) and nuclear magnetic resonance. They provide insights into the affinity, stability and stoichiometry of the G-quadruplex-ligand complex. Further, structural elucidation of ligand-G-quadruplex complex was obtained using Nuclear Magnetic Resonance (NMR) techniques in combination with restrained Molecular Dynamics (rMD) simulations. Finally, TRAP assay

reactions were carried out with these ligands to assess their ability towards telomerase enzyme inhibition, which in turn can throw light about their anticancer property.

So, in order to investigate the binding, stabilization and inhibition properties of mitoxantrone with human G-quadruplex DNA, several spectroscopic and thermodynamic techniques were employed. Binding of MTX to quadruplex showed hypochromicity and red shift in the visible band of MTX. Apparently two modes of binding was observed one at higher D/N ratios and another at low D/N ratio. This dual mode of interaction was further revealed by fluorescence studies, which not only showed a higher binding affinity of MTX to quadruplex but also gave the probable stoichiometry of both 1:1 and 2:1 for MTX-d-(TTAGGGT)₄ complex. The stoichiometry obtained from job plot correlated with this finding. Fluorescence life time studies also confirm the existence of two species with an increase in a fluorescence life time value compared to that of free MTX. Presence of induced negative CD (ICD) band within the absorption range of MTX molecule, gives a clear proof of the formation of bound complex of MTX-d-(TTAGGGT)₄. The binding of MTX leads to thermal stabilization of G-quadruplex structure which was confirmed independently by CD thermal melting studies and DSC studies. Both results showed a net stabilization 13°C on the binding of MTX. MTX shows a dose dependent telomerase inhibition revealed by TRAP assay (IC₅₀=2µM). This inhibition is owing to the stabilization of G-quadruplex structure. These findings reveal that MTX can be a promising G4 ligand with implications towards G-quadruplex mediated telomerase inhibition for anticancer therapy. Luteolin also shows a dose dependent telomerase inhibition but the extent of inhibition was less compared to MTX (30-35 µM). This difference in inhibition is due to the structural change of both the ligand since MTX has both aromatic ring and side chains which enhances its binding to quadruplex.

In order to know the exact mode of binding and forces involved in the interaction of MTX and luteolin with G-quadruplex structure, NMR techniques followed by restrained Molecular Dynamics (rMD) simulations were employed. Binding of both the ligand have not altered the four fold symmetry of G-quadruplex, which is evident by the presence of all the sequential connectivities between base and G-tetrads. Presence of all the sequential connectivities between base H8/H6 with H1'/H2'/H2'' sugar protons along with the absence of significant downfield shift (>1.5 ppm) in ³¹P NMR exclude the possibility of opening of base pair at any step to permit intercalative mode of binding. Single set of quadruplex and ligand protons were observed at all D/N ratios, during the course of titration indicating that the binding is fast in NMR time scale. Upfield shift of imino signal was observed in both the complexes which is indicative of stacking

interaction. In case of luteolin there was a significant shift in the G6pT7 step of both the quadruplex (d-(TTAGGGT)₄ and d-(TTGGGGT)₄). But the magnitude of shift was greater in case of d-(TTGGGGT)₄. Both the MTX and luteolin protons showed an upfield shift on binding. In case of MTX 2/3 H, 1/4 OH and 11 CH₂ showed maximum upfield shift while in case of luteolin all the proton signals were upfield shifted from their corresponding positions in free luteolin by 0.67-0.80 ppm. Both the MTX and luteolin proton signal did not shift any further beyond D/N 0.25, i.e., with increasing D/N. This showed that both the ligands are completely bound at all D/N ratios in both the complexes. This binding lead to the stabilization of all the three complexes but the extent of stability was different. The stability of MTX/Luteolin-d-(TTAGGGT)₄ complexes was greater (25°C) than that of luteolin-d-(TTGGGGT)₄ (10°C). This is because in the former two ligand molecules are involved in the binding.

The NOESY spectra of all the complexes showed several intramolecular NOE connectivities within quadruplex and ligand in addition to intermolecular connectivities between quadruplex and ligand. In case of MTX-d-(TTAGGGT)₄ complex, most of the intermolecular NOE connectivities were observed between MTX protons 11 NH, 1/4 OH and 6/7 H with sugar (H1', H2'/H2'', H4') and CH₃ protons of T1, T2, and T7 bases of DNA. This showed that the binding of MTX is at two steps. One at T1pT2 step and other at G6pT7 step. Similar kind of observation was observed in case of luteolin-d-(TTAGGGT)₄ complex while in case of luteolin-d-(TTGGGGT)₄ complex the NOEs were mostly centred at G5, G6 and T7 residues. The rMD results clearly revealed the exact mode of binding in all the complexes. In case of MTX-d-(TTAGGGT)₄ complex two molecules of MTX partially stacked at T1pT2 step and G6pT7 step. The aromatic rings of MTX were involved in partial stacking while the side chains interact with groove. The complex was stabilized by both stacking, H-bonding and electrostatic interactions. In case of luteolin-d-(TTAGGGT)₄ complex a dual mode of interaction occurs i.e., both groove (at T1pT2 step) and partial end-stacking (at G6pT7 step) was observed. The complex was stabilized by stacking as well as electrostatic interactions. On the other hand, only a single mode of binding (groove binding) occurs in case of luteolin-d-(TTGGGGT)₄ complex. The complex was stabilized by H-bonding and electrostatic interactions. The result showed that binding of luteolin is different in both the complexes. But one binding site in common for both the complexes. The difference in binding is probably due to differences in the structures, which is basically in the third base. Thus we can deduce that the substitution of A with G in the heptamer sequence has marked effect on the binding of luteolin.

In a nut shell we conclude that both MTX and luteolin are a good G- quadruplex binders. MTX is a better binder than luteolin. The extent of binding is more with the parallel quadruplex sequence having adenine. The studies provided thought provoking insights into the structure-function paradigm of quadruplex-ligand interactions and highlighted their biological significance. Henceforth, these results can facilitate a rational structure-based drug design approaches in order to synthesize novel therapeutic molecules that can specifically interact with G-quadruplexes and regulate telomerase inhibition during the progression of cancer cell growth.

List of publications

1. Research Papers

1. Mitrasinovic P M, Palakshan. P T, **Tripathi. S**, Tripathi. AN.
On the affinity and specificity of quercetin to DNA. *Med Chem.* 2013 Mar; 9(2):193-202.
Pubmed ID: 22779797.
2. Dogra. S, Awasthi. P, **Tripathi. S**, Pradeep. TP, Nair. MS, Barthwal. R.
NMR-based structure of anticancer drug mitoxantrone stacked with terminal base pair of DNA hexamer sequence d-(ATCGAT)₂. *J Biomol Struct Dyn.* 2014 Jul; 32(7): 1164-83.
Pubmed ID: 23808712.
3. Dogra. S, Awasthi. P, **Tripathi. S**, Pradeep. TP, Barthwal. R.
Multispectroscopic methods reveal interaction of anticancer drug mitoxantrone with DNA hexanucleotide sequence d-(ATCGAT)₂. (Communicated to *Spectrochimica Acta. A Molecular and Biomolecular Spectroscopy*).
4. **Sweta Tripathi**, Pradeep T Palakshan and Ritu Barthwal.
Multi-spectroscopic studies of interaction of anti-tumor anthraquinone drug, mitoxantrone with parallel human tetramolecular G-Quadruplex DNA. (To be communicated).
5. **Sweta Tripathi**, Pradeep T Palakshan and Ritu Barthwal.
Solution structure of anti-tumor drug Mitoxantrone-d-(TTAGGGT)₄ G-Quadruplex DNA. (To be communicated).
6. **Sweta Tripathi**, Pradeep T Palakshan and Ritu Barthwal.
Solution structure of luteolin, a flavonoid glycoside with tetramolecular Quadruplex DNA. (To be communicated)

2. Papers in Conference and poster papers:

1. NMR Structure of Mitoxantrone bound to human G-quadruplex DNA sequence establishes stabilization of G quadruplex, **Sweta Tripathi** and Ritu Barthwal. Recent Advances in Structural Biology and Drug Discovery, IIT Roorkee, 9th -11th October 2014
2. Mitoxantrone inhibits telomerase enzyme by forming stable complex with G-quadruplex d-(TTGGGGT)₄ , Pradeep T Palakshan, **Sweta Tripathi**, Ritu Barthwal, ICMRBS XXVI International Conference on Magnetic Resonance in Biological Systems, Dallas, Texas, USA, 24-29 August 2014.

3. Affinity of adriamycin for G-quadruplex telomeric DNA sequence d-(TTGGGGT)₄ is greater than that with 4'-epiadriamycin, Ritu Barthwal, Zia Tariq, Ashhar Musharib Firdausi, Rajgopal Rudrarapu, **Sweta Tripathi**, Pradeep T Palakshan, ICMRBS XXVI International Conference on Magnetic Resonance in Biological Systems, Dallas, Texas, USA, 24-29 August 2014.
4. NMR based structural analysis of 4'-epiadriamycin bound to G-quadruplex telomeric DNA sequence d-(TTGGGGT)₄, Ashhar Musharib Firdausi, Zia Tariq, **Sweta Tripathi**, Ritu Barthwal, National Conference on Recent Trends in Chemical Sciences, Engineering and Technology (RTCET) 2014, National Institute of Technology Hamipur H.P., 29-30 May 2014.
5. NMR based structure of berberine bound to parallel stranded DNA quadruplex d-(TTAGGGT)₄ containing human telomeric repeat, Ritu Barthwal, Rahul Yadav, **Sweta Tripathi**, Tarikere Palakashan Pradeep , Albany 2013, The 18th Conversation, State University of New York, SUNY at Albany, New York, USA, 11-15 June 2013.
6. Interaction of flavone, luteolin with Parallel –stranded G-quadruplex sequence d-(TTGGGGT)₄, **Sweta Tripathi**, Pradeep T.P, Maya.S. Nair and Ritu Barthwal. Symposium on New Developments in NMR and Conference of the National Magnetic Resonance Society (NMRS-2012), Bangalore, February 5-8 2012.
7. Interaction of flavonoid, rutin with telomeric G-quadruplex sequence d-(TTGGGGT)₄, Pradeep. T. P, **Sweta Tripathi**, Maya S. Nair and Ritu Barthwal. Symposium on New Developments in NMR and Conference of the National Magnetic Resonance Society (NMRS- 2012), Bangalore, February 5-8 2012.
8. Binding of Berberrubine Dimer To Minor Groove Of Promoter Sequence d(CCAATTGG)₂, **Sweta Tripathi**, Pradeep T.P, Sayed Asif Hassan, Nair Maya S, Ritu Barthwal. 7th Asian Biophysics Association (ABA) Symposium and Annual Meeting of the Indian Biophysical Society (IBS), New Delhi, 30th Jan – 2nd Feb 2011

References

1. Aboul-ela, F., Murchie, A. I., Lilley, D. M., NMR study of parallel-stranded tetraplex formation by the hexadeoxynucleotide d(TG4T), *Nature*, 1992, 360, 280-282.
2. Ahmed, M.S., Ramesh, V., Nagaraja, V., Parish, J. and Hadi, S. Mode of binding of quercetin to DNA, *Mutagenesis*, 1994, 9, 193-197.
3. Alberti, P., Lacroix, L., Guittat, L., Helene, C., and Mergny, J. L., Nucleic acids as targets for antitelomerase agents, *Mini reviews in medicinal chemistry*, 2003, 3, 23-36.
4. Allsopp, R. C., and Harley, C. B., Evidence for a critical telomere length in senescent human fibroblasts, *Experimental cell research*, 1995, 219, 130-136.
5. Alvi, N. K., Rizvi, R. Y., and Hadi, S. M., Interaction of quercetin with DNA, *Bioscience reports*, 1986, 6, 861-868.
6. Ambrus, A., Chen, D., Dai, J., Jones, R. A., Yang, D. Z., Solution structure of the biologically relevant G-quadruplex element in the human c-MYC promoter. Implications for G-quadruplex stabilization, *Biochemistry*, 2005, 44, 2048–2058.
7. Aviñó, A., Mazzini, S., Ferreira, R., Gargallo, R., Marquez, V.E. and Eritja, R. The effect on quadruplex stability of *i> North</i>-nucleoside derivatives in the loops of the thrombin-binding aptamers, *Bioorg. Med. Chem.*, 2012, 20, 4186-4193.*
8. Aviñó, A., Portella, G., Ferreira, R., Gargallo, R., Mazzini, S., Gabelica, V., Orozco, M. and Eritja, R. Specific loop modifications of the thrombin-binding aptamer trigger the formation of parallel structures, *FEBS Journal.*, 2013, 281.
9. Awasthi, P., Dogra, S., and Barthwal, R., Multispectroscopic methods reveal different modes of interaction of anti cancer drug mitoxantrone with Poly (dG-dC). Poly (dG-dC) and Poly (dA-dT). Poly (dA-dT), *Journal of Photochemistry and Photobiology B: Biology*, 2013, 127, 78-87.
10. Babayan, Y. S., Sngryan, A. E., Kazaayran, Avetisyan, M. G. , Sogomonyan, L.R., and Garibyan, D. V., Interactions of antitumor drugs mitoxantrone and Ametantrone with DNA as Determined from the Changes in Circular Dichorism Spectra, *Mol. Biophys.*, 1998, 43, 398-402.

11. Bailly, C., Routier, S., Bernier, J. L., and Waring, M. J., DNA recognition by two mitoxantrone analogues: influence of the hydroxyl groups, *FEBS letters*, 1996, 379, 269-272.
12. Balasubramanian, S., and Neidle, S., G-quadruplex nucleic acids as therapeutic targets, *Current Opinion in Chemical Biology*, 2009, 13, 345-353.
13. Balasubramanian, S., Hurley, L. H., and Neidle, S., "Targeting G-quadruplexes in gene promoters: a novel anticancer strategy?", *Nat Rev Drug Discov.*, 2011, 10, 261-275.
14. Baumann, P., and Cech, T. R., Pot1, the putative telomere end-binding protein in fission yeast and humans, *Science*, 2001, 292, 1171-1175.
15. Beal, P. A., Dervan, P. B., Second structural motif for recognition of DNA by oligonucleotide-directed triple-helix formation. *Science*, 1991, 251, 1360-1363.
16. Beattie, T. L., Zhou, W., Robinson, M. O., and Harrington, L., Functional multimerization of the human telomerase reverse transcriptase, *Molecular and cellular biology*, 2001, 21, 6151-6160.
17. Beattie, T., Zhou, W., Robinson, M., & Harrington, L., Reconstitution of human telomerase activity in vitro, *Current Biology*, 1998, 8, 177-180.
18. Beecher, G. R., Overview of dietary flavonoids: nomenclature, occurrence and intake, *J. Nutr.*, 2003, 133, 3248-3254.
19. Benesi, H.A., Hildebrand, J.H., A Spectrophotometric Investigation of the Interaction of Iodine with Aromatic Hydrocarbons, *J. Am. Chem. Soc.*, 1949, 71, 2703- 2707.
20. Bessi, I., Bazzicalupi, C., Richter, C., Jonker, H. R., Saxena, K., Sissi, C., ... and Gratteri, P., Spectroscopic, molecular modeling, and NMR-spectroscopic investigation of the binding mode of the natural alkaloids berberine and sanguinarine to human telomeric G-quadruplex DNA, *ACS chemical biology*, 2012, 7, 1109-1119.
21. Bhadra, K., and Kumar, G. S., Interaction of berberine, palmatine, coralyne, and sanguinarine to quadruplex DNA: a comparative spectroscopic and calorimetric study, *Biochimica et Biophysica Acta (BBA)-General Subjects*, 2011, 1810, 485-496.
22. Bharti, S. K., and Roy, R., Quantitative ¹H NMR spectroscopy, *TrAC Trends in Analytical Chemistry*, 2012, 35, 5-26.
23. Bhatia, A., Bharti, S.K., Tewari, S.K., Sidhu, O.P. and Roy, R., Metabolic profiling for studying chemotype variations in *Withania somnifera* (L.) Dunal fruits using GC-MS and NMR spectroscopy, *Phytochemistry*, 2013, 93, 105-115.

24. Bi, S., Qiao, C., Song, D., Tian, Y., Gao, D., Sun, Y., and Zhang, H., Study of interactions of flavonoids with DNA using acridine orange as a fluorescence probe, *Sensors and Actuators B: Chemical*, 2006, 119, 199-208.
25. Bilaud, T., Brun, C., Ancelin, K., Koering, C. E., Laroche, T., and Gilson, E., Telomeric localization of TRF2, a novel human telobox protein, *Nature genetics*, 1997, 17, 236-239.
26. Blackburn, E. H., Structure and function of telomeres, *Nature*, 1991, 350, 569-573.
27. Blackburn, E. H., Telomere states and cell fates, *Nature*, 2000, 408, 53-56.
28. Bock, L. C., Griffin, L. C., Latham, J. A., Vermaas, E. H. and Toole, J. J., Selection of single-stranded DNA molecules that bind and inhibit human thrombin, *Nature*, 1992, 355, 564-566.
29. Bonadonna, G., Monfardini, S., Marmont, A., Damasio, E., and Rossi, F., Cardiac toxicity of daunorubicin, *The Lancet*, 1969, 293, 837-838.
30. Bossone, S. A., Asselin, C., Patel, A. J., and Marcu, K. B., MAZ, a zinc finger protein, binds to c-MYC and C2 gene sequences regulating transcriptional initiation and termination, *Proceedings of the National Academy of Sciences*, 1992, 89, 7452-7456.
31. Bowden, G.T., Roberts, R., Alberts, D.S., Peng, Y.M., Garcia, D., Comparative molecular pharmacology in leukemic L1210 cells of the anthracene anticancer drugs mitoxantrone and bisantrene, *Cancer Res.*, 1985, 45, 4915-4920.
32. Braunschweiler, L., Ernst, R.R., Coherence transfer by isotropic mixing -application to proton correlation spectroscopy, *Journal of Magnetic Resonance*, 1983, 53, 521-528.
33. Broccoli, D., Chong, L., Oelmann, S., Fernald, A. A., Marziliano, N., van Steensel, B., and de Lange, T., Comparison of the human and mouse genes encoding the telomeric protein, TRF1: chromosomal localization, expression and conserved protein domains, *Human molecular genetics*, 1997, 6, 69-76.
34. Broccoli, D., Smogorzewska, A., Chong, L., and de Lange, T., Human telomeres contain two distinct Myb-related proteins, TRF1 and TRF2, *Nature genetics*, 1997, 17, 231-235.
35. Brooks, T. A., Hurley, L. H., The role of supercoiling in transcriptional control of MYC and its importance in molecular therapeutics, *Nature Rev. Cancer*, 2009, 9, 849-861.
36. Brouillard, R. Cheminat, A., Flavonoids and plant color. *Prog. Clin. Biol. Res.*, 1988, 280, 93-106.
37. Brown, J. E., and Rice-Evans, C. A., Luteolin-rich artichoke extract protects low density lipoprotein from oxidation in vitro, *Free Radical Research*, 1998, 29, 247-255.

38. Bryan, T. M., and Cech, T. R., Telomerase and the maintenance of chromosome ends, *Current opinion in cell biology*, 1999, 11, 318-324.
39. Burger, A. M., Dai, F., Schultes, C. M., Reszka, A. P., Moore, M. J., Double, J. A. and Neidle, S., The G-quadruplex-interactive molecule BRACO-19 inhibits tumor growth, consistent with telomere targeting and interference with telomerase function, *Cancer Res.*, 2005, 65, 1489–1496.
40. Cairns, D., Michalitsi, E., Jenkins, T.C., and Mackay, S. P., Molecular modelling and cytotoxicity of substituted anthraquinones as inhibitors of human telomerase, *Bioorganic and medicinal chemistry*, 2002, 10, 803-807.
41. Campbell, N.H., Parkinson, G.N., Reszka, A.P., Neidle, S., Structural basis of DNA quadruplex recognition by an acridine drug, *J. Amer. Chem. Soc.*, 2008, 130, 6722–6724.
42. Capranico, G., Palumbo, M., Tinelli, S., Mabilia, M., Pozzan, A., and Zunino, F. Conformational drug determinants of the sequence specificity of drug-stimulated topoisomerase II DNA cleavage, *Journal of molecular biology*, 1994, 235, 1218-1230.
43. Catasti, P., Chen, X., Moyzis, R. K., Bradbury EM, Gupta G. Structure-function correlations of the insulin-linked polymorphic region, *J Mol Biol.*, 1996, 264, 534-545.
44. Cavaliere, C., Foglia, P., Pastorini, E., Samperi, R., and Lagana, A., Identification and mass spectrometric characterization of glycosylated flavonoids in *Triticum durum* plants by high-performance liquid chromatography with tandem mass spectrometry, *Rapid Communications in Mass Spectrometry*, 2005,19, 3143–3158.
45. Chai, J., Wang, J., Xu, Q., Hao F., and Liu, R., Multi-spectroscopic methods combined with molecular modeling dissect the interaction mechanisms of ractopamine and calf thymus DNA, *Mol. BioSyst.*, 2012, 8, 1902-1907.
46. Cheong, C. and Moore, P. B., Solution structure of an unusually stable RNA tetraplex containing G- and U-quartet structures, *Biochemistry*, 1992, 31, 8406–8414.
47. Chowdhury, A. R., Sharma, S., Mandal, S., Goswami, A., Mukhopadhyay, S., Majumder, H. K., Luteolin, an emerging anti-cancer flavonoid, poisons eukaryotic DNA topoisomerase I, *Biochem. J.*, 2002, 366, 653-61.
48. Chung, H. J., and Levens, D., c-myc expression: keep the noise down!, *Mol. Cells*, 2005, 20, 157–166.

49. Clark, G. R., Pytel, P. D., and Squire, C. J., The high-resolution crystal structure of a parallel intermolecular DNA G-4 quadruplex/drug complex employing syn glycosyl linkages, *Nucleic acids research*, 2012, 40, 5731-5738.
50. Clark, G. R., Pytel, P. D., Squire, C. J., and Neidle, S., Structure of the first parallel DNA quadruplex-drug complex, *Journal of the American Chemical Society*, 2003, 125, 4066-4067.
51. Cogoi, S., Xodo, L. E., G-quadruplex formation within the promoter of the KRAS protooncogene and its effect on transcription, *Nucleic Acids Res.*, 2006, 34, 2536-2549.
52. Colgin, L. M., Baran, K., Baumann, P., Cech, T. R., and Reddel, R. R., Human POT1 facilitates telomere elongation by telomerase, *Current biology*, 2003, 13, 942-946.
53. Conomos, D., Pickett, H.A., Reddel, R. R., Alternative lengthening of telomeres: Remodeling the telomere architecture. *Front. Oncol.*, 2013, 3.
54. Cook, N. C., Samman, S., Flavonoids: Chemistry, metabolism, cardioprotective effects and dietary sources, *Nutritional Biochemistry*, 1996, 7, 66-76.
55. Cookson, J. C., Dai, F., Smith, V., Heald, R. A., Laughton, C. A., Stevens, M. F., Burger, A.M., Pharmacodynamics of the G-quadruplex-stabilizing telomerase inhibitor 3,11-difluoro-6,8, 13-trimethyl-8H-quinol[4,3,2-kl]acridinium methosulfate (RHPS4) in vitro: Activity in human tumor cells correlates with telomere length and can be enhanced, or antagonized, with cytotoxic agents, *Mol. Pharmacol.*, 2005, 68, 1551–1558.
56. Cooney, M., Czernuszewicz, G., Postel, E. H., Flint, S. J., and Hogan, M. E., Site-specific oligonucleotide binding represses transcription of the human c-myc gene in vitro, *Science*, 1988, 241, 456-459.
57. Cosconati, S., Marinelli, L., Trotta, R., Virno, A., De Tito, S., Romagnoli, R., ... and Randazzo, A., Structural and conformational requisites in DNA quadruplex groove binding: another piece to the puzzle, *Journal of the American Chemical Society*, 2010, 132, 6425-6433.
58. Cox, P. J., Kumarasamy, Y., Nahar, L., Sarker, S. D., and Shoeb, M., Luteolin, *Acta Crystallographica Section E: Structure Reports Online*, 2003, 59, o975-o977.
59. Cunningham, A., Andrews, L., and Tollefsbol, T., Retrovirus-mediated RNA interference. Targeting hTERT through stable expression of short-hairpin RNA, *Methods in Molecular Biology* (Clifton, N.J.), 2007, 405, 39–46.

60. Cushnie, T. P., and Lamb, A. J., Antimicrobial activity of flavonoids, *International journal of antimicrobial agents*, 2005, 26, 343-356.
61. Cuyckens, F., Shahat, A.A., Van den Heuvel, H., Abdel- Shafeek, K.A., El-Messiry, M.M., Seif-El Nasr, M.M., et al., The application of liquid chromatography–electrospray ionization mass spectrometry and collision-induced dissociation in the structural characterization of acylated flavonol O-glycosides from the seeds of *Carrichtera annua.*, *European journal of mass spectrometry*, 2003, 9, 409–420.
62. Dai, J., Chen, D., Jones, R. A., Hurley, L. H. and Yang, D., NMR solution structure of the major G-quadruplex structure formed in the human BCL2 promoter region, *Nucleic acids research*, 2006, 34, 5133-5144.
63. Dai, J., Dexheimer, T. S., Chen, D., Carver, M., Ambrus, A., Jones, R. A., Yang, D., An intramolecular G-quadruplex structure with mixed parallel/ antiparallel G-strands formed in the human BCL-2 promoter region in solution, *J. Am. Chem. Soc.*, 2006, 128, 1096-1098.
64. Davies, D. B., Djimant, L. N., and Veselkov, A. N., ¹H NMR investigation of self-association of aromatic drug molecules in aqueous solutions, *J. Chem. Soc., Faraday Trans.*, 1996, 92, 383–390.
65. Davies, D. B., Veselkov, D. A., Evstigneev, M. P., and Veselkov, A. N., Self-association of the antitumour agent novatrone (mitoxantrone) and its hetero-association with caffeine, *Journal of the Chemical Society, Perkin Transactions*, 2001, 2, 61-67.
66. Davis, W. L., and Matthew, S. B., “Antioxidants and cancer III: quercetin,” *Alternative Medicine Review*, 2000, 5, 196–208.
67. De Armond, R., Wood, S., Sun, D., Hurley, L. H. and Ebbinghaus, S. W., Evidence for the presence of a guanine quadruplex forming region within a polypurine tract of the hypoxia inducible factor 1alpha promoter, *Biochemistry*, 2005, 44,16341–16350.
68. De Cian, A., Lacroix, L., Douarre, C., Temime-Smaali, N., Trentesaux, C., Riou, J. F., and Mergny, J. L., Targeting telomeres and telomerase, *Biochimie*, 2008, 90, 131-155.
69. De Groot, H., Raven, U., Tissue injury by reactive oxygen species and the protective effects of flavonoids, *Fundam. Clin. Pharma. Col.*, 1998, 12, 249-255.
70. De Lange, T., Shelterin: the protein complex that shapes and safeguards human telomeres, *Genes & development*, 2005, 19, 2100-2110.

71. de Soultrait, V. R., Lozach, P.-Y., Altmeyer, R., Tarrago-Litvak, L., Litvak, S. and Andre'ola, M. L., DNA aptamers derived from HIV-1 RNase H inhibitors are strong anti-integrase agents, *J. Mol. Biol.*, 2002, 324, 195–203.
72. Deng, J., Xiong, Y. and Sundaralingam, M., X-ray analysis of an RNA tetraplex (UGGGGU)₄ with divalent Sr²⁺ ions at subatomic resolution (0.61 Å), *Proc. Natl Acad. Sci. USA*, 2001, 98, 13665–13670.
73. Dexheimer, T. S., Fry, M. and Hurley, L. H., DNA quadruplexes and gene regulation. In Neidle, S., and Balasubramanian, S. (eds), *Quadruplex Nucleic Acids*, RSC Publishing, Cambridge, UK, 2006, pp. 180–207.
74. Dogra, S., Awasthi, P., Nair, M., & Barthwal, R., Interaction of anticancer drug mitoxantrone with DNA hexamer sequence d-(CTCGAG)₂ by absorption, fluorescence and circular dichroism spectroscopy, *Journal of Photochemistry and Photobiology B: Biology*, 2013, 123, 48-54.
75. Drygin, D., Siddiqui-Jain, A., O'Brien, S., Schwaebe, M., Lin, A., Bliesath, J., ... & Rice, W. G., Anticancer activity of CX-3543: a direct inhibitor of rRNA biogenesis, *Cancer research*, 2009, 69, 7653-7661.
76. Duan, W., Rangan, A., Vankayalapati, H., Kim, M. Y., Zeng, Q., et al., Design and synthesis of fluoroquinophenoxazines that interact with human telomeric G-quadruplexes and their biological effects, *Mol. Cancer Ther.*, 2001, 1, 103–120.
77. Duquette, M. L., Pham, P., Goodman, M. F. and Maizels, N., AID binds to transcription-induced structures in c-MYC that map to regions associated with translocation and hypermutation, *Oncogene*, 2005, 24, 5791–5798.
78. E.M. Rezler, D.J. Bearss, L.H. Hurley, Telomeres and telomerases as drug targets, *Curr. Opin. Pharmacol.*, 2002, 2, 415–423.
79. Eddy, J., and Maizels, N., Gene function correlates with potential for G4 DNA formation in the human genome, *Nucleic Acids Res*, 34, 3887–3896.
80. El Daly, H., and Martens, U., Telomerase inhibition and telomere targeting in hematopoietic cancer cell lines with small non-nucleosidic synthetic compounds (BIBR1532), *Methods in Molecular Biology* (Clifton, N.J.), 2007, 405, 47–60.
81. Ellestad, G.A., Drug and Natural products binding to nucleic acids analyzed by electronic circular dichroism, in N. Berova, P.L. Polavarapu, K. Nakanishi, R.W. Woody (Eds.), *Comprehensive Chiroptical Spectroscopy*, Vol. 2: Application in Stereochemical Analysis

of Synthetic Compounds, Natural Products and Biomolecules, John Wiley & Sons, New Jersey, 2012, pp. 635-664.

82. Enache, M., and Volanschi, E., Spectral characterization of self-association of antitumor drug mitoxantrone, *Rev. Roum. Chim.*, 2010, 55, 255-262.
83. Fang, G. and Cech, T. R., The beta subunit of Oxytricha telomere-binding protein promotes G-quartet formation by telomeric DNA, *Cell*, 1993, 74, 875–885.
84. Faulds, D., Balfour, J. A., Chrisp, P. and Langtry, H. D., Mitoxantrone. A review of its pharmacodynamics and pharmacokinetic properties and therapeutic potential in the chemotherapy of cancer, *Drugs*, 1991, 41, 440–449.
85. Fedoroff, O. Y., Salazar, M., Han, H., Chemeris, V. V., Kerwin, S. M., and Hurley, L. H., NMR-based model of a telomerase-inhibiting compound bound to G-quadruplex DNA, *Biochemistry*, 1998, 37, 12367-12374.
86. Feigon, J., Koshlap, K.M., Smith, F.W., *Methods Enzymol.*, 1995, 261, 225–255.
87. Felsenfeld, G., Davies, D. R., Rich, A., Formation of a three-stranded polynucleotide molecule, *J. Am. Chem. Soc.*, 1957, 79, 2023-2024.
88. Feng, J., Funk, W. D., Wang, S. S., Weinrich, S. L., Avilion, A. A., Chiu, C. P., ... and Yu, J., The RNA component of human telomerase, *Science*, 1995, 269, 1236-1241.
89. Fernando, H., Reszka, A. P., Huppert, J., Ladame, S., Rankin, S., Venkitaraman, A. R., Neidle, S. and Balasubramanian, S., A conserved quadruplex motif located in a transcription activation site of the human c-kit oncogene, *Biochemistry*, 2006, 45, 7854–7860.
90. Ferreyra, M. L. F., Rius, S. P., and Casati, P., Flavonoids: biosynthesis, biological functions, and biotechnological applications, *Frontiers in plant science*, 2012, 3.
91. Fletcher, T., Cathers, B., Ravikumar, K., Mamiya, B., and Kerwin, S., Inhibition of human telomerase by 7-deaza-2'-deoxyguanosine nucleoside triphosphate analogs: Potent inhibition by 6-thio-7-deaza-2'-deoxyguanosine 5'-triphosphate, *Bioorganic Chemistry*, 2001, 29, 36–55.
92. Franceschin, M., Rizzo, A., Casagrande, V., Salvati, E., Alvino, A., Altieri, A., Ciammaichella, A., Iachettini, S., Leonetti, C., Ortaggi, G., Porru, M., Bianco, A., Biroccio, A., Aromatic core extension in the series of N-cyclic bay-substituted perylene G-quadruplex ligands: Increased telomere damage, antitumor activity, and strong selectivity for neoplastic over healthy cells, *Chem. Med. Chem.*, 2012, 7, 2144–2154.

93. Franceschin, M., Rossetti, L., D'Ambrosio, A., Schirripa, S., Bianco, A., Ortaggi, G., Savino, M., Schultes, C., Neidle, S., Natural and synthetic G-quadruplex interactive berberine derivatives, *Bioorganic & Medicinal Chemistry Letters*, 2006, 16, 1707-1711.
94. Fry, M., Tetraplex DNA and its interacting proteins, *Front. Biosci.*, 2007, 12, 4336–4351.
95. Fujimori, J., Matsuo, T., Shimose, S., Kubo, T., Ishikawa, M., Yasunaga, Y., Ochi, M., Antitumor effects of telomerase inhibitor TMPyP4 in osteosarcoma cell lines, *J. Orthop. Res.*, 2011, 29, 1707–1711.
96. Gai, W., Yang, Q., Xiang, J., Jiang, W., Li, Q., Sun, H., ... and Tang, Y., A dual-site simultaneous binding mode in the interaction between parallel-stranded G-quadruplex [d-(TGGGGT)]₄ and cyanine dye 2, 2'-diethyl-9-methyl-selenacarbocyanine bromide, *Nucleic acids research*, 2013, 41, 2709-2722.
97. Gavathiotis, E., and Searle, M. S., Structure of the parallel-stranded DNA quadruplex d(TTAGGGT)₄ containing the human telomeric repeat: evidence for A-tetrad formation from NMR and molecular dynamics simulations, *Org. Biomol. Chem.*, 2003, 1, 1650–1656.
98. Gavathiotis, E., Heald, R. A., Stevens, M. F., and Searle, M. S., Drug Recognition and Stabilisation of the Parallel-stranded DNA Quadruplex d (TTAGGGT)₄ Containing the Human Telomeric Repeat. *Journal of molecular biology*, 2003, 334, 1, 25-36.
99. Gellert, G. C., Jackson, S. R., Dikmen, Z. G., Wright, W. E., and Shay, J. W. Telomerase as a therapeutic target in cancer, *Drug Discovery Today: Disease Mechanisms*, 2005, 2, 159-164.
100. Gellert, M., Lipsett, M. N. and Davies, D. R., Helix formation by guanylic acid, *Proc. Natl Acad. Sci. USA*, 1962, 48, 2013–2018.
101. Germann, M. W., Zhou, N., Van de Sande, J. H., and Vogel, H. J., [9] Parallel-stranded duplex DNA: An NMR perspective, *Methods in enzymology*, 1995, 261, 207-225.
102. Gil-Izquierdo, A., Gil, M. I., Ferreres, F., and Tomas-Barber'an, F. A., "In vitro availability of flavonoids and other phenolics in orange juice," *Journal of Agricultural and Food Chemistry*, 2001, 49, 1035–1041.
103. Giraldo, R. and Rhodes, D., The yeast telomere-binding protein RAP1 binds to and promotes the formation of DNA quadruplexes in telomeric DNA, *EMBO J.*, 1994, 13, 2411–2420.
104. Goddard, T.D., DGK, SPARKY 3., University of California, San Francisco, USA., 2004.

105. Gomez, D., Aouali, N., Renaud, A., Douarre, C., Shin-Ya, K., Tazi, J., Martinez, S., Trentesaux, C., Morjani, H., Riou, J. F., Resistance to senescence induction and telomere shortening by a G-quadruplex ligand inhibitor of telomerase, *Cancer Res.*, 2003, 63, 6149–6153.
106. Gomez, D., Lemarteleur, T., Lacroix, L., Mailliet, P., Mergny, J.L., Riou, J. F., Telomerase downregulation induced by the G-quadruplex ligand 12459 in A549 cells is mediated by hTERT RNA alternative splicing, *Nucleic Acids Res.*, 2004, 32, 371–379.
107. Gorenstein, D. G., and Kar, D., ³¹P chemical shifts in phosphate diester monoanions. Bond angle and torsional angle effects, *Biochem. Biophys. Res. Commun.*, 1975, 65, 1073.
108. Gorenstein, D. G., in “Phosphorus-31 NMR: Principles and Applications” (D. G Gorenstein ed.) p.7. Academic Press, Orlando, Florida, 1984.
109. Gorenstein, D.G., ³¹P NMR of DNA Spectroscopic methods for analysis of DNA, *Methods in Enzymology*, 1992, 211, 254–285.
110. Gowan, S. M., Harrison, J. R., Patterson, L., Valenti, M., Read, M. A., Neidle, S., and Kelland, L. R., A G-quadruplex-interactive potent small-molecule inhibitor of telomerase exhibiting in vitro and in vivo antitumor activity, *Molecular pharmacology*, 2002, 61, 1154-1162.
111. Gowan, S. M., Heald, R., Stevens, M. F., Kelland, L. R., Potent inhibition of telomerase by smallmolecule pentacyclic acridines capable of interacting with g-quadruplexes, *Mol. Pharmacol.*, 2001, 60, 981–988.
112. Greider, C. W., and Blackburn, E. H., Identification of a specific telomere terminal transferase activity in Tetrahymena extracts, *Cell*, 1985, 43, 405-413.
113. Griffith, J. D., Comeau, L., Rosenfield, S., Stansel, R. M., Bianchi, A., Moss, H. and De Lange, T., Mammalian telomeres end in a large duplex loop. *Cell*, 1999, 97, 503-514.
114. Günther, U. L., Ludwig, C., and Rüterjans, H., NMRLAB—advanced NMR data processing in MATLAB, *Journal of Magnetic Resonance*, 2000, 145, 201-208.
115. Günther, U. L., Ludwig, C., and Rüterjans, H., WAVEWAT—improved solvent suppression in NMR spectra employing wavelet transforms, *Journal of Magnetic Resonance*, 2002, 156, 19-25.
116. Hagemester, F., Cabanillas, F., Coleman, M., Gregory, S. A., and Zinzani, P. L., The role of mitoxantrone in the treatment of indolent lymphomas, *The oncologist*, 2005, 10, 150-159.

117. Haider, S., Parkinson, G. N., Neidle, S., Crystal structure of the potassium form of an Oxytricha nova G-quadruplex, *J. Mol. Biol.*, 2002, 320, 189-200.
118. Hajihassan, Z., and Chadegani, A. R., Interaction of mitoxantrone, as an anticancer drug, with chromatin proteins, core histones and H1, in solution, *Int. J. Biol. Macromol.*, 2011, 48, 87-92.
119. Hajihassan, Z., and Chadegani, A. R., Studies on the binding affinity of anticancer drug mitoxantrone to chromatin, DNA and histone proteins, *J. Biom. Sci.*, 2009, 16, 31-38.
120. Han, H. and Hurley, L. H., G-quadruplex DNA: a potential target for anti-cancer drug design. *Trends in pharmacological sciences*, 2000, 21, 136-142.
121. Hara, Y., Luo, S. J., Wickremasinghe, R. L., and Yamanishi, T., "Special issue on tea," *Food Reviews International*, 1995, 11, 371–542.
122. Harley, C. B., Futcher, A. B., and Greider, C. W., Telomeres shorten during ageing of human fibroblasts, *Nature*, 1990, 345, 458-460.
123. Harrison, R.J., Gowan, S.M., Kelland, L.R., Neidle, S., Human telomerase inhibition by substituted acridine derivatives, *Bioorg. Med. Chem. Lett.*, 1999, 9, 2463–2468.
124. Heim, K. E., Tagliaferro, A. R., Bobliya, D. J., Flavonoids antioxidants: Chemistry, metabolism and structure-activity relationships, *The Journal of Nutritional Biochemistry*, 2002, 13, 572-584.
125. Hertog, M. G., Hollman, P. C., and Katan, M. B., Content of potentially anticarcinogenic flavonoids of 28 vegetables and 9 fruits commonly consumed in the Netherlands, *Journal of agricultural and food chemistry*, 1992, 40, 2379-2383.
126. Hollman, P. C. H., Buijsman, M. N. C. P., van Gameren, Y. , Cnossen, P. J., de Vries, J. H. M., and Katan, M. B., "The sugar moiety is a major determinant of the absorption of dietary flavonoid glycosides in man," *Free Radical Research*, 1999, 31, 569–573.
127. Hosur R. V., Ravikumar M., Roy K. B., Kunn T. Z. and Miles H. T. and Govil G, In 'Magnetic resonance in Biology and medicine, (Eds. Govil, G. Khetrapal C. L. and Saran, A.) Tata Mc Graw Hill, New Delhi, 1985.
128. Hosur, R. V., Govil, G., and Miles, H. T., Application of two-dimensional NMR spectroscopy in the determination of solution conformation of nucleic acids, *Magnetic resonance in chemistry*, 1988, 26, 927-944.

129. Hsu, S. T., et al., A G-rich sequence within the c-kit oncogene promoter forms a parallel Gquadruplex having asymmetric G-tetrad dynamics, *J. Am. Chem. Soc.*, 2009, 131, 3399–13409.
130. Huang, C.Y., Determination of binding stoichiometry by the continuous variation method: The Job plot, *Methods Enzymol.*, 1982, 87 509–525.
131. Huang, H. S., Chen, T. C., Chen, R. H., Huang, K. F., Huang, F. C., Jhan, J. R., ... & Lin, J. J. Synthesis, cytotoxicity and human telomerase inhibition activities of a series of 1, 2-heteroannulated anthraquinones and anthra [1, 2- d] imidazole-6, 11-dione homologues, *Bioorganic & medicinal chemistry*, 2009, 17, 7418-7428.
132. Huang, H. S., Huang, K. F., Li, C. L., Huang, Y.Y., Chiang, Y.H., Huang, F.C., Lin, J. J., Synthesis, human telomerase inhibition and anti-proliferative studies of a series of 2,7-bis-substituted amido-anthraquinone derivatives, *Bioorg. Med. Chem.*, 2008, 16, 6976–6986.
133. Huber, M. D., Duquette, M. L., Shiels, J. C. and Maizels, N., A conserved G4 DNA binding domain in RecQ family helicases, *J. Mol. Biol.*, 2006, 358, 1071–1080.
134. Hud, N.V., and Plavec, J., The role of cations in determining quadruplex structure and stability. In Neidle, S. and Balasubramanian, S. (eds), *Quadruplex Nucleic Acids*, RSC Publishing, Cambridge, UK, 2006, pp. 100–130.
135. Hudson, J. S., Brooks, S. C., and Graves, D. E., Interactions of actinomycin D with human telomeric G-quadruplex DNA. *Biochemistry*, 2009, 48, 21, 4440-4447.
136. Hughes, R.J., Croley, T.R., Metcalfe, C.D., and March, R.E., A tandem mass spectrometric study of selected characteristic flavonoids. *International Journal of Mass Spectrometry*, 2001, 210, 371–385.
137. Huppert, J. L. and Balasubramanian, S., Prevalence of quadruplexes in the human genome, *Nucleic Acids Res.*, 2005, 33, 2908–2916.
138. Huppert, J. L., Balasubramanian, S., G-quadruplexes in promoters throughout the human genome, *Nucleic Acids Res.*, 2007, 35, 406-413.
139. Huppert, J. L., Hunting G-quadruplexes, *Biochimie*, 2008, 90, 1140-1148.
140. Ibrahim, M.S., Voltammetric studies of the interaction of nogalamycin antitumor drug with DNA, *Anal. Chim. Acta.*, 2001, 443, 63– 72.
141. Ishikawa, F., Regulation mechanisms of mammalian telomerase. A review, *Biochemistry. Biokhimiia*, 1997, 62, 1332–1337.

142. Islam, S. A., Neidle, S., Gandecha, B. M., Partridge, M., Patterson, L.H. and Brown, J. R., Comparative computer graphics and solution studies of the DNA interaction of substituted anthraquinones based on doxorubicin and mitoxantrone, *J. Med. Chem.*, 1985, 28, 857–864.
143. Iwashina, T., The structure and distribution of the flavonoids in plants. *Journal of Plant Research*, 2000, 113, 287–299
144. Jin, Y., Li, H., and Bai, J., Homogeneous selecting of a quadruplex-binding ligand-based gold nanoparticle fluorescence resonance energy transfer assay, *Analytical chemistry*, 2009, 81, 5709-5715.
145. Jin, Y., Li, H., and Liu, P., Label-free electrochemical selection of G-quadruplex-binding ligands based on structure switching, *Biosensors and Bioelectronics*, 2010, 25, 2669-2674.
146. Job, P., Formation and stability of inorganic complexes in solution, *Ann.Chim.*, 1928, 9, 113–203.
147. Johnson, I. M., Kumar, S. B., & Malathi, R., De-intercalation of ethidium bromide and acridine orange by xanthine derivatives and their modulatory effect on anticancer agents: a study of DNA-directed toxicity enlightened by time correlated single photon counting, *Journal of Biomolecular Structure and Dynamics*, 2003 20, 5, 677-685.
148. Johnson, J. E., Smith, J. S., Kozak, M. L., Johnson, F. B., In vivo veritas: Using yeast to probe the biological functions of G-quadruplexes, *Biochimie*, 2008, 90, 1250-1263.
149. Joshi, B., Roy, R., Chattopadhyay, S. and Madhusudanan, K., An NMR and LC–MS based approach for Mixture Analysis involving Taxoid molecules from *Taxus wallichiana*, *J. Molec. Struc.*, 2003, 645, 235-248,.
150. Jurasekova, Z., Marconi, G., Sanchez-Cortes, S., and Torreggiani, A., Spectroscopic and molecular modeling studies on the binding of the flavonoid luteolin and human serum albumin, *Biopolymers*, 2009, 91, 917-927.
151. Justesen, U., Knuthsen, P., and Leth, T., Quantitative analysis of flavonols, flavones, and flavanones in fruits, vegetables and beverages by high-performance liquid chromatography with photo-diode array and mass spectrometric detection, *Journal of Chromatography A*, 1998, 799, 101–110.
152. Kang, C., Zhang, X., Ratliff, R., Moyzis, R., Rich, A., Crystal structure of four-stranded Oxytricha telomeric DNA, *Nature* 1992, 356, 126-131.

153. Kapuscinski, J., and Darzynkiewicz, Z., Relationship between the pharmacological activity of antitumor drugs ametantrone and mitoxantrone (Novatrone) and their ability to condense nucleic acids. *Proc. Natl. Acad. Sci., USA*, 1986, 83, 6303–6306.
154. Kapuscinski, J., Darzynkiewicz, Z., Traganos, F., and Melamed, M. R., Interactions of a new antitumor agent, 1, 4-dihydroxy-5, 8-bis [[2-[(2-hydroxyethyl) amino]-ethyl] amino]-9, 10-anthracenedione, with nucleic acids, *Biochemical pharmacology*, 1981, 30, 231-240.
155. Karplus, M., *Journal of Chemical Physics*, 1959, 30, 1, 11–15.
156. Keniry, M. A., *Biopolymers*, 2001, 56, 123-146.
157. Keniry, M. A., Quadruplex structures in nucleic acids, *Biopolymers*, 2001, 56, 123-146.
158. Kerwin, S. M., *Curr. Pharm. Des.*, 2000, 6, 441-478.
159. Kettani, A., Gorin, A., Majumdar, A., Hermann, T., Skripkin, E., Zhao, H., Jones, R., Patel, D. J. A., dimeric DNA interface stabilized by stacked A•(G•G•G•G)•A hexads and coordinated monovalent cations, *J. Mol. Biol*, 2000, 297, 627-644.
160. Kieper, I., Schmidt, T., Fera, B., and Rüterjans, H., ¹⁵N-Labeled Oligodeoxynucleotides- Useful Probes for ¹H-NMR Investigations, *Nucleosides & nucleotides*, 1998, 7, 821-825.
161. Kim, M.Y.; Duan, W.; Gleason-Guzman, M.; Hurley, L.H. Design, synthesis, and biological evaluation of a series of fluoroquinoanthroxazines with contrasting dual mechanisms of action against topoisomerase II and G-quadruplexes, *J. Med. Chem.*, 2003, 46, 571–583.
162. Kim, N. W., Clinical implications of telomerase in cancer, *European Journal of Cancer*, 1997, 33, 781-786.
163. Kim, N. W., Piatyszek, M. A., Prowse, K. R., Harley, C. B., West, M. D., Ho, P. D. L., ... and Shay, J. W., Specific association of human telomerase activity with immortal cells and cancer, *Science*, 1994, 266, 2011-2015.
164. Koeppel, F., Riou, J. F., Laoui, A., Mailliet, P., Arimondo, P. B., Labit, D., Petitgenet, O., Helene, C., Mergny, J. L., “Ethidium derivatives bind to G-quartets, inhibit telomerase and act as fluorescent probes for quadruplexes”, *Nucleic Acids Res.*, 2001, 29, 1087.
165. Kondo, Y., & Kondo, S., Telomerase RNA inhibition using antisense oligonucleotide against human telomerase RNA linked to a 2',5'-oligoadenylate, *Methods in Molecular Biology* (Clifton, N.J.), 2007, 405, 97–112.
166. Kostjukov, V.V., Pahomov, V. I, Andrejuk, D. D., Davies, D. B., Evstigneev, M.P., Investigation of the complexation of the anti-cancer drug novantrone with the hairpin

- structure of the deoxyheptanucleotide 5'-d(GpCpGpApApGpC), *J. Mol. Struct.*, 2007, 843, 78-86
167. Kotovych, G., Lown, J. W and Tong, P. K., High field ^1H and ^{31}P NMR studies on the binding of the anticancer agent mitoxantrone to d-[CpGpApTpCpG]₂, *J Biomol Struct Dyn.*, 1986, 4, 111–125.
168. Kreft, S., Knapp, M., and Kreft, I., Extraction of rutin from buckwheat (*Fagopyrum esculentum* Moench) seeds and determination by capillary electrophoresis, *Journal of agricultural and food chemistry*, 1999, 47, 4649-4652.
169. Krishnamoorthy, C. R., Yen, S. F., Smith, J. C., Lown, J. W., and Wilson, W. D., Stopped-flow kinetic analysis of the interaction of anthraquinone anticancer drugs with calf thymus DNA, poly[d(G-C)].poly[d(G-C)], and poly[d(A-T)].poly[d(A-T)], *Biochemistry*, 1986, 25, 5933-5940.
170. Krugh, T.R., Reinhardt, C.G., Evidence for sequence preferences in the intercalative binding of ethidium bromide to dinucleoside monophosphates, *J. Mol. Biol.*, 1975, 97, 133-162.
171. Kuhna, J., The flavanoids. A class of semi-essential food components: their role in human nutrition, *World Rev. Nutr. Diet.*, 1976, 24, 117-191.
172. Kumar, A., Ernst, R.R., Wuthrich, K., A two-dimensional nuclear overhauser enhancement (2D NOE) experiment for the elucidation of complete proton-proton cross-relaxation network in biological macromolecules. *Biochemical and Biophysical Research Communications*, 1980, 95, 1–6.
173. Kumar, S., and Pandey, A. K., Chemistry and biological activities of flavonoids: an overview, *The Scientific World Journal*, 2013, 2013.
174. Kumar, V., Dwivedi, D.K. and Jagannathan, N.R., High-resolution NMR spectroscopy of human body fluids and tissues in relation to prostate cancer, *NMR in Biomedicine*, 2014, 27, 80-89.
175. Kumar, V., Sharma, U. and Jagannathan, N., In vivo magnetic resonance spectroscopy of cancer, *Biomedical Spectroscopy and Imaging*, 2012, 1, 89-100.
176. Kumari, S., Bugaut, A., Huppert, J. L. and Balasubramanian, S., An RNA G-quadruplex in the 50 UTR of the N-RAS proto-oncogene modulates translation, *Nat. Chem. Biol.*, 2007, 3, 218–221.

177. Kuryavyi, V., Phan, A. T., Patel, D. J., Solution structures of all parallel-stranded monomeric and dimeric G-quadruplex scaffolds of the human c-kit2 promoter. *Nucleic Acids Res.*, 2010, 38, 6757–6773.
178. Kypr, J., Kejnovska, I., Bednarova, K., Vorlickova, M., Circular Dichroism of Nucleic acids, in N. Berova, P.L. Polavarapu, K. Nakanishi, R.W. Woody (Eds.), *Comprehensive Chiroptical Spectroscopy, Vol. 2: Application in Stereochemical Analysis of Synthetic Compounds, Natural Products and Biomolecules*, John Wiley & Sons, 2012, pp. 575-585.
179. Lai, S., Andrews, L., and Tollefsbol, T., hTERT knockdown in human embryonic kidney cells using double-stranded RNA, *Methods in Molecular Biology (Clifton, N.J.)*, 2007, 405, 23–29.
180. Lai, S., Andrews, L., and Tollefsbol, T., RNA interference using a plasmid construct expressing short-hairpin RNA, *Methods in Molecular Biology (Clifton, N.J.)*, 2007, 405, 31–37.
181. Lakowicz, J.R., *Principles of Fluorescence Spectroscopy*, third ed., Springer, New York, 2006.
182. Larson, E. D., Duquette, M. L., Cummings, W. J., Streiff, R. J. and Maizels, N., MutSalpha binds to and promotes synapsis of transcriptionally activated immunoglobulin switch regions, *Curr. Biol.*, 2005, 15, 470–474.
183. Larson, R. A., The antioxidants of higher plants, *Phytochemistry*, 1988, 27, 969-978.
184. Lee, B. S., and Dutta, P. K., Optical spectroscopic studies of the antitumor drug 1, 4-dihydroxy-5, 8-bis [[2-[(2-hydroxyethyl) amino] ethyl] amino]-9, 10-anthracenedione (mitoxantrone), *The Journal of Physical Chemistry*, 1989, 93, 5665-5672.
185. Leonetti, C., Amodei, S., D'Angelo, C., Rizzo, A., Benassi, B., Antonelli, A., Elli, R., Stevens, M. F., D'Incalci, M., Zupi, G., Biroccio, A., Biological activity of the G-quadruplex ligand RHPS4 (3,11-difluoro-6,8,13-trimethyl-8H-quino[4,3,2-kl]acridinium methosulfate) is associated with telomere capping alteration, *Mol. Pharmacol.*, 2004, 66, 1138–1146.
186. Leopoldini, M., Pitarch, I. P., Russo, N., and Toscano, M., Structure, conformation, and electronic properties of apigenin, luteolin, and taxifolin antioxidants. A first principle theoretical study, *The Journal of Physical Chemistry A*, 2004, 108, 92-96.
187. Li, H., Katik, I., & Liu, J., Uses of telomerase peptides in anti-tumor immune therapy, *Methods in Molecular Biology (Clifton, N.J.)*, 2007, 405, 61–86.

188. Li, N., Ma, Y., Yang, C., Guo, L., Yang, X., Interaction of anticancer drug mitoxantrone with DNA analyzed by electrochemical and spectroscopic methods, *Biophys. Chem.*, 2005, 116, 199-205.
189. Li, Q., Xiang, J. F., Yang, Q. F., Sun, H. X., Guan, A. J., & Tang, Y. L., G4LDB: a database for discovering and studying G-quadruplex ligands, *Nucleic acids research*, 2013, 41, D1115-D1123.
190. Li, Q., Xiang, J., Li, X., Chen, L., Xu, X., Tang, Y., ... and Xu, G., Stabilizing parallel G-quadruplex DNA by a new class of ligands: two non-planar alkaloids through interaction in lateral grooves, *Biochimie*, 2009, 91, 811-819.
191. Li, Q., Xiang, J., Li, X., Chen, L., Xu, X., Tang, Y., and Xu, G., Stabilizing parallel G-quadruplex DNA by a new class of ligands: two non-planar alkaloids through interaction in lateral grooves. *Biochimie*, 2009, 91, 7, 811-819.
192. Li, S., Nosrati, M., and Kashani-Sabet, M., Knockdown of telomerase RNA using hammerhead ribozymes and RNA interference, *Methods in Molecular Biology* (Clifton, N.J.), 2007, 405, 113–131.
193. Li, W., Zhang, M., Zhang, J. L., Li, H. Q., Zhang, X. C., Sun, Q., and Qiu, C. M. Interactions of daidzin with intramolecular G-quadruplex, *FEBS letters*, 2006, 580, 4905-4910.
- ligands, *Biochemistry*, 1999, 38, 16067e16075.
194. Lin, S., and Struve, W.S., Solvatochromism and Time-Resolved Fluorescence of the Antitumor Agent Mitoxantrone and its Analogues in Solution and in DNA, *J. Phys. Chem.*, 1991, 2251-2256.
195. Lin, Y., Shi, R., Wang, X., and Shen, H. M., Luteolin, a flavonoid with potentials for cancer prevention and therapy, *Current cancer drug targets*, 2008, 8, 634.
196. Liu, J. N., Deng, R., Guo, J. F., Zhou, J. M., Feng, G. K., Huang, Z. S., Gu, L. Q., Zeng, Y. X., Zhu, X. F., Inhibition of myc promoter and telomerase activity and induction of delayed apoptosis by SYUIQ-5, a novel G-quadruplex interactive agent in leukemia cells, *Leukemia*, 2007, 21,1300–1302.
197. Lopez, M., Martinez, F., Del Valle, C., Orte, C., and Miro, M., Analysis of phenolic constituents of biological interest in red wines by high-performance liquid chromatography, *Journal of Chromatography A*, 2001, 922, 359-363.

198. Lopez-Lazaro, M., Distribution and biological activities of the flavonoid luteolin, Mini review in medicinal chemistry, 2009, 9, 31-59.
199. Lown, J. W. and Hanstock, C. C., High field $^1\text{H-NMR}$ analysis of the 1:1 intercalation complex of the antitumor agent mitoxantrone and the DNA duplex [d(CpGpCpG)]. *J. Biomol. Struct. Dyn.*, 1985b, 2, 1097–1106.
200. Lown, J. W., Morgan, A. R., Yen, S. F., Wang, Y. H., and Wilson, W. D., Characteristics of the binding of the anticancer agents mitoxantrone and ametantrone and related structures to deoxyribonucleic acids, *Biochemistry*, 1985a, 24, 4028-4035.
201. Lown, J.W., Morgan, A.R., Yen, S –F., Wang, Y–H., Wilson, W.D., Characteristics of the binding of the anticancer agents mitoxantrone and ametantrone and related structures to deoxyribonucleic acids, *Biochemistry*, 1985, 24, 4028–4035.
202. Lutz, W., Leon, J., and Eilers, M., "Contributions of Myc to tumorigenesis," *BBA-Rev Cancer*, 2002, 1602, 61-71.
203. Macaya, R. F., Schultze, P., Smith, F. W., Roe, J. A., Feigon, J., Thrombin-binding DNA aptamer forms a unimolecular quadruplex structure in solution, *Proc. Natl. Acad. Sci. USA*, 1993, 90, 3745-3749.
204. Maizels, N., Dynamic roles for G4 DNA in the biology of eukaryotic cells, *Nat. Struct. Mol. Biol.*, 2006, 13, 1055–1059.
205. Manach, C., Scalbert, A., Morand, C., Remesy, C., Jimenez, L., Polyphenols: food sources and bioavailability, *Am. J. Clin. Nutr.*, 2004, 79, 727-747.
206. Manet, I., Manoli, F., Zambelli, B., Andreano, G., Masi, A., Cellai, L., & Monti, S., Affinity of the anthracycline antitumor drugs Doxorubicin and Sabarubicin for human telomeric G-quadruplex structures, *Physical Chemistry Chemical Physics*, 2011, 13, 540-551.
207. Marcu, K. B., Bossone, S. A., Patel AJ, myc function and regulation, *Annu. Rev. Biochem.*, 1992, 61, 809-860.
208. Martino, L., Virno, A., Pagano, B., Virgilio, A., Di Micco, S., Galeone, A., ... and Randazzo, A., Structural and thermodynamic studies of the interaction of distamycin A with the parallel quadruplex structure [d(TGGGGT)]₄, *Journal of the American Chemical Society*, 2007, 129, 16048-16056.

209. Masiero, S., Trotta, R., Pieraccini, S., De Tito, S., Perone, R., Randazzo, A., & Spada, G. P., A non-empirical chromophoric interpretation of CD spectra of DNA G-quadruplex structures, *Organic & biomolecular chemistry*, 2010, 8, 12, 2683-2692.
210. Masiero, S., Trotta, R., Pieraccini, S., De Tito, S., Perone, R., Randazzo, A., & Spada, G. P., A non-empirical chromophoric interpretation of CD spectra of DNA G-quadruplex structures, *Organic & biomolecular chemistry*, 2010, 8, 12, 2683-2692.
211. McElligott, R., and Wellinger, R. J., The terminal DNA structure of mammalian chromosomes, *The EMBO journal*, 1997, 16, 3705-3714.
212. Mergny, J. L., Lacroix, L., Teulade-Fichou, M. P., Hounsou, C., Guittat, L., Hoarau, M., ... and Hélène, C., Telomerase inhibitors based on quadruplex ligands selected by a fluorescence assay, *Proceedings of the National Academy of Sciences*, 2001, 98, 3062-3067.
213. Micheli, E., D'Ambrosio, D., Franceschin, M., Savino, M., Water soluble cationic perylene derivatives as possible telomerase inhibitors: The search for selective G-quadruplex targeting, *Mini Rev. Med. Chem.*, 2009, 9, 1622–1632.
214. Middleton, E. J., “Effect of plant flavonoids on immune and inflammatory cell function,” *Advances in Experimental Medicine and Biology*, 1998, 439, 175–182.
215. Middleton, E., “The flavonoids,” *Trends in Pharmacological Sciences*, 1984, 5, 335–338.
216. Middleton, E., and Kandaswami, C., “Effects of flavonoids on immune and inflammatory cell functions,” *Biochemical Pharmacology*, 1992, 43, 1167–1179.
217. Mills, M., Lacroix, L., Arimondo, P.B., Leroy, J.L., Francois, J.C., Klump, H., & Mergny, J.L., Unusual DNA conformations: implications for telomeres, *Curr Med Chem Anticancer Agents*, 2002, 2, 627-644.
218. Mishra, A., Sharma, A. K., Kumar, S., Saxena, A. K., and Pandey, A. K., *Bauhinia variegata* leaf extracts exhibit considerable antibacterial, antioxidant, and anticancer activities, *BioMed research international*, 2013, 2013.
219. Mita, H., Ohyama, T., Tanaka, Y., Yamamoto, Y., Formation of a complex of 5,10,15,20-tetrakis(N-methylpyridinium-4-yl)-21H23H-porphyrin with G-quadruplex DNA, *Biochemistry*, 2006, 45, 6765–6772.
220. Miyake, Y., Shimoi, K., Kumazawa, S., Yamamoto, K., Kinae, N., and Osawa, T., Identification and antioxidant activity of flavonoid metabolites in plasma and urine of eriocitrin-treated rats, *Journal of agricultural and food chemistry*, 2000, 48, 3217-3224.

221. Mocellin, S., Pooley, K. A., Nitti, D., Telomerase and the search for the end of cancer, *Trends Mol. Med.*, 2013, 19, 125–133.
222. Monchaud, D., Teulade-Fichou, M. P., A hitchhiker's guide to G-quadruplex ligands, *Org. Biomol. Chem.*, 2008, 6, 627-636.
223. Murdock, K. C., Child, R. G., Fabio, P. F., Angier, R. B., Wallace, T. E., Durr, F. E. and Citarella, R. V., Antitumor agents.1, 4 Bis-[aminoalkyl) amino]-9, 10 anthracenedione, *J. Med.Chem.*, 1979, 22, 1024–1030.
224. Nakamura, T. M., Morin, G. B., Chapman, K. B., Weinrich, S. L., Andrews, W. H., Lingner, J., ... and Cech, T. R., Telomerase catalytic subunit homologs from fission yeast and human, *Science*, 1997, 277, 955-959.
225. Nanjunda, R., Owens, E. A., Mickelson, L., Dost, T. L., Stroeva, E. M., Huynh, H. T., Germann, M. W., Henary, M. M., and Wilson, W. D., Selective G-Quadruplex DNA Recognition by a New Class of Designed Cyanines, *Molecules*, 2013, 18, 13588-13607.
226. Neidle, S., and Balasubramanian, S. (Eds.), *Quadruplex nucleic acids*, Royal Society of Chemistry, 2006, Vol. 7.
227. Neidle, S., and Kelland, L. R., Telomerase as an anti-cancer target: current status and future prospects, *Anti-cancer drug design*, 1999, 14, 341-347.
228. Neidle, S., and Parkinson, G. N., The structure of telomeric DNA, *Curr. Opin.Struct. Biol.*, 2003, 13, 275-283.
229. Neidle, S., and Waring, M. J., *Molecular Aspects of Anti-cancer Drug Action*, Macmillan, London, 1983.
230. Neidle, S., Human telomeric G-quadruplex: The current status of telomeric G-quadruplexes as therapeutic targets in human cancer, *FEBS journal*, 2010, 277, 1118-1125.
231. Neidle, S., In: *Topics in Antibiotic Chemistry*, Vol. 2 (Ed Sammes P), Wiley, New York, 1978, pp. 261-271.
232. Neidle, S., Parkinson, G. N., Telomere maintenance as a target for anticancer drug discovery, *Nature Review Drug Discovery* 2002, 1, 383-93.
233. Nerdal, W., Andersen, O. M., and Sletten, E., NMR Studies of a Plant Flavonoid-DNA Oligonucleotide Complex, *Acta chemica scandinavica*, 1993, 47, 658-658.
234. Nissler, L., Gebhardt, R., and Berger, S., Flavonoid binding to a multi-drug-resistance transporter protein: an STD-NMR study, *Analytical and bioanalytical chemistry*, 2004, 379, 1045-1049.

235. Nugent, C. I., and Lundblad, V., The telomerase reverse transcriptase: components and regulation, *Genes & development*, 1998, 12, 1073-1085.
236. O'Connor, M. S., Safari, A., Xin, H., Liu, D., and Songyang, Z., A critical role for TPP1 and TIN2 interaction in high-order telomeric complex assembly, *Proceedings of the National Academy of Sciences*, 2006, 103, 11874-11879.
237. Ohishi, T., Tsuruo, T., and Seimiya, H., Evaluation of tankyrase inhibition in whole cells, *Methods in Molecular Biology (Clifton, N.J.)*, 2007, 405, 133–146.
238. Otter, A., Lown, J. W., and Kotovych, G., Sequential assignments in deoxyribonucleotide tetramers by $^{31}\text{P}/^1\text{H}$ two-dimensional shift correlation NMR spectroscopy, *Magnetic resonance in chemistry*, 1986, 24, 251-254.
239. Owen, R. W., Haubner, R., Mier, W., Giacosa, A., Hull, W. E., Spiegelhalder, B., and Bartsch, H., Isolation, structure elucidation and antioxidant potential of the major phenolic and flavonoid compounds in brined olive drupes, *Food and Chemical Toxicology*, 2003, 41, 703-717.
240. Paeschke, K., Simonsson, T., Postberg, J., Rhodes, D., Lipps, H. J., Telomere end-binding proteins control the formation of G-quadruplex DNA structures in vivo, *Nat. Struct. Mol. Biol.*, 2005. 12, 847-854.
241. Pal, S., Kumar, G. S., Debnath, D., and Maiti, M., Interaction of the antitumour alkaloid coralyne with duplex deoxyribonucleic acid structures: spectroscopic and viscometric studies, *Indian journal of biochemistry & biophysics*, 1998, 35, 321-332.
242. Pan, B., Xiong, Y., Shi, K., Deng, J. and Sundaralingam, M., Crystal structure of an RNA purine-rich tetraplex containing adenine tetrads: implications for specific binding in RNA tetraplexes, *Structure*, 2003, 11, 815–823.
243. Panousis C., Kettle A. J. and Phillips D. R. Myeloperoxidase oxidizes mitoxantrone to metabolites which bind covalently to DNA and RNA. *Anti-Cancer Drug Design*, 1995, 10, 593–605
244. Panousis, C., Kettle A. L., Phillips, D. R., Oxidative metabolism of mitoxantrone by the human neutrophil enzyme myeloperoxidase, *Biochem. Pharmacol*, 1994, 48, 2223-2230.
245. Parker, B. S., Cullinane, C., and Phillips, D. R., Formation of DNA adducts by formaldehyde-activated mitoxantrone. *Nucleic Acids Research*, 1999, 27, 2918–2923.
246. Parkinson, G. N., Lee, M. P., and Neidle, S., Crystal structure of parallel quadruplexes from human telomeric DNA, *Nature*, 2002, 417, 876-880.

247. Parkinson, G.N., Ghosh, R., Neidle, S., Structural basis for binding of porphyrin to human telomeres, *Biochemistry*, 2007, 46, 2390–2397.
248. Pasternack, R. F., Gibbs, E. J., and Villafranca, J. J., Interactions of porphyrins with nucleic acids, *Biochemistry*, 1983, 22, 2406-2414.
249. Patel, D. J. and Canuel, L. L., Ethidium bromide-(dC–dG–dC–dG)₂ complex in solution: intercalation and sequence specificity of drug binding at the tetranucleotide duplex level, *Proc. Natl. Acad. Sci. USA.*, 1976, 73, 3343-3347.
250. Patel, D. J., Phan, A. T., & Kuryavyi, V., Human telomere, oncogenic promoter and 5'-UTR G-quadruplexes: diverse higher order DNA and RNA targets for cancer therapeutics. *Nucleic acids research*, 2007, 35, 7429-7455.
251. Patel, D.J., Helix-coil transition of the dG-dC-dG-dC self-complementary duplex and complex formation with daunomycin in solution, *Biopolymers*, 1979, 18, 553.
252. Patel, D.J., Tonelli, A.E., *Biopolymers*, 1974, 13, 1943–1964.
253. Pennarun, G., Granotier, C., Gauthier, L. R., Gomez, D., Hoffschir, F., Mandine, E., Riou, J. F., Mergny, J. L., Mailliet, P., Boussin, F. D., Apoptosis related to telomere instability and cell cycle alterations in human glioma cells treated by new highly selective G-quadruplex ligands, *Oncogene*, 2005, 24, 2917–2928.
254. Percivalle, C., Sissi, C., Greco, M. L., Musetti, C., Mariani, A., Artese, A., ... and Freccero, M., Aryl ethynyl anthraquinones: a useful platform for targeting telomeric G-quadruplex structures, *Organic & biomolecular chemistry*, 2014, 12, 3744-3754.
255. Phan, A. T., and Mergny, J. L., Human telomeric DNA: G-quadruplex, i-motif and Watson–Crick double helix, *Nucleic acids research*, 2002, 30, 4618-4625.
256. Phan, A. T., Kuryavyi, V., Burge, S., Neidle, S., Patel, D. J., Structure of an unprecedented G-quadruplex scaffold in the human c-kit promoter, *J. Am. Chem. Soc.*, 2007, 129, 4386–4392.
257. Phan, A. T., Kuryavyi, V., Gaw, H. Y., Patel, D. J., Small-molecule interaction with a five-guanine-tract G-quadruplex structure from the human MYC promoter. *Nature Chem. Biol.*, 2005, 1, 167–173.
258. Phan, A. T., Luu, K. L. and Patel, D. J., Different loop arrangements of intramolecular human telomeric (3C1) G-quadruplexes in KC solution. *Nucleic Acids Res.*, 2006, 34, 5715–5719.

259. Phan, A. T., Modi, Y. S. and Patel, D. J., Propellor-type parallel-stranded G-quadruplexes in the human c-myc promoter. *J. Am. Chem. Soc.*, 2004, 126, 8710–8716.
260. Phatak, P., Cookson, J. C., Dai, F., Smith, V., Gartenhaus, R. B., Stevens, M. F. G., and Burger, A. M., Telomere uncapping by the G-quadruplex ligand RHPS4 inhibits clonogenic tumour cell growth in vitro and in vivo consistent with a cancer stem cell targeting mechanism, *British journal of cancer*, 2007, 96, 1223-1233.
261. Phillips, K., Dauter, Z., Murchie, A. I., Lilley, D. M., Luisi, B., The crystal structure of a parallelstranded guanine tetraplex at 0.95 Å resolution, *J. Mol. Biol.*, 1997, 273, 171-182.
262. Praseuth, D., Guieysse, A. L., Helene, C., Triple helix formation and the antigene strategy for sequence-specific control of gene expression, *Biochim Biophys Acta*, 1999, 1489, 181-206.
263. Qin, Y., Hurley, L. H., Structures folding patterns and functions of intramolecular DNA G-quadruplexes found in eukaryotic promoter regions, *Biochimie*, 2008, 90, 1149–1171.
264. Ragazzon, P. A., Iley, J., and Missailidis, S., Structure-activity Studies of the Binding of the Flavonoid Scaffold to DNA, *Anticancer research*, 2009, 29, 2285-2293.
265. Ranaud, S., de Lorgeril, M., Wine, alcohol, platelets, and the french paradox for coronary heart disease, *Lancet*, 1992, 339, 1523-1526.
266. Randazzo, A., Galeone, A., Esposito, V., Varra, M., and Mayol, L., Interaction of distamycin A and netropsin with quadruplex and duplex structures: a comparative ¹H-NMR study, *Nucleosides, Nucleotides and Nucleic Acids*, 2002, 21, 535-545.
267. Rangan, A., Fedoroff, O. Y. and Hurley, L. H., Induction of duplex to G-quadruplex transition in the c-myc promoter region by a small molecule, *J. Biol. Chem.*, 2001, 276, 4640–4646.
268. Rankin, S., Reszka, A. P., Huppert, J., Zloh, M., Parkinson, G. N., Todd, A. K., Ladame, S., Balasubramanian, S., Neidle, S., Putative DNA quadruplex formation within the human c-kit oncogene, *J. Am. Chem. Soc.*, 2005, 127, 10584–10589.
269. Read, M. A., Wood, A. A., Harrison, J. R., Gowan, S. M., Kelland, L. R., Dosanjh, H. S., and Neidle, S., Molecular modeling studies on G-quadruplex complexes of telomerase inhibitors: structure-activity relationships, *Journal of medicinal chemistry*, 1999, 42, 4538-4546.

270. Read, M. A., Wood, A. A., Harrison, R. J., Gowan, S. M., Kelland, L. R., Dosanjh, H. S., and Neidle, S., Molecular modelling studies on G-quadruplex complexes of telomerase inhibitors: structure-activity relationships, *J Med Chem.*, 1999, 42, 4538–4546.
271. Read, M., Harrison, R. J., Romagnoli, B., Tanious, F. A., Gowan, S. H., Reszka, A. P., Wilson, W. D., Kelland, L. R., Neidle, S., Structure-based design of selective and potent G quadruplex-mediated telomerase inhibitors, *Proc. Natl. Acad. Sci. USA*, 2001, 98, 4844–4849.
272. Reinli, K., and Block, G., Phytoestrogen content of foods—a compendium of literature values, *Nutrition and cancer*, 1996, 26, 123-148.
273. Ren, J., and Chaires, J.B., Sequence and structural selectivity of nucleic acid binding
274. Rha, S.Y., Izbicka, E., Lawrence, R., Davidson, K., Sun, D., Moyer, M.P., Roodman, G.D., Hurley, L., Von Hoff, D. Effect of telomere and telomerase interactive agents on human tumor and normal cell lines, *Clin. Cancer Res.*, 2000, 6, 987–993.
275. Rice-Evans, C. A., Miller, N. J., and Paganga, G., Structure-antioxidant activity relationships of flavonoids and phenolic acids, *Free radical biology and medicine*, 1996, 20, 933-956.
276. Riethman, H., Human telomere structure and biology, *Annu. Rev. Genomics Hum.Genet*, 2008, 1, 1-19.
277. Rijke, E. D., Out, P., Niessen, W. M. A., Ariese, F., Goojer, C., Brinkman, U. A. T., Analytical separation and detection methods for flavonoids, *Journal of Chromatography A*, 2006, 1112, 31-63.
278. Riou, J.F., Guittat, L., Mailliet, P., Laoui, A., Renou, E., Petitgenet, O., Megnin-Chanet, F., Helene, C., Mergny, J. L., Cell senescence and telomere shortening induced by a new series of specific G-quadruplex DNA ligands, *Proc. Natl. Acad. Sci. USA*, 2002, 99, 2672–2677.
279. Robards, K., and Antolovich, M., Analytical Chemistry of Fruit Bioflavonoids A Review, *Analyst*, 1997, 122, 11R-34R.
280. Robards, K., Li, X., Antolovich, M., and Boyd, S., Characterisation of citrus by chromatographic analysis of flavonoids. *Journal of the Science of Food and Agriculture*, 1997, 75, 87–101.
281. Rossetti, L., Franceschin, M., Schirripa, S., Bianco, A., Ortaggi, G., Savino, M., Selective interactions of perylene derivatives having different side chains with inter- and

- intramolecular G-quadruplex structures. A correlation with telomerase inhibition, *Bioorganic & Medicinal Chemistry Letters*, 2005, 15, 413-420.
282. Rousseff, R. L., Martin, S. F., and Youtsey, C. O., "Quantitative survey of narirutin, naringin, hesperidin, and neohesperidin in citrus," *Journal of Agricultural and Food Chemistry*, 1987, 35, 6, 1027–1030.
283. Rujan, I. N., Meleney, J. C., and Bolton, P. H., Vertebrate telomere repeat DNAs favor external loop propeller quadruplex structures in the presence of high concentrations of potassium, *Nucleic acids research*, 2005, 33, 2022-2031.
284. S.M. Gowan, R. Heald, M.F. Stevens, L.R. Kelland, Potent inhibition of telomerase by small-molecule pentacyclic acridines capable of interacting with G-quadruplexes, *Mol. Pharmacol.*, 2001, 60, 981–988.
285. Schaffitzel, C., Berger, I., Postberg, J., Hanes, J., Lipps, H. J., Pluckthun, A., In vitro generated antibodies specific for telomeric guanine-quadruplex DNA react with *Stylonychia lemnae macronuclei*, *Proc. Natl. Acad. Sci. U.S.A.*, 2001, 98, 8572-8577.
286. Schultze, P., Macaya, R. F., Feigon, J., Three-dimensional solution structure of the thrombinbinding DNA aptamer d(GGTTGGTGTGGTTGG), *J. Mol. Biol.*, 1994, 235, 1532-1547.
287. Seelinger, G., Merfort, I., Wölfle, U., and Schempp, C. M., Anti-carcinogenic effects of the flavonoid luteolin, 2008, *Molecules*, 13, 2628-2651.
288. Seenisamy, J., Rezler, E. M., Powell, T. J., Tye, D., Gokhale, V., Joshi, C. S., Siddiqui-Jain, A. and Hurley, L. H., The dynamic character of the G-quadruplex element in the c-myc promoter and modification by TMPyP4, *J. Am. Chem. Soc.*, 2004, 126, 8702–8709.
289. Sen, D., and Gilbert, W., A sodium-potassium switch in the formation of four-stranded G4-DNA. *Nature*, 1990, 344, 410-414.
290. Sen, D., Gilbert, W., Formation of parallel four-stranded complexes by guanine-rich motifs in DNA and its implications for meiosis, *Nature*, 1988, 334, 364-366.
291. Sengupta, B., Pahari, B., Blackmon, L., and Sengupta, P. K., Prospect of bioflavonoid fisetin as a quadruplex DNA ligand: a biophysical approach, *PloS one*, 2013, 8, e65383.
292. Shamma, M. A., Shmookler Reis, R. J., Li, C., Koley, H., Hurley, L.H., Anderson, K. C., Munshi, N. C., Telomerase inhibition and cell growth arrest after telomestatin treatment in multiple myeloma, *Clin. Cancer Res.*, 2004, 10, 770–776.

293. Shan, C., Tan, J. H., Ou, T. M., and Huang, Z. S., Natural products and their derivatives as G-quadruplex binding ligands, *Science China Chemistry*, 2013, 56, 1351-1363.
294. Sharma, S., Raymond, E., Soda, H., Sun, D., Hilsenbeck, S. G., Sharma, A., ... and Von Hoff, D. D., Preclinical and clinical strategies for development of telomerase and telomere inhibitors*, *Annals of oncology*, 1997, 8, 1063-1074.
295. Sharma, U., Danishad, K. K. A., Seenu, V., and Jagannathan, N. R., Longitudinal study of the assessment by MRI and diffusion-weighted imaging of tumor response in patients with locally advanced breast cancer undergoing neoadjuvant chemotherapy, *NMR in Biomedicine*, 2009, 22, 104-113.
296. Shay, J. W., and Gazdar, A. F., Telomerase in the early detection of cancer, *Journal of clinical pathology*, 1997, 50, 106-109.
297. Shen, Y., Myslinski, P., Treszczanowicz, T., Liu, Y., and Koningstein, J. A., Picosecond laser-induced fluorescence polarization studies of mitoxantrone and tetrakis porphine/DNA complexes, *The Journal of Physical Chemistry*, 1992, 96, 19, 7782-7787.
298. Shi, R. X., Ong, C. N., Shen, H. M., Luteolin sensitizes tumor necrosis factor-alpha-induced apoptosis in human tumor cells, *Oncogene*, 2004, 23, 7712-21.
299. Shimoi, K., Masuda, S., Furugori, M., Esaki, S., Kinae, N., Radioprotective effect of antioxidative flavonoids in gamma-ray irradiated mice, *Carcinogenesis*, 1994, 15, 2669-72.
300. Shin-ya, K., Wierzba, K., Matsuo, K., Ohtani, T., Yamada, Y., Furihata, K., Hayakawa, Y., Seto, H., Telomestatin, a novel telomerase inhibitor from *Streptomyces anulatus*, *J. Am. Chem. Soc.*, 2001, 123, 1262-1263.
301. Siddiqui-Jain, A., Grand, C. L., Bearss, D. J., Hurley, L. H., Direct evidence for a G-quadruplex in a promoter region and its targeting with a small molecule to repress c-MYC transcription, *Proc. Natl. Acad. Sci. USA*, 2002, 99, 11593-11598.
302. Siddiqui-Jain, A., Grand, C. L., Bearss, D. J., Hurley, L. H., Direct evidence for a G-quadruplex in a promoter region and its targeting with a small molecule to repress c-MYC transcription, *Proc. Natl. Acad. Sci. USA*, 2002, 99; 11593-11598.
303. Simonsson, T., Pecinka, P. and Kubista, M., DNA tetraplex formation in the control region of c-myc. *Nucleic Acids Res.*, 1998, 26, 1167-1172.
304. Sinha, R., and Kumar, G. S., Interaction of isoquinoline alkaloids with an RNA triplex: Structural and thermodynamic studies of berberine, palmatine, and coralyne binding to poly (U). poly (A)* poly (U), *The Journal of Physical Chemistry B*, 2009, 113, 13410-13420.

305. Sinha, R., Gadhwal, M. K., Joshi, U. J., Srivastava, S., and Govil, G., Interaction of quercetin with DPPC model membrane: Molecular dynamic simulation, DSC and multinuclear NMR studies, *Journal of the Indian Chemical Society*, 2011, 88, 1203.
306. Smith, F. W., Feigon, J., Quadruplex structure of Oxytricha telomeric DNA oligonucleotides, *Nature* 1992, 356, 164-168.
307. Smith, I. E., Mitoxantrone (novantrone): a review of experimental and early clinical studies, *Cancer Treat Rev.*, 1983, 10, 103–115.
308. Smith, Paul J., Sally A. Morgan, Mary E. Fox, and James V. Watson. "Mitoxantrone-DNA binding and the induction of topoisomerase II associated DNA damage in multi-drug resistant small cell lung cancer cells." *Biochemical pharmacology*, 1990, 40, 2069-2078.
309. Solimani, R., Bayon, F., Domini, I., Pifferi, P.G., Todesco, P.A., Marconi, G., Samorì, B., Flavonoid-DNA Interaction Studied with Flow Linear Dichroism Technique, *J. Agric. Food Chem.*, 1995, 43, 876–882.
310. Spring, A. M., and Germann, M. W., Supercooled aqueous nuclear magnetic resonance using agarose gels, *Analytical biochemistry*, 2012, 427, 79-81.
311. Stewart, A. J., Bozonnet, S., Mullen, W., Jenkins, G. I., Lean, M. E., and Crozier, A., "Occurrence of flavonols in tomatoes and tomato-based products," *Journal of Agricultural and Food Chemistry*, 2000, 48, 7, 2663–2669.
312. Stobiecki, M., Malosse, C., Kerhoas, L., Wojlaszek, P., & Einhorn, J., Detection of isoflavonoids and their glycosides by liquid chromatography/electrospray ionization mass spectrometry in root extracts of lupin (*Lupinus albus*). *Phytochemical Analysis*, 1999, 10, 198–207,
313. Sumi, M., Tauchi, T., Sashida, G., Nakajima, A., Gotoh, A., Shin-Ya, K., Ohyashiki, J.H., Ohyashiki, K. A., G-quadruplex-interactive agent, telomestatin (SOT-095), induces telomere shortening with apoptosis and enhances chemosensitivity in acute myeloid leukemia, *Int. J. Oncol.*, 2004, 24, 1481–1487.
314. Sun, D., Guo, K., Rusche, J. J. and Hurley, L. H., Facilitation of a structural transition in the polypurine/polypyrimidine tract within the proximal promoter region of the human VEGF gene by the presence of potassium and G-quadruplex-interactive agents, *Nucleic Acids Res.*, 2005, 33, 6070–6080.

315. Sun, D., Thompson, B., Cathers, B. E., Salazar, M., Kerwin, S. M., Trent, J. O., Jenkins, T. C., Neidle, S., Hurley, L. H., Inhibition of human telomerase by a G-quadruplex-interactive compound, *J. Med. Chem.*, 1997, 40, 2113-2116.
316. Sun, D.; Pourpak, A.; Beetz, K.; Hurley, L. H., Direct evidence for the formation of G-quadruplex in the proximal promoter region of the RET protooncogene and its targeting with a small molecule to repress RET protooncogene transcription, *Clin. Cancer Res.*, 2003, 9, A218.
317. Sun, H., Karow, J. K., Hickson, I. D. and Maizels, N., The Bloom's syndrome helicase unwinds G4 DNA. *J. Biol. Chem.*, 1998, 273, 27587-27592.
318. Sun, H., Tang, Y., Xiang, J., Xu, G., Zhang, Y., Zhang, H., and Xu, L., Spectroscopic studies of the interaction between quercetin and G-quadruplex DNA, *Bioorganic & medicinal chemistry letters*, 2006, 16, 3586-3589.
319. Sun, H., Xiang, J., Tang, Y., and Xu, G., Regulation and recognition of the extended G-quadruplex by rutin, *Biochemical and biophysical research communications*, 2007, 352, 942-946.
320. Sun, J. S., Garestier, T., Helene, C., Oligonucleotide directed triple helix formation, *Curr Opin Struct Biol*, 1996, 6, 327-333.
321. Tauchi, T., Shin-Ya, K., Sashida, G., Sumi, M., Nakajima, A., Shimamoto, T., ... and Ohyashiki, K., Activity of a novel G-quadruplex-interactive telomerase inhibitor, telomestatin (SOT-095), against human leukemia cells: involvement of ATM-dependent DNA damage response pathways, *Oncogene*, 2003, 22, 5338-5347.
322. Tsavaris, N., Kosmas, C., Kavantzias, N., Lazaris, A., Skopelitis, E., Dimitrakopoulos, A., ... and Pangalis, G. A., Breast cancer following curative chemotherapy for non-Hodgkin's lymphoma and the effect of drug resistance proteins to the final outcome. A retrospective study, *Journal of BU ON.: official journal of the Balkan Union of Oncology*, 2004, 10, 71-76.
323. Ueda, H., Yamazaki, C., and Yamazaki, M., Luteolin as an anti-inflammatory and anti-allergic constituent of *Perilla frutescens*, *Biological and Pharmaceutical Bulletin*, 2002, 25, 1197-1202.
324. van Dongen, M. J., Doreleijers, J. F., van der Marel, G. A., van Boom, J. H., Hilbers, C. W., & Wijmenga, S. S., Structure and mechanism of formation of the H-y5 isomer of an intramolecular DNA triple helix, *Nature Structural & Molecular Biology*, 1999, 6, 854-859.

325. Wan, C., Cui, M., Song, F., Liu, Z., and Liu, S., A study of the non-covalent interaction between flavonoids and DNA triplexes by electrospray ionization mass spectrometry, *International Journal of Mass Spectrometry*, 2009, 283, 48-55.
326. Wang, A.H., Quigley, G.J., Kolpak, F.J., Crawford, J.L., van Boom, J.H., van der Marel, G., and Rich, A., Molecular structure of a left-handed double helical DNA fragment at atomic resolution, *Nature*, 1979, 282, 680-686.
327. Wang, J., Xie, L. Y., Allan, S., Beach, D., and Hannon, G. J., Myc activates telomerase, *Genes & development*, 1998, 12, 1769-1774.
328. Wang, Y., and Patel, D. J., Solution structure of the human telomeric repeat d [AG3(T2AG3)3] G-tetraplex, *Structure*, 1993, 1, 263-282.
329. Wang, Y., Patel, D. J., Guanine residues in d(T2AG3) and d(T2G4) form parallel-stranded potassium cation stabilized G-quadruplexes with anti glycosidic torsion angles in solution, *Biochemistry*, 1992, 31, 8112-8119.
330. Wang, Y., Patel, D. J., Solution structure of a parallel stranded G-quadruplex DNA. *J. Mol. Biol.*, 1993a, 234, 1171-1183.
331. Wang, Y., Patel, D. J., Solution structure of the human telomeric repeat d[AG3(T2AG3)3] G-tetraplex, *Structure*, 1993, 1, 263-282.
332. Wang, Y., Patel, D. J., Solution structure of the *Oxytricha* telomeric repeat d[G4(T4G4)3] G tetraplex, *J. Mol. Biol.*, 1995, 251, 76-94.
333. Wang, Y., Patel, D.J., *Biochemistry*, 1992, 31, 8112–8119.
334. Wang, Z., Cui, M., Song, F., Lu, L., Liu, Z., and Liu, S., Evaluation of flavonoids binding to DNA duplexes by electrospray ionization mass spectrometry, *Journal of the American Society for Mass Spectrometry*, 2008, 19, 914-922.
335. Watson, J. D., and Crick, F. H., Molecular structure of nucleic acids, *Nature*, 1953, 171, 737-738.
336. Webba da Silva M., NMR methods for studying quadruplex nucleic acids., *Methods*, 2007, 43, 264-277.
337. Wei, C., Jia, G., Yuan, J., Feng, Z., and Li, C., A spectroscopic study on the interactions of porphyrin with G-quadruplex DNAs. *Biochemistry*, 2006, 45, 21, 6681-6691.
338. Wei, C., Wang, J., and Zhang, M., Spectroscopic study on the binding of porphyrins to (G₄T₄G₄)₄ parallel G-quadruplex. *Biophysical chemistry*, 2010, 148, 51-55.

339. Weinrich, S. L., Pruzan, R., Ma, L., Ouellette, M., Tesmer, V. M., Holt, S. E.,... and Morin, G. B., Reconstitution of human telomerase with the template RNA component hTR and the catalytic protein subunit hTRT, *Nature genetics*, 1997, 17, 498-502.
340. Weinrich, S., Pruzan, R., Ma, L., Ouellette, M., Tesmer, V., Holt, S., et al. Reconstitution of human telomerase with the template RNA component hTR and the catalytic protein subunit hTERT, *Nature Genetics*, 1997, 17, 498–502.
341. Wheelhouse, R. T., D. Sun, H. Han, F. X. Han and Hurley, L. H., "Cationic Porphyrins as Telomerase Inhibitors: the Interaction of Tetra-(N-methyl-4-pyridyl)porphine with Quadruplex DNA." *J Am Chem Soc.*, 1998, 120, 3261-3262.
342. Wheelhouse, R. T., Sun, D. K., Han, H.Y., Han, F. X., Hurley LH Cationic porphyrins as telomerase inhibitors: the interaction of tetra-(N-methyl-4- pyridyl)porphine with quadruplex DNA, *J. Am. Chem. Soc.*, 1998, 120, 3261–3262.
343. Wierstra, I. and Alves, J., The c-myc Promoter: Still MysterY and Challenge, *Advances in Cancer Research*, 2008, 99, 113-333.
344. Williamson, G., Common features in the pathways of absorption and metabolism of flavonoids. In: Meskin, MS, R. BW, Davies AJ, Lewis DS, Randolph RK, eds. *Phytochemicals: Mechanisms of Action*. Boca Raton: CRC Press, 2004, 21-33.
345. Wilson, W. D. and Jones, R. L. Interaction of actinomycin D, ethidium, quinacrine daunorubicin, and tetralysine with DNA: ³¹P NMR chemical shift and relaxation investigation, *Nucleic Acids. Res.*, 1982, 10, 1399-1410.
346. Winkel-Shirley, B., Flavonoid biosynthesis. A colorful model for genetics, biochemistry, cell biology, and biotechnology, *Plant physiology*, 2001, 126, 485-493.
347. Wright, W. E., Tesmer, V. M., Huffman, K. E., Levene, S. D., and Shay, J. W., Normal human chromosomes have long G-rich telomeric overhangs at one end, *Genes & development*, 1997, 11, 2801-2809.
348. Wuthrich, K., *NMR of Proteins and Nucleic Acid*, John Wiley & Sons, New York, 1986.
349. Wyatt, J. R. et al., Combinatorially selected guanosine-quartet structure is a potent inhibitor of human immunodeficiency virus envelope-mediated cell fusion. *Proc. Natl Acad. Sci. USA*, 1994, 91, 1356–1360.
350. Xu, D., Li, H., and Liu, J., Inhibition of telomerase by targeting MAP kinase signalling, *Methods in Molecular Biology (Clifton, N.J.)*, 2007, 405, 147–165.

351. Xu, Y., and Sugiyama, H., Formation of the G-quadruplex and i-motif structures in retinoblastoma susceptibility genes (Rb), *Nucleic acids research*, 2006, 34, 949-954.
352. Yang, D., and Okamoto, K., Structural insights into G-quadruplexes: towards new anticancer drugs, *Future medicinal chemistry*, 2010, 2, 619-646.
353. Yang, Y., Hu, Q., Fan, Y., and Shen, H., Study on the binding of luteolin to bovine serum albumin, *Spectrochimica Acta Part A: Molecular and Biomolecular Spectroscopy*, 2008, 69, 432-436.
354. Zagotto, G., Ricci, A., Vasquez, E., Sandoli, A., Benedetti, S., Palumbo, M., & Sissi, C., Tuning G-quadruplex vs double-stranded DNA recognition in regioisomeric lysyl-peptidyl-anthraquinone conjugates, *Bioconjugate chemistry*, 2011, 22, 2126-2135.
355. Zagotto, G., Sissi, C., Lucatello, L., Pivetta, C., Cadamuro, S. A., Fox, K. R., ... and Palumbo, M., Aminoacyl- Anthraquinone Conjugates as Telomerase Inhibitors: Synthesis, Biophysical and Biological Evaluation, *Journal of medicinal chemistry*, 2008, 51, 5566-5574.
356. Zahler, A. M., Williamson, J. R., Cech, T. R., Prescott DM Inhibition of telomerase by G-quartet DNA structures, *Nature*, 1991, 350, 718-720.
357. Zahler, A. M., Williamson, J. R., Cech, T. R., Prescott, D. M., Inhibition of telomerase by G-quartet DNA structures, *Nature*, 1991, 350, 718-720.
358. Zaug, A. J., Podell, E. R., Cech, T. R., Human POT1 disrupts telomeric G-quadruplexes allowing telomerase extension in vitro, *Proc. Natl. Acad. Sci. U.S.A.*, 2005, 102, 10864-10869.
359. Zhang, J. L., Fu, Y., Zheng, L., Li, W., Li, H., Sun, Q., ..and Geng, F., Natural isoflavones regulate the quadruplex-duplex competition in human telomeric DNA, *Nucleic acids research*, 2009, 37, 2471-2482.
360. Zhang, N., Gorin, A., Majumdar, A., Kettani, A., Chernichenko, N., Skripkin, E., Patel, D. J., V-shaped scaffold: a new architectural motif identified in an A•(G•G•G•G) pentad-containing dimeric DNA quadruplex involving stacked G(anti)•G(anti)•G(anti)•G(syn) tetrads, *J. Mol. Biol.*, 2001, 311, 1063-1079.
361. Zhang, S., Ling, B., Qu, F., and Sun, X., Investigation on the interaction between luteolin and calf thymus DNA by spectroscopic techniques, *Spectrochimica Acta Part A: Molecular and Biomolecular Spectroscopy*, 2012, 97, 521-525.

362. Zhang, W. J., Ou, T. M., Lu, Y. J., Huang, Y. Y., Wu, W. B., Huang, Z. S., ... and Gu, L. Q., 9-Substituted berberine derivatives as G-quadruplex stabilizing ligands in telomeric DNA, *Bioorganic & medicinal chemistry*, 2007, 15, 5493-5501.
363. Zheng, S., Chen, Yu., Donahue, C. P., Wolfe, M. S., Varani, G., Structural basis for stabilization of the tau pre-mRNA splicing regulatory element by novantrone (mitoxantrone), *Chem. Biol.*, 2009, 16, 557-566.
364. Zhong, Z. H. O. N. G., Shiue, L. I. L. Y., Kaplan, S. H. A. W. N., and de Lange, T. I. T. I. A., A mammalian factor that binds telomeric TTAGGG repeats in vitro, *Molecular and cellular biology*, 1992. 12, 4834-4843.
365. Zhou, J. M., Zhu, X. F., Lu, Y.J., Deng, R., Huang, Z. S., Mei, Y.P., Wang, Y., Huang, W. L., Liu, Z.C., Gu, L. Q., Zeng, Y. X., Senescence and telomere shortening induced by novel potent G-quadruplex interactive agents, quindoline derivatives, in human cancer cell lines, *Oncogene*, 2006, 25, 503–511.
366. Zhou, T. M., Lin, J., Lu, Y. J., Hou, J. Q., Tan, J. H., Chen, S. H., Li, Z., Li, Y. P., Li, D., Gu, L. Q., et al., Inhibition of cell proliferation by quindoline derivative (SYUIQ-05) through its preferential interaction with c-myc promoter G-quadruplex. *J. Med. Chem.*, 2011, 54, 5671–5679.